

A Novel Antibiofilm Treatment for Surgical Site Infections



A thesis submitted for the degree of

Doctor of Philosophy

at the

Adelaide Medical School, Discipline of Surgery

Faculty of Health and Medical Sciences

University of Adelaide, Adelaide, Australia

&

Doctor rerum naturalium (Dr. rer. nat.)

at the

Department of Pharmaceutics

Faculty of Chemistry and Pharmacy

Albert-Ludwigs-Universität Freiburg, Freiburg im Breisgau, Germany

by

Laurine Dorothea Kaul

from Le Chesnay

March 2023

A Novel Antibiofilm Treatment for Surgical Site Infections



THE UNIVERSITY
of ADELAIDE

A thesis submitted for the degree of

Doctor of Philosophy

at the

Adelaide Medical School, Discipline of Surgery

Faculty of Health and Medical Sciences

University of Adelaide, Adelaide, Australia

by

Laurine Dorothea Kaul

March 2023



I certify that this work contains no material which has been accepted for the award of any other degree or diploma in my name, in any university or other tertiary institution and, to the best of my knowledge and belief, contains no material previously published or written by another person, except where due reference has been made in the text. In addition, I certify that no part of this work will, in the future, be used in a submission in my name, for any other degree or diploma in any university or other tertiary institution without the prior approval of the University of Adelaide and where applicable, any partner institution responsible for the joint award of this degree.

The author acknowledges that copyright of published works contained within the thesis resides with the copyright holder(s) of those works.

I give permission for the digital version of my thesis to be made available on the web, via the University's digital research repository, the Library Search and also through web search engines, unless permission has been granted by the University to restrict access for a period of time.

Date: 06.03.2023

A Novel Antibiofilm Treatment for Surgical Site Infections



Dissertation

submitted for the degree

Doctor rerum naturalium (Dr. rer. nat.)

at the

Faculty of Chemistry and Pharmacy

University of Freiburg

by

Laurine Dorothea Kaul

from Le Chesnay

2023



Die vorliegende Dissertationsschrift wurde von Januar 2019 bis März 2023 unter Anleitung von Frau Prof. Dr. Regine Süss, Frau Dr. Katharina Richter und Herr Prof. Dr. Andrew Zannettino am Lehrstuhl für Pharmazeutische Technologie und Biopharmazie des Instituts für Pharmazeutische Wissenschaften der Albert-Ludwigs-Universität Freiburg im Breisgau und an der Adelaide Medical School der University of Adelaide (Australien) angefertigt.

Laurine Dorothea Kaul

A novel antibiofilm treatment for surgical site infections, 2023

Chairman of the Doctoral Committee

Prof. Dr. Stefan Weber

Dean of the Faculty

Prof. Dr. Andreas Bechthold

Supervisors

Dr. Katharina Richter

Prof. Dr. Regine Süss

Prof. Dr. Andrew Zannettino

Examiners

Assistant Prof. Lene Bay

Prof. Natasa Skalko-Basnet

Oral examination

18 May 2023

Acknowledgements

I would like to take this opportunity to acknowledge and thank all the people that have contributed to this project and supported me during my PhD.

I am grateful for the supervision and guidance of Dr Katharina Richter, Prof Dr Regine Süss and Prof Dr Andrew Zannettino over the last four years.

I thank Katharina, my supervisor from the University of Adelaide, for her mentorship, and for trusting me to be her first PhD student. You supported me from the first email on, guided me through the application and enrolment process, taught me all your biofilm knowledge and got your hands dirty with me in the lab when I needed help. I thank you for embracing my curiosity, for being open to my ideas, for cheering at every presentation and for taking the time to discuss problems. You always have my best interests at heart, you gave me many opportunities to attend conferences and visit labs and convinced me that presenting can be fun. I am also very grateful for our adventures outside of work, including eating Knöpfle late at night, waffles brunches and being by your side at important events.

Similarly, I thank Regine, my supervisor from the University of Freiburg, for all the effort to make this Joint PhD possible, for the warm welcome in Freiburg and for always being available no matter the time zone. You allowed me to discover a different way to do research and built a creative space that embraces the development of ideas and encourages out-of-the-box thinking. Thank you for your trust in letting me work independently and supervising and teaching other students. You know how much I value our discussions, particularly your honesty and feedback, and I thank you for always having my back. I am also grateful for your flexibility, when my return to Australia was uncertain, for our many meetings over coffee, and for your help, no matter the problem. It was a joy spending time with you in Australia, discussing past experiences and life plans whilst sharing our love of mussels. Lastly, I thank you for showing me the importance of making lists and having the confidence to believe that everything will be ticked off.

I thank my co-supervisor Andrew for taking on the role as my primary supervisor for the first two years. I'm also grateful for your valuable perspective, and for reviewing everything I send you. I appreciate your excitement about my progress at every meeting and for your quick problem-solving skills during challenging presentations.

I would also like to acknowledge the institutions which have contributed to the success of my project over the last four years.

I am grateful for the scholarship and travel support provided by the University of Adelaide, and for the financial support of conferences and lab visits by the Australian Society for Microbiology and The Hospital Research Foundation. I thank Prof Dr Simon Swift and his team at the University of Auckland, and Prof Dr Tom Coenye at Ghent University, for giving me the opportunity to do research in their labs. I would also like to thank Prof Dr Hans-Georg Koch and his team at the University of Freiburg for giving a home to my bacteria, letting me use their facilities for experiments, involving me in collaborations, and for always being helpful.

I appreciate the time of all the people who proofread this thesis and gave constructive feedback. I thank Artur Weiz and Hanna Löffler for generating valuable data for this project as a part of their master's internship and diploma thesis, respectively. I acknowledge the 1000 larvae that have sacrificed their lives for my research.

I am grateful for the friendly environment at the Basil Hetzel Institute for Translational Health Research and the privilege of being part of the surgery department. I thank Dr Makutiro Masavuli for providing entertainment during many hours in the level 1 lab, for the vivid discussions and the endless supply of cake.

It was a joy to be a part of the Richter Lab and I thank every team member for their input, the interesting discussions, the encouraging words, and fun meetings. I would especially like to thank Dr Adrian Abdo for managing the lab and contributing to the outstanding atmosphere in our shared office. Your accompaniment on countless coffee and lunch breaks is also appreciated. Despite the rocky start, when you tried (and failed) to help me fix the Fluostar, your assistance turned out to be crucial for cell culture experiments! Thank you for proofreading everything that I put on paper, including this whole thesis. I am so lucky to have you as my work husband to help guide me through my daily ups and downs. Thank you for sharing the excitement of every single dog photo, for embracing the drama, for not believing in my Australian accent and for being Terry.

Furthermore, I thank Prof Dr Heiko Heerklotz for welcoming me into the Pharmaceutical Technology group. Despite COVID disruptions and uncertainties regarding the length of my stay in Freiburg, my colleagues and friends from the Techno AG made every moment there outstanding. Some special moments I remember fondly are the result of time spent with Hannah and include intense discussions during runs and the power of her flirty look. I thank Eva Dengler, Birgit Erhard, Dr Monika Köll-Weber, Nuria Beltrán-Sánchez, and Dr Martin Holzer for their help in organising labs, administrative tasks, and teaching activities. I especially thank Monika for her incredible assistance in the lab, her dedication to the project, providing moral support and for organising and sponsoring the team building BBQ. You made my life so much easier by helping me in the cell culture lab, from the tedious cell ordering process to preparing every single cell culture plate.

I cannot mention the part of this project at the University of Freiburg without acknowledging the amazing time that I had with the Sonnenstraßen sweeties. So many fond memories remain of the entertaining coffee and lunch breaks, ice cream excursions and after-hours activities. You were a key factor for the success of this PhD and get the credit for many smiles and laughter. I thank Friederike for introducing me to the world of $\text{Cu}(\text{DDC})_2$ -liposomes, and for showing me what life after PhD looks like during our frequent catch ups. Thank you, Benedikt, for always grinning when everyone else was serious and for the educational yet unfiltered conversations. I also thank the “pöbel”-king and animal fact lover, Laurens, for being my liposome production partner and for all the funny burger and whisky moments. A special thanks to Clara and Carolin for making me a part of the loser office. Clara, I thank you for paving the way in the gel struggle, for stabilising my raft before every waterfall, and for sharing the donkey and cow worries. Carolin, I thank you for all the moments we shared life-stories, laughed, and made plans for the future — while running, over the phone or on a blanket in a park with a gourmet meal and wine in cups.

As they had to keep up with weird stories from the lab and provide food during stressful times, I thank my housemates in Freiburg and Adelaide (Basti, Louise, Robin, Esther, and Matt). Louise, thank you for listening to me complain about work, helping me practice my presentations and celebrating my successes with our “late-to-catch-the-bus-drinks”, and for accompanying me to countless gigs. In addition, I am incredibly grateful for all my friends that have been by my side throughout my life: the French school-friends, the German friends from university, and previous housemates, as well as my Aussie friends. I thank my bouldering partner Chris for the morally-uplifting philosophical discussions on life and for regularly checking up on me, especially when I work too much. Lena and Mimi, thank you for continuously being the most exceptional friends.

Celebrating my successes, comforting me during difficult times, coming to visit me in Australia, and keeping me sane with voice messages, girls' nights and amazing food has meant the world. Moreover, Australia would not feel like home without the East family, and especially Lord Gerard and Karen. I am incredibly thankful for the chance to call you my second family, for the safe haven you provide at the other end of the world and the certainty of a red wine with amazing company.

Lastly, this PhD would not have been possible without the support and encouragements of my partner and family. To my partner Robin, thank you for doing this crazy life with me. It is an immense pleasure to plan, execute and recount adventures with you and an honour to call you out on your proud smiles. To my family, the nicest know-it-all, you accept my decisions, even if they lead me far away. Thank you, Mum and Dad, for always believing in me and for the hints to help me solve the riddles of life. Thank you, Camilla, for the emotional support over world-class food and exquisite wine, and for sponsoring my award-winning outfits. I thank my brother Patrick for teaching me that with courage and creativity you can achieve anything. And finally, I thank my sister Lea for inspiring me to be kind-hearted, brave, and strong — you truly are the best sister in the world.

*« On ne fait jamais attention à ce qui été fait ;
on ne voit que ce qui reste à faire »*

Marie Curie

Abstract

Surgical site infections (SSIs) are the most common postoperative complication, causing frequent hospital readmissions, significant mortality and representing an economic burden for the healthcare system. The pathogens typically associated with SSIs are *Staphylococcus aureus* (*S. aureus*) and *Staphylococcus epidermidis* (*S. epidermidis*). Prophylaxis and treatment of SSIs with antibiotics frequently fail due to increased antibiotic-resistance of bacteria and their ability to reside as clusters within a matrix. This form of life is called a biofilm and offers the bacteria protection against antibiotics and the immune system. To eradicate biofilms, high systemic concentrations of antibiotics are needed, often causing toxic side effects, emphasising the need for novel therapeutic strategies that can be administered locally on SSIs.

Repurposed diethyldithiocarbamate (DDC⁻), a metabolite of the old anti-alcoholic drug Disulfiram, previously showed antibacterial activity against mycobacteria and streptococci in combination with copper ions (Cu²⁺) but had not been investigated against *S. aureus* and *S. epidermidis* biofilms. In this thesis, the antibacterial and antibiofilm activities of DDC⁻ with Cu²⁺ were examined and an injectable gel containing the combination was developed for application on SSIs.

The antibacterial and antibiofilm activity of DDC⁻ was strictly Cu²⁺-dependent and linked to the formation of Cu(DDC)₂ (2:1 molar ratio of DDC⁻ and Cu²⁺) with excess Cu²⁺. This combination inhibited bacterial growth, multiple steps in the biofilm formation, including bacterial attachment and bacterial aggregation, and reduced biofilm viability. Furthermore, DDC⁻ and Cu²⁺ demonstrated either synergistic or additive antibiofilm effects against the staphylococci tested and synergised with multiple antibiotics. *In vitro* cell culture studies, at relevant concentrations, showed no toxicity of the DDC⁻ and Cu²⁺ combination in human dermal fibroblast cells. Antibacterial activity and non-toxicity of Cu(DDC)₂ + Cu²⁺ was also confirmed *in vivo* in a *Galleria mellonella* infection model.

To enable prolonged exposure of the combination at surgical sites, a depot system was developed for controlled drug release. As Cu(DDC)₂ is water-insoluble, the complex was first encapsulated into PEGylated liposomes. Cu²⁺-liposomes were produced by thin-film hydration and extrusion, then Cu(DDC)₂-liposomes were formed by diffusion of DDC⁻ into the liposomal core and complexation with encapsulated Cu²⁺. Like free Cu(DDC)₂ + Cu²⁺, the liposomal combination showed antibiofilm activity *in vitro* and antibacterial effects and non-toxicity *in vivo*, making it a water-soluble formulation for Cu(DDC)₂. Following lyophilisation, the liposomes were stable below 6 °C for over six months and able to be incorporated within a gel. A biocompatible mixture, comprising chitosan and beta-glycerophosphate, was fluid at ambient temperature and formed a gel at body temperature. These thermosensitive properties were maintained following sterilisation, storage at -20 °C and liposomes incorporation. The liposomal gel prevented biofilm formation and reduced *S. aureus* and *S. epidermidis* biofilm viability.

The combination of DDC⁻ and Cu²⁺ has potential as antibacterial and antibiofilm treatment against *S. aureus* and *S. epidermidis*. An application at the surgical site is possible when liposomal Cu(DDC)₂ + Cu²⁺ is incorporated into an injectable gel. This antibacterial gel represents an innovative therapeutic approach for the prophylaxis and treatment of SSIs.

Kurzzusammenfassung

Chirurgische Wundinfektionen gehören zu den häufigsten postoperativen Komplikationen und führen zu verlängerten Krankenhausaufenthalten, erhöhter Sterblichkeitsrate sowie erheblichen Kosten für das Gesundheitssystem. Oftmals sind *Staphylococcus aureus* und *Staphylococcus epidermidis* die dafür verantwortlichen Keime, welche in der Regel durch prophylaktische und therapeutische Gabe von Antibiotika bekämpft werden. Jedoch ist durch die steigende Zahl resistenter Keime und der Bildung von Biofilmen die Behandlung mit Antibiotika häufig unzureichend. Biofilme bestehen aus bakteriellen Gruppierungen, die in eine Schleimschicht eingebettet und vor Antibiotika und dem Immunsystem geschützt sind. Um Biofilme zu bekämpfen, bedarf es deshalb der systemischen Verabreichung hoher Dosen an Antibiotika, welche vermehrt zu Nebenwirkungen führen. Zur Behandlung postoperativer Wundinfektionen werden daher dringend alternative und lokal anwendbare Therapieansätze benötigt.

Ein Ansatz besteht aus der Neupositionierung bereits zugelassener Wirkstoffe, wie z.B. Disulfiram, welches zur Alkoholentwöhnung eingesetzt und im Körper zu Diethyldithiocarbamat (DDC⁻) metabolisiert wird. Die bereits nachgewiesene antibakterielle Wirkung von DDC⁻ gegen Mykobakterien und Streptokokken ist abhängig von der Anwesenheit zweiwertigen Kupfers (Cu²⁺), wurde aber noch nicht gegen *S. aureus* und *S. epidermidis* Biofilme untersucht. In der vorliegenden Arbeit wurde DDC⁻ mit Cu²⁺ auf antibakterielle Eigenschaften erforscht und ein lokal injizierbares Hydrogel zur Prophylaxe und Therapie von chirurgischen Wundinfektionen entwickelt.

Die antibakterielle Aktivität von DDC⁻ und Cu²⁺ gegen *S. aureus* und *S. epidermidis*, vorliegend als einzelne Bakterien oder als Biofilme, erfolgte nur in Anwesenheit des Cu(DDC)₂ Komplexes (molares 2:1-Verhältnis von DDC⁻ zu Cu²⁺) und einem Überschuss an Cu²⁺. Diese Kombination hemmte *in vitro* Bakterienwachstum, mehrere Schritte der Biofilmbildung und reduzierte die Lebensfähigkeit ausgereifter Biofilme. Die antibakterielle Aktivität von Cu(DDC)₂ + Cu²⁺ konnte durch gleichzeitige Anwendung von Antibiotika verstärkt werden. Bei relevanten Konzentrationen in Zellkulturen von humanen dermalen Fibroblasten wurde keine Zytotoxizität beobachtet. Außerdem wurde die Wirkung und Verträglichkeit der Kombination in infizierten *Galleria mellonella* Larven bestätigt.

Um einen konstanten Effekt am Behandlungsort zu erreichen, wurden die Wirkstoffe aus einem Depot freigesetzt. In einem ersten Schritt wurde das wasserunlösliche Cu(DDC)₂ in Liposomen verkapselt, indem Cu²⁺-Liposomen mit DDC⁻ beladen wurden. Durch vergleichbare Wirkungen der liposomalen Formulierung und der freien Kombination gegen Biofilme *in vitro* und infizierten Larven *in vivo* wurden Liposomen als geeignetes hydrophiles Trägersystem identifiziert. In einem zweiten Schritt wurden die Liposomen gefriergetrocknet, um eine Lagerstabilität über mindestens 6 Monate zu erhalten und die Weiterverarbeitung in einem Gel zu erleichtern. Letztlich erfolgte die Hydrogel-Entwicklung mit einer biokompatiblen Mischung aus Chitosan und β -Glycerophosphat, die bei Raumtemperatur flüssig ist und bei Körpertemperatur in ein Gel übergeht. Diese thermosensitiven Eigenschaften blieben auch nach der Sterilisation, Lagerung bei -20 °C und dem Einbringen von Liposomen erhalten. Das liposomale Gel verhinderte die Biofilmbildung und senkte die Lebensfähigkeit ausgereifter *S. aureus* und *S. epidermidis* Biofilme.

Damit gelang in dieser Arbeit die Entdeckung und der Nachweis der antimikrobiellen Wirkung von Cu(DDC)₂ + Cu²⁺ gegen *S. aureus* und *S. epidermidis* Biofilme. Durch das Einarbeiten der wirkstoffbeladenen Liposomen in ein injizierbares Gel wird eine lokale Anwendung in der chirurgischen Wunde ermöglicht. Dieses antibakterielle Hydrogel stellt einen innovativen Ansatz zur Prophylaxe und Behandlung von postoperativen Wundinfektionen dar.

Contents

Abbreviations.....	xix
1 Introduction.....	1
1.1 Surgical site infections.....	1
1.1.1 Definition and significance	1
1.1.2 Variations in surgical site infection incidences.....	2
1.1.3 Pathogens associated with surgical site infections	3
1.2 Biofilms.....	5
1.2.1 Biofilm characteristics	5
1.2.2 Biofilm life cycle.....	6
1.2.3 Tolerance and resistance mechanisms	7
1.3 Prevention and treatment of surgical site infections	9
1.3.1 Prevention of surgical site infections.....	9
1.3.2 Treatment options for surgical site infections	11
1.4 Novel strategies to control staphylococci biofilm-associated infections	13
1.4.1 Non-pharmacological approaches for surgical site infections.....	13
1.4.2 Novel antibiofilm agents in the development pipeline	14
1.5 Repurposing drugs as antibiofilm agents against <i>S. aureus</i>	20
1.5.1 Benefits of drug repurposing	20
1.5.2 Investigating drugs for antimicrobial activity against <i>S. aureus</i>	22
1.5.3 Disulfiram and diethyldithiocarbamate.....	23
1.6 Administration of diethyldithiocarbamate and copper ions on surgical site infections	30
1.6.1 Low solubility of Cu(DDC) ₂	30
1.6.2 Local application for surgical site infections	35
1.7 Aim of this work.....	40
2 Antibacterial activity of diethyldithiocarbamate and copper ions	41
2.1 Publication: “The combination of diethyldithiocarbamate and copper ions is active against <i>Staphylococcus aureus</i> and <i>Staphylococcus epidermidis</i> biofilms <i>in vitro</i> and <i>in vivo</i> ”	41
2.1.1 Publication title page	44
2.1.2 Abstract.....	45
2.1.3 Introduction.....	45
2.1.4 Materials and methods	46

2.1.5	Results.....	50
2.1.6	Discussion.....	58
2.1.7	Supplementary files	61
2.2	Effect of Cu(DDC) ₂ + Cu ²⁺ on biofilm dispersal	62
3	Assessing Cu(DDC)₂ + Cu²⁺ for surgical site infections	65
3.1	Publication: “ <i>In vitro</i> and <i>in vivo</i> evaluation of diethyldithiocarbamate with copper ions and its liposomal formulation for the treatment of <i>Staphylococcus aureus</i> and <i>Staphylococcus epidermidis</i> biofilms”	65
3.1.1	Publication title page	68
3.1.2	Graphical abstract.....	69
3.1.3	Abstract.....	69
3.1.4	Introduction.....	69
3.1.5	Materials and methods	71
3.1.6	Results.....	74
3.1.7	Discussion.....	80
3.1.8	Conclusion	82
3.1.9	Supplementary file.....	82
4	Development of an injectable gel for local delivery of Cu(DDC)₂ + Cu²⁺	83
4.1	Publication: “A thermosensitive, chitosan-based hydrogel as delivery system for antibacterial liposomes to surgical site infections”	83
4.1.1	Publication title page	86
4.1.2	Graphical abstract.....	87
4.1.3	Abstract.....	87
4.1.4	Introduction.....	87
4.1.5	Materials and methods	89
4.1.6	Results and discussion.....	94
4.1.7	Conclusion	106
4.1.8	Supplementary file.....	107
4.2	Management of hydrogel prior to administration.....	107
4.2.1	Stability of hydrogel at -20 °C.....	107
4.2.2	Estimated time for preparation and administration of the hydrogel	108
5	Discussion and future perspectives	111
5.1	DDC ⁻ and Cu ²⁺ as antibacterial agents	111
5.2	Liposomal formulation of Cu(DDC) ₂ + Cu ²⁺	113

5.3	Injectable hydrogel as drug-delivery platform for Cu(DDC) ₂ -liposomes and Cu ²⁺ -liposomes.....	115
6	Conclusion	117
7	Appendix.....	118
8	Bibliography.....	121

Publications arising from this thesis

Laurine Kaul, Regine Süß, Andrew Zannettino, Katharina Richter

The revival of dithiocarbamates: from pesticides to innovative medical treatments.

iScience, 2021, Volume 24, Issue 2, 102092

[doi:10.1016/j.isci.2021.102092](https://doi.org/10.1016/j.isci.2021.102092)

Parts of this publication are incorporated into Chapter 1.5.3.2 – 1.5.3.4

Laurine Kaul, Adrian Abdo, Tom Coenye, Bastiaan Krom, Michel Hoogenkamp, Andrew Zannettino, Regine Süß, Katharina Richter

The combination of diethyldithiocarbamate and copper ions is active against *Staphylococcus aureus* and *Staphylococcus epidermidis* biofilms *in vitro* and *in vivo*.

Frontiers in Microbiology, 2022, Volume 13, 999893

[doi:10.3389/fmicb.2022.999893](https://doi.org/10.3389/fmicb.2022.999893)

This publication is shown in Chapter 2.1

Laurine Kaul, Clara Grundmann, Monika Köll-Weber, Hanna Löffler, Artur Weiz, Andrew Zannettino, Katharina Richter, Regine Süß

A thermosensitive, chitosan-based hydrogel as delivery system for antibacterial liposomes to surgical site infections.

Pharmaceutics, 2022, Volume 14, Issue 12, 2841

[doi:10.3390/pharmaceutics14122841](https://doi.org/10.3390/pharmaceutics14122841)

This publication is shown in Chapter 4.1

Laurine Kaul, Adrian Abdo, Tom Coenye, Simon Swift, Andrew Zannettino, Regine Süß, Katharina Richter

***In vitro* and *in vivo* evaluation of diethyldithiocarbamate with copper ions and its liposomal formulation for the treatment of *Staphylococcus aureus* and *Staphylococcus epidermidis* biofilms.**

Biofilm, 2023, Volume 5, 10013

[doi: 10.1016/j.bioflm.2023.100130](https://doi.org/10.1016/j.bioflm.2023.100130)

This publication is shown in Chapter 3.1

Presentations arising from this thesis

Oral presentations

Repurposing the metal chelator diethyldithiocarbamate to inhibit bacterial growth of staphylococci.

2019 Annual Meeting of the Australian Society for Microbiology, Adelaide, Australia.

Toxic cocktail for bacteria – staphylococci party ends deadly.

2019 Annual Meeting of the New Zealand Microbiology Society, Palmerston North, New Zealand.

Biofilm presence on hernia meshes and a new treatment combination to fight staphylococci.

2019 Annual The Queen Elizabeth Hospital Research Expo, Adelaide, Australia.

Revival of an old anti-alcoholic drug to fight staphylococcal infections.

2020 Annual Meeting of the Australian Society for Medical Research, virtual.

Old anti-alcoholic drug to fight biofilms on hernia meshes.

2021 Annual Student Night, Australian Society for Microbiology South Australia/Northern Territory Branch and 2021 Annual Meeting of the Australian Society for Microbiology, virtual.

Pre-clinical validation of a newly developed treatment combination for surgical site infections.

2022 Annual Scientific Meeting of the Australian Society for Medical Research South Australia, Adelaide, Australia.

Efficacy of a metal chelator as antibacterial agent against staphylococci biofilms.

2022 Annual Meeting of the Australian Society for Microbiology, virtual.

An antibacterial gel against staphylococci biofilms to prevent surgical site infections.

2022 Annual The Queen Elizabeth Hospital Research Expo, Adelaide, Australia.

Poster presentations

Kaul L, Zannettino A, Süß R, Richter K. **Repurposing metal chelators to combat staphylococci biofilms.** 6th EuroBioFilms Meeting (2019), Glasgow, United Kingdom.

Kaul L, Zannettino A, Süß R, Richter K. **Revival of an old anti-alcoholic drug to fight biofilm infections on hernia meshes.** 31st European Congress of Clinical Microbiology & Infectious Diseases (ECCMID 2021), virtual.

Kaul L, Zannettino A, Süß R, Richter K. **The revival of an old anti-alcoholic drug to fight staphylococci biofilms on hernia meshes.** 2021 Online Research Conference for Remote & Joint HDR of the University of Adelaide, virtual.

Kaul L, Abdo A, Zannettino A, Süß R, Richter K. **Efficacy of a metal chelator as therapeutic agent against staphylococci biofilms.** 7th EuroBioFilms Meeting (2022), Palma de Mallorca, Spain.

Kaul L, Abdo A, Zannettino A, Süß R, Richter K. **Development of a new antibacterial treatment for surgical site infections.** 2022 Annual Florey Postgraduate Research Conference, Adelaide, Australia.

Awards and prizes arising from this thesis

2019:

- Winner Best Oral Presentation Junior PhD Student (Laboratory), The Queen Elizabeth Hospital Research Expo
- NZMS Postgraduate Research Travel Award, the Australian Society for Microbiology

2021:

- Nancy Millis Student Award, the Australian Society for Microbiology

2022:

- Tanya Monro Best Student Oral Presentation Prize, Institute for Photonics and Advanced Sensing
- Finalist for Ross Wishart Memorial Award, the Australian Society for Medical Research South Australia
- BHI Conference and Travel Grant, The Hospital Research Foundation
- Adelaide Medical School – Department of Surgical Specialties Prize, Florey Postgraduate Research Conference
- Winner Best Oral Presentation Senior PhD Student (Laboratory), The Queen Elizabeth Hospital Research Expo

Abbreviations

°C	Degree Celsius
λ	Wavelength
$\times g$	Relative centrifugal force
Σ FICI	Sum of fractional inhibitory concentration index
Agr	Accessory gene regulator
AIP	Autoinducing peptide
ALDH	Aldehyde dehydrogenase
Amik	Amikacin
ANOVA	Analysis of variance
ATCC	American type culture collection
β GP	β -Glycerophosphate
Ca ²⁺	Calcium(II) ions
Ceft	Ceftazidime
CFU	Colony forming units
Chol	Cholesterol
CI	Cell index
Cip	Ciprofloxacin
COVID-19	Coronavirus disease-19
Cryo-EM	Cryogenic-electron microscopy
CS	Chitosan
CS ₂	Carbon disulphide
Cu(DDC) ₂	Cupric-diethyldithiocarbamate
Cu ²⁺	Copper(II) ions
CuS	Copper sulphide
DDC ⁻	Diethyldithiocarbamate
DEA	Diethylamine
d _h	Hydrodynamic diameter
DLS	Dynamic light scattering
DNA	Desoxyribonucleic acid
Doxy	Doxycycline
DSF	Disulfiram
DSPC	1,2-Distearoyl-sn-glycero-3-phosphocholine

Abbreviations

DSPE-mPEG ₂₀₀₀	1,2-Distearoyl-sn-glycero-3-phosphoethanolamin-N-[methoxy-poly(ethylene glycol)-2000]
eDNA	Extracellular DNA
EDTA	Ethylenediaminetetraacetic acid
EPS	Extracellular polymeric substances
Ery	Erythromycin
FDA	Food and drug administration (USA)
Fe ²⁺	Iron(II) ions
G'	Storage modulus
G''	Loss modulus
Ga ³⁺	Gallium(III) ions
HIV	Human immunodeficiency virus
Hz	Hertz
kDa	Kilodalton
LCST	Low critical solution temperature
mDa	Megadalton
Me-DDC	Methyl diethyldithiocarbamate
Meth	Methicillin
MERS-CoV	Middle East respiratory syndrome coronavirus
Mg ²⁺	Magnesium(II) ions
MIC	Minimum inhibitory concentration
MRSA	Methicillin-resistant <i>S. aureus</i>
MWCO	Molecular weight cut-off
NaCl	Sodium chloride
NIR	Near infrared light
NP	Nanoparticle
OD ₆₀₀	Optical density at 600 nm
PBS	Phosphate buffered saline, pH 7.4
PDI	Polydispersity index
PEG	Polyethylene glycol
PLGA	Poly(lactic-co-glycolic acid)
QS	Quorum sensing
RNA	Ribonucleic acid
ROS	Reactive oxygen species
rpm	Rounds per minute

RTCA	Real-time cell analysis
SARS-CoV	Severe acute respiratory syndrome coronavirus
SD	Standard deviation
SH	Sucrose HEPES buffer, pH 7.4
SSI	Surgical site infection
Tg'	Glass transition temperature of the maximally freeze-concentrated amorphous phase
TSA	Tryptone soya agar
TSB	Tryptone soya broth
UV-Vis	Ultraviolet-visible
Van	Vancomycin
WHO	World Health Organization
Zn ²⁺	Zinc(II) ions

1 Introduction

Parts of this Chapter were published as part of a literature review: Kaul, L.; Süß, R.; Zannettino, A.; Richter, K. "The revival of dithiocarbamates: From pesticides to innovative medical treatments." *iScience* **2021**, *24*, 102092, doi:10.1016/j.isci.2021.102092.

1.1 Surgical site infections

1.1.1 Definition and significance

Approximately 310 million major surgeries are performed every year, with approximately 40 to 50 million performed in the US and 20 million in Europe [1]. The most common postoperative complication is surgical site infection (SSI) [2], which occurs in up to 22% of surgical procedures [3]. These are infections that occur in a wound created by a surgical procedure within 30 days and can be classified, according to Figure 1.1, as (i) superficial incisional infections affecting the skin and subcutaneous tissue, (ii) deep incisional infections affecting deeper tissue, such as muscles and fascial planes, and (iii) organs and spaces that are opened or manipulated during the surgical procedure [4,5]. In addition, the timeframe for monitoring and identifying postoperative infection is extended to 90 days, when a surgical procedure includes the placement of an implant [6,7].

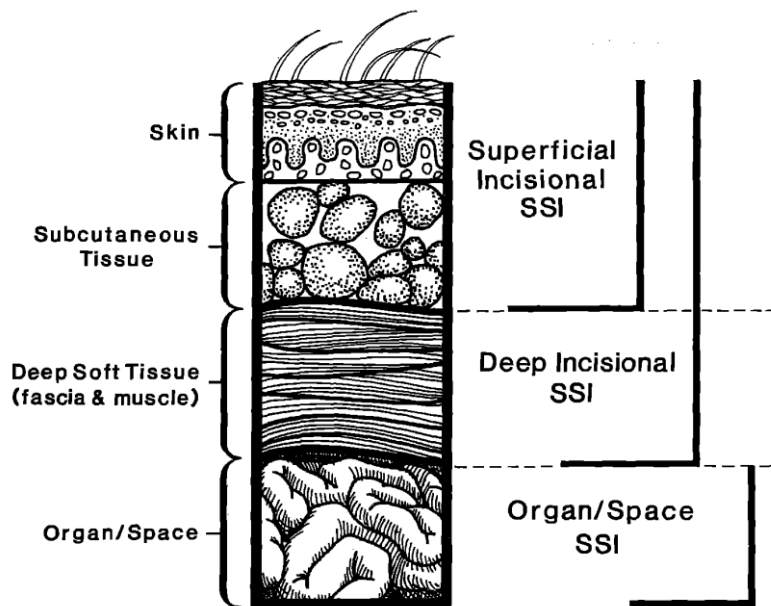


Figure 1.1: Schematic of the anatomy of surgical site infections (SSI) and their appropriate classifications. Reprinted with permission from Horan, *et al.* [5].

SSIs increase morbidity and mortality and represent a significant economic burden for healthcare systems [1,8,9]. Across the world, medical costs per SSI are estimated to range from US\$ 15,800 to 43,900 [10], accumulating to annual expenses of up to US\$ 45 billion in the US [8] and up to € 19.1 billion in Europe [11]. In the presence of antimicrobial-resistant bacteria or device-related infections, the costs are estimated to exceed US\$ 90,000 per SSI [12]. Depending on the type of surgery performed [9], these expenses can, in part, be attributed to increased length of hospital stay, rehospitalisation, revision surgeries, and additional medication [9,12].

1.1.2 Variations in surgical site infection incidences

While SSIs are amongst the most frequent healthcare-associated infections, their incidence varies depending on multiple factors, including country, surveillance method, surgical technique, and type of surgery (Figure 1.2) [11].

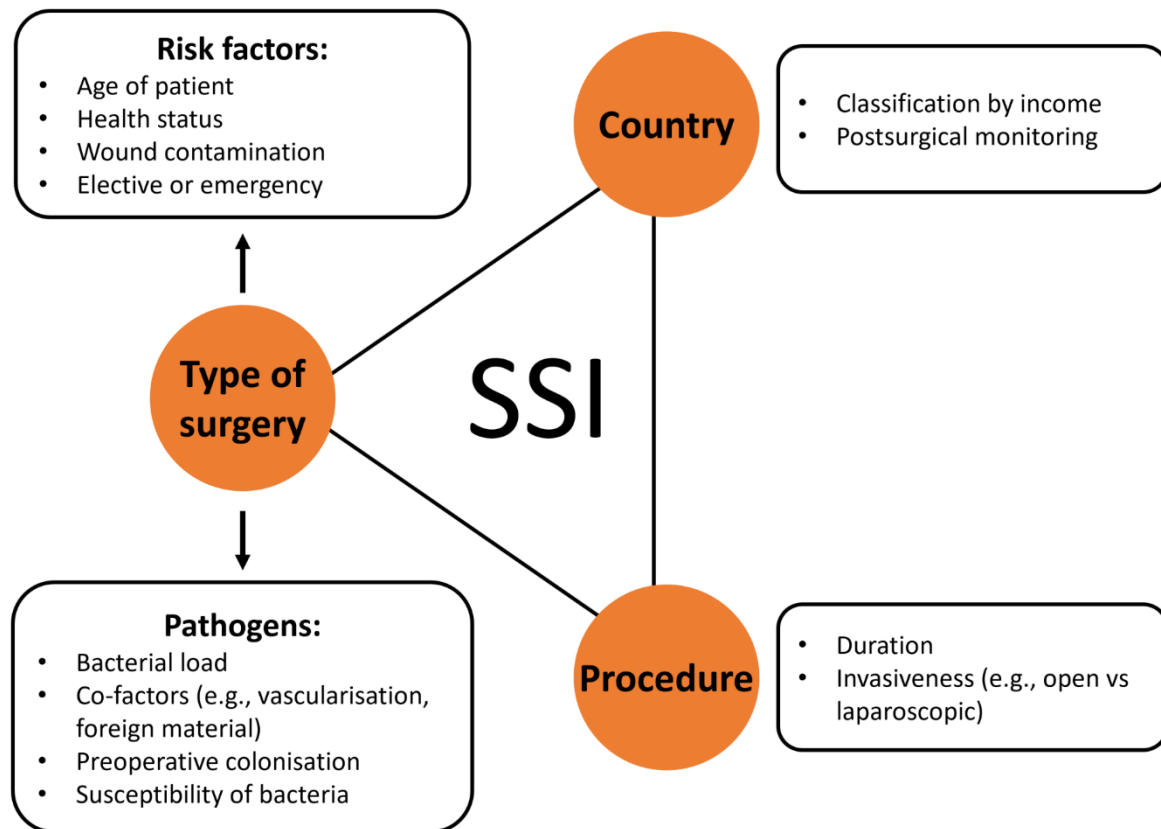


Figure 1.2: Factors influencing the risk for surgical site infections (SSIs).

The incidence of reported SSI varies between high-income countries and low- and middle-income countries. While 1.9% SSIs of surgical procedures were reported in the US from 2006 to 2009 [12], 1.6% SSIs in Europe in 2017 [7] and 2.8% SSIs in Australia from 2002 to 2013 [13,14], an overall SSI rate of 22% in seven low- and middle-income countries was determined [3]. Similarly, the World Health Organization (WHO) reported that SSIs affect up to one-third of patients undergoing surgical procedure in low- and middle-income countries [11].

However, the variations in incidence of SSI are difficult to compare between countries, as national registration systems are not standardised and vary in the definition of SSIs, postoperative routines, and data reporting [11,15]. Consequently, superficial surgical wound infections are not always reported after discharge from hospital. However, up to 60% of SSIs are detected after the patient has been discharged from the hospital [6], which can be attributed to risk minimisation procedures, such as short postoperative hospital stays [7,15].

The overall risk of SSI development decreases every year, which has been attributed to improved surgical techniques, such as conducting minimal invasive procedures [6,14]. For example, laparoscopic surgeries have the advantage to decrease the size and surgical manipulation of the wound, and consequently reduce the SSI rates compared to open surgeries. These reductions in SSI rates were reported for colorectal, cholecystectomy and hernia mesh repair surgeries [7,16].

However, despite novel technologies and improved surgical techniques, the SSI incidence of some surgical procedures is increasing. For instance, incidence of SSI following prosthetic surgeries is estimated to triple by 2030 due to the increasing number of implant surgeries [12].

Consequently, SSI rates also depend on the type of surgical procedures [7]. Reviews and reports typically focus on selected examples of surgical procedure within a specific type of surgery, such as coronary artery bypass graft, caesarean, hip or knee prosthesis, colon surgery and cholecystectomy [7,14,15]. However, SSIs also play an important role in neurological, cardiovascular, colorectal, breast or skin, gastrointestinal, orthopaedic, and gynaecologic surgeries (Table 1.1). The highest SSI rates were observed following colorectal surgeries, while lowest rates were observed following caesareans [7,14,17]. According to the American Society of Anaesthesiologists, the risk factors linked to the type of surgeries include differences in clinical characteristics, such as age, physical status (from ‘normal healthy patient to moribund patient’), duration of surgical procedure, and contamination of the wound [6,7,11,13]. The United States Centers for Disease Control and Prevention and the European Centre for Disease Prevention and Control classify surgical wounds in four wound contamination classes from ‘clean’ to ‘dirty or infected’ and the prevalence of SSI progressively increases with increasing wound contamination [18,19]. It was also reported that the SSI incidence for clean procedures can be as low as <1%, while it can be up to 30% for some colorectal procedures [14]. Moreover, the risk for SSI is increased in patients undergoing emergency surgery compared to elective surgery [20] and when patients are carriers of nosocomial *Staphylococcus aureus* (*S. aureus*) [21].

Table 1.1: Surgical site infection (SSI) incidence (per 100 procedures) of selected type of surgery.

Type of surgery	Procedure examples	SSI incidence rate *	References
Neurosurgeries	Craniotomy	0.8 – 11%	[22,23]
Skin, tissue, breast surgeries	Mastectomy	1 – 30%	[24,25]
Cardiovascular surgeries	Coronary artery bypass graft	2.2 - 11.9%	[7,15]
Gastrointestinal surgeries	Colorectal surgery	4.1 - 15.9%	[7,15]
	Cholecystectomy	0.6 - 7.1%	[7,15]
	Hernia repair	1 – 10%	[15,16,26]
Obstetric and gynaecologic surgeries	Caesarean	0.7 - 9.8%	[7,15]
Orthopaedic surgeries	Hip or knee prosthesis	0.9 - 7.8%	[7,15]

* The incidence rate depend on the surgical procedure and country (within high-income countries) where surgery is performed.

1.1.3 Pathogens associated with surgical site infections

The pathogens responsible for the SSI originate from the patient’s microbiota, the flora of the operating personnel or the environment prior, during or following the surgical procedure [6,15]. While exogenous microbial flora primarily consist of aerobe Gram-positive bacteria, microorganisms from the patient’s microbiota vary depending on the location of the incision (e.g., skin flora and faecal flora), the presence of *S. aureus* in the patients’ nose or of Gram-negative rods

1 Introduction

in their airways, and if an organ is opened during a procedure [10,15]. Consequently, depending on the type of surgical procedure, different pathogens can be isolated (Figure 1.3).

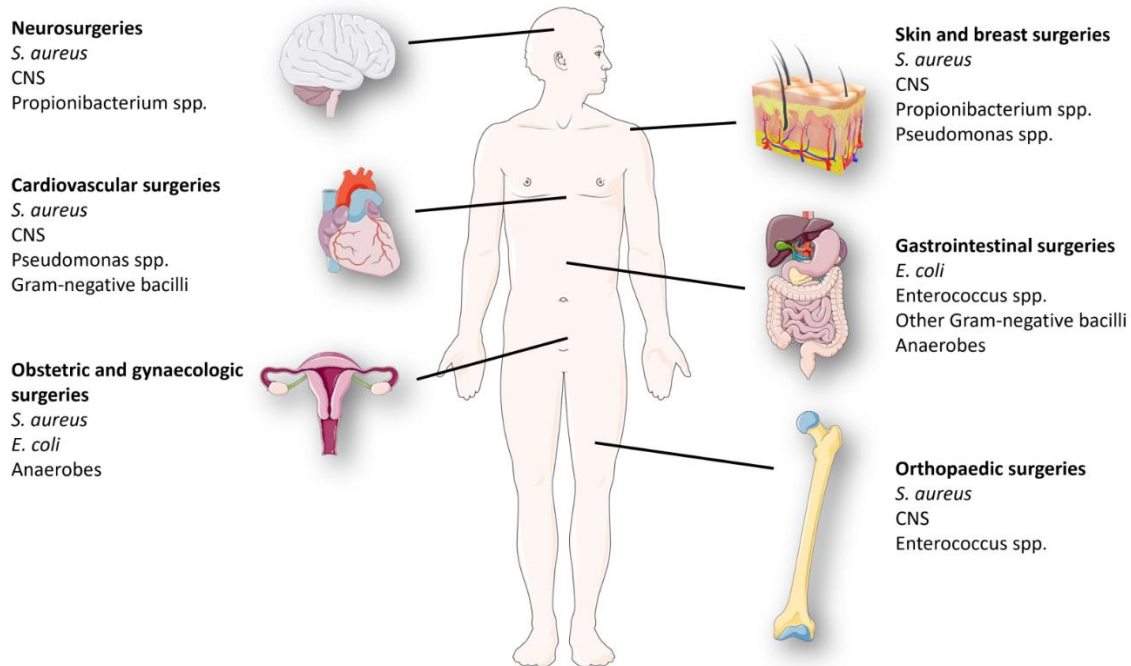


Figure 1.3: Most common pathogens isolated in different types of surgeries. Based on Owens and Stoessel [6], European Centre for Disease Prevention and Control [7], Worth, *et al.* [14] and Hrynshyn, *et al.* [27]. Additional reference for neurosurgery [22] and skin and breast surgeries [24,25]. CNS = coagulase negative staphylococci.

Overall, the most common pathogens causing SSIs are *S. aureus*, which is present in 21.5 to 46.5% of cases, coagulase negative staphylococci including *Staphylococcus epidermidis* (*S. epidermidis*), Enterococcus spp., and Gram-negative bacilli including *Escherichia coli* (*E. coli*) [7,11,14]. Moreover, an increasing number of SSIs are attributed to fungi and antibiotic-resistant bacteria, such as methicillin-resistant *S. aureus* (MRSA) [6,10,28]. Presence of MRSA in SSIs is linked to additional costs, longer hospital stays, more frequent hospital readmission and a higher mortality rate [15].

Not every surgical site contaminated with microorganisms will result in a SSI. The development of a SSI is based on 4 factors: innate and acquired host defence, micro-environment in the surgical wound (necrotic tissue, vascularisation, foreign bodies), bacterial inoculum, and bacterial virulence, including the formation of biofilms. It was quantitatively determined that a surgical site contaminated with over 10^5 colony forming units (CFU) per gram of tissue increases the risk of SSI. However, this threshold can be as low as 10 - 20 bacteria in the presence of a foreign material, such as sutures, meshes or prostheses [6,10,15], due to formation of device-associated biofilms and delayed detection by the immune system. In addition, as almost all bacteria can form biofilms [29], the National Institute of Health estimated that approximately 80% of SSIs are associated with the formation of biofilms [27,30].

1.2 Biofilms

1.2.1 Biofilm characteristics

A biofilm is defined as agglomerations of microbial cells, free-floating or on a surface, enclosed in a self-produced matrix [31]. This sessile lifestyle is considered the primary mode of growth for bacteria in most environments, including in infections [32], and offers bacteria protection against environmental, chemical, and mechanical stresses [33]. In its mature state, biofilms exhibit a heterogeneous structure based on bacterial cells and matrix, with a distinctive intricate water channel network, transporting nutrients, oxygen, and waste throughout the different areas of the biofilm (Figure 1.4) [33,34].

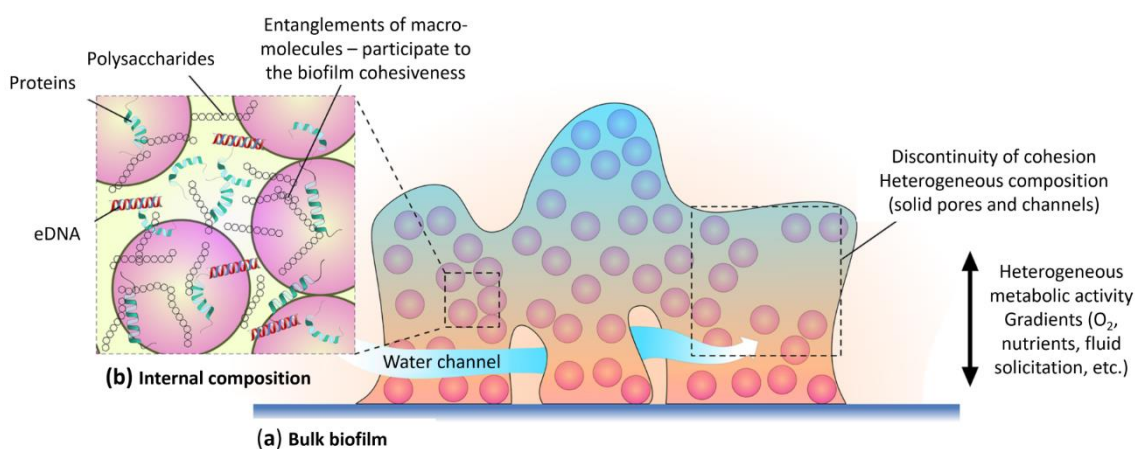


Figure 1.4: Physical heterogeneities of *in vitro* grown biofilms: biofilms are heterogeneous in their composition. **(a)** Biofilms are made of reinforcements (bacteria) surrounded with a matrix (extracellular polymeric substance: EPS). The influence of the scale of the mechanical study is not insignificant. Moreover, metabolic gradients (oxygen, nutrient, physical stress, etc.) result in heterogeneity in mechanical parameters. **(b)** A focus on the internal composition reveals that EPS matrix is made of many components. Entanglements of molecules within the EPS matrix have a key role in the biofilm behaviour. Adapted from Boudarel, *et al.* [33].

Biofilms are frequently composed of multiple microbial species and bacterial cells account for less than 10% of the dry biofilm mass. The matrix is the major component of the biofilm and consists of highly hydrated extracellular polymeric substances (EPS) and trapped exogenous nutrients and minerals, such as nitrogen, carbon, and phosphate [35]. The EPS comprises a conglomeration of biopolymers, including polysaccharides, proteins (enzymes and signalling molecules), extracellular DNA (eDNA) from lysed bacteria, surfactants, and lipids. [36,37]. In staphylococci biofilms, the matrix composition can be divided into three categories: polysaccharide matrix, proteinaceous matrix, and eDNA-dependent matrix. In *S. aureus* and *S. epidermidis* biofilms consisting of a polysaccharide matrix, the main EPS component is polysaccharide intercellular adhesin, a poly-N-acetylglucosamine. In contrast, proteinaceous matrices are based on the promotion of cell-cell interactions of bacterial cell wall-anchored proteins, the formation of amyloid-like scaffolds by biofilm associated proteins, and self- and intercellular adhesion of the surface protein Aap. Proteinaceous matrices are mainly observed in MRSA and *S. epidermidis* clinical isolates [38]. These differences in the matrix composition of staphylococci biofilms depend on environmental conditions present during biofilm formation [39].

1.2.2 Biofilm life cycle

The biofilm lifecycle is a complex process that can be divided into three major steps: (i) attachment and aggregation, (ii) growth and accumulation, and (iii) disaggregation and detachment (Figure 1.5) [40,41].

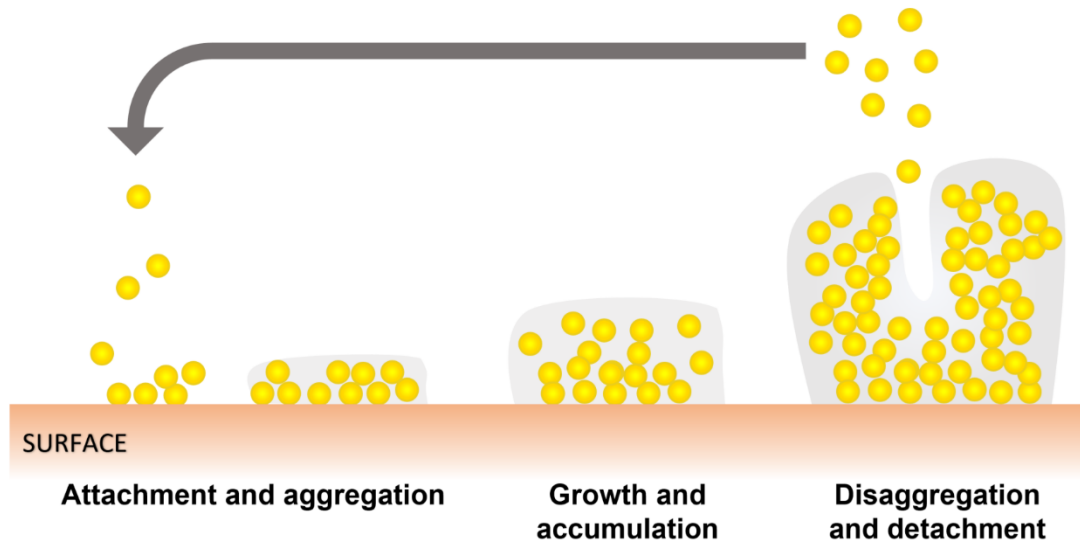


Figure 1.5: Simplified illustration of major steps in biofilm formation on surface exemplified by *Staphylococcus aureus*.

First, free-floating bacteria bind reversibly to each other, or to a biotic or abiotic surface. The docking can vary between bacterial species and is initiated by nonspecific interactions, like hydrophobic effects, van der Waals forces or hydrodynamic processes, but also by specific interactions, such as pili and flagella receptors [42]. The attachment of *S. aureus* on biotic surfaces, is regulated by a range of bacterial cell-wall anchored proteins that recognise components of the extracellular matrix of the host. These proteins include fibronectin-binding proteins, clumping factors, members of the serine-aspartate repeat family proteins and the bone sialoprotein-binding protein. They recognise adhesive matrix molecules, such as fibrinogen, fibronectin, collagen, and keratin [38,43-45]. Similar bacterial cell wall-anchored proteins regulate the attachment of *S. epidermidis* on biotic surfaces [38]. The attachment of staphylococci on abiotic surfaces, such as implants or surfaces of laboratory equipment, is facilitated through hydrophobic and electrostatic interactions by wall teichoic acid. Other contributors of the attachment are major autolytic enzymes, which are hypothesised to change the bacterial surface hydrophobicity [38].

When bacteria start secreting EPS, the adhesion becomes irreversible. Aggregated bacteria expand by replicating and recruiting surrounding bacterial cells and forming the biofilm matrix [46]. Once the biofilm reaches a mature state, a complex three-dimensional structure has been formed containing bacteria, matrix and channels for nutrient and waste exchange (Figure 1.4). Lastly, bacterial cells or cell-clusters detach from the biofilm and can start a new biofilm lifecycle in a new area [42,47]. The degradation and interruption of the biofilm matrix is caused by the activities of different enzymes and molecules on specific matrix components. For example, *S. aureus* produces and secretes (i) proteases, which are often responsible for the dispersal of biofilms; (ii) nucleases that can degrade eDNA; (iii) glycoside hydrolases that degrade exopolysaccharides; and (iv) surfactants, such as phenol-soluble modulins that can disrupt non-covalent interactions between

matrix components [38,48]. The biofilm dispersal is triggered by environmental changes, such as reduced levels of nutrients and oxygen, accumulation of toxic by-products, or challenges by bacteriophages, phagocytes, and antimicrobial agents [49].

The biofilm life cycle is dependent on different habitats, conditions, and microenvironments [41]. For instance, bacteria prefer forming biofilms in high shear stress environments [34], or bacteria are depleted from polymers when entering a surgical site but can exploit the hosts' polymers to drive bacterial aggregation [41]. These variations in the formation and the composition of biofilms, combined with resistance and tolerance mechanisms make biofilm-associated infections difficult to treat [31].

1.2.3 Tolerance and resistance mechanisms

Bacteria in biofilms are more tolerant to the host immune system and to antimicrobial agents. While the immune system can typically detect and clear planktonic bacteria, there is no specific immune response for biofilms [50]. In addition, biofilms employ multiple strategies to tolerate host defences, that can be categorised into nutrient depletion, immune modulation, and virulence factors production. Consumption of local nutrients increases during biofilm growth, thus creating an unfavourable environment for leukocytes by reducing their phagocytic activity and expressing anti-inflammatory cytokines. To evade humoral detection of the innate response, biofilms prevent the activation of complement components and block opsonisation, leading to delays of innate immune recruitment [51]. In addition, the immune cell activity is affected by the activation of response regulators, genetic switches, and the mediation of suppressor cells. *S. aureus* can secrete factors and modify polysaccharide intercellular adhesin to mediate resistance to neutrophil phagocytosis and skew inflammatory responses in the early stages of biofilm formation to cause tissue damage and subsequently promote further biofilm development [38,50]. Moreover, the production of virulence factors, such as auto-inducing peptides and toxins, can directly combat leukocytes and promote biofilm dispersal [51].

Similarly, bacteria within biofilms possess several tolerance and resistance mechanisms to evade antimicrobial agents (Figure 1.6), causing them to be up to 1000-fold less susceptible compared to planktonic bacteria [52-54]. Antibiotic resistance is an inherited or acquired mechanism, that alters the genetic background of bacteria to enable growth despite high concentrations of antibiotics. Antibiotic tolerance is the capacity of bacteria to survive a transient exposure of antibiotics, which can be associated with biofilm properties, such as the matrix and bacterial cell heterogeneity [55,56].

The biofilm matrix also presents a physical barrier for antibiotics, as penetration can be delayed by binding of antibiotics to matrix components or bacterial membranes. For example, positively charged antibiotics, such as the aminoglycoside antibiotic amikacin can interact with negatively charged EPS or eDNA, resulting in lower antibiotic concentrations reaching bacteria and subsequently promoting bacterial tolerance [52,55].

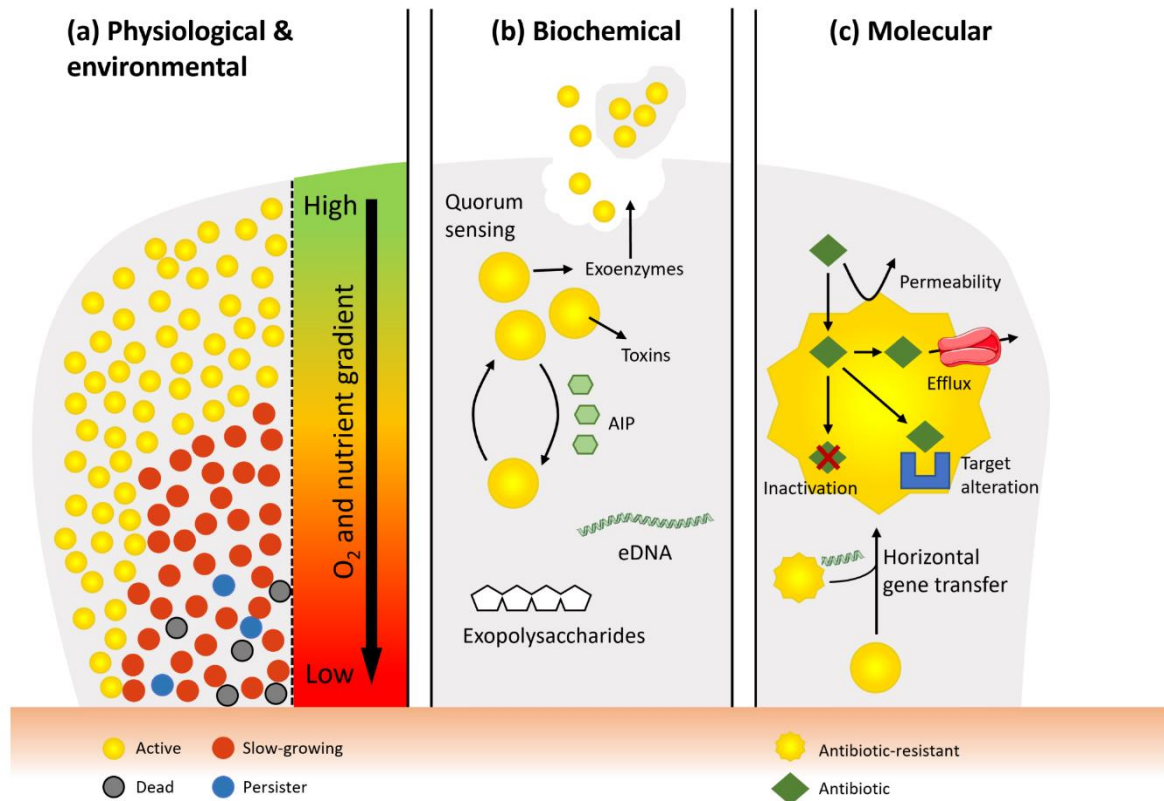


Figure 1.6: Tolerance and resistance mechanisms of *S. aureus* biofilms to antibacterial agents exemplified on an illustration of a biofilm grown *in vitro* on a surface. **(a)** Metabolic activity of bacteria is associated with oxygen and nutrient levels in the biofilms. Metabolically active bacteria are present at the surface of the biofilm with high concentrations of oxygen and nutrients, while slow-growing, persister and dead bacteria are present deep in the biofilm with low oxygen and nutrient levels. **(b)** *S. aureus* bacteria communicate with each other using autoinducing peptides (AIP) as part of quorum sensing. Quorum sensing is responsible for secretion of toxins and degradative exoenzymes. Matrix elements including exopolysaccharides and eDNA can interact with antibiotics. **(c)** Antibiotic-resistance mechanisms can be transferred between bacteria using horizontal gene transfer and include reduced permeability, inactivation through enzymes, altering the target, and multidrug efflux pumps.

Physiological tolerances are based on heterogeneous metabolic bacterial cell states within biofilms, due to nutrient and oxygen gradients. While high levels of nutrients and oxygen at the periphery of biofilms result in the presence of metabolically active bacteria, low levels in the inner parts of the biofilms lead to bacteria progressively shutting down metabolic processes and entering slow-growing and dormant stages or bacterial death. However, numerous antibiotics target metabolic processes of bacteria, such as replication, transcription, and bacterial cell-wall synthesis, or require aerobic conditions. Consequently, oxygen depleted biofilm areas and slow-growing or dormant bacteria can display increased antibiotic tolerance. Dormant bacteria, also called ‘persisters’, are viable but incapable of growth and make up less than 1% of the population in biofilms. They tolerate antibiotic exposure and can resuscitate when environmental conditions become favourable again, resulting in repopulation of biofilms and renewed infection [51,55]. In addition, the metabolic heterogeneity within biofilms is regulated by quorum sensing (QS). QS is a bacterial communication system based on the production and detection of signal molecules, which regulates metabolic activity, production of virulence factors and other bacterial responses in a cell density-dependent manner [47,57]. The main QS system of *S. aureus* is called accessory gene regulator (Agr) and controls the extracellular autoinducing peptide (AIP) signal. Agr is responsible for increased expression of many toxins and degradative exoenzymes and decreased expression of

surface proteins. This system is important for the timing of virulence factors, such as detachment of bacterial cells or cell-clusters in high cell density biofilms [38,58].

In addition to the protective mechanisms provided by the environment within a biofilm, bacteria also possess resistance mechanisms against antibiotics. Resistance mechanisms of *S. aureus* can be categorised as intrinsic or acquired. Intrinsic resistance mechanisms include decrease of membrane permeability, active drug efflux systems and enzymatic drug inactivation (e.g., β -lactamase). Acquired resistance mechanisms are based on mutations of the bacterial genome or horizontal gene transfer and include alteration of drug-binding sites, reduction of target outer membrane proteins and expression of multidrug resistant efflux pumps. Horizontal gene transfer is favoured in biofilms due to the close proximity of bacteria, and genetic material is shared between bacteria through DNA fragments [56,59].

The protective mechanisms of bacteria and biofilms against the immune system and antibiotics, highlight the importance of effective preventive measures and adequate treatment options for surgical sites infections.

1.3 Prevention and treatment of surgical site infections

1.3.1 Prevention of surgical site infections

As biofilms are the underlying reason for prolonged infections and delayed wound healing, preventing the formation of biofilms in surgical site infections is an important consideration before undergoing a surgical procedure [30]. In general, it is estimated that up to 60% of SSIs can be prevented by applying practical measures [12,15], including:

- Informing patient on preparation steps (e.g., body wash, minimising risk factors) and pre- and postoperative measures (e.g., avoid unnecessary hospital stay, sterile technique when changing wound dressing).
- If possible, clearing pre-existing infections of patient.
- Preparing the surgical site prior to the surgical procedure (e.g., disinfection).
- Preparing the operating room by ensuring the environment (including air quality, personnel, surgical technique) is aseptic and decontaminating medical devices and surgical instruments.
- Prophylactically administering antibiotics and dressing wounds appropriately.

The WHO released global guidelines for the prevention of SSIs in 2018 with evidence-based recommendations for interventions prior, during or following a surgical procedure (Table 1.2). The strength of each recommendation was assessed by the WHO based on the quality of evidence [11].

Table 1.2: Recommendations of the World Health Organization for preventive measures against surgical site infections. Continuously = pre-, intra-, and postoperative. Adapted from World Health Organization [11].

Timing	Recommendation	Strength
Patient		
Preoperative	No hair removal, with a clipper if absolutely necessary	Strong
	Mechanical bowel preparation with antibiotics for elective colorectal surgery	Conditional - strong
	No discontinuation of immunosuppressive medication	Conditional
	Bathing or showering of patient with use of plain soap or antimicrobial soap	Conditional
Pre- and/or intraoperative	Enhanced nutritional support for underweight patients undergoing a major surgery	Conditional
	Use of warming devices in the operation room and during the procedure for maintaining normal body temperature	Conditional
Intraoperative	Goal directed fluid therapy for prevention of tissue hypoxia	Conditional
Intra- and postoperative	Oxygenation with 80% fraction of inspired oxygen for patients undergoing general anaesthesia with tracheal intubation	Conditional
Continuously	Protocols for intensive monitoring of blood glucose	Conditional
Environment in operating room		
Preoperative	Surgical hand preparation by scrubbing with antimicrobial soap and water or suitable alcohol-based hand rub before donning sterile gloves	Strong
Intraoperative	No laminar airflow ventilation system for patients undergoing total arthroplasty surgery	Conditional
	Use of sterile disposable non-woven or sterile reusable woven gowns	Conditional
	No use of plastic adhesive incise drapes with or without antimicrobial properties	Conditional
	Use of wound protector device in clean-contaminated, contaminated, and dirty abdominal surgical procedures	Conditional
Bacterial load at the surgical site		
Preoperative	Antibiotic prophylaxis within 120 min before incision but depending on half-life of antibiotic	Strong
	Use of chlorhexidine gluconate antiseptic solution for surgical site skin preparation	Strong
	No antimicrobial sealants after surgical site skin preparation	Conditional
Intraoperative	Irrigation of incisional wound with aqueous povidone-iodine solution before wound closure in clean and clean-contaminated wounds	Conditional
	Use of triclosan-coated sutures	Conditional
	No irrigation of incisional wound with antibiotics	Conditional
Postoperative	No prolonged antibiotic prophylaxis after completion of surgery	Strong
	Prophylactic negative wound therapy on closed surgical incisions in high-risk wounds	Conditional
	No use of any type of advanced dressing over standard dressing	Conditional
	Removal of the wound drain when clinically indicated but no continuation of antibiotic prophylaxis in the presence of a wound drain	Conditional
Continuously	Intranasal application of mupirocin with or without chlorhexidine gluconate body wash for patients with nasal <i>S. aureus</i> colonisation	Conditional - strong

While many preventive measures minimise the risk of pathogen transmission into the wound, disinfection and antibiotic prophylaxis reduce the bacterial load within the surgical wound. The antibiotics recommended for prophylaxis of SSI are based on the type of surgical procedures, as the pathogens causing the SSI vary [27]. In addition, to avoid postoperative colonisation of the wound and infection with multidrug-resistant microorganisms present within the hospital environment, patients are discharged from the hospital as quickly as possible [30].

1.3.2 Treatment options for surgical site infections

Indicators of an acute wound infection include symptoms like pain, fever, swelling, redness, and purulent drainage. When a wound persists over 30 days, it is called a chronic wound and typically exhibits lack of healing, putrid smell, necrotic and/or friable tissue, and persistent wound drainage [27,30]. However, a clinically visible inflammation is not always observed in the early stages of an infection and can result in a delay of SSI detection [60]. The wound healing process, including the early inflammatory response and healing cascade, is hindered by the rapid formation of biofilms in acute wounds. In addition, diagnosis of biofilms in the wound is typically not possible by culture of conventional swabbing but requires microscopical and culture analysis of biopsy samples [12,30]. Biofilms are present in up to 70% of open wounds and in almost all chronic wounds [12] and treatment of established biofilms is often a long-term, costly challenge [30,60] with significantly lower chance of successful treatment compared to acute infection. Treatment strategies of SSIs are described in Figure 1.7.

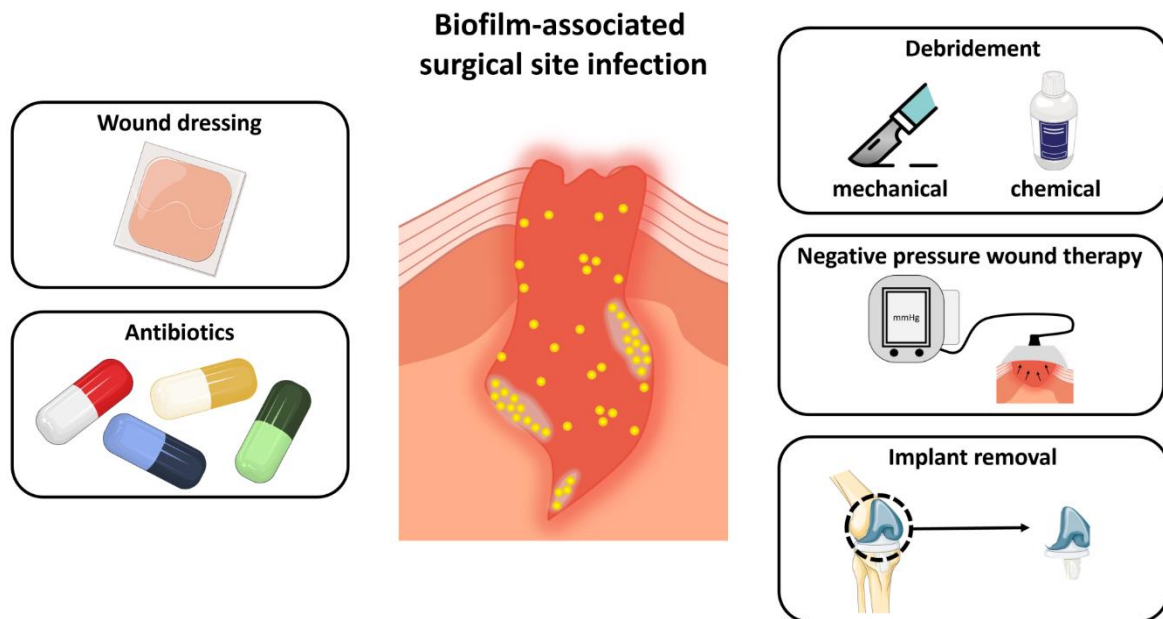


Figure 1.7: Treatment strategies for biofilm-associated surgical site infections.

Wound dressings and antibiotics are routinely employed for the prevention and treatment of SSIs. The primary role of a wound dressing is to form a barrier between the wound and environmental contamination and to absorb exudation [61]. While standard dressings should be used for prophylaxis, advanced dressings such as hydrocolloid dressings, hydrogel dressings and antimicrobial dressings can be used for the treatment of SSIs [62]. However, the wound dressing can sometimes also act as a bioreactor by creating a favourable environment for biofilm formation. A pH and oxygen gradient can develop in the covered wound bed, skewing the bacterial phenotype

1 Introduction

from planktonic to biofilms and favouring the transfer of resistant components between species [63]. In addition, dressings with incorporated gels or forming gels when absorbing exudation can encapsulate and immobilise bacteria, thereby serving as a reservoir [30]. Novel dressings minimise the development of a microenvironment by showing good breathability and incorporation of antimicrobials into wound dressings to defend against planktonic bacteria [61]. The clinically appropriate antibiotic for the treatment of SSIs is typically chosen based on the microorganisms detected in the wound and laboratory antimicrobial efficacy testing. However, little therapeutical guidance to manage biofilm-associated SSI with antibiotics is provided by microbiological analysis of conventional wound swab and *in vitro* susceptibility assessment, due to the presence of multi-species biofilms and increased recalcitrance to antimicrobials once biofilms are established in a wound [30].

As biofilms in surgical wounds often defy eradication, additional therapeutic options target the disruption of biofilms to make the bacteria more susceptible to topical or systemic antibiotics [30,60]. Depending on the location and stage of the infection, the techniques employed to disaggregate or detach biofilms include debridement, negative pressure wound therapy and removal of the implant (Figure 1.7). While, superficial SSIs can be opened and drained easily, deep incisional SSIs frequently require debridement [27]. Debridement is the removal of necrotic and infected tissue or cellular debris, with the goal to remove biofilms or force biofilm dispersion. Corresponding methods can be categorised into chemical and mechanical debridement. Chemical debridement methods include pulsed lavage and antiseptics. Mechanical debridement is widely used and consists of scraping the wound with a scalpel, scissors, loop, and curette, as part of a surgical procedure or routinely when the wound dressing is changed [27,60]. However, mechanical debridement comes with significant risks and discomfort for the patients [30]. Negative pressure wound therapy combines debridement and wound dressings. It consists of a foam or open-pore gauze dressing, which is sealed over the infected site and connected to a gentle vacuum pump [64]. Wound fluid and bacteria are drawn out and growth of new tissue is promoted by increased blood supply in the wound and facilitated granulation and epithelisation [64,65]. While debridement and negative pressure wound therapy are employed on superficial and deep wounds, device-related infections, such as infections of hip prostheses or hernia meshes, typically require the removal of the implant [27]. This is the case when the infection is detected late (> 3 weeks), a tunnelling wound is present, and treatment with antibiotics failed, due to antibiotic resistance and the presence of biofilms [60,66]. Moreover, biofilms on medical implants often lead to failure of the device and delayed or silent infections, which can contribute to additional clinical complications [67,68]. For example, bacterial biofilms were found on hernia meshes explanted due to clinical complications, despite no signs of infections [67,69]. In addition, replacing the infected device with a new implant bears the risk of a new biofilm-associated SSI [66].

Consequently, the first component of an effective antibiofilm strategy for SSIs remains the prevention of biofilm formation [30]. Once a biofilm is present in the surgical wound, therapeutic options are limited to disrupting the biofilm by debridement or implant removal, followed by administration of antibiotics to eradicate planktonic bacteria and delay biofilm reformation [60]. The drawback to this is the high doses, long treatment duration, and combination therapy of antibiotics required for a successful SSI treatment, which bear the risk of severe side effects and the emergence of new antibiotic-resistant bacterial infections [70]. Therefore, new antibiofilm strategies for SSIs are needed to inhibit biofilm formation and to control existing biofilms in surgical wounds.

1.4 Novel strategies to control staphylococci biofilm-associated infections

1.4.1 Non-pharmacological approaches for surgical site infections

Current strategies for prevention and treatment of SSIs are challenged by the formation of biofilms and the spread of antibiotic resistant bacteria, resulting in a need for novel antibacterial and antibiofilm strategies [27]. Research on new antibiofilm strategies not only includes the development of drugs with intrinsic bactericidal effects or as adjunct therapy to standard of care antibiotics, but also focuses on non-pharmacological approaches. For example, hyperbaric oxygen therapy targets the decreased local blood and oxygen (O₂) levels that stimulate SSIs. Patients breathe 100% O₂ at greater than one atmospheric pressure to increase levels of circulating and tissue O₂ levels [71], thereby diminishing low oxygen zones in the wound environment and improving host response [72]. Hyperbaric oxygen therapy is already used to prevent SSIs in contaminated colorectal surgeries and showed promise as adjuvant treatment in a range of SSIs, such as brain abscess surgery and gender affirmation surgery [71,73].

In device-related SSIs, the surface of the implant plays an important role in the development of biofilms [74]. For example, bacterial colonisation of hernia meshes was reported to be influenced by the mesh material, structure, and effective porosity [75-77]. To prevent bacterial adhesion, the surface of implants can be altered by chemical or physical modifications to repel or kill bacteria (Figure 1.8). Attachment of bacteria to the surface can be inhibited by modifying the properties of the surface, such as topography, surface charge and wettability. For example, exposure to gaseous plasma or creation of nanosurfaces can prevent bacterial adhesion [78-80]. Another technology to repulse bacteria from the surface is based on electrostatic or steric effects by coating the device with antifouling agents, including the hydrophilic polymer polyethylene glycol (PEG) and zwitterionic units [78,79]. In contrast, antimicrobial coatings of surfaces prevent biofilm formation by contact killing of bacteria or by releasing antibacterial agents embedded in the layer. Non-releasing coatings are typically based on polymers with antibacterial activity or metal-oxide nanoparticles. Cationic biocidal polymers, such as chitosan and polyethyleneimine derivatives, bind to the negatively charged bacterial membrane, causing its disassembly and leakage of intracellular low-molecular proteins [79]. The antibiofilm activity of metallic nanoparticles that can be incorporated in coatings is further explained in Chapter 1.4.2.4. Lastly, releasing coatings are based on antibacterial agents that separate from the surface to interact with bacteria. These drug eluting coatings can contain antibiotics, antiseptics, or other antibacterial agents, such as metals which are attached to the surface by impregnation, physical adsorption, conjugation or complexation [79]. For example, hernia meshes can be coated with antimicrobial metals (e.g., silver, zinc, gold), antibiotics or antiseptics to reduce bacterial load [81]. Recently, the US Food and Drug Administration (FDA) approved an antibiotic-coated mesh from Ariste Medical LLC containing minocycline and rifampicin for hernia repair (FDA 510(k) Number: K211132). Similarly, orthopaedic implants can be coated with antibacterial agents, such as antibiotics or antimicrobial silver to combat inflammation, bacterial colonisation, and biofilm formation. The compounds can be covalently bound or loaded into a hydrogel, such as “Defensive Antibacterial Coating”, DAC[®] (Novagenit Srl, Mezzolombardo, Italy), for attachment on the implant [82]. However, coatings releasing antibacterial agents can fail to prevent biofilm formation when bacteria colonising the

device are resistant to the coated treatment [78]. Consequently, there is a need for the development of novel antibiofilm agents.

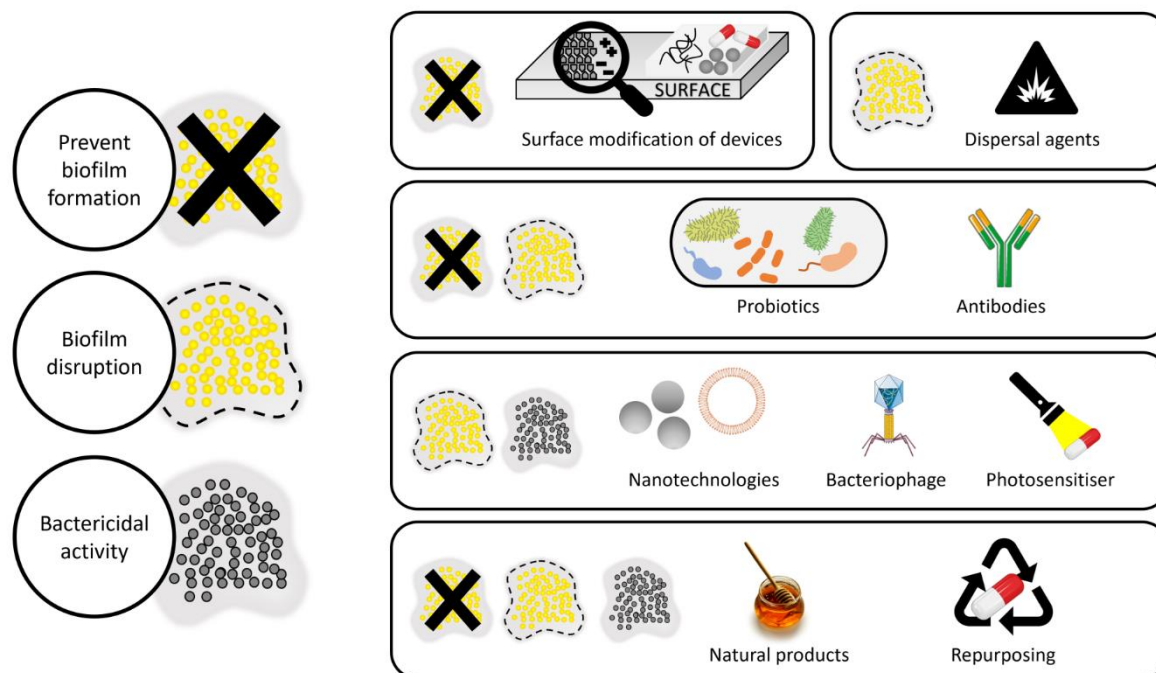


Figure 1.8: Example of *S. aureus* antibiofilm treatment strategies by preventing biofilm formation, disrupting biofilms or bactericidal effects in pre-clinical and/or clinical development.

1.4.2 Novel antibiofilm agents in the development pipeline

Despite the emergence and spread of antibiotic resistance in bacteria that endanger the efficacy of many treatments and consequently the safety of patients, a lack of antibiotic discovery and development has been observed since the early 1980s. Some reasons include the long timeframe and high investments to bring one new antibiotic substance to the market. In addition, once a new agent is approved, it is often considered a last resort treatment to limit the formation of resistances [83]. In recent years, the need for increased research and development of new antibacterial therapies was highlighted and translated into various new initiatives [84]. According to the World Health Organization [85] twelve new antibiotics were approved by the FDA or the European Medicines Agency since July 2017. However, ten of the newly approved drugs belong to existing antibiotic classes with known resistance mechanisms. Moreover, the current clinical antibacterial pipeline contains 77 agents, with the majority being conventional antibiotics [85]. Nevertheless, non-traditional antibacterial treatments are also being developed. Table 1.3 describes nine agents in the current clinical antibacterial pipeline that show activity against staphylococci and/or staphylococci biofilms [85]. Based on their mode of action or composition, novel treatment strategies are categorised as immunomodulators, antibodies, bacteriophages, anti-virulence agents, natural products, probiotics, nanotechnologies, and repurposed drugs (Figure 1.8). Immunomodulating agents are not discussed here, as their therapeutic effect is based on decreasing inflammation by overcoming harmful effects of microorganisms on the immune system, and they do not interact with bacteria or biofilms [86,87].

Table 1.3: New antimicrobial agents against *Staphylococcus aureus* and *Staphylococcus epidermidis* in the current development pipeline according to the World Health Organization with or without activity against biofilms or biofilm components. Modified from World Health Organization [85].

Category	Name	Target	Anti-biofilm? 1	Application	Clinical trial phase	Clinical trial update ²
Immuno-modulating	Reltecimod (AB103)	Synthetic peptide antagonist of both superantigen exotoxins and the CD28 T cell receptor	N	i.v. as adjunctive therapy for necrotising soft tissue infection	Pending FDA approval	
	Rhu-pGSN	Recombinant human plasma protein gelsolin to help regulate homeostasis	N	i.v. as adjunct to standard of care for severe COVID-19 pneumoniae	Phase 2	NCT04358406 Results [87]
Antibody	Tosatoxumab (AR-301)	virulence factor α -toxin	Y [88]	i.v. as adjunctive treatment of <i>S. aureus</i> ventilator associated pneumoniae	Phase 3	NCT03816956 Recruiting
	Suvratoxumab (AR-302)	virulence factor α -toxin and surface-localised clumping factor A	Y [89]	i.v. for ventilated adults colonised or at high-risk of <i>S. aureus</i> pneumoniae	Phase 3	NCT05331885 Not yet recruiting
	9MW1411	Pore-forming α -toxin protein	/	i.v. for acute <i>S. aureus</i> skin and skin structure infection	Phase 2	NCT05339802 Recruiting
					Phase 1	NCT04784312 Completed
	TRL1086	DNABII to disrupt biofilms	Y [90]	i.v. for periprosthetic joint infection	Phase 1	NCT04763759 Recruiting
				i.v. for chronic rhinosinusitis with nasal polyps	Phase 1	NCT05355207 Not yet recruiting
Phage	Exabacase (CF-301)	Prophage with lysin to destroy bacteria by targeting cell wall	Y [91]	i.v. with antibiotics for <i>S. aureus</i> bloodstream infection	Phase 3	NCT04160468 Terminated
		liquid pyo-bacteriophage complex	/	Inhalation for acute tonsillitis in children	Phase 3	NCT04682964 Active
	Tonabacase (LSVT-1701)	Phage encoded lysin for enzymatic hydrolyse of cell wall	Y [92]	i.v. with standard treatment for persistent <i>S. aureus</i> bacteraemia	Phase 2	NCT05329168 Withdrawn
	PP1493 + PP1815	Anti-staphylococcal phage cocktail	Y [93]	Intra-articular injection after DAIR procedure with suppressive antibiotic treatment for prosthetic joint infection	Phase 2	NCT05369104 Recruiting
		Anti-staphylococcal bacteriophage cocktail	/	Topical for <i>S. aureus</i> infected diabetic foot ulcers	Phase 1/2	NCT02664740 Not yet recruiting

1 Introduction

Category	Name	Target	Anti-biofilm? ¹	Application	Clinical trial phase	Clinical trial update ²
Phage	TP-102	Phage cocktail	/	Topical for non-infected and <i>P. aeruginosa</i> , <i>S. aureus</i> and/or <i>A. baumannii</i> infected diabetic foot ulcer	Phase 1/2	NCT04803708 Completed
	PhageBank™ bacteriophage	Phage cocktail	/	Intraoperative and i.v. with standard of care antibiotics after DAIR procedures for treatment of chronic prosthetic joint infection	Phase 1/2	NCT05269121 Recruiting
	BACTELIDE	Phage cocktail	/	Topical as an adjunct to standard therapy for prevention and treatment of <i>S. aureus</i> , <i>P. aeruginosa</i> , or <i>K. pneumoniae</i> colonised pressure ulcers	Phase 1/2	NCT04815798 Not yet recruiting
	AP-SA02	Anti-staphylococcal bacteriophage	Y*	i.v. as adjunct to best available antibiotic therapy for treatment of <i>S. aureus</i> bacteraemia	Phase 1/2	NCT05184764 Recruiting
	Phage Cocktail-SPK		/	Topical as spray for second degree burn wounds susceptible for infections by <i>S. aureus</i> , <i>P. aeruginosa</i> or <i>K. pneumoniae</i> .	Phase 1	NCT04323475 Not yet recruiting
	AB-SA01	Phage cocktail	Y [94]	Intranasal irrigation for treatment of <i>S. aureus</i> -associated chronic rhinosinusitis	Phase 1	ACTRN1261-600002482 Results [95]
Anti-virulence	ALS-4	Staphyloxanthin inhibitor	biosynthesis	/	Oral for <i>S. aureus</i> infection	Phase 1 NCT05274802 Completed
	Recombinant <i>S. aureus</i> vaccine (rFSAV)	Antigens against surface virulence factors (e.g., staphylococcal protein A) and secreted toxins		/	Intramuscular injection in healthy patients	Phase 1 NCT02804711 NCT03966040 Results [96]

¹ Antibiofilm activity determined in pre-clinical experiments with reference if applicable. Y = Yes; N = No; / = no information.

² Updated according to clinicaltrials.gov, accessed on 25th January 2023.

* According to US Patent Number: US20210252083A1.

DAIR = Debridement, antibiotics, and implant retention; i.v. = intravenous; *Staphylococcus aureus* (*S. aureus*); *Pseudomonas aeruginosa* (*P. aeruginosa*); *Klebsiella pneumoniae* (*K. pneumoniae*); *Acinetobacter baumannii* (*A. baumannii*).

1.4.2.1 Antibodies

Antibodies are protein molecules that play an important role in the humoral immune response. Their antibacterial activity is based on binding to a bacterial target and (i) mediate microbial clearance by phagocytes, (ii) activate the classic complement cascade to recruit immune cells, (iii) neutralise the action of secreted proteins, (iv) inhibit bacterial attachment and subsequent biofilm formation or (v) disrupt the biofilm formation [88]. Therefore, targets of antibodies include bacterial surface proteins, cell wall enzymes and extracellular secreted elements, such as toxins and matrix components [88,97]. The high specificity of antibodies to their target ensures low toxicity towards the hosts microbiota but can also restrict the antibacterial effect to single bacterial species [97]. In addition, targets can vary within bacterial species, depending on the strain and the presence of the biofilm or planktonic form. For example, monoclonal antibodies targeting the *S. aureus* biofilm matrix component poly-N-acetyl glucosamine can lack efficacy if the biofilm matrix is not primarily composed of polysaccharides but a proteinaceous or eDNA-dependent matrix (see Chapter 1.2.1) and binding of antibodies on the surface protein wall teichoic acid can be disrupted by the presence of glycosylation in some *S. aureus* strains, as a result of environmental adaptation [98].

As described by Han and Poma [88], antibodies for a broad range of targets are being investigated in pre-clinical studies. Currently in clinical trials are the human monoclonal antibodies tosatoxumab, suvratoxumab and 9MW1411 that target the virulence factor α -toxin, and TRL1086 that targets DNA-binding proteins. The efficacy and safety of tosatoxumab as adjunct therapy and monotherapy of suvratoxumab have been investigated in phase 3 clinical trials for the treatment of ventilator associated pneumoniae caused by *S. aureus* (ClinicalTrials.gov Identifier: NCT03816956) and to prevent pneumoniae by *S. aureus* in high-risk patients (ClinicalTrials.gov Identifier: NCT05331885), respectively. Monotherapy of suvratoxumab did not reduce the incidence of *S. aureus* pneumoniae in patients receiving mechanical ventilation with confirmed *S. aureus* colonisation in the respiratory tract compared to placebo in a phase 2 clinical study [99]. Tosatoxumab was investigated as adjunct therapy with antibiotics, appeared safe and decreased the ventilation duration compared to the placebo group in a phase 2 clinical study [100]. 9MW1411 also binds α -toxin and inhibits binding to the cellular receptor disintegrin and metalloproteinase 10 [85], which plays an important role in the homeostatic regulation of acute inflammatory diseases [101]. The safety, tolerability, and pharmacokinetic properties of 9MW1411 were evaluated in a phase 1 clinical trial (ClinicalTrials.gov Identifier: NCT04784312). While the results of this phase 1 study have not been published, a phase 2 clinical trial (ClinicalTrials.gov Identifier: NCT05339802) is recruiting patients with acute *S. aureus* skin and skin structure infection to investigate the efficacy and safety of two doses of 9MW1411 combined with linezolid. The therapeutic approach of human monoclonal antibody TRL1086 is the disruption of biofilms by targeting DNA-binding proteins that are critical structural components within eDNA scaffolds and responsible for the biofilm's structural support [90]. Following promising results as combination therapy with antibiotics in animal models [102,103], the safety and efficacy of TRL1086 is currently being investigated in patients with prosthetic joint infection of the knee or hip (ClinicalTrials.gov Identifier: NCT04763759) and in patients with chronic rhinosinusitis and nasal polyps (ClinicalTrials.gov Identifier: NCT05355207).

1.4.2.2 Bacteriophages

Bacteriophages are host specific viruses that selectively target and specifically kill bacteria by self-replication. They diffuse or actively penetrate through the extracellular polymeric matrix, degrade

1 Introduction

or disrupt the biofilm structure and kill bacteria within the biofilm [104]. Due to the narrow host ranges of the individual phage, the use of phage cocktails can broaden the spectrum of activity, overcome phage resistance, and complement each other [104,105]. Treatment with phage cocktails alone or in combination with antibiotics showed antibacterial activity against *S. aureus* in animal models and in case studies for a range of infections, including osteomyelitis, prosthetic knee-joint infection, cardiovascular infections, and diabetic wounds [106]. For example, Morris, *et al.* [107] reported *in vivo* safety and efficacy of a phage cocktail comprising five *S. aureus* specific bacteriophages in combination with vancomycin against *S. aureus* biofilm-associated prosthetic joint infections in rats. Combined preparations of bacteriophages, such as liquid pyobacteriophage complexes are available in Poland, Russia and Georgia for various types of infections [108] and are being investigated as part of a phase 3 clinical trial as inhalation therapy for tonsillitis (ClinicalTrials.gov Identifier: NCT04682964). In addition, clinical trials are underway to determine the safety and efficacy of bacteriophage therapy with or without antibiotics in multiple *S. aureus* infections that are typically associated with biofilm formation, such as chronic rhinosinusitis (anzctr.gov.au; ACTRN1261600002482), bacteraemia (ClinicalTrials.gov Identifier: NCT05184764), diabetic foot ulcers (ClinicalTrials.gov Identifier: NCT04803708, NCT02664740), pressure ulcers (ClinicalTrials.gov Identifier: NCT04815798), wound infections (ClinicalTrials.gov Identifier: NCT04323475) and prosthetic joint infections (ClinicalTrials.gov Identifier: NCT05269121, NCT05369104). Details on these clinical trials are displayed in Table 1.3.

Furthermore, bacteriophages produce lysin enzymes, which show antibiofilm activity as part of the phage or as free enzymes. Lysins degrade the biofilm extracellular polymeric matrix and cleave the bacterial cell wall by binding polysaccharides and peptidoglycan [105]. Exebacase (CF-301) and tonabacase (LSVT-1701) are purified recombinant lysins with antibiofilm activity against *S. aureus* and *S. epidermidis* [91,92]. In a phase 2 clinical trial (ClinicalTrials.gov Identifier: NCT03163446), treatment of MRSA bloodstream infection with exebacase in combination with antibiotics showed superior clinical outcome and similar safety compared to treatment with antibiotics alone [109]. However, the phase 3 clinical trial (ClinicalTrials.gov Identifier: NCT04160468) was recently terminated for futility after interim efficacy analysis. The phase 2 clinical trial investigating tonabacase (LSVT-1701) for bacteraemia was withdrawn. While this is a setback for the development of endolysin treatments, their antimicrobial activity, synergistic effects, and high specificity, make them a promising approach to combat biofilms [105].

1.4.2.3 Anti-virulence agents

As described in Chapter 1.2.3, *S. aureus* produces a range of virulence factors which help the bacteria evade the hosts immune system. Virulence factors are regulated by QS and contribute to disease pathogenesis, tissue injury and treatment failure, making virulence factors a therapeutic target for antibacterial strategies. Anti-virulence agents disarm bacteria by targeting toxins, immune evasion mechanisms, and the QS system. These agents typically do not reduce pathogen viability and rely on the immune system or additional treatment with antibiotics to clear the infection [110]. Pore-forming toxins, such as α -toxin and leukocidins, are one of the largest classes of bacterial virulence factors that bind to receptors on the host cell membrane, form pores and disrupt membrane integrity [111]. Anti-virulence agents targeting pore-forming toxins, include monoclonal antibodies, small molecules and nanotherapeutics. Monoclonal antibodies bind and neutralise the toxins and are investigated in clinical trials as described in Chapter 1.4.2.1. In pre-clinical development are small molecules, such as flavonoid compounds and peptides, that bind toxins or inhibit pore assembly, and nanotherapeutics, such as liposomes, micelles and red blood

cells mimicking poly(lactic-co-glycolic acid) (PLGA)-based nanoparticles, that act as decoy receptors for toxins [110,111].

While toxins kill host cells, the mechanisms of the virulence factors staphyloxanthin and bacterial cell wall-anchored proteins, such as staphylococcal protein A, are based on evading the immune cells. Staphyloxanthin acts as an antioxidant against reactive oxygen species (ROS) secreted by neutrophils and consequently protects *S. aureus* against bacterial damage and death [112]. The small molecule ALS-4 inhibits the biosynthesis of staphyloxanthin [85] and its safety, tolerability and pharmacokinetic effects are investigated as part of a phase 1 clinical trial (ClinicalTrials.gov Identifier: NCT05274802) in healthy subjects. The virulence factor staphylococcal protein A disturbs recognition and ingestion of *S. aureus* by phagocytic cells [113]. It is the target of the monoclonal antibody omodenbamab, which was not further investigated in clinical trials since completion of a phase 1 clinical trial [85]. Staphylococcal protein A is also one of the targets of the five-antigen *S. aureus* vaccine rFSAV. The vaccine contains three antigens for *S. aureus* surface virulence factors and two for *S. aureus*-secreted toxins. In two phase 1 clinical trials, rFSAV was highly immunogenic, yet deemed safe and well tolerated in healthy adults [96], but evidence of safety is limited as severe reactions were detected in a small trial of just 108 subjects receiving the vaccine.

As many *S. aureus* virulence factors are regulated by Agr-mediated QS, such as the production of toxins and phenol-soluble modulins, targeting the QS system can result in the simultaneous inhibition of multiple downstream virulence factors [57]. One approach is based on inhibiting the production or sensing of the extracellular QS signal AIP, thereby interrupting the feedback loop required for transcription of *agr*. To inhibit binding of AIP to the Agr receptor or response modulator, derivatives of AIP were investigated to compete for binding sites [110]. Alternatively, savarin and staquorsin showed anti-Agr activity by inhibiting the transcription of one of the four *agr* genes [114].

1.4.2.4 Other antibiofilm agents

The clinical pipeline and recently approved antibacterial agents described by the WHO are insufficient to tackle the challenge of the emergence and spread of antimicrobial resistance [85]. Therefore, more antibiofilm agents are being developed and are the focus of multiple research groups around the world. To tackle biofilm-associated infections, strategies are based on inhibition of biofilm formation, disruption of the mature biofilm structure, or killing bacteria within the biofilm (Figure 1.8) [27,38]. Similar to the approach of anti-virulence agents, biofilm dispersal agents are used as adjunctive therapy to antibiotics. By dispersing the biofilm, released bacterial cells are no longer protected by the matrix and are more accessible for traditional antimicrobial therapies [49]. This can be achieved passively by debridement (see Chapter 1.3.2) or actively by triggering the biofilm microbes through environmental changes (see Chapter 1.2.2) and dispersal agents. Biofilm degradation can be induced by dispersal signals recognised by bacteria, by destabilising the matrix structure or by interfering with biofilm-sustaining signals [49].

Natural products have been extensively investigated *in vitro* and showed some antibiofilm activity *in vivo*. These include complex mixtures of natural remedies, such as honey and essential oils, phytochemicals, such as catechins extracted from tea, and antimicrobial peptides [115,116].

Furthermore, probiotics and their metabolites can be used to displace the biofilm by disrupting the architecture of the biofilm, to prevent biofilm infections by competing with pathogenic cells for bacterial attachment and by forming probiotic biofilms on surfaces to hinder adhesion of

pathogens. Lactic acid bacteria, such as *Lactobacillus*, *Bifidobacterium* and *Lactococcus*, are commonly used bacterial species and their metabolites include biosurfactants, bacteriocins, EPS and bacteria-free supernatant [117]. In multiple animal models of SSIs, the use of probiotics promoted wound healing by attracting inflammatory cells, inhibiting pathogens, and increasing epithelisation and vascularisation [118].

Antimicrobial photodynamic therapy uses harmless visible light or near infrared light (NIR) to activate a photosensitiser, resulting in the production of ROS. Irradiation with light, at a specific wavelength, leads to a change of the low photosensitisers' energy level to the excited state. In presence of ambient oxygen, ROS is generated by electrons and energy transfer. The highly reactive singlet oxygen and toxic reactive oxygen species, such as hydrogen peroxide, attack various components of the biofilm matrix (polysaccharides, proteins, lipids, DNA), damage the bacterial cell surface and reduce intracellular metabolism [119,120]. Photosensitisers commonly employed for antimicrobial photodynamic therapy are dyes, such as methylene blue [121] and porphyrin [122], and nanotechnologies, such as copper sulphide nanoparticles (see Chapter 1.6.1.2).

Nanotechnologies can be used as drug-delivery vehicles for antibiofilm agents and show intrinsic antibiofilm activity. Lipid-based nanoparticles, such as liposomes (see Chapter 1.6.1.3) and micelles, and polymeric based nanoparticles, such as PLGA, chitosan and dendrimers, are used to improve cellular uptake of antibacterial drugs, to protect the drug from drug-degrading enzymes present in the biofilm and improve efficacy by enabling drug combinations [123,124]. In contrast, the intrinsic antibacterial activity of metal-based nanoparticles is associated with the release of the corresponding metal ions or metal oxide, the production of ROS, the disruption of bacterial cell membranes, and the inhibition of exopolysaccharide synthesis and QS. The most commonly researched metallic nanoparticles are silver and gold, but other metals, including zinc, copper, titanium and selenium, are also being investigated. Facal Marina, *et al.* [125] provided an overview of metallic nanoparticles investigated as part of clinical trials for a range of infections, including wound infections, surgical site infections and infections of medical devices.

While many novel treatment strategies to combat *S. aureus* biofilms show promising pre-clinical and clinical results, the path to market-approval is arduous and uncertain. The research and development of new drugs is a lengthy and costly process that impedes a fast availability of new therapies. In addition, high numbers of drugs fail in clinical trials due to safety and toxicity issues [126]. To accelerate the development process and reduce the risk of failure in clinical trials, repurposed drugs are being investigated as alternative strategy for the treatment of *S. aureus* biofilms.

1.5 Repurposing drugs as antibiofilm agents against *S. aureus*

1.5.1 Benefits of drug repurposing

Repurposing or repositioning drugs investigates the use of an approved drug for new therapeutic purposes. As safety and toxicological evaluation of the drug were typically assessed for the original indication, the risks of failing in clinical trials are minimised and the regulatory process for licensing of repurposed compounds can be shortened compared to the development of new drugs (Figure 1.9). In addition, the investment risks are lowered, as the pre-clinical phase is reduced, and extensive phase 1 clinical trials can be waived [127,128].

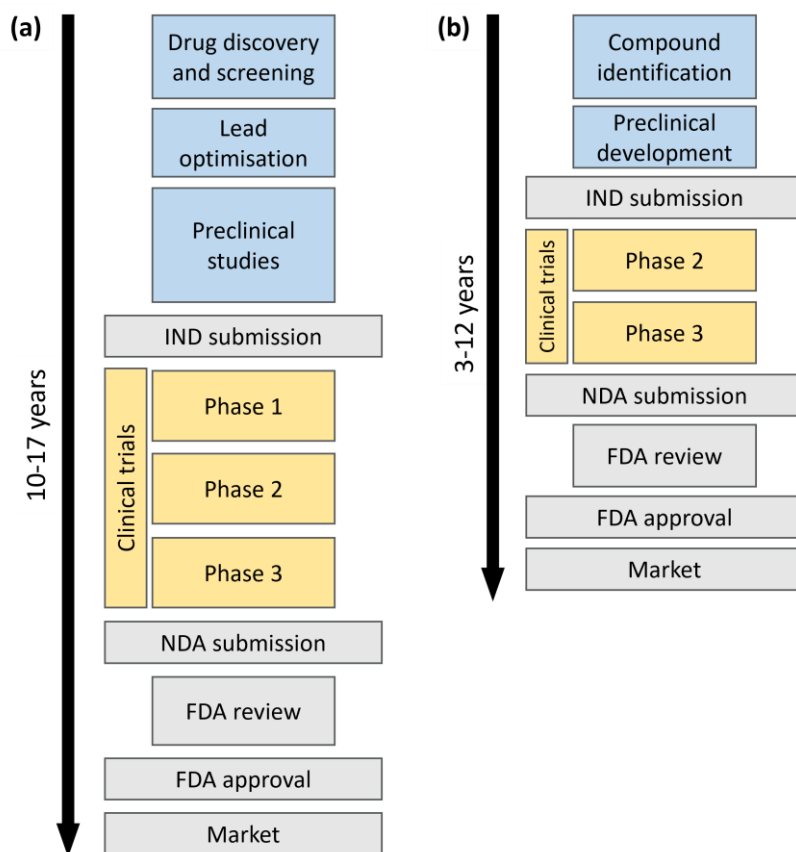


Figure 1.9: Schematic representation of the regulatory process for licensing conventional versus repurposed compounds. **(a)** The typical route to the clinic for *de novo* drug development first involves intellectual property filing and preclinical studies. If successful, an Investigational New Drug Application (IND) is filed with the FDA in preparation, for example, for the US marketplace. The drug candidate is then evaluated in humans through a series of clinical trials (Phase 1–3). Success here leads to a New Drug Application (NDA) that allows entry into the marketplace for prescription and sales to patients/consumers. **(b)** Repurposing efforts bypass much of the discovery and preclinical stages and typically forgo extensive Phase 1 studies for safety, entering clinical trials at Phase 2. Successful clinical trials lead to a NDA and the repurposed drug enters the market. Adapted with permission from Farha and Brown [128].

Repurposed drugs account for approximately 30% of all FDA approved drugs. Notable examples include the repositioning of the antihypertensive drugs sildenafil for the treatment of erectile dysfunction and minoxidil for treatment of hair loss [128]. While no repurposed drugs have received regulatory approval as antibacterial agents to date [129], a range of existing drugs were investigated *in vivo* or in clinical trials for antibiofilm activity against *S. aureus* (Table 1.4).

Table 1.4: Repurposed drugs with *in vivo* antibiofilm activity against *S. aureus*.

Clinical use	Drug	Reference
Anti-inflammatory	Acetylsalicylic acid	Paes Leme and da Silva [130]
	Diclofenac	Abbas, <i>et al.</i> [131]
	Diflunisal	Hendrix, <i>et al.</i> [132]
	Flufenamic acid	Zhang, <i>et al.</i> [133]
	Auranofin	Thangamani, <i>et al.</i> [134]
Anticancer	Idarubicin	She, <i>et al.</i> [135]
	5-fluorouracil	Sedlmayer, <i>et al.</i> [136]
	Streptozotocin	Yeo, <i>et al.</i> [137]
	Floxuridine	Yeo, <i>et al.</i> [137]
Antipsychotic	Penfluridol	Liu, <i>et al.</i> [138]
Antidiabetic	Sitagliptin	Khayat, <i>et al.</i> [139]
Thrombopoietin receptor agonist	Eltrombopag	She, <i>et al.</i> [140]
Antihypertensive	Candesartan	Xu, <i>et al.</i> [141]
Antihyperlipidemic	Simvastatin	Sun, <i>et al.</i> [142]
Antihistamine	Loratadine	Zheng, <i>et al.</i> [143]
Antiviral	Simeprevir	Li, <i>et al.</i> [144]
Antiparasitic	Nitazoxanide	Kaul, <i>et al.</i> [145]
Anthelmintic	Pyrrvinium	Mahey, <i>et al.</i> [146]
	Niclosamide	Weiss, <i>et al.</i> [147]
Anti-alcoholic	Disulfiram	Thakare, <i>et al.</i> [148]

1.5.2 Investigating drugs for antimicrobial activity against *S. aureus*

The discovery of novel clinical opportunities for drugs can be serendipitous through the observation of side effects or the result of drug library screens. Drug candidates are tested for growth inhibition, target-based phenotypic screened to block a specific pathway, screened for synergising with antibiotics or screened *in silico* by virtually predicting molecular docking of agents on the target's binding sites [128].

Both whole bacterial cell screens (i.e., growth inhibition) and target-based screens are high throughput screens that enable the investigation of compound libraries or compound groups. Whole bacterial cell library screenings of approved drugs, such as the FDA-approved drug library, revealed the antibiofilm activity of the antihistaminic drug loratadine, the anti-hepatitis C drug simeprevir and the antiparasitic drug nitazoxanide [143-145]. In addition, the discovery of antibacterial activity against *S. aureus* of the anthelmintic drug niclosamide was the result of drug libraries and salicylanilide derivatives screenings [149,150]. A 2% niclosamide ointment was tested as part of a randomised, double-blind, and placebo-controlled phase 2 clinical trial on infected atopic dermatitis (ClinicalTrials.gov Identifier: NCT03009734). The twice-daily treatment was well tolerated, reduced *S. aureus* colonisation in atopic dermatitis lesions and increased the skin microbiome diversity [147]. Furthermore, target-based screenings of drug libraries identified 5-

fluorouracil as promising antibiofilm agent based on the inhibition of AIP production [136], as well as streptozotocin and floxuridine based on the inhibition of the virulence factor regulator SaeRS [137].

While libraries contain a wide range of different compounds, the screening can be limited to specific groups of compounds, based on chemical structure and clinical application. For example, non-steroidal anti-inflammatory drugs are amongst the best known and most widely used class of drugs and employed for their anti-inflammatory, analgesic, and antipyretic properties [130,151]. Diclofenac, diflunisal and flufenamic acid showed *in vivo* activity against *S. aureus* biofilms, and beneficial effects of acetylsalicylic acid were observed in combination with standard of care antibiotics in periprosthetic joint infections as part of a single-centre database search [130]. A trend of superior time-to-infection resolution was observed in patients receiving a daily dose of 100 mg acetylsalicylic acid for previous cardiovascular diseases [152]. Other compounds with antibacterial properties discovered during the screening of chemical groups are the lipid-lowering drug simvastatin as part of a statin screening [153] and the antidiabetic drug sitagliptin as part of a gliptin screening. Sitagliptin was also screened for *in silico* molecular docking to *S. aureus* QS receptors, to confirm observed downregulation of genes associated with QS and biofilm formation [139].

Moreover, some drugs are being investigated for potential antibiofilm activity based on previous repurposing attempts. For example, the antirheumatic drug auranofin is being repurposed for cancer, HIV, neurodegenerative disorders, and parasitical and bacterial infections. The broad spectrum of activity can be explained by its anti-inflammatory properties, high affinity for thiols and selenoproteins and inhibition of ROS controlling enzymes [154]. The same properties contributed to clearing MRSA in a subcutaneous abscess in mice when auranofin was combined with phenethyl isothiocyanate [155]. Similarly, idarubicin inhibits the DNA topoisomerase for its anticancer activity, which is also part of the mechanism for the antibacterial activity against MRSA [135]. In contrast, some drugs showed potential for repurposing in a variety of different diseases, including effects against *S. aureus* but the different mechanisms behind the activities are not linked. These include the antihypertensive drug candesartan that was previously investigated for chronic heart failure and as antiviral treatment for Zika virus [141], the thrombopoietin receptor agonist eltrombopag that showed antibacterial activity against *Mycobacterium tuberculosis* (*M. tuberculosis*) and antifungal effects against *Cryptococcus neoformans* [140], and the anthelmintic drug pyrvinium pamoate that is under investigation as an anticancer drug (ClinicalTrials.gov Identifier: NCT05055323). The previous repurposing attempts of the anti-alcoholic drug disulfiram, for a variety of indications, resulted in the discovery of its antibacterial activity *in vitro* and *in vivo* as described in the next section.

1.5.3 Disulfiram and diethyldithiocarbamate

Disulfiram (DSF), or tetraethylthiuram disulphide, is the active ingredient in Antabuse®, a drug for the treatment of chronic alcoholism. Its discovery was serendipitous, when workers who used disulfiram to accelerate the vulcanisation of natural rubber observed a drastically reduced tolerance to alcohol. The potential medical use as treatment of alcoholism was first reported by Dr E. E. Williams in 1937. DSF was approved as a drug in Denmark and Sweden in 1949 and by the FDA in 1951 as therapy to prevent the consumption of alcohol [156,157]. DSF is administered as a daily dose of 125-500 mg and has been used for over 70 years [157,158].

1 Introduction

The alcohol detoxification in the human body contains two steps: First, ethanol is converted into the toxic acetaldehyde by the enzyme alcohol dehydrogenase. Secondly, acetaldehyde is metabolised to the well tolerated acetate by an aldehyde dehydrogenase (ALDH). DSF blocks the activity of ALDH by irreversibly binding to the enzyme and thereby prevents the detoxifying second step. Consequently, toxic acetaldehyde is not converted into acetate and accumulates in the body, resulting in an unpleasant reaction similar to a “hangover”, such as headaches, flushing, sweating, vertigo and nausea [158-160].

1.5.3.1 Metabolic activity of disulfiram

DSF is administered orally as dispersible tablet and is metabolised as described in Figure 1.10. As DSF is unstable under acidic conditions, it rapidly reduces to the polar and hydrophilic monomer diethyldithiocarbamate (DDC⁻). DSF and metallic complexes of DDC⁻ permeate the intestinal wall and travel to the liver, where they are metabolised or degraded. DDC⁻ is unstable in biological tissues and spontaneously converts to carbon disulphide (CS₂) and diethylamine (DEA) or is transformed in the liver or kidney by the S-methyltransferase to methyl diethyldithiocarbamate (Me-DDC) [161,162]. The stable Me-DDC is further metabolised by cytochrome P450 enzymes to bioactive molecules that bind ALDH and exert the anti-alcoholic properties [160,163]. DDC⁻ happens to also be a strong chelator of transient divalent metal cations [164]. For example, in the presence of copper salts or protein bound copper (Cu²⁺), 1 mol of Cu²⁺ will bind 2 mol of DDC⁻ and form the cupric-diethyldithiocarbamate (Cu(DDC)₂) complex [160].

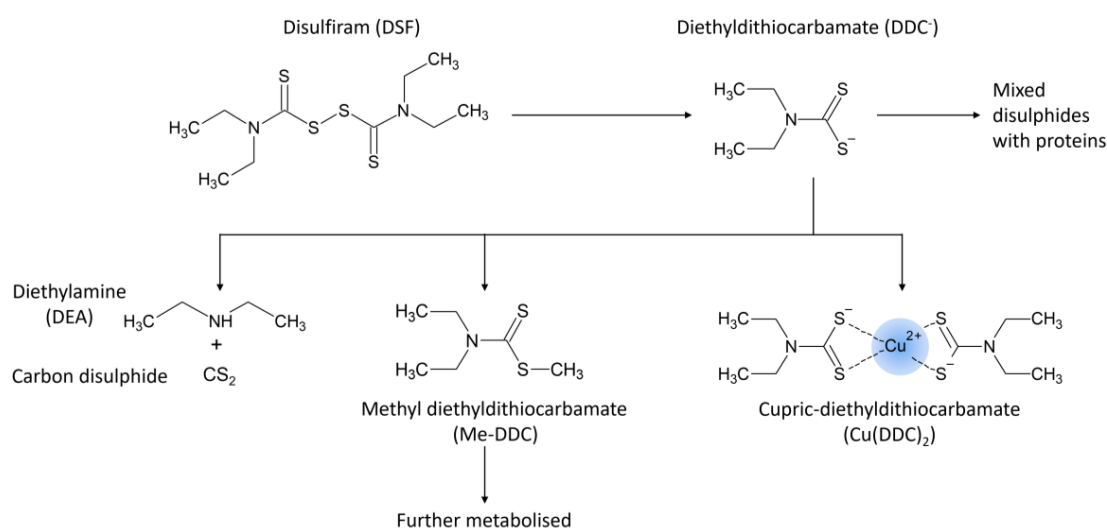


Figure 1.10: Metabolic pathway of disulfiram in the human body. Modified from Johansson [160].

1.5.3.2 Repurposing of disulfiram

“The anticancer activity of DSF was first observed when an alcoholic patient showed complete remission of metastatic breast cancer when being treated with the anti-alcoholic drug DSF in 1977 [165]” [166]. Since then, the activity of DSF has been investigated against a range of cancer cell lines and resulted in 23 clinical trials (according to ClinicalTrials.gov, accessed 24/01/2023) with the focus on metastatic breast, prostate, gastric and pancreatic cancer, glioblastoma, sarcoma, and melanoma. In these trials, DSF was investigated alone, in combination, or as adjuvant to standard chemotherapy. As the anticancer activity of DSF was potentiated by the combination with Cu²⁺ [162,167,168] or zinc salts (Zn²⁺) [169], clinical trials have also been investigating these

combinations. In addition, multiple completed, ongoing, or recruiting clinical trials are described in Table 1.5, which evaluate DSF as treatment for a range of different diseases, including cocaine addiction, obesity, retinal degeneration, HIV, COVID-19, and Lyme disease. By going into clinical trials for viral and bacterial infections, DSF shows potential as treatment against microbial diseases.

Table 1.5: Examples of clinical trials investigating the activity of repurposed disulfiram.

Indication	Example	Phase	Status	Clinical trial number
Cancer	Advance gastric cancer	Not applicable	Not yet recruiting	NCT05667415
	Metastatic breast cancer	2	Recruiting	NCT03323346
	Multiple Myeloma	1	Recruiting	NCT04521335
Cocaine addiction		2	Completed	NCT00395850
Obesity		1	Enrolling by invitation	NCT05162001
Retinal degeneration		1/2	Not yet recruiting	NCT05626920
Virus	COVID-19	2	Completed	NCT04594343
		2	Suspended	NCT04485130
	HIV	1/2	Completed	NCT01944371
Lyme disease		1/2	Completed	NCT03891667

1.5.3.3 Disulfiram and diethyldithiocarbamate as antimicrobial agents

The antimicrobial activity of DSF against parasites, viruses, fungi, and bacteria (Figure 1.11) was recently reviewed by Custodio, *et al.* [170]. In addition, the antibacterial and anti-parasitic activity of DSF was the focus of reviews by Meneguello, *et al.* [171] and Shirley, *et al.* [172]. DSF and DDC⁻ are either investigated alone, as adjuvants to antibiotics or to counter drug resistance [170].

Parasites

The activity of DSF against parasites was observed as early as 1947, when it was recognised as scabicide and vermicide [157]. Since 1982, a cutaneous emulsion called Tenutex[®], containing 2% DSF and 22.5% benzyl benzoate, has been used in Sweden for the treatment of scabies and pediculosis. Tenutex[®] eradicated sheep lice after 6h in an *ex vivo* experiment and killed both the adult *Pediculus humanus* and its eggs *in vitro* [173].

The antiparasitic activity of DSF and DDC⁻, as monotherapy or in combination with standard of care therapy, was also investigated *in vitro* and *in vivo* for a range of different diseases, such as schistosomiasis caused by the helminth *Schistosoma mansoni* [174], giardiasis caused by the trophozoite *Giardia duodenalis* [175], chagas disease caused by *Trypanosoma cruzi* [176], leishmaniasis caused by *Leishmania braziliensis* [177] and malaria caused by different *Plasmodium* strains [178].

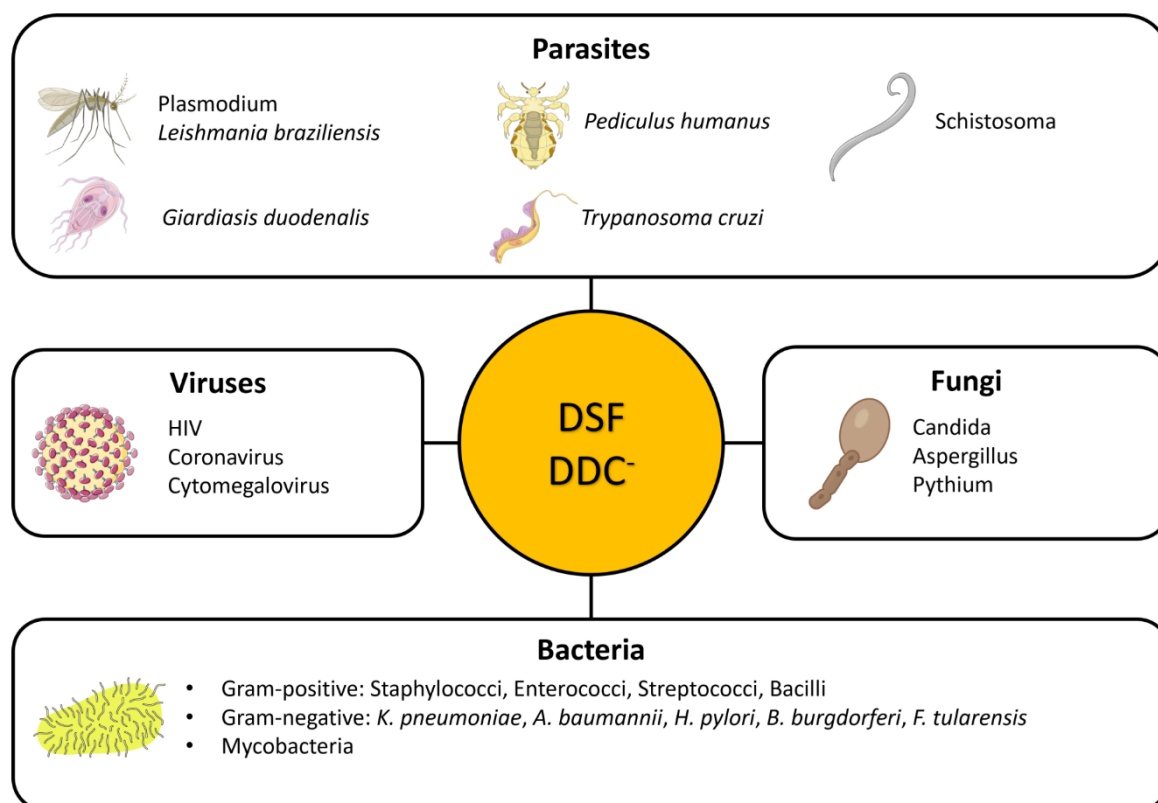


Figure 1.11: Antimicrobial activity of disulfiram (DSF) and diethyldithiocarbamate (DDC⁻) against examples of parasites, viruses, fungi, and bacteria. HIV = human immunodeficiency virus; *Klebsiella pneumoniae* (*K. pneumoniae*); *Acinetobacter baumannii* (*A. baumannii*); *Helicobacter pylori* (*H. pylori*); *Borrelia burgdorferi* (*B. burgdorferi*), *Francisella tularensis* (*F. tularensis*).

Viruses

DSF has been investigated as antiviral treatment against cytomegalovirus, multiple coronaviruses, and the human immunodeficiency virus. In cytomegalovirus pneumonia-infected mice, DSF improved survival and reduced hyperinflammatory effects, pulmonary injury, and viral load [179]. DSF also inhibited proteases that are crucial for viral replication of the Middle East respiratory syndrome coronavirus (MERS-CoV) and severe acute respiratory syndrome coronavirus (SARS-CoV) *in vitro* [180]. In addition, a retrospective cohort study showed a trend of reduced COVID-19 incidence and severity in veterans treated with DSF for alcohol use disorder [181]. This led to two clinical trials investigating the safety and efficacy of DSF treatment in patients with COVID-19 (Table 1.5). One clinical trial was completed (NCT04594343) but no results are available yet, and the clinical trial DISCO (NCT04485130) was suspended due to low case numbers and progress of competing treatments.

The antiviral activity of DSF and its metabolite DDC⁻ against human immunodeficiency virus (HIV)-1 is based on the approach termed the “shock and kill strategy”. It aims to reactivate the latent, replication-competent virus reservoirs, which are then the target of standard anti-retroviral therapy [182]. “Clinical studies performed in 2011 (NCT01286259) and 2013 (NCT01944371) showed that treatment with DSF resulted in a dose-dependent increase of cell-associated unspliced HIV-RNA and plasma HIV-RNA [161,183,184]. However, a reduction of the size of the latent reservoir could not be achieved. It was postulated that this was the result of a lack of potency of DSF, the challenges of measuring the size of the reservoir, and the presence of additional viral reservoirs, such as in the central nervous system [185]” [166]. An additional study

(NCT03198559) investigating the changes in HIV-RNA levels after treatment with DSF and another latency-reversing agent, vorinostat, had to be terminated due to neurotoxicity [186]. Nevertheless, more research was conducted and showed that DSF with the antiretroviral drug maraviroc did not alter resting CD4 T cell viability or proliferation and enhanced HIV replication *in vitro* [187].

Fungi

DSF showed activity against fungal pathogens, such as *Candida* and *Aspergillus* isolates [188] and the fungus-like pathogen *Pythium insidiosum* (*P. insidiosum*) [189]. DSF and DDC⁻ inhibited growth of several *Candida* species, including *Candida albicans* (*C. albicans*), *Candida tropicalis* and *Candida auris*, and reduced *Candida* biofilm viability [190,191]. For example, DDC⁻ inhibited the biofilm persistence mechanism superoxide dismutase and combined with amphotericin B reduced *C. albicans* biofilm viability [192]. Furthermore, DSF shows potential as therapy for fungal keratitis. In an early-stage *Aspergillus fumigatus* keratitis mice model, DSF suppressed inflammation by inhibiting secretion of proinflammatory cytokines and improved the corneal transparency when combined with the antifungal natamycin [193]. Similarly, DSF inhibited growth of *P. insidiosum*, which is mostly found in water and is associated with infections of the eye's cornea [189].

Bacteria

“In 1987, Taylor, et al. [194] were the first group investigating the antibacterial properties of DDC⁻ against MRSA. Subsequent to these studies, Phillips, et al. [195] investigated the antibacterial properties of DSF against a range of Gram-positive and Gram-negative bacteria. They concluded that DSF inhibits the growth of Gram-positive bacteria, such as MRSA, but not Enterobacteriaceae or *Pseudomonas aeruginosa*” [166]. Recent studies confirmed the antibacterial activity of DSF in Gram-positive bacteria [196,197], especially in *S. aureus* and MRSA [198,199], streptococci [200], enterococci [201] and bacilli [196]. Thakare, et al. [148] reported the ability of DSF to diminish *S. aureus* biofilm mass, intracellular killing and to reduce bacterial load in a murine neutropenic thigh *S. aureus* infection. DSF synergised with a range of antibiotics, such as gentamycin, linezolid, vancomycin and fosfomycin [148,196,199]. Additionally, derivatives of DSF and DDC⁻ were synthesised to increase the antibacterial activity [197,202].

Interestingly, the lack of activity against Enterobacteriaceae or *Pseudomonas aeruginosa* (*P. aeruginosa*) was not observed for other Gram-negative bacteria, as recent studies revealed antibacterial activity of DSF against *Helicobacter pylori* (*H. pylori*), *Klebsiella pneumoniae* (*K. pneumoniae*), *Acinetobacter baumannii* (*A. baumannii*), *Francisella tularensis* (*F. tularensis*), and *Borrelia burgdorferi* (*B. burgdorferi*) [170,171]. By blocking the activity of ureases, DSF inhibited growth of *H. pylori*, altered the bacterial cell morphology, and prevented killing of gastric cells by the pathogen *in vitro* [203]. Treatment with DSF also enhanced the disruption of *K. pneumoniae* membrane with polymyxin B and the combination increased the survival rate of infected mice [204]. The combination of DSF and meropenem reduced the *A. baumannii* load *in vivo* [205] and treatment with DSF alone inhibited *A. baumannii* growth and biofilm formation by blocking a key molecule of the QS system [206]. In addition, high *in vitro* activity of DSF was observed against the tick-transmitted *B. burgdorferi* [207] but DSF alone and in combination with antibiotics did not inhibit regrowth of persisters [208]. In a case study of three patients with symptoms of chronic relapsing neurological Lyme disease and relapsing babesiosis, daily administration of DSF enabled all patients to discontinue antimicrobial treatment and to remain

1 Introduction

clinically well for 6 months [209]. Based on these results, a clinical trial (NCT03891667) examined the safety and efficacy of a treatment with DSF to reduce symptoms in patients with post-treatment Lyme disease symptoms [210].

As a metabolite of DSF, DDC⁻ was also investigated for antibacterial activity against Gram-positive and Gram-negative bacteria but showed no significant growth inhibition, except for *Bacillus anthracis* [196]. However, superior effects in reducing intracellular growth of *F. tularensis* in human monocytic cells were observed when treated with DDC⁻ compared to DSF [211]. DDC⁻ also inhibited the metalloenzymes carbonic anhydrase of *Legionella pneumophila* [212], *Neisseria gonorrhoeae* [213] and *S. aureus* [214], as well as the *cyn* operon gene of *E. coli* encoding for β -carbonic anhydrase [215]. The carbonic anhydrase is responsible for the catalytic reaction of CO₂ to bicarbonate, which can play a significant role in the pathogenicity, invasion and survival of bacteria and is therefore considered a promising target of novel antibiotics [212,214].

In addition, DDC⁻ was highly active against growing and nongrowing persister *M. tuberculosis* and enhanced the activity of established tuberculosis drugs [216]. DSF showed *in vitro* and *in vivo* antibacterial activity against non-tuberculosis mycobacteria, such as *Mycobacterium fortuitum* and *Mycobacterium abscessus*, and synergised with multiple antibiotics [217,218].

While the mechanisms behind the antibacterial activity of DSF and DDC⁻ are not fully understood, it is partly attributed to (i) thiol interactions with cysteines from several targets, such as ureases [203], (ii) binding of divalent metals in the catalytic site of enzymes, such as zinc ions in carbonic anhydrase [219], and (iii) chelation of metal micronutrients, such as extracellular ferric ions [170,171,196]. The high affinity of DSF and DDC⁻ to metal ions, the bactericidal effects of Cu²⁺-complexes [170] and the enhancement of anticancer activity observed when DSF or DDC⁻ are combined with Cu²⁺ [166,220] fuel the hypothesis that the combination of DSF or DDC⁻ with Cu²⁺ show synergistic antibacterial activity.

1.5.3.4 Antibacterial activity of disulfiram and DDC⁻ with Cu²⁺

DSF is a poor metal chelator and reductively dissociates to DDC⁻ in an acidic environment or an aqueous Cu²⁺ solution, but not in the presence of other divalent metal ions, such as cobalt, iron, nickel, manganese, or zinc ions. In contrast, DDC⁻ is a strong metal chelator and forms complexes with many metal ions, often resulting in a change of colour [221]. Dalecki, *et al.* [221] observed no noteworthy antibacterial activity of DDC⁻ with nickel, iron, cobalt, manganese, and zinc ions but growth inhibition of *M. tuberculosis* in the presence of Cu²⁺. DDC⁻ forms the Cu(DDC)₂ complex by binding Cu²⁺ in a 2:1 molar ratio (Figure 1.12) [162], which is considered the most stable metal ion-DDC⁻ complex [222].

1.5 Repurposing drugs as antibiofilm agents against *S. aureus*

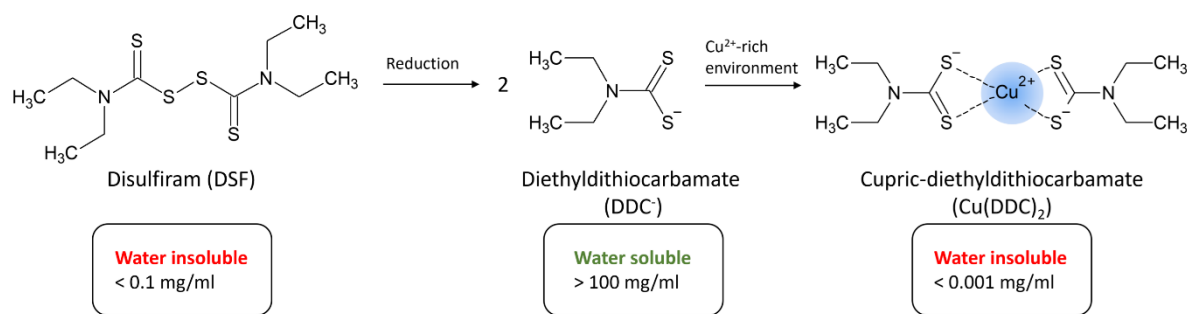


Figure 1.12: Formation of the Cu(DDC)₂ complex. The water-insoluble disulfiram (DSF) reductively dissociates to two molecules of water-soluble diethyldithiocarbamate (DDC⁻) in acidic or copper ion (Cu²⁺)-rich environments. In the presence of Cu²⁺, DDC⁻ forms the water insoluble Cu(DDC)₂ complex at a molar ratio of 2:1 [DDC⁻:Cu²⁺]. The value for water solubility of Cu(DDC)₂ was sourced from Wehbe, *et al.* [223], and that of DSF and DDC⁻ were sourced from the National Center for Biotechnology Information. PubChem Compound Summary for CID 3117, Disulfiram and CID 533728, Sodium diethyldithiocarbamate. <https://pubchem.ncbi.nlm.nih.gov>. Accessed Jan. 30, 2023.

To date, only a small number of articles have described the antibacterial properties of DDC⁻ or DSF combined with Cu²⁺ (Table 1.6). Dalecki, *et al.* [221] demonstrated that the concentration ratio of DSF and Cu²⁺ that inhibited growth of *M. tuberculosis* was consistent with the formation of Cu(DDC)₂. This was further confirmed when Cu²⁺ outcompeted zinc ions (Zn²⁺) in the Zn(DDC)₂ complex and the resulting Cu(DDC)₂ complex displayed an identical inhibition profile to that of DSF with Cu²⁺. It was further suggested that Cu(DDC)₂ penetrates the mycobacterial cell envelope, protects Cu²⁺ from copper resistance proteins and induces intracellular copper stress response by inhibiting intracellular protein functions [221]. Similarly, Totten, *et al.* [224] described that in the presence of Cu²⁺, the minimal inhibitory concentration (MIC) of DSF against *Mycoplasma hominis* was reduced by four- to eight-fold. Interestingly, Menghani, *et al.* [222] observed no bactericidal activity against *Streptococcus pneumoniae* (*S. pneumoniae*) when treated with DSF and Cu²⁺ but showed concentration dependent antibacterial activity of DDC⁻ with Cu²⁺. DSF might interact with bacterial cell components that prevent dissociation to DDC⁻ and be unavailable for the formation of the Cu(DDC)₂ complex. In contrast, the combination of DSF and Cu²⁺ was synergistic and inhibited growth of *Streptococcus mutans* (*S. mutans*). The antibacterial activity of the combination was not only observed against planktonic forms of *S. mutans* but also against biofilm [225].

Table 1.6: Combination of copper ions (Cu²⁺) with disulfiram (DSF) or diethyldithiocarbamate (DDC⁻) that showed antibacterial activity.

Reference	DSF or DDC ⁻	Bacteria	Biofilm ¹
Dalecki, <i>et al.</i> [221]	DSF	<i>Mycobacteria tuberculosis</i>	N
	DDC ⁻	<i>Mycobacteria smegmatis</i>	
Saputo, <i>et al.</i> [225]	DSF	<i>Streptococcus mutans</i>	Y
Totten, <i>et al.</i> [224]	DSF	<i>Mycoplasma hominis</i>	N
Menghani, <i>et al.</i> [222]	DDC ⁻	<i>Streptococcus pneumoniae</i>	N

¹ The activity of DSF and DDC⁻ in combination with Cu²⁺ was investigated against biofilms: N= No; Y = Yes.

Little research has been done to investigate the activity of DSF or DDC⁻ against biofilms. The antibiofilm activity of DSF was only investigated without Cu²⁺ against *A. baumannii* [206] and *S. aureus* [148], and in combination with Cu²⁺ against *S. mutans* [225]. Moreover, the antibiofilm

activity of DDC⁻ has not been investigated yet and based on promising synergistic effects of DSF and DDC⁻ combined with Cu²⁺ against planktonic bacteria, the combination should be further examined for antibiofilm activity.

While the antibacterial activity of DSF against MRSA appeared to be Cu²⁺-independent [226], previous results by Menghani, *et al.* [222] demonstrated effects of DDC⁻ with Cu²⁺ against *S. pneumoniae* despite the lack of effects observed when Cu²⁺ is combined with DSF. This warrants the investigation of DDC⁻ in combination with Cu²⁺ as antibacterial agent against a range of bacteria and their biofilms found in SSIs, including the pathogens *S. aureus* and *S. epidermidis*.

1.6 Administration of diethyldithiocarbamate and copper ions on surgical site infections

1.6.1 Low solubility of Cu(DDC)₂

1.6.1.1 Limits of an oral or intravenous administration of DSF or DDC⁻ with Cu²⁺

Following oral administration, DSF either rapidly degrades in the acidic environment of the gastrointestinal tract or is absorbed by the gastrointestinal mucosa into the bloodstream. DSF is then reduced to its monomer DDC⁻, which converts to DEA and CS₂ and/or accumulates in the liver where it is enzymatically transformed into Me-DDC or chelates metal ions, such as Cu²⁺. In contrast, the metabolites of DDC⁻ are lacking the functional thiol groups that are crucial for chelating Cu²⁺ and consequently cannot form a Cu²⁺-dithiocarbamate complex. The short plasma half-life of DSF is due to the bio-instability in the bloodstream but varies considerable between individuals [160,161]. Therefore, reaching steady *in vivo* doses of DSF or DDC⁻ is problematic and oral or intravenous administration of DSF and Cu²⁺ separately might not result in the formation of Cu(DDC)₂ [167]. In addition, intravenous and topical application of DSF and Cu(DDC)₂ is limited by the low water solubility of both structures (Figure 1.12). Poor solubility and bio-instability of pharmaceutical compounds are common limitations for the administration and treatment efficacy of drugs. Amongst various strategies to overcome these challenges, the encapsulation of the respective drug into a carrier-system is regarded as one of the most promising approaches [227]. By incorporating DDC⁻ with Cu²⁺ into a nanoparticle, the intravenous or topical application can be facilitated due to increased solubility of Cu(DDC)₂ and protection of DDC⁻ from degradation.

1.6.1.2 Nanoparticles for the delivery of DSF or DDC⁻ with Cu²⁺

Many different nanoparticles were recently developed for an intravenous application of DSF or DDC⁻ with Cu²⁺ as anticancer treatment [228-230]. As depicted in Figure 1.13, the nanosystems can be categorised into three approaches:

(a) Nanoparticles containing DSF (DSF-NPs) are co-administered with free Cu²⁺ or copper-nanoparticles (Cu-NPs).

A range of different DSF-NPs were developed, such as dendrimers [231], cyclodextrins [232], liposomes [233], micelles [234], and nanocrystals [235], but only few were investigated in combination with Cu²⁺. DSF liposomes [236,237], nanocomplexes [238], lipid NPs [239], and polymer NPs [240] were combined with free Cu²⁺, and DSF micelles were investigated with copper sulphide (CuS) NPs [241] or Cu²⁺-oleate liposomes [242]. In contrast, only He, *et al.* [243] described the development of a polymer nanoparticle containing DDC⁻ that was investigated for anticancer activity with free Cu²⁺.

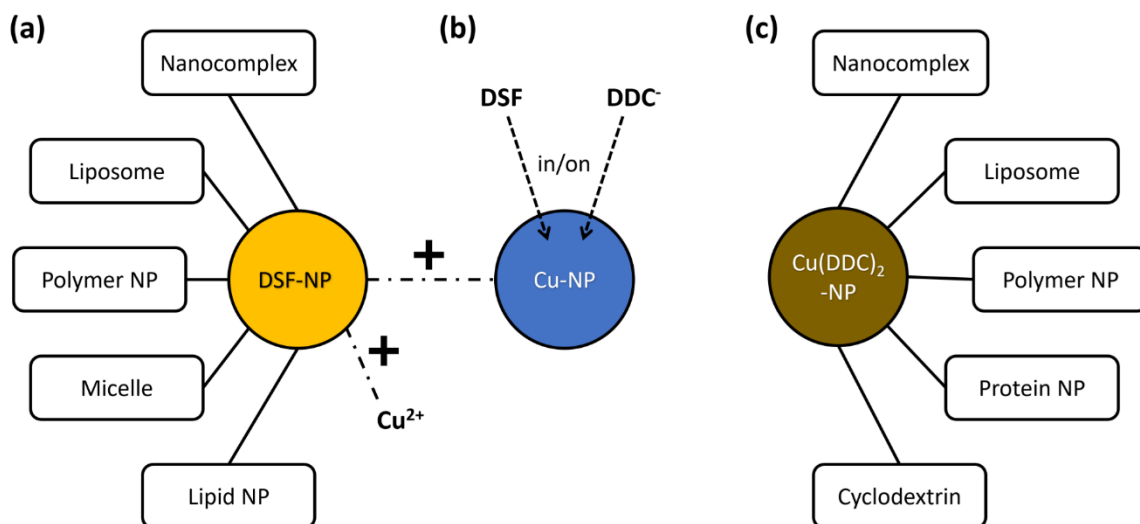


Figure 1.13: Nanoparticles (NP) developed for disulfiram (DSF) or diethyldithiocarbamate (DDC⁻) with copper ions (Cu²⁺). **(a)** DSF-NPs, categorised (—) as nanocomplexes, liposomes, polymer NPs, micelles, and lipid NP, are co-administered (---) with free Cu²⁺ or Cu-NPs. **(b)** DSF or DDC⁻ can be inserted in or attached onto (---) Cu-NPs. **(c)** Cu(DDC)₂-NPs can be categorised as nanocomplexes, liposomes, polymer NPs, protein NPs and cyclodextrins.

(b) DSF or DDC⁻ is incorporated into or attached onto Cu-NPs.

Biodegradable CuS-NPs have been investigated for anticancer and antibacterial activity as part of a photodynamic therapy (see Chapter 1.4.2.4). In addition to ROS generation upon activation of photothermal effects with NIR light, the release of Cu²⁺ from CuS-NPs can also promote the ROS generation and interact with DDC⁻ [244]. Therefore, DSF was encapsulated in the large cavities and mesoporous shells of hollow CuS-NPs [245] or attached to their surface for on-site formation of Cu(DDC)₂ [246]. Alternatively, Cu(DDC)₂ was transported to the target site by loading DDC⁻ on the surface of CuS-NPs through complexation with Cu²⁺ [244]. Other Cu-NPs were also investigated, such as copper oxide NPs with DDC⁻ attached to the surface [247].

(c) Nanoparticles containing Cu(DDC)₂ (Cu(DDC)₂-NP).

The developed Cu(DDC)₂-NPs can be differentiated into polymer NPs, protein NPs, cyclodextrins, nanocomplexes and liposomes. For the production of polymer NPs, one strategy is based on stabilising Cu(DDC)₂ by incorporating the complex in polymer structures or coating it with polymers. For instance, Cu(DDC)₂ was successfully integrated into micelles using the stabilised metal ion ligand complex technique [248,249]. Other examples include the formation of nanocrystals using the antisolvent precipitation method [250] or controlled particle growth by mixing Cu(DDC)₂ with the polymer polyvinylpyrrolidone [251]. In another method for the production of polymer NPs, Cu²⁺ or DSF was first incorporated into a polymer mix to form a NP and subsequently the other components were added to form Cu(DDC)₂ *in situ* within the polymer structure [252]. Protein NPs were developed by stabilising Cu(DDC)₂ in bovine serum albumin [253] or by embedding Cu(DDC)₂ in apoferritin [254]. Cyclodextrins are cyclic oligosaccharides with a truncated-cone-shaped structure that can form inclusion complexes on the hydrophilic surface or in the hydrophobic cavity. As cyclodextrins typically enhance drug solubility and stability, Cu(DDC)₂ was mixed with the FDA approved inactive pharmaceutical excipients hydroxypropyl beta-cyclodextrin or sulfobutylether beta-cyclodextrin [255]. Furthermore, nanocomplexes consist of a matrix that forms and stabilises Cu(DDC)₂ within the NP or releases

Cu^{2+} and DSF or DDC^- for *in situ* chelation at the target site. The release from the structure can be triggered by photothermal effects and/or by the environment at the target site (e.g., acidic tumour environment). For a photodynamic triggered release, the structure itself can be a photothermal agent, such as Prussian blue NPs [256] and ultrasmall melanin NPs [257], or a NIR-dye can be added to the matrix [230]. Materials of matrices that degrade depending on environmental conditions, include mesoporous silica NPs [258] and hexagonal layered double hydroxide NPs [259]. Similarly, $\text{Cu}(\text{DDC})_2$ can be attached or *in situ* chelated using metal organic frameworks, such as the acid-sensitive zeolitic imidazolate framework or a Cu^{2+} -based 2 methyl-imidazole framework [229,260,261]. Lastly, the developed $\text{Cu}(\text{DDC})_2$ -liposomes are described in Chapter 1.6.1.4.

1.6.1.3 Liposomes as vehicle for delivery of antibacterial agents

Liposomes are spherical lipid vesicles based on a minimum of one lipid bilayer that encapsulate an aqueous core (Figure 1.14a) [262]. They are amongst the most used nanoparticles for drug delivery due to their biocompatibility, size, and drug loading efficiency [263,264]. The structure of liposomes enables lipophilic drugs to be incorporated into the membrane bilayer, while hydrophilic drugs are encapsulated in the aqueous core. The drug encapsulation efficiency of hydrophilic compounds decreases with the increasing number of bilayer membranes [264]. Liposomes protect the drug from degradation, increase its solubility, prevent accelerated renal clearance, and increase blood circulation time [262,265]. For a good circulation half-life, the size of liposomes should range between 50 and 200 nm [266].

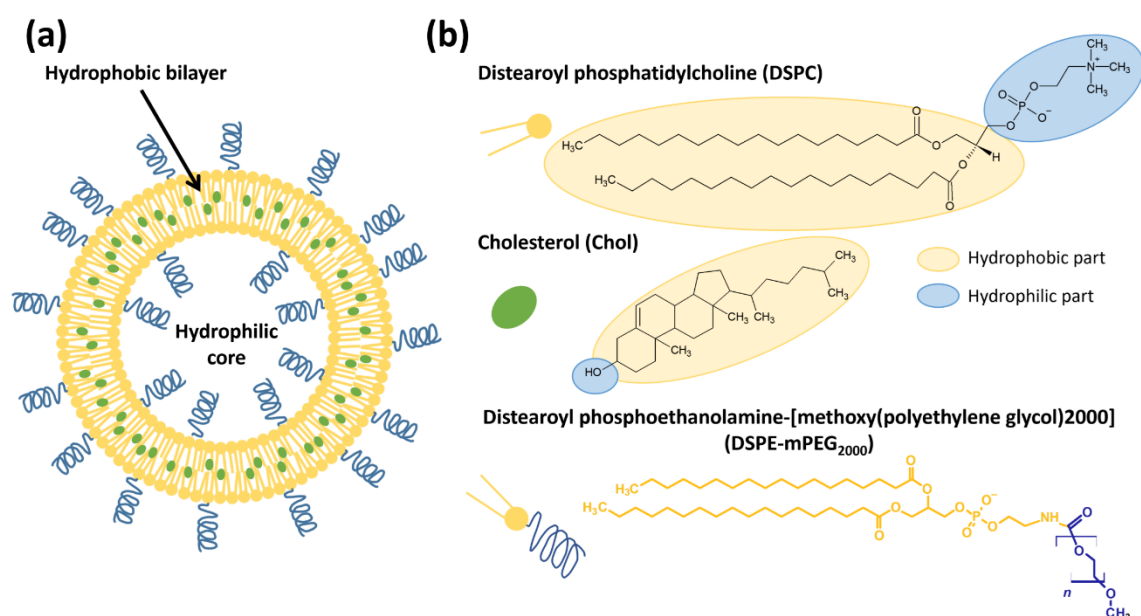


Figure 1.14: Liposome structure and composition. (a) Schematic representation of a liposome with one lipid bilayer. (b) Chemical structure of phospholipids and steroids used to produce liposomes according to Hartwig, *et al.* [228].

The primary component of liposomes are glycerophospholipids (also called phospholipids), such as distearoyl phosphatidylcholine (DSPC). Fatty acid chains forming the hydrophobic “tails” of the phospholipids align to decrease the interaction with the aqueous solution and the hydrophilic heads remain in contact with water, thereby assembling to a lipid bilayer (Figure 1.14). The polarity of the hydrophilic groups and the saturation, symmetry and acyl chain length of the hydrophobic

group affect the liposome characteristics. For example, liposomes containing charged lipids are typically stable during storage, as electrostatic repulsion between the liposomes prevents aggregation, but are less stable in the bloodstream, due to interaction with blood components. To modulate membrane permeability and fluidity, as well as stabilise the liposomal structure, cholesterol (Chol) can be incorporated into the membrane [264]. In addition, surface decoration with polymers, such as poly(ethylene glycol) (PEG), increases stability during storage and delays the clearance process by the mononuclear phagocyte system. PEGylation of liposomes prevents tagging with opsonising proteins, such as complement proteins and fibronectin, and consequently hinders recognition by macrophages and phagocytosis (“stealth” liposomes) [267]. However, PEGylated liposomes can lead to the development of anti-PEG-antibodies, which might result in an accelerated blood clearance but can be prevented using PEG alternatives [268].

Currently, liposomes are applied clinically as drug delivery vesicles for the treatment of cancer, fungal infections, and pain management [264]. In addition, liposomal formulations are being investigated to combat *S. aureus* biofilm infections as nanotraps for bacterial virulence factors by sequestering pore-forming toxins [269], and as drug delivery system for antibacterial agents, such as antibiotics [270]. Liposomes can transport the antibacterial agent into the biofilm, protect the drug from interactions with biofilm matrix components and enzymatic degradation, and prevent the development of resistance by gene transfer [271]. Upon reaching the bacteria, liposomes interact with the bacterial membrane due to similar phospholipid composition, by adsorption [272], endocytosis [273] or fusion, and release the entrapped antibacterial agents intracellularly [274,275].

The properties of the liposomes need to be designed around the delivery of antibacterial agents. Liposomes need to navigate the water channels to reach and penetrate biofilms, restricting their size to below 200 nm [275]. In addition, changes to the surface charge and the fluidity of the liposomes can facilitate the penetration into the biofilm matrix and the interaction with the bacterial membrane. It should be noted that contradictory reports regarding the beneficial effects of PEG-phospholipids incorporation in the liposomal membrane for increased antibacterial activity have been published [276,277]. While it was shown that PEGylated liposomes increased the antibacterial effect against *S. aureus* [276], there was reduced adsorption of PEGylated liposomes to *S. aureus* biofilms [277]. Site-specific delivery of the liposomal formulation can be improved by attaching target ligands to the surface of liposomes or to initiate drug release upon stimuli at the site of action. Modified liposomes can target bacterial or biofilm components through surface attachment of peptides, proteins, antibodies, or aptamers [278]. For example, immunoliposomes were developed with attached antibodies targeting *S. aureus* alpha-toxin [279]. Similarly, short, single-stranded DNA or RNA molecules called aptamers can be attached to PEG polymers and bind either whole *S. aureus* or *S. aureus* proteins with high affinity [280]. Furthermore, the acidic environment in biofilms can be used for targeted delivery of antibiotics encapsulated in pH-responsive liposomes [281].

1.6.1.4 Development of Cu(DDC)₂-liposomes

Multiple Cu(DDC)₂-liposomes were recently developed for cancer treatment, as detailed in Table 1.7. While most developed liposomes are “symmetrical”, several asymmetrical lipid bilayer liposomes were produced that contain a different lipid composition in the outer and inner layer of the membrane. For the development of symmetrical liposomes, Cu(DDC)₂ was either directly mixed with the lipids or DDC⁻ was loaded remotely into Cu²⁺-liposomes. For example, Hartwig, *et al.* [228] developed Cu²⁺-liposomes consisting of DSPC, Chol and distearoyl phosphoethanolamine-

[methoxy(polyethylene glycol)-2000] (DSPE-mPEG₂₀₀₀) (Figure 1.14b). Upon DDC⁻ diffusing through the membrane, Cu(DDC)₂ was formed and trapped within the liposomes, producing Cu(DDC)₂-liposomes [228,282]. The development of an asymmetrical lipid bilayer can promote fusion with cell membranes and facilitate the loading of hydrophilic and hydrophobic drugs [283]. Liu, *et al.* [284] formed an asymmetrical lipid bilayer liposome by producing dioleoyl-3-trimethylammonium methyl sulphate-encapsulated Cu(DDC)₂-NPs, which were decorated with a phospholipid layer containing DSPE-mPEG₂₀₀₀. The asymmetrical lipid bilayer liposomes of Li, *et al.* [285] and Chen, *et al.* [286] consist of a dioleoyl glycerophosphate-encapsulated Cu²⁺ core and a second lipid layer containing DSF, that is released at the target site and forms Cu(DDC)₂ *in situ*. Similarly, Huang, *et al.* [287] incorporated DDC⁻ linked with a ROS-responsive phenylboronic ester into the outer layer of liposomes containing a Cu²⁺ core.

Table 1.7: Liposomes for the delivery of disulfiram (DSF) or diethyldithiocarbamate (DDC⁻) in combination with Cu²⁺.

Reference	DSF/DDC ⁻	Lipid composition	Method
Paun, <i>et al.</i> [288]	Cu(DDC) ₂	DSPC/DSPE-PEG-COOH/Chol	Ethanol injection method
Zheng, <i>et al.</i> [289]	Cu(DDC) ₂	SPC/Chol/DSPE-PEG	Thin-film hydration extrusion method
Wehbe, <i>et al.</i> [282] Hartwig, <i>et al.</i> [228] Marengo, <i>et al.</i> [263]	Cu ²⁺ Cu(DDC) ₂	DSPC/Chol/DSPE-PEG or DSPC/Chol/DSPE-mPEG	Thin-film hydration-extrusion method for production of Cu ²⁺ -liposomes, then remote loading of DDC ⁻ in Cu ²⁺ -liposomes
Liu, <i>et al.</i> [290]	Cu ²⁺ Cu(DDC) ₂	SM/Chol/DSPE-mPEG	
Liu, <i>et al.</i> [284]*	Cu(DDC) ₂	Inner layer: DOPA Outer layer: DOTAP/DSPE-PEG	Reversed phase micro-emulsion followed by thin-film hydration
Li, <i>et al.</i> [285]*	Cu ²⁺ + DSF	Inner layer: DOPA Outer layer: DPPC/Chol/DSPE-mPEG	
Huang, <i>et al.</i> [287]*	Cu ²⁺ + DDC ⁻	Inner layer: DOPA	Reversed phase micro-emulsion followed by mixing with lipids and DSF/DDC ⁻ and solvent removal
Chen, <i>et al.</i> [286]*	Cu ²⁺ + DSF	Outer layer: DOPC/Chol/DSPE-PEG	

DSPC = Distearoyl phosphatidylcholine; Chol = Cholesterol; DSPE-PEG = Distearoyl phosphoethanolamine-(polyethylene glycol); DSPE-PEG-COOH = DSPE-[PEG-carboxylic acid]; DSPE-mPEG = DSPE-[methoxy(PEG)]; SPC = Soybean phosphatidylcholine; SM = Sphingomyelin; DOPA = Dioleoyl glycerophosphate; DOTAP = Dioleoyl-3-trimethylammonium methyl sulphate; DPPC = Dipalmitoyl phosphatidylcholine; DOPC = Dioleoyl phosphocholine.

* Asymmetrical lipid bilayer liposomes

While many new DSF or DDC⁻ and Cu²⁺ nanoparticles were developed over the last 5 years, their activity was almost exclusively investigated in the context of cancer [291]. However, nanoparticles, such as liposomes, have also shown to be a suitable drug delivery system for antibacterial agents in biofilm infections [271]. Despite previously determined antibacterial activity of DSF, alone or in combination with Cu²⁺, against a range of bacterial species in pre-clinical experiments (see Chapter 1.5.3.4), there has been limited translation into clinic due to the problematic administration of the compounds. To date, no DSF or DDC⁻ and Cu²⁺ nanoparticles have been investigated as potential drug delivery system for the treatment of bacterial infections. This is in part due to the challenging administration of the compounds, which will be addressed in this thesis.

1.6.2 Local application for surgical site infections

The development of Cu(DDC)₂-NPs enables the intravenous administration of Cu(DDC)₂ and provides the possibility of targeting infection sites. Nevertheless, systemic application always bears the risk of toxic side effects in different organs and/or rapid clearance. In contrast, a topical application offers the opportunity to deliver high concentrations of antibacterial agents directly to the site of infection, thereby increasing treatment efficacy and reducing side effects. For the topical treatment of SSIs, wound dressings and lavages are mostly used (see Chapter 1.3.2).

1.6.2.1 Topical application of DSF or DDC⁻

Due to the low water solubility of DSF and Cu(DDC)₂, only few topical formulations have been developed thus far. These include eye drops, a nose-to-brain formulation, and dermal formulations, such as emulsions, creams, and membranes as wound dressings. Eye drops were developed for ocular lesions as part of an autoimmune blistering disease by dissolving DSF in hydroxypropyl methylcellulose [292] and for cataract, endotoxin-induced uveitis, and glaucoma by incorporating DSF in cyclodextrins [293-295]. An ion-sensitive nanoemulsion *in situ* gel was developed for intranasal delivery of DSF to the brain. The nanoemulsion consists of an oily core containing DSF that is surrounded by emulsifier, co-emulsifier, and DSPE-PEG. The gelling properties are based on ion-sensitive deacetylated gellan gum that interacts with nasal fluid to improve mucosal absorption and minimise mucociliary clearance. In combination with oral administration of Cu²⁺, the *in situ* forming nanogel inhibited glioblastoma growth *in vivo* [296]. The first established dermal application of DSF is an emulsion combining DSF with benzyl benzoate (Tenutex®) that is used against scabies, as described in Chapter 1.5.3.3 [173,297]. A modified version of the Tenutex® emulsion without benzyl benzoate was recently investigated as candidate for the treatment of skin infections. DSF showed antibacterial activity against *S. aureus* and *Streptococcus pyogenes*. Following exposure to the emulsion, no permeation in the dermis of pig skin was observed but DSF was retained in the first layers of the skin [298]. Furthermore, DSF mixed with medium-chain triglycerides and embedded in base cream (DAC Deutscher Arzneimittelcodex) was applied on irritant contact dermatitis and showed anti-inflammatory properties [299]. Lastly, membranes or fibre scaffolds to cover wounds or lesions can be used to avoid physical damage, balance the microenvironment, act as drug carrier, and promote healing. As topical treatment of cutaneous leishmaniasis, bacterial cellulose membranes loaded with DDC⁻ reduced the parasite load and decreased the lesion size [300]. A biocompatible fibre membrane loaded with DSF was developed as wound dressing and showed antibacterial effects against *E. coli* and *S. aureus* [301].

While some of the developed dermal formulations could be used for SSIs, no topical formulation incorporating DDC⁻ in combination with Cu²⁺ has been developed. Therefore, an alternative drug delivery system for DDC⁻ and Cu²⁺ needs to be designed to facilitate the application on surgical wounds, independent of the wound depth or the presence of an implant, such as a hernia mesh, and to accomplish a prolonged drug delivery.

1.6.2.2 Characteristics of injectable gels

An alternative system for the prolonged delivery of a DDC⁻ and Cu²⁺ liposomal formulation that can be applied on wounds are hydrogels. Hydrogels are three-dimensional polymeric networks with an intrinsic hydrophilic character, formed by one or more polymers covalently and/or physically cross-linked. The chemical and physical properties of the hydrogel, such as biocompatibility, degradation, and environmental responsiveness, are regulated by the composition and preparation method and can be adapted depending on the medical application [302]. However, pre-formed hydrogels are

difficult to administer at surgical sites, especially when the surgery is performed in deep tissue, is minimal invasive or results in an unevenly shaped surgical wound, as the gel cannot adapt to niches within the wound. Injectable hydrogels are a promising approach, as the polymer mixture is injected as a fluid and the hydrogel formation occurs *in situ* under physiological conditions [303,304].

Important factors for the development of an injectable hydrogel are the injectability of the liquid form, the gelation process, the mechanical stability, and the drug release properties (Figure 1.15). These mostly depend on the characteristics of the polymers and the polymer to cross-linking agent ratio. The injectability and the mechanical stability of the gel are determined by the concentration of the cross-linking agent, as it affects the viscosity of the liquid mixture and the density of the hydrogel [302]. Therefore, the concentration of the cross-linking agent requires careful consideration, as the viscosity of the liquid form needs to be low enough to disperse the drug homogeneously and to pass through a canula during injection, and at the same time high enough to form a strong gel depot. Furthermore, the gelation process should not occur in the syringe during the injection process but only at the target site within the body. When the polymer to cross-linking agent ratio is shifted in favour of the cross-linker, the time until sol-gel transition is reduced. Lastly, the release rate of compounds from the gel is dependent on the density and mechanical stability of the gel [303]. With increasing density and mechanical stability of the gel, the release of drugs from the gel is prolonged due to slow diffusion.

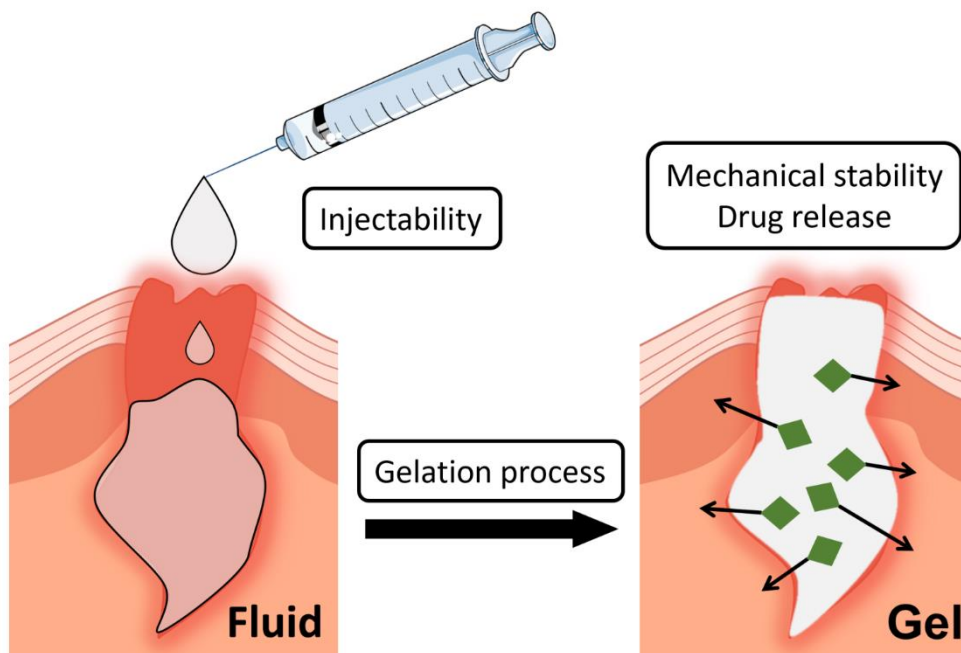


Figure 1.15: Characteristics of an injectable hydrogel. The injectability is dependent on the viscosity and the time until sol-gel transition of the polymer and cross-linker mixture. The gelation process should only occur at the target site after injection. The *in situ* formed hydrogel needs to be mechanically stable and serves as depot system for the release of drugs over a period of time.

1.6.2.3 Polymer dependent gelation process of injectable hydrogels

The characteristics of the polymers determine the cross-linking methods and consequently the gelation process. The polymers can be differentiated into natural (such as chitosan, alginate, hyaluronic acid, collagen, and gelatine) and synthetic (such as PEG, polyacrylamide, and poly(vinyl

alcohol)) [305]. Synthetic polymers have the advantage that their properties can be adapted according to a specific application or to incorporate drugs. Natural polymers, on the other hand, are typically biodegradable and less toxic [303]. Different cross-linking methods of *in situ* forming injectable hydrogels were investigated, such as ionic, chemical, pH-dependent, photoactivated, enzymatic and thermal crosslinking. These have been extensively reviewed by Dimatteo, *et al.* [305], Li, *et al.* [303], Parhi [306] and Zawani and Fauzi [304]. Here, the focus is on thermally annealing hydrogels, as the mediation by temperature is considered constant throughout the body and among patients, thus enabling application at various surgical sites. Thermosensitive hydrogels contain a delicate balance of hydrophobic and hydrophilic components that shift with temperature changes. The liquid or solid state of the hydrogel depends on the low critical solution temperature (LCST). Typically, the polymers are soluble below this temperature. When the temperature rises above the LCST, the polymers collapse into hydrophobic and insoluble structures [307]. Polymers used for thermosensitive hydrogels are poly(N-isopropylacrylamide) and derivatives, poloxamers, PEG-PLGA and chitosan. Based on the limitation for clinical application of the different thermosensitive hydrogel systems described in Table 1.8 and the innate antibacterial activity of chitosan [308], chitosan-based thermosensitive hydrogels are described further.

Table 1.8: Overview of thermosensitive *in situ* forming hydrogels. LCST = lower critical solution temperature. Modified from Huang, *et al.* [307].

Hydrogel	Composition	LCST	Mechanism	Limitation
NIPAAAM	Poly (N-isopropyl acrylamide) (NIPAAAM) is a homopolymer with hydrophilic amide groups and hydrophobic isopropyl groups	32 °C	<u>At low temperatures:</u> the polymer is coiled and flexible. <u>At temperatures above the LCST (32 °C):</u> the polymer shrinks and discharges water	Not biocompatible in clinical application
Poloxamer (PEO-PPO-PEO)	Triblock copolymer of poly (ethylene oxide) (PEO) and poly (propylene oxide) (PPO): hydrophilic ethylene oxide and hydrophobic propylene oxide	Dependent on polymer concentration	<u>At high temperatures:</u> formation of a micelle structure of PEO wrapped around a PPO inner core. <u>Concentration above critical micelle concentration:</u> micelles aggregate and entangle to form gel structure	Undegradable <i>in vivo</i> and diluted by body fluid
PEG-PLGA-PEG	Triblock copolymer of poly[(lactic acid) co-(glycolic acid)] (PLGA) and poly(ethylene glycol)	Dependent on the length of the PLGA and PEG block	<u>At low temperatures:</u> formation of micelles <u>At high temperatures:</u> micelle expansion and aggregation by hydrophobic forces	Diluted by body fluid
Chitosan	(1–4)-2-amino-2-deoxy-β-D-glucan (CS) in combination with β-glycerophosphate	Physiological temperatures	<u>At low temperatures:</u> polyol protective layer around CS chains <u>At high temperatures:</u> polyol layer destroyed and hydrophobic bonds between CS chains	Low mechanical strength

1.6.2.4 Chitosan-based thermosensitive hydrogel

Chitosan (CS) is the partially deacetylated product of the natural polysaccharide chitin that is often found in the shell of marine crustaceans. It is composed of randomly distributed β-(1,4)-linked D-glucosamine and N-acetyl-D-glucosamine (Figure 1.16a), where the high degree of deacetylation

favours biocompatibility. CS is dissolved in acidic aqueous solution with protonated amino groups and the pH is subject to the deacetylation degree and molecular weight, which affects the viscosity and consequently the gelation properties [309].

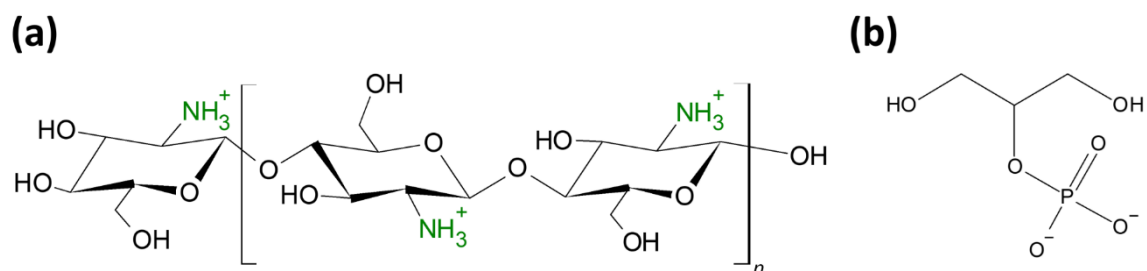


Figure 1.16: Chemical structure of (a) cationic chitosan and (b) beta-glycerophosphate.

As CS alone is not a thermosensitive polymer, the formation of a thermally induced hydrogel that is fluid at ambient temperature and transitions to a gel at high temperatures, requires catalysis by beta-glycerophosphate (β GP). β GP is the conjugate base of phosphoric ester glycerol that is found naturally in the body (Figure 1.16b) [310]. The mechanism behind the formation of the CS- β GP thermosensitive hydrogel is displayed in Figure 1.17. When β GP is added to the acidic CS solution, the pH increases to physiological range, but despite this CS remains in solution because of minimised electrical repulsions between the CS chains, and ionic interactions between the amino groups of CS and the phosphate groups of β GP. At low temperature, enclosed structures of water molecules surround the polymer chains and prevent CS chain aggregation. When the temperature rises, the water is removed by the glycerol moieties and hydrophobic CS chains associate, inducing the formation of the gel [311-313].

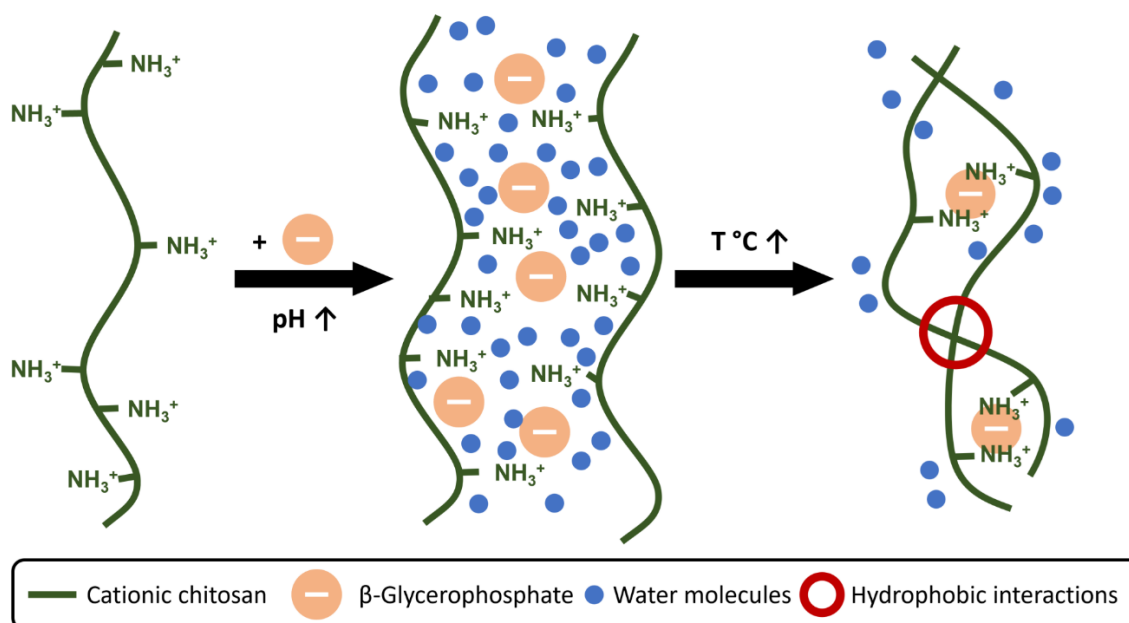


Figure 1.17: Mechanisms behind the temperature sensitive sol-gel transition of cationic chitosan (CS) and β -glycerophosphate (β GP). β GP induces a protective hydration layer that enables CS to remain in solution despite the increased pH and inhibits the immediate precipitation of the gel. With rising temperatures, the hydration layer is removed, and the sol-gel transition is initiated by CS-CS hydrophobic interactions.

1.6 Administration of diethyldithiocarbamate and copper ions on surgical site infections

The time and temperature of CS- β GP sol-gel transition is dependent on the degree of deacetylation of CS, the pH, and concentration of the CS solution and the β GP solution. As most of these factors are connected, finding the appropriate concentration and CS to β GP ratio is crucial. For example, a high pH of the CS- β GP solution can be the result of elevated β GP concentrations, and lead to reduced temperature and accelerated sol-gel transition [311]. A similar effect on the sol-gel transition time is the result of high CS concentrations that are associated with more viscous CS- β GP solutions and increased CS- β GP interactions. The CS- β GP interactions can also be enhanced by increasing the CS deacetylation degree, as more amino groups are available [310]. Ideally, the presence of a drug should not affect the structure of the CS- β GP hydrogel and the gelation process. However, the sol-gel transition can be altered depending on the characteristics of the drug or the nanocarrier. The size or amount of the drug can physically interfere with the formation of polymer crosslinks and anionic and hydrophobic material can interact with CS [314].

CS- β GP hydrogels were developed as drug delivery systems for a range of applications, such as nasal [315], ocular [316], subcutaneous [317], intra-articular [318], and dermal application [319], and for a variety of indications, such as treatment of Alzheimer disease [315], diabetes [317], cancer [320], glaucoma [316], peri-implant inflammation [321], and bacterial infections [322-324]. Furthermore, CS- β GP enable the delivery of vaccines [325], insulin [317], stem cells [326], and nanoparticles [314]. For example, diclofenac was incorporated into CS- β GP as alginate microsphere for intra-articular administration [318], curcumin as cyclodextrins for cutaneous wound infection [319], and doxorubicin in liposomes for cancer treatment [327]. In addition, the injection of a CS- β GP hydrogel containing a liposomal formulation (lipogel) of the antimicrobial drug danofloxacin in mice prolonged the drug release and increased persistence in blood circulation [328]. While the antibacterial activity of the lipogels was not investigated, the pharmacokinetic results warrant the consideration of antibacterial lipogels as treatment for microbial infections. Furthermore, free antibiotics and other antibacterial agents were also incorporated into CS- β GP and showed promising results for the treatment of periodontitis [322,323], osteomyelitis [324], conjunctivitis [329,330], and wound infections [319].

The thermosensitive properties of the CS- β GP hydrogel enable application to essentially all sites in the body, including on SSIs. The hydrogel provides a depot of antibacterial agents, as free drugs or encapsulated in nanoparticles, that can be released over time directly at the site of infection. While applying an antibacterial hydrogel on a surgical wound could prevent the formation of biofilms, the sustained local release of antibacterial agents could also result in the eradication of established biofilms. For example, a vancomycin loaded CS- β GP hydrogel was developed for prevention of SSIs on bone tissue and showed antibacterial activity *in vitro* and *in vivo* against *S. aureus* [331]. However, this would appear to be the only publication of an antibacterial CS- β GP hydrogel for the treatment of SSIs to date.

1.7 Aim of this work

In healthcare settings around the world, up to 20% of surgical sites become infected with antibiotic-resistant bacteria, in particular *S. aureus* and *S. epidermidis* [332]. Staphylococci form biofilms, which enable bacteria to persist in hostile conditions, communicate with each other and become highly resistant to antibiotics. Biofilms require higher concentrations of antibiotics to be eradicated compared to planktonic forms, exceeding the maximum therapeutic dose, and risking toxic effects. Further, the increased tolerance to antibiotics renders the antibiotic therapy insufficient, accelerating antibiotic resistance. This is a major concern, as biofilms are present in at least 80% of SSIs and are a major cause of delayed wound healing [333]. Courses of various antibiotics and surgical removal of the infected tissue are the main interventions to control SSIs, and yet, both are progressively ineffective against staphylococci biofilm infections.

The aim of this project was to develop a novel topical antibiofilm treatment for surgical site infections. Specifically, the antibacterial and antibiofilm activity of DDC⁻ in combination with Cu²⁺ was evaluated as possible repurposed treatment for bacterial infections. Furthermore, a liposomal formulation of DDC⁻ and Cu²⁺ was embedded in a biocompatible, injectable hydrogel, suitable for application on surgical site infections.

Chapter 2 describes DDC⁻ and Cu²⁺ as antibacterial treatment. The antibacterial activity of DDC⁻ was investigated against a range of bacterial species and in combination with different divalent metal ions. The combination of DDC⁻ and Cu²⁺ was further examined against multiple *S. aureus* and *S. epidermidis* strains in planktonic and biofilm form to determine the optimal ratio of the compounds. Moreover, possible synergistic effects with antibiotics, the effect on biofilm formation, and cytotoxic effects of the combination against human cells were evaluated. Lastly, an *in vivo* invertebrate staphylococci-infection model was used to determine efficacy and non-toxicity of DDC⁻ and Cu²⁺.

Chapter 3 considers the combination as potential treatment for surgical site infections. *In vitro* biofilm models mimicking surgical site infections were used to assess the antibacterial effect of DDC⁻ with Cu²⁺. A liposomal formulation comprising Cu²⁺-liposomes and Cu(DDC)₂-liposomes was used to overcome the poor water solubility of Cu(DDC)₂. The *in vitro* antibiofilm activity of the liposomes was evaluated and the *in vivo* efficacy and non-toxicity examined using the previously established invertebrate infection model.

Chapter 4 depicts the incorporation of the liposomal Cu(DDC)₂ + Cu²⁺ formulation in an injectable gel for surgical site infections. A chitosan-β-glycerophosphate hydrogel was chosen as the drug delivery system for the liposomes. Liposomes were lyophilised prior to incorporation into the hydrogel and their colloidal stability determined following storage conditions. The effect of liposome incorporation into the hydrogel on thermosensitive properties and the mechanical stability of the lipogel were characterised using rheological measurements. An estimation of the liposome release from the lipogel was performed and the ability of the hydrogel itself and the lipogel to prevent and eradicate biofilms was examined *in vitro*.

2 Antibacterial activity of diethyldithiocarbamate and copper ions

2.1 Publication: “The combination of diethyldithiocarbamate and copper ions is active against *Staphylococcus aureus* and *Staphylococcus epidermidis* biofilms *in vitro* and *in vivo*”

Statement of authorship

Title of Paper	The combination of diethyldithiocarbamate and copper ions is active against <i>Staphylococcus aureus</i> and <i>Staphylococcus epidermidis</i> biofilms <i>in vitro</i> and <i>in vivo</i>
Publication Status	<input checked="" type="checkbox"/> Published <input type="checkbox"/> Submitted for Publication <input type="checkbox"/> Accepted for Publication <input type="checkbox"/> Unpublished and Unsubmitted work written in a manuscript style
Publication Details	Kaul L, Abdo AI, Coenye T, Krom BP, Hoogenkamp MA, Zannettino ACW, Süß R & Richter K. The combination of diethyldithiocarbamate and copper ions is active against <i>Staphylococcus aureus</i> and <i>Staphylococcus epidermidis</i> biofilms <i>in vitro</i> and <i>in vivo</i> . <i>Front Microbiol.</i> 2022;13:999893; doi:10.3389/fmicb.2022.999893.

Principal author

Name of Principal author	Laurine Kaul			
Contribution to the Paper	Conceptualisation of the project, development of methods, investigation, formal analysis of data, writing – original draft preparation			
Overall percentage (%)	70%			
Certification	This paper reports on original research I conducted during the period of my Higher Degree by Research candidature and is not subject to any obligations or contractual agreements with a third party that would constrain its inclusion in this thesis. I am the primary author of this paper.			
Signature	<table border="1" style="width: 100%;"> <tr> <td style="width: 70%;"></td> <td style="width: 10%;">Date</td> <td style="width: 20%;">08.02.2023</td> </tr> </table>		Date	08.02.2023
	Date	08.02.2023		

Co-author

By signing the Statement of Authorship, each author certifies that:

- i. The candidate’s stated contribution to the publication is accurate (as detailed above).
- ii. Permission is granted for the candidate to include the publication in the thesis; and
- iii. The sum of all co-author contributions is equal to 100% less the candidate’s stated contribution.

2 Antibacterial activity of diethyldithiocarbamate and copper ions

Name of Co-Author	Adrian Abdo		
Contribution to the Paper	Analysis of data, contributed to the result section, review and editing of manuscript		
Signature		Date	08.02.2023

Name of Co-Author	Tom Coenye		
Contribution to the Paper	Methodology and technical assistance, review and editing of manuscript		
Signature		Date	16.02.2023

Name of Co-Author	Bastiaan Krom		
Contribution to the Paper	Methodology and technical assistance, review and editing of manuscript		
Signature		Date	21/2/23

Name of Co-Author	Michel Hoogenkamp		
Contribution to the Paper	Methodology and technical assistance, review and editing of manuscript		
Signature		Date	20/02/2023

Name of Co-Author	Andrew Zannettino		
Contribution to the Paper	Supervision, review and editing of manuscript		
Signature		Date	15/02/23

Name of Co-Author	Regine Süß		
Contribution to the Paper	Conceptualisation of the project, supervision, review and editing of manuscript		
Signature		Date	15/2/2023

Name of Co-Author	Katharina Richter		
Contribution to the Paper	Conceptualisation of the project, investigation, supervision, review and editing of manuscript, corresponding author		
Signature		Date	8/2/23

2.1.1 Publication title page



OPEN ACCESS

EDITED BY
Nagendran Tharmalingam,
Rhode Island Hospital,
United States

REVIEWED BY
Arshad Rizvi,
Emory University,
United States
Soojin Jang,
Korea Pasteur Institute,
South Korea
Charuta Agashe,
Icahn School of Medicine at Mount Sinai,
United States

*CORRESPONDENCE
Katharina Richter
katharina.richter@adelaide.edu.au

SPECIALTY SECTION
This article was submitted to
Antimicrobials, Resistance and
Chemotherapy,
a section of the journal
Frontiers in Microbiology

RECEIVED 21 July 2022
ACCEPTED 18 August 2022
PUBLISHED 09 September 2022

CITATION
Kaul L, Abdo AI, Coenye T, Krom BP,
Hoogenkamp MA, Zannettino ACW,
Süss R and Richter K (2022) The
combination of diethyldithiocarbamate and
copper ions is active against
Staphylococcus aureus and
Staphylococcus epidermidis biofilms *in vitro*
and *in vivo*.
Front. Microbiol. 13:999893.
doi: 10.3389/fmicb.2022.999893

COPYRIGHT
© 2022 Kaul, Abdo, Coenye, Krom,
Hoogenkamp, Zannettino, Süss and
Richter. This is an open-access article
distributed under the terms of the [Creative Commons Attribution License \(CC BY\)](https://creativecommons.org/licenses/by/4.0/). The
use, distribution or reproduction in other
forums is permitted, provided the original
author(s) and the copyright owner(s) are
credited and that the original publication in
this journal is cited, in accordance with
accepted academic practice. No use,
distribution or reproduction is permitted
which does not comply with these terms.

The combination of diethyldithiocarbamate and copper ions is active against *Staphylococcus aureus* and *Staphylococcus epidermidis* biofilms *in vitro* and *in vivo*

Laurine Kaul^{1,2,3}, Adrian I. Abdo^{1,3}, Tom Coenye⁴,
Bastiaan P. Krom⁵, Michel A. Hoogenkamp⁵,
Andrew C. W. Zannettino^{3,6,7}, Regine Süss² and
Katharina Richter^{1,3,8*}

¹Richter Lab, Basil Hetzel Institute for Translational Health Research, Department of Surgery, University of Adelaide, Adelaide, SA, Australia, ²Department of Pharmaceutical Technology and Biopharmacy, Institute of Pharmaceutical Sciences, University of Freiburg, Freiburg, Germany, ³Faculty of Health and Medical Sciences, Adelaide Medical School, University of Adelaide, Adelaide, SA, Australia, ⁴Laboratory of Pharmaceutical Microbiology, Ghent University, Ghent, Belgium, ⁵Department of Preventive Dentistry, Academic Center for Dentistry Amsterdam (ACTA), University of Amsterdam and Vrije Universiteit Amsterdam, Amsterdam, Netherlands, ⁶Precision Medicine Theme, South Australian Health & Medical Research Institute, Adelaide, SA, Australia, ⁷Central Adelaide Local Health Network, Adelaide, SA, Australia, ⁸Institute for Photonics and Advanced Sensing, University of Adelaide, Adelaide, SA, Australia

Staphylococcus aureus and *Staphylococcus epidermidis* are associated with life-threatening infections. Despite the best medical care, these infections frequently occur due to antibiotic resistance and the formation of biofilms of these two bacteria (i.e., clusters of bacteria embedded in a matrix). As a consequence, there is an urgent need for effective anti-biofilm treatments. Here, we describe the antibacterial properties of a combination treatment of diethyldithiocarbamate (DDC) and copper ions (Cu²⁺) and their low toxicity *in vitro* and *in vivo*. The antibacterial activity of DDC and Cu²⁺ was assessed *in vitro* against both planktonic and biofilm cultures of *S. aureus* and *S. epidermidis* using viability assays, microscopy, and attachment assays. Cytotoxicity of DDC and Cu²⁺ (DDC-Cu²⁺) was determined using a human fibroblast cell line. *In vivo* antimicrobial activity and toxicity were monitored in *Galleria mellonella* larvae. DDC-Cu²⁺ concentrations of 8 µg/ml DDC and 32 µg/ml Cu²⁺ resulted in over 80% MRSA and *S. epidermidis* biofilm killing, showed synergistic and additive effects in both planktonic and biofilm cultures of *S. aureus* and *S. epidermidis*, and synergized multiple antibiotics. DDC-Cu²⁺ inhibited MRSA and *S. epidermidis* attachment and biofilm formation in the xCELLigence and Bioflux systems. *In vitro* and *in vivo* toxicity of DDC, Cu²⁺ and DDC-Cu²⁺ resulted in >70% fibroblast viability and >90% *G. mellonella* survival. Treatment with DDC-Cu²⁺ significantly increased the survival of infected larvae (87% survival of infected, treated larvae vs. 47% survival of infected, untreated larvae, *p* < 0.001). Therefore, DDC-Cu²⁺ is a promising new antimicrobial with activity against planktonic and biofilm cultures of *S. epidermidis* and *S. aureus* and low

2.1.2 Abstract

S. aureus and *S. epidermidis* are associated with life-threatening infections. Despite the best medical care, these infections frequently occur due to antibiotic resistance and the formation of biofilms of these two bacteria (i.e., clusters of bacteria embedded in a matrix). As a consequence, there is an urgent need for effective antibiofilm treatments. Here, we describe the antibacterial properties of a combination treatment of DDC⁻ and Cu²⁺ and their low toxicity *in vitro* and *in vivo*. The antibacterial activity of DDC⁻ and Cu²⁺ was assessed *in vitro* against both planktonic and biofilm cultures of *S. aureus* and *S. epidermidis* using viability assays, microscopy, and attachment assays. Cytotoxicity of DDC⁻ and Cu²⁺ (DDC-Cu²⁺) was determined using a human fibroblast cell line. *In vivo* antimicrobial activity and toxicity were monitored in *Galleria mellonella* larvae. DDC-Cu²⁺ concentrations of 8 µg/ml DDC⁻ and 32 µg/ml Cu²⁺ resulted in over 80% MRSA and *S. epidermidis* biofilm killing, showed synergistic and additive effects in both planktonic and biofilm cultures of *S. aureus* and *S. epidermidis*, and synergised multiple antibiotics. DDC-Cu²⁺ inhibited MRSA and *S. epidermidis* attachment and biofilm formation in the xCELLigence and Bioflux systems. *In vitro* and *in vivo* toxicity of DDC⁻, Cu²⁺ and DDC-Cu²⁺ resulted in > 70% fibroblast viability and > 90% *G. mellonella* survival. Treatment with DDC-Cu²⁺ significantly increased the survival of infected larvae (87% survival of infected, treated larvae *vs.* 47% survival of infected, untreated larvae, $p < 0.001$). Therefore, DDC-Cu²⁺ is a promising new antimicrobial with activity against planktonic and biofilm cultures of *S. epidermidis* and *S. aureus* and low cytotoxicity *in vitro*. This gives us high confidence to progress to mammalian animal studies, testing the antimicrobial efficacy and safety of DDC-Cu²⁺.

2.1.3 Introduction

The Gram-positive bacteria *S. aureus* and *S. epidermidis* are notable human pathogens, causing infections ranging from mild skin infection to life-threatening bacteraemia [334,335], endocarditis [336], osteoarticular [337] and medical device related infections [67,338,339]. Furthermore, *S. aureus* is the most common pathogen isolated from surgical site infections [340]. Typically, a bacterial infection is treated with antibiotics [341], e.g., intervention against *S. aureus* infections is executed with either β-lactams, lincosamides, lipopeptides, tetracyclines, glycopeptides, linezolid, or adjunct trimethoprim-sulfamethoxazole therapy [342]. However, these therapies are frequently failing due to the rise of antibiotic resistance and the formation of biofilms [343].

Biofilms are aggregates of bacteria embedded in a protective matrix [31] and are known to be up to 1,000-fold more tolerant to antimicrobial agents compared to planktonic cells [52]. The biofilm matrix, a conglomeration of extracellular polymeric substances, prevents diffusion of the drug and modulates or reduces their metabolic activity [344]. In addition, staphylococci developed penicillin-resistance, including MRSA with rates varying between 1.5 and over 50% in different parts of the world [345-347] and methicillin-resistant *S. epidermidis* with reported rates over 70% [348]. The implications of antimicrobial resistance are devastating, as exemplified by MRSA-associated surgical site infections, which is associated with 2- to 11-fold increased patient mortality [28]. Therefore, *S. aureus* is listed as a high priority pathogen for research and development by the WHO, emphasising the urgency for new treatments [349].

Innovative strategies against *S. aureus* and *S. epidermidis* in the research and development pipeline include newly synthesised compounds [350-352], bacteriophages [353,354], metals [355,356] and repurposed drugs [357,358]. Repurposing of drugs has a history of multiple benefits

and safe uses, allowing for a faster bench to bedside translation and lower drug development costs [127].

An excellent candidate for drug repurposing is DDC⁻. DDC⁻ is the metabolite of disulfiram, an FDA-approved drug for the treatment of chronic alcoholism, which have both recently resurfaced as potentially useful in other medical fields, such as cancer, cocaine addiction, or infections with fungi, parasites, viruses, and bacteria [166]. DDC⁻ showed high antifungal activity against *Candida albicans* and *Candida tropicalis* biofilms [190], reduced the load of *Leishmania braziliensis* [177,300] and, in combination with copper ions (Cu²⁺), showed anti-SARS-CoV-2 activity by targeted oxidation strategies [359]. The suggested mechanisms behind the antimicrobial activity of DDC⁻ is based on chelating vital metals and inhibiting enzymes [195], such as the carbonic anhydrases present in *Legionella pneumophila* [212] or the superoxide dismutase present in *Candida albicans* [192], *Leishmania braziliensis* [177] or *Bacillus anthracis* [196]. An additional advantage of DDC⁻ is a lack of teratogenic, mutagenic, or carcinogenic effects in animal models [360].

Based on the anticancer activity of DDC⁻ being linked to the addition of Cu²⁺ and on limited activity against Gram-positive bacteria of DDC⁻ as monotherapy, DDC⁻ was combined with Cu²⁺ and showed promising results against mycobacteria and streptococci [221,222]. However, the combination of DDC⁻ with metal ions, such as Cu²⁺ has not been further investigated against staphylococci and their biofilms. Thus, this study presents the antibacterial activity of DDC⁻ and Cu²⁺ against planktonic and biofilm *S. aureus* and *S. epidermidis* including *in vivo* safety and efficacy in an infected *Galleria mellonella* model.

2.1.4 Materials and methods

2.1.4.1 Bacterial strains and cell cultures

S. epidermidis ATCC 35984 and ATCC 14990, *S. aureus* ATCC 25923 and ATCC 700699 (also known as MRSA Mu50), and *E. coli* ATCC 25922 were purchased from the American Type Culture Collection (Manassas, VA, United States). Three clinical isolates, i.e., MRSA 1, 2 and 3 were obtained from Adelaide Pathology Partners (Mile End, Australia). *P. aeruginosa* PAO1 was obtained from the School of Molecular Medical Sciences, University of Nottingham (Nottingham, United Kingdom). Unless stated otherwise, bacterial suspensions were prepared by dissolving colonies in 0.9% saline and adjusted to the appropriate McFarland units before being further diluted in broth and incubated at 37 °C under aerobic conditions. Cell culture studies were carried out using control human fibroblast cells (Coriell Cat# GM00038, RRID: CVCL_7271) obtained from the Coriell Institute for Medical Research (Camden, NJ, United States). Unless stated otherwise, all experiments were carried out at least in triplicate and all chemicals, media and supplements were purchased from Sigma-Aldrich (Steinheim, Germany).

2.1.4.2 Minimal inhibitory concentration and checkerboard analysis

The MIC values of DDC⁻ (Carl Roth, Karlsruhe, Germany) and the antibiotics methicillin (Meth), ceftazidime (Ceft), vancomycin (Van), ciprofloxacin (Cip), doxycycline (Doxy), amikacin (Amik) and erythromycin (Ery) towards the staphylococci *S. aureus* and *S. epidermidis* and the Gram-negative bacteria *E. coli* and *P. aeruginosa* were determined in a 96-well microtiter plate using the broth microdilution method [361]. Bacterial suspensions were adjusted to 0.5 ± 0.1 McFarland units, further 1: 100 (v/v) diluted in Mueller-Hinton broth (Thermo Fisher) and mixed with equal volumes of treatments or antibiotics. Treatment concentrations of DDC⁻ ranged from 0.5 to

128 µg/ml and for antibiotics from 0.125 to 64 µg/ml. Furthermore, the broth microdilution method was adapted to investigate the MIC of gallium nitrate hydrate (Ga³⁺), iron sulphate heptahydrate (Fe²⁺), calcium chloride dihydrate (Ca²⁺), magnesium sulphate (Mg²⁺), zinc sulphate heptahydrate (Zn²⁺) and copper sulphate pentahydrate (Cu²⁺) alone or in combination with DDC⁻. The MIC was determined as the lowest concentration of treatment required to inhibit visual growth by the unaided eye [361].

2.1.4.3 Biofilm checkerboard assay

Black 96-well microtiter plates (Costar, Corning Incorporated, NY, United States) were inoculated with 100 µl of a 1: 100 (v/v) diluted *S. aureus*, MRSA or *S. epidermidis* bacterial suspension in nutrient broth, adjusted to 0.5 ± 0.1 McFarland units, and incubated at 37 °C for 24 h on a rotating platform at 70 rpm (3D Gyrotory Mixer, Ratek Instruments, Boronia, Australia). After washing once with sterile 0.9% w/v saline to remove planktonic bacteria, biofilms were exposed to serial dilutions of (i) 1 to 256 µg/ml DDC⁻, (ii) 4 to 256 µg/ml Cu²⁺, (iii) mixture of DDC⁻ and Cu²⁺, (iv) antibiotics with concentrations ranging from 0.5 to 128 µg/ml, including Meth, Ceft, Van, Cip, Doxy, Amik and Ery or (v) a mixture of DDC-Cu²⁺ and antibiotics, and further incubated at 37 °C on a rotating platform for 24 h. After a second washing step to remove the treatments, bacterial viability was assessed by the alamarBlue™ Cell Viability assay [362,363]. Briefly, 100 µl of a freshly prepared 10% (v/v) alamarBlue (Thermo Fisher, MA, United States) solution in nutrient broth (Thermo Fisher) were added to each well and incubated, protected from light, for up to 5 h at 37 °C on a rotating platform. The fluorescence was determined hourly using a FLUOstar OPTIMA plate reader (BMG LABTECH, Offenburg, Germany) at $\lambda_{\text{excitation}}/\lambda_{\text{emission}} = 530/590$ nm. After reaching maximum fluorescence the relative biofilm killing efficacy was quantified according to Equation 2.1.

$$\% \text{ Biofilm killing} = \left(1 - \frac{I_{\text{treatment}} - I_{\text{blank}}}{I_{\text{untreated}} - I_{\text{blank}}} \right) \times 100 \quad (2.1)$$

Antibiofilm activity of the different treatments was determined as percentage of biofilm killing, where the fluorescence intensity of treated and untreated biofilms is represented by $I_{\text{treatment}}$ and $I_{\text{untreated}}$, respectively, and I_{blank} represents the background fluorescence of the 10% (v/v) alamarBlue solution [363].

2.1.4.4 Synergy of compounds

The fractional inhibitory concentration index (FIC_i) was used to describe synergistic, additive, and antagonistic effects between DDC⁻ and Cu²⁺, or between DDC-Cu²⁺ and antibiotics. The equation for calculating the sum of FIC_i (Σ FIC_i) is based on the planktonic and biofilm checkerboard assay and exemplified for planktonic bacteria in Equation 2.2 using the MICs.

$$\Sigma \text{FIC}_i = \frac{\text{MIC}_{\text{ab}}}{\text{MIC}_a} + \frac{\text{MIC}_{\text{ba}}}{\text{MIC}_b} \quad (2.2)$$

MIC_{ab} = MIC of compound a in combination with b; MIC_a = MIC of compound a; MIC_{ba} = MIC of compound b in combination with a; MIC_b = MIC of compound b [177]. Similarly, the equation for biofilms was adapted by replacing the MIC with the minimum biofilm inhibitory concentration, correlating to a minimum of 80% biofilm killing. According to previous literature, the Σ FIC_i was interpreted as: (i) synergy; Σ FIC_i ≤ 0.5, (ii) additivity; Σ FIC_i between 0.5 and 1, (iii) indifference; Σ FIC_i ≥ 1 and ≤ 4, and (iv) antagonism; Σ FIC_i ≥ 4 [364].

2.1.4.5 Confocal microscopy

An 8-well chamber slide (μ -Slide, Ibidi, Gräfelfing, Germany) was inoculated with 300 μ l of a 1: 100 (v/v) dilution of a bacterial suspension of MRSA Mu50 or *S. epidermidis* ATCC 35984 adjusted to 0.5 ± 0.1 McFarland units in nutrient broth and incubated for 24 h at 37 °C on a rotating platform at 70 rpm (3D Gyrotory Mixer, Ritek Instruments, Boronia, Australia). Biofilms were rinsed with phosphate buffered saline, followed by exposure to DDC-Cu²⁺ (8 μ g/ml DDC⁻ + 32 μ g/ml Cu²⁺) or nutrient broth alone for 24 h at 37 °C on a rotating platform. After a second washing step, a 1: 1000 (v/v) dilution of LIVE/DEAD BacLight staining (SYTO 9/propidium iodide; Life Technologies, Scoresby, Australia) was incubated in the dark for 30 min, then imaged by confocal laser scanning microscopy (Olympus FV3000, Shinjuku, Japan) using a 20 \times and 100 \times objective. The excitation/emission wavelengths of the LIVE/DEAD BacLight staining were 488/520 nm and 543/619 nm, respectively. The images were quantified using ImageJ Software (1.53q, NIH, University of Wisconsin, WI, United States). Due to the number of layers of cells in the biofilm and the magnification objective, live/dead cell count was not possible. Instead, measurement of total red and green fluorescence ratio was used to semi-quantitatively calculate the live/dead cell ratio.

2.1.4.6 Prevention of bacterial attachment

The activity of DDC-Cu²⁺ to inhibit bacterial attachment was determined using the xCELLigence real-time cell analysis (RTCA; Agilent, CA, United States). This technology measures the impedance through gold electrode sensors placed on the bottom of each well of the RTCA E-plate 16 (Agilent, CA, United States). When cells attach onto the electrodes, a larger impedance is detected, leading to an increase of the cell index (CI) compared to the baselines.

To measure the baselines, 50 μ l of nutrient broth and 100 μ l of 8 μ g/ml DDC⁻, 32 μ g/ml Cu²⁺, DDC-Cu²⁺ (8 μ g/ml DDC⁻ + 32 μ g/ml Cu²⁺) dissolved in nutrient broth or media alone were added to each well. A bacterial overnight culture in nutrient broth was adjusted to OD₆₀₀ of 0.4 for MRSA Mu50 and *S. epidermidis* ATCC 35984. A 1: 4 (v/v) dilution of the bacterial suspension was added to the appropriate wells. The impedance of the cells was continuously and automatically measured every 15 min for 48 h while statically incubated at 37 °C. Wells with bacterial suspension in broth (100% bacterial attachment), wells with broth alone (background) and wells with compounds in broth (0% bacterial attachment, reflecting the compounds' influence on impedance) were assessed as controls.

2.1.4.7 Bioflux

The Bioflux system (Fluxion, United States) was used to determine inhibition of biofilm growth under flow conditions, as previously described [365]. All media was pre-warmed to 37 °C before use. Bioflux plates were primed with 350 μ l half-strength tryptone soy broth (TSB, BD, Sparks, MD, United States) and inoculated with 70 μ l of a bacterial overnight culture (either MRSA Mu50 or *S. epidermidis* ATCC 35984) adjusted to OD₆₀₀ of 0.2. Following bacterial attachment for 30 min at 37 °C and no flow, bacteria were exposed to either half-strength TSB or half-strength TSB supplemented with DDC-Cu²⁺ (8 μ g/ml DDC⁻ + 32 μ g/ml Cu²⁺) for 24 h at 37 °C under steady nutrient flow (0.5 dyne/cm²). Biofilm growth was monitored through brightfield microscopy (20 \times objective), and images were automatically taken every 15 min.

2.1.4.8 In vitro cytotoxicity

The GM00038 normal human skin fibroblast cell line was cultured in Eagle's Minimum Essential Medium with Earle's salts and non-essential amino acids supplemented with 15% foetal bovine

serum (Biochrom, Berlin, Germany) and 2.2 g/l sodium bicarbonate anhydrous. Fibroblasts were seeded at 5×10^4 cells/100 μ l culture medium per well in black 96-well flat-bottom plates and incubated at 37 °C in 5% CO₂ for 24 h to allow attachment. Cells were separately treated with either 8 μ g/ml DDC⁻, 32 μ g/ml Cu²⁺ or DDC-Cu²⁺ (8 μ g/ml DDC⁻ + 32 μ g/ml Cu²⁺) for 18 h. The effect of the compounds on fibroblast viability was assessed with the CellTiter-Glo[®] Luminescent Viability Assay (Promega Corporation, WI, United States) according to the manufacturer's instructions and luminescence was measured on a FLUOstar OPTIMA plate reader. Equation 2.3 was used to quantify the percentage of fibroblast viability, where the luminescence intensity of treated and untreated fibroblast cells is represented by I_{treatment} and I_{untreated}, respectively, and I_{blank} represents the background luminescence of the CellTiter-Glo[®] reagent.

$$\% \text{ Fibroblast viability} = \left(\frac{I_{\text{treatment}} - I_{\text{blank}}}{I_{\text{untreated}} - I_{\text{blank}}} \right) \times 100 \quad (2.3)$$

2.1.4.9 *In vivo* cytotoxicity and efficacy

Galleria mellonella larvae (Hengelsport De Poorterwere, Ghent, Belgium) were stored in the dark at 13 °C and used within 3 days of receipt. Each treatment group was assigned 30 larvae. Larvae were injected in the last proleg with micro-fine (30 gauge) needle insulin syringes (BD, Franklin Lakes, NJ, United States). Three control groups were included, (i) larvae injected with 0.9% saline (uninfected, untreated control), (ii) larvae injected with treatment (uninfected, treated control to determine treatment toxicity) and (iii) larvae injected with a bacterial suspension (infected, untreated control). To determine treatment efficacy, larvae were injected with a bacterial suspension (either MRSA Mu50 or *S. epidermidis* ATCC 35984) and with DDC⁻, Cu²⁺ or DDC-Cu²⁺. Considering the dilution factor within the larvae, the concentrations of the DDC-Cu²⁺ were increased a 10-fold and based on the average weight of the larvae (250 mg) was determined as 6.4 mg/kg DDC⁻ and 25.6 mg/kg. A total volume of 20 μ l was injected comprising treatment or saline in a 1:1 mix with a bacterial suspension in nutrient broth. The final bacterial density was OD₆₀₀ 0.05. Larvae were housed in petri dishes in the dark at 37 °C and the larvae mortality was monitored daily over 4 days.

2.1.4.10 Statistical analysis

Results were statistically analysed using GraphPad Prism (RRID:SCR_002798) version 9.00 for Windows (GraphPad Software, CA, United States) and statistical significance was determined with an $\alpha = 0.05$. Parametric data (MIC, biofilm killing and cytotoxicity) are represented by the mean \pm standard deviation (SD), which was analysed using one-way analysis of variance (ANOVA) with Dunnett's (for MICs, biofilm checkerboard, microscopy) or Tukey's (for xCELLigence) multiple comparison test for finding statistical differences between treatment groups. *G. mellonella* survival data was analysed using Kaplan–Meier survival curves with significant differences between groups determined by log-rank test, significance was Bonferroni-Holm-corrected for multiple comparisons.

2.1.5 Results

2.1.5.1 Minimal inhibitory concentration

As shown in Table 2.1, DDC⁻ displayed low antibacterial activity against *S. epidermidis* ATCC 35984 with a MIC of 64 µg/ml. To increase the antibacterial activity of DDC⁻, a selection of metal salts was evaluated against *S. epidermidis* ATCC 35984 in the presence or absence of DDC⁻. The MIC of the metal salts alone was 128 µg/ml for Cu²⁺ and above 128 µg/ml for all other metal ions (Table 2.1). In combination with Ga³⁺, Fe²⁺ and Ca²⁺, the MIC of DDC⁻ was not reduced. In contrast, the MIC of DDC⁻ was reduced to 16 µg/ml in the presence of Mg²⁺ and Zn²⁺ and to 1 µg/ml when combined with Cu²⁺ (Table 2.1).

Table 2.1: Minimum inhibitory concentration (MIC) of diethyldithiocarbamate (DDC⁻), metal ions and the combination of both against *S. epidermidis* ATCC 35984.

Metal ion	MIC (µg/ml)	
	DDC ⁻	Metal ion DDC ⁻ (a)-Metal ion (b)
	64	
Ga³⁺	> 128	64/> 128
Ca²⁺	> 128	64/> 128
Fe²⁺	> 128	32/4
Mg²⁺	> 128	16/4
Zn²⁺	> 128	16/4
Cu²⁺	128	1/8

(a) MIC of DDC⁻ in combination with metal ion.

(b) MIC of metal ion in combination with DDC⁻.

Since the DDC⁻ combination with Cu²⁺ resulted in a substantial MIC reduction in *S. epidermidis* ATCC 35984, the MIC of DDC⁻ in the presence or absence of Cu²⁺ was further investigated in a range of bacteria. In *S. aureus*, MRSA and *S. epidermidis*, the MICs of DDC⁻ ranged from 32 to 128 µg/ml. The MIC of DDC⁻ against *E. coli* and *P. aeruginosa* was above 128 µg/ml. The extensive MIC reduction of DDC⁻ in the presence of Cu²⁺ was also observed with other *S. aureus*, MRSA and *S. epidermidis* strains (Table 2.2). Both the MIC of DDC⁻ in the presence of Cu²⁺ and the MIC of Cu²⁺ in the presence of DDC⁻ were reduced in all *S. aureus* and *S. epidermidis* strains tested. Interestingly, the MIC values of the combination were the highest with 4 µg/ml DDC⁻ and 64 µg/ml Cu²⁺ in *S. aureus* ATCC 25923, the most antibiotic susceptible strain, while the MIC values of the combination were lowest, with 0.5 µg/ml DDC⁻ and 2 µg/ml Cu²⁺ in MRSA 2 and MRSA Mu50, the strain with the highest antibiotic MICs. In all strains tested, the lowest concentration of Cu²⁺ required to inhibit *S. aureus* and *S. epidermidis* growth exceeded the lowest DDC⁻ concentration.

Table 2.2: Minimal inhibitory concentration of the antibiotics methicillin (Meth), ceftazidime (Ceft), ciprofloxacin (Cip), vancomycin (Van), doxycycline (Doxy), amikacin (Amik), erythromycin (Ery) and the compounds diethyldithiocarbamate (DDC⁻) and Cu²⁺ towards planktonic *S. aureus*, MRSA, *S. epidermidis*, *E. coli* and *P. aeruginosa*. Antibacterial activity and synergistic effects of the combination of both compounds (DDC-Cu²⁺) against planktonic *S. aureus*, MRSA and *S. epidermidis*. ND = Not determined.

Bacterial strain	MIC (µg/ml)										Synergy	
	Meth	Ceft	Cip	Van	Doxy	Amik	Ery	DDC ⁻	Cu ²⁺	DDC ⁻ (a)- Cu ²⁺ (b)	ΣFICi (c)	Result (d)
<i>S. aureus</i> ATCC 25923		32	0.25	1	≤ 0.125	8	0.5	32	> 128	4/64	1.23	I
MRSA Mu50	> 64	> 64	16	2	4	32	> 64	64	> 128	≤ 0.5/2	0.14*	S
MRSA 1	2	32	0.25	1	≤ 0.125	8	0.25	128	> 128	2/8	0.67	A
MRSA 2		> 64	2	1	≤ 0.125	8	0.5	32	> 128	≤ 0.5/2	0.19*	S
MRSA 3	2	32	0.5	1	≤ 0.125	4	> 64	128	> 128	2/16	0.88	A
<i>S. epidermidis</i> ATCC 14990		8	≤ 0.125	1	≤ 0.125	0.5	≤ 0.125	32	> 128	2/16	0.93	A
<i>S. epidermidis</i> ATCC 35984	64	64	≤ 0.125	1	≤ 0.125	8	> 64	64	128	1/8	0.87	A
<i>E. coli</i> ATCC 25922								> 128	> 128	ND	ND	ND
<i>P. aeruginosa</i> PAO1								> 128	> 128	ND	ND	ND

(a) MIC of DDC⁻ in combination with Cu²⁺.

(b) MIC of Cu²⁺ in combination with DDC⁻.

(c) average of all calculated fractional inhibitory concentration index sums of DDC-Cu²⁺ (ΣFICi) (n=3).

(d) results: synergy (S) ≤ 0.5; additivity (A) > 0.5 to ≤ 1; indifferent (I) > 1.

* ΣFICi values calculated with the lowest concentration of DDC⁻ in combination with Cu²⁺ measured (0.5 µg/ml) and not with MIC.

2.1.5.2 Effect of different DDC⁻ and Cu²⁺ concentrations on biofilms

MRSA and *S. epidermidis* biofilms were exposed to combined treatments of DDC⁻ (1 to 256 µg/ml) and Cu²⁺ (4 to 256 µg/ml). In Figure 2.1, the MRSA Mu50, MRSA 2, *S. epidermidis* ATCC 35984 and *S. epidermidis* ATCC 14990 biofilm killing of different DDC⁻ and Cu²⁺ combination (DDC-Cu²⁺) ratios were compared to the effect of single Cu²⁺ treatment. Overall, treatment with DDC⁻ alone, Cu²⁺ alone and combinations involving Cu²⁺ concentrations below 16 µg/ml resulted in low antibiofilm activity against *S. aureus* and *S. epidermidis* with less than 31.2% biofilm killing, except for Cu²⁺ 256 µg/ml against *S. epidermidis* ATCC 14990 resulting in 70.8% biofilm killing (Figure 2.1d). The highest biofilm killing was 95.8, 99.6, 99.3 and > 99.9% with 256 µg/ml Cu²⁺ in combination with 8 µg/ml DDC⁻ in MRSA Mu50 (Figure 2.1a), MRSA 2 (Figure 2.1b), *S. epidermidis* ATCC 35984 (Figure 2.1c) and *S. epidermidis* ATCC 14990 (Figure 2.1d), respectively. The minimal concentrations of DDC-Cu²⁺ that resulted in above 80.0% biofilm killing were 8 µg/ml DDC⁻ and 16 µg/ml Cu²⁺ in MRSA Mu50 (81.0% biofilm killing, $p \leq 0.001$; Figure 2.1a), 4 µg/ml DDC⁻ and 32 µg/ml Cu²⁺ in MRSA 2 (98.6% biofilm killing, $p \leq 0.001$, Figure 2.1b), 4 µg/ml DDC⁻ and 16 µg/ml Cu²⁺ in *S. epidermidis* ATCC 35984 (85.0% biofilm killing; $p \leq 0.001$; Figure 2.1c) and 8 µg/ml DDC⁻ and 32 µg/ml Cu²⁺ in *S. epidermidis* ATCC 14990 (83.7% biofilm killing, $p \leq 0.01$; Figure 2.1d). Complementing the results obtained against planktonic MRSA and

2 Antibacterial activity of diethyldithiocarbamate and copper ions

S. epidermidis, low antibiofilm activity was observed when DDC⁻ concentrations exceeded Cu²⁺ concentrations, suggesting the importance of a DDC-Cu²⁺ ratio range. The lowest concentration of DDC⁻ and Cu²⁺ with over 80.0% biofilm killing in all strains tested was 8 µg/ml and 32 µg/ml Cu²⁺, therefore this concentration was chosen for further experiments. This concentration was also effective against *S. aureus* ATCC 25923, MRSA 1 and MRSA 3 biofilms (data not shown).

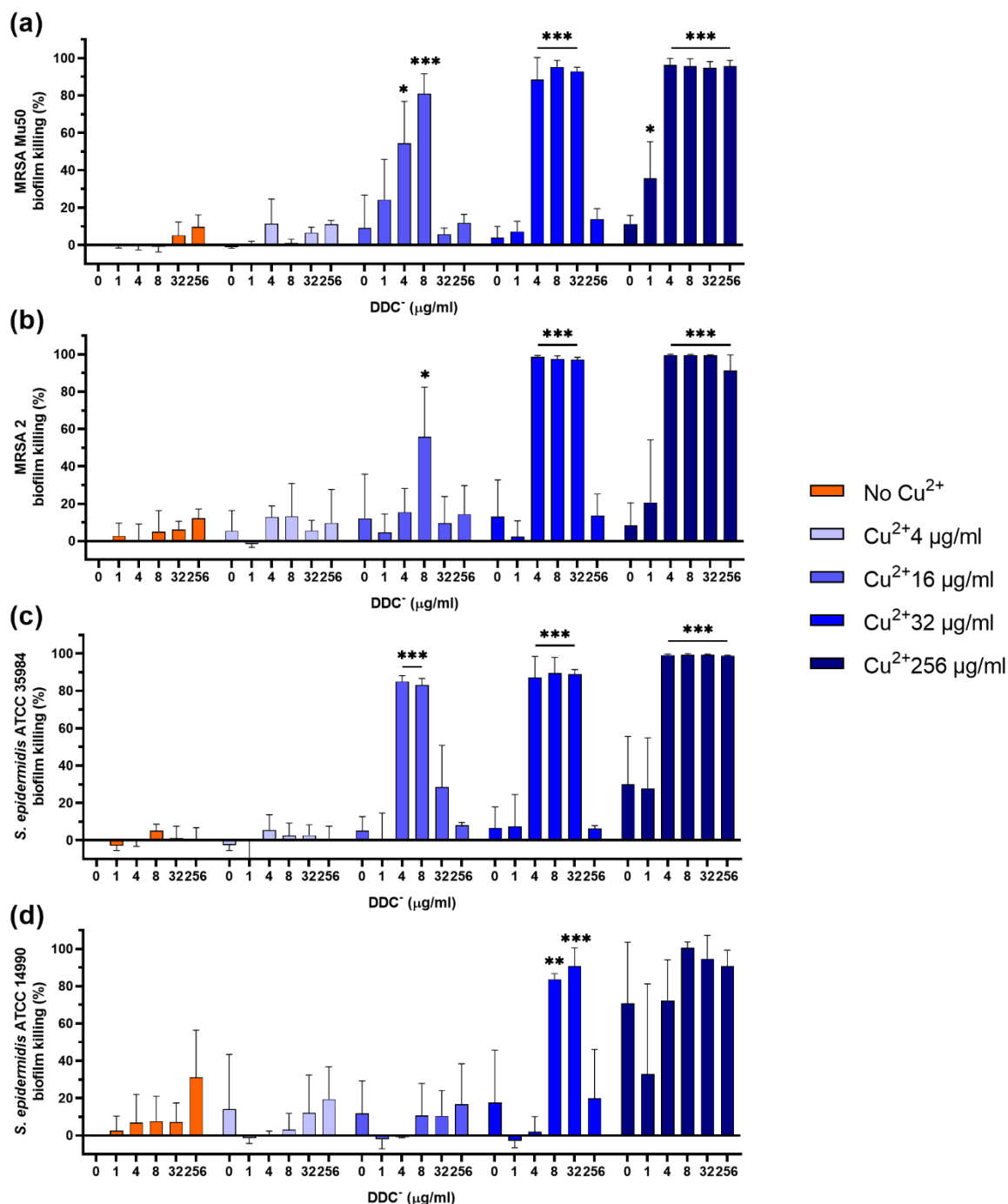


Figure 2.1: Effect of diethyldithiocarbamate (DDC⁻) and Cu²⁺ concentrations (in µg/ml) on the viability of (a) MRSA Mu50, (b) MRSA 2, (c) *S. epidermidis* ATCC 35984 and (d) *S. epidermidis* ATCC 14990 biofilms compared to monotherapy with Cu²⁺ ($n = 3$; * $p < 0.05$; ** $p < 0.01$; *** $p < 0.001$).

2.1.5.3 Synergistic effects of DDC⁻ and Cu²⁺ in combination with different antibiotics

Synergistic and additive effects of DDC⁻ and Cu²⁺ were observed against all planktonic MRSA (ΣFICi : MRSA Mu50 = 0.14; MRSA 1 = 0.67; MRSA 2 = 0.19; MRSA 3 = 0.88) and *S. epidermidis* strains (ΣFICi : *S. epidermidis* ATCC 14990 = 0.93; *S. epidermidis* ATCC 35984 = 0.87), except for *S. aureus* ATCC 25923 (ΣFICi = 1.23; Table 2.2). Against the biofilm form of the same strains, the ΣFICi of DDC-Cu²⁺ was reduced in most strains (Table 2.3). Synergistic effects of the combination were reached against MRSA Mu50 (ΣFICi = 0.26), and additive effects were reached against both *S. epidermidis* strains (ΣFICi : *S. epidermidis* ATCC 14990 = 0.86; *S. epidermidis* ATCC 35984 = 0.58), *S. aureus* ATCC 25923 (ΣFICi = 0.80) and the other MRSA strains (ΣFICi : MRSA 1 = 0.53; MRSA 2 = 0.64; MRSA 3 = 0.66). The synergistic effects of DDC-Cu²⁺ in planktonic MRSA 2 and planktonic and biofilm MRSA Mu50 were not observed in the other MRSA strains tested, which showed additive effects of DDC-Cu²⁺. This difference should be investigated based on the phenotype and genotype of the different strains tested. As the MICs of multiple antibiotics were the highest for MRSA Mu50 and *S. epidermidis* ATCC 35984, respectively, these strains were chosen as representatives for *S. aureus* and *S. epidermidis* in the following experiments.

Table 2.3: Synergistic effects of diethyldithiocarbamate in combination with Cu²⁺ against *S. aureus*, MRSA and *S. epidermidis* biofilms.

Bacterial strain	Synergy	
	ΣFICi (a)	Results (b)
<i>S. aureus</i> ATCC 25923	0.80	A
MRSA Mu50	0.26	S
MRSA 1	0.53	A
MRSA 2	0.64	A
MRSA 3	0.66	A
<i>S. epidermidis</i> ATCC 14990	0.86	A
<i>S. epidermidis</i> ATCC 35984	0.58	A

(a) average of all calculated fractional inhibitory concentration index sums (ΣFICi) (n=3).

(b) results: synergy (S) ≤ 0.5 ; additivity (A) > 0.5 to ≤ 1 ; indifferent (I) > 1 .

The ΣFICi of the DDC-Cu²⁺ combination was further investigated with representatives of different classes of antibiotics against MRSA Mu50 biofilms (Table 2.4). The MRSA Mu50 strain was chosen based on the high antibiotics MICs in the planktonic form and on the biofilms not inhibited by antibiotics at concentrations of 128 $\mu\text{g/ml}$ or lower, except for the tetracycline representative Doxy and the cell wall synthesis inhibitor Van (over 70% biofilm killing with concentrations of 16 $\mu\text{g/ml}$). When the antibiotics were combined with DDC-Cu²⁺, the minimum concentration to kill at least 80% of bacteria within the biofilm, was reduced at least 16-fold, except for the combination of Ery with DDC-Cu²⁺ (no change). In addition, DDC-Cu²⁺ showed additive effect with Amik and the β -lactam antibiotics Meth and Ceft. Synergistic effects were observed when DDC-Cu²⁺ was combined with Cip, Doxy, and Van. However, no difference was observed with Ery.

2 Antibacterial activity of diethyldithiocarbamate and copper ions

Table 2.4: Minimal concentration to kill over 80% biofilm and synergistic effects of antibiotics, diethyldithiocarbamate and Cu²⁺ (DDC-Cu²⁺) and the combination against MRSA Mu50 (n=3).

Treatment	Minimal concentration to kill over 80% biofilm (µg/ml)			Synergy	
	Antibiotic	DDC-Cu ²⁺	Antibiotic ^(a) /DDC-Cu ²⁺ ^(b)	ΣFICi ^(c)	Results ^(d)
DDC-Cu²⁺		4-16			
Meth	> 128		8/0.5-2	0.63	A
Ceft	> 128		8/0.5-2	0.71	A
Van	16		0.5/0.5-2	0.50	S
Cip	> 128		4/0.5-2	0.45	S
Doxy	16		1/0.5-2	0.44	S
Amik	> 128		1/0.5-2	0.55	A
Ery	> 128		> 128/4-16	1.43	I

^(a) lowest concentration of antibiotic in combination with DDC-Cu²⁺.

^(b) lowest concentration of DDC-Cu²⁺ in combination with antibiotic.

^(c) average of all calculated fractional inhibitory concentration index sums (ΣFICi) (n=3).

^(d) results: synergy (S) ≤ 0.5; additivity (A) > 0.5 to ≤ 1; indifferent (I) > 1.

2.1.5.4 Visualising biofilms after DDC-Cu²⁺ treatment

Confocal microscopy images of the untreated control of *S. epidermidis* ATCC 35984 biofilms were characterised by a large, dense, and undisturbed biofilm with mostly viable bacteria (Figure 2.2a). After exposure to DDC-Cu²⁺ (8 µg/ml DDC + 32 µg/ml Cu²⁺), the biofilm structure was disturbed and less dense. In addition, an increase in number of red, indicating dead bacteria was observed (Figure 2.2b). Similar observations were made in MRSA Mu50 biofilm images (Supplementary Figure S2.1). The quantification of the fluorescence showed a significant decrease of the green/red ratio between untreated biofilm and biofilm treated with DDC-Cu²⁺ (Figure 2.2c). This ratio was also observed when using a 100 × objective on a DDC-Cu²⁺ treated *S. epidermidis* ATCC 35984 biofilm that showed dead bacteria with only few viable bacteria (Figure 2.2d).

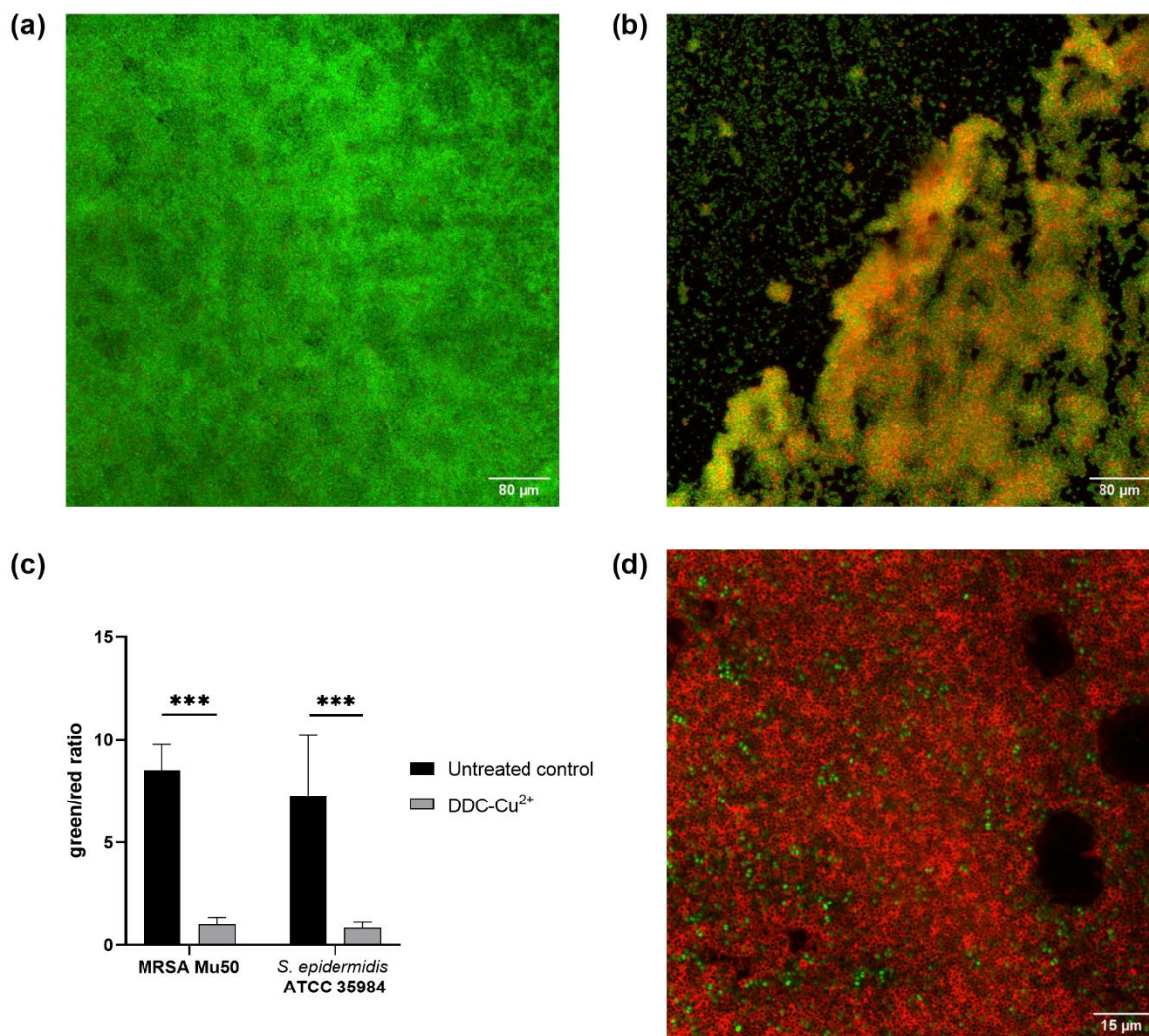


Figure 2.2: Comparison of stained MRSA Mu50 and *S. epidermidis* ATCC 35984 biofilms with LIVE/DEAD BacLight staining after treatment with 8 µg/ml diethyldithiocarbamate and 32 µg/ml Cu²⁺ (DDC-Cu²⁺). Confocal microscopy images results: green = viable bacteria; red = dead bacteria. **(a)** Untreated *S. epidermidis* ATCC 35984 biofilm at 20×. *S. epidermidis* ATCC 35984 biofilm after treatment with DDC-Cu²⁺ at **(b)** 20 × and **(d)** 100 ×. **(c)** Quantification of images as green/red ratio of untreated control (black) and treatment with DDC-Cu²⁺ (grey) of MRSA and *S. epidermidis* ATCC 35984 biofilms ($n = 3-8$; *** $p < 0.001$).

2.1.5.5 DDC-Cu²⁺ inhibits bacterial attachment

Prevention of biofilm growth was examined in MRSA Mu50 (Figure 2.3**Figure 2.3a,b**) and *S. epidermidis* ATCC 35984 (Figure 2.3c,d) with the xCELLigence RTCA system over 48 h. A high cell index (CI) correlates with bacteria attaching to the gold electrodes located at the bottom of the well [366]. For both *S. aureus* and *S. epidermidis*, the untreated control showed a high increase in CI within the first 12 h, reaching a CI of 0.32 in MRSA Mu50 (Figure 2.3a) and 0.25 in *S. epidermidis* ATCC 35984 (Figure 2.3c), before steadily increasing at a slower rate to reach 0.50 in MRSA Mu50 and 0.45 in *S. epidermidis* ATCC 35984 after 48 h. Monotherapy of DDC⁻ (8 µg/ml) and Cu²⁺ (32 µg/ml) resulted in a faster CI increase compared to the untreated control, reaching a maximum after 5 h in MRSA Mu50 (CI: DDC⁻ = 0.40; Cu²⁺ = 0.19) and 6 h in *S. epidermidis* ATCC 35984 (CI: DDC⁻ = 0.35; Cu²⁺ = 0.18). The fast CI increase of DDC⁻ or Cu²⁺ treated bacteria should not be a result of DDC⁻ or Cu²⁺ salts interacting with the gold electrodes or the impedance, as these were assessed with the baselines. The initial increased bacterial attachment when treated with DDC⁻ or Cu²⁺ can be explained by the subinhibitory concentration of DDC⁻ or Cu²⁺ alone used in this

experiment. Treatment with DDC⁻ and Cu²⁺ can induce oxidative stress and the production of reactive oxygen species in *S. aureus*, which play a role in the control of different cellular processes, such as biofilm formation [367]. Treatment with DDC⁻ alone showed no significant difference from the mean CI (12–48 h) compared to the untreated control (CI: 0.44 MRSA Mu50 and 0.38 *S. epidermidis* ATCC 35984). Treatment with Cu²⁺ alone resulted in approximately half the CI compared to untreated control (CI: 0.22 MRSA Mu50 and 0.18 *S. epidermidis* ATCC 35984), translating in less bacteria attaching to the bottom of the well and forming biofilms. Lastly, treatment with DDC-Cu²⁺ (8 µg/ml DDC⁻ + 32 µg/ml Cu²⁺) resulted in a CI of 0 after 12 h and a mean CI of 0.04 and 0.03 after 48 h in MRSA Mu50 (Figure 2.3b) and *S. epidermidis* ATCC 35984 (Figure 2.3d), respectively. Therefore, treatment with DDC-Cu²⁺ prevented the attachment of bacteria over 48 h, which can be a result of high bacterial killing at the tested concentrations. To determine if bacterial killing was responsible for prevention of bacterial attachment, lower DDC-Cu²⁺ concentrations can be investigated.

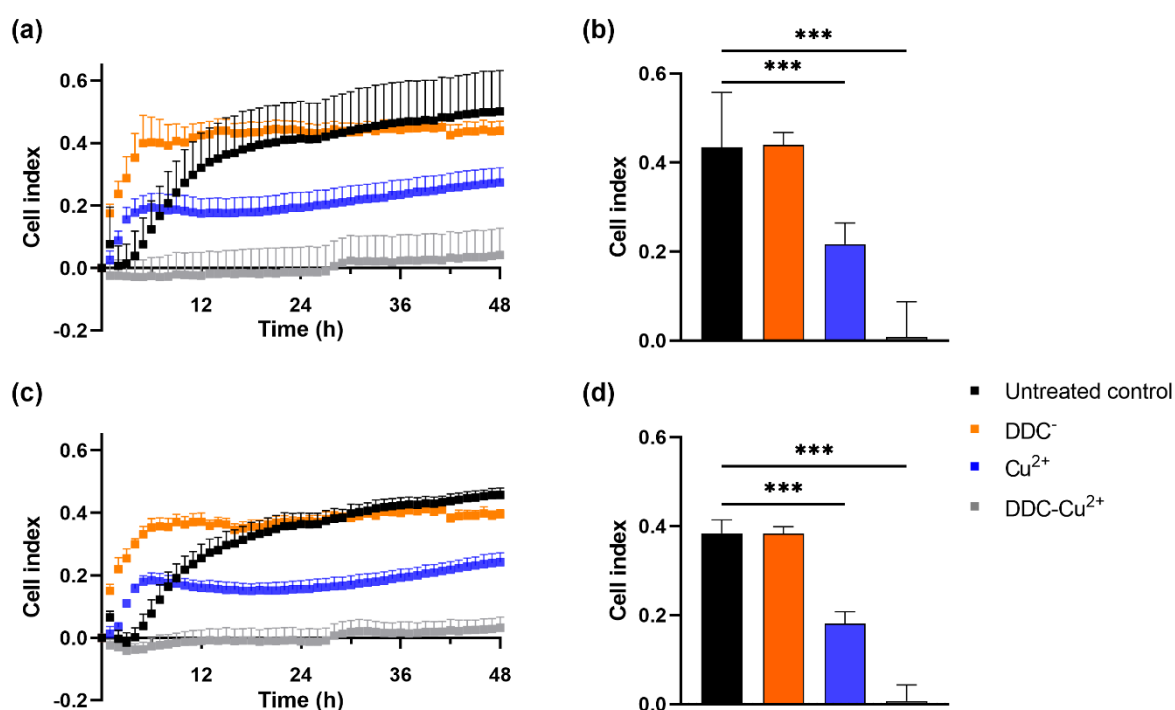


Figure 2.3: Effect of 8 µg/ml diethyldithiocarbamate (DDC⁻; orange), 32 µg/ml Cu²⁺ (blue) and combined DDC-Cu²⁺ (grey) on (a) the cell index of MRSA Mu50 and (c) *S. epidermidis* ATCC 35984 over 48 h compared to the untreated control (black). Comparison of the mean cell index between 12 and 48 h for each treatment of (b) MRSA Mu50 and (d) *S. epidermidis* ATCC 35984 ($n > 3$; *** $p < 0.001$).

2.1.5.6 DDC-Cu²⁺ inhibits biofilm growth

Similar results were observed with the Bioflux system (Figure 2.4). In the untreated control, under constant nutrient flow, MRSA Mu50 bacteria started to aggregate within 8 h, formed biofilms within 16 h that continuously increased in size within 24 h (Figure 2.4, top time lapse). When DDC-Cu²⁺ was added to the constant nutrient flow, inhibition of biofilm growth was achieved over 24 h (Figure 2.4; bottom time lapse. Supplementary File S2.2: Video footage). Similar observations were made in *S. epidermidis* ATCC 35984 biofilms (data not shown).

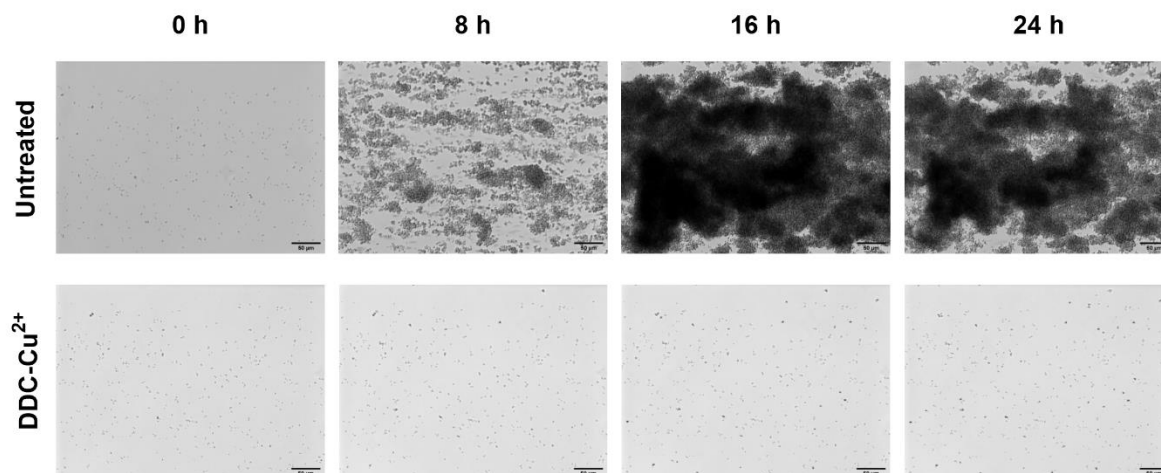


Figure 2.4: Monitoring of MRSA Mu50 biofilm formation over 24 h when left untreated or treated with a combination of 8 µg/ml diethyldithiocarbamate and 32 µg/ml Cu^{2+} combination (DDC- Cu^{2+}) using the Bioflux system. Scale bar represents 50 µm.

2.1.5.7 Cytotoxicity of DDC- Cu^{2+} *in vitro*

The *in vitro* cytotoxicity of the compounds was investigated in fibroblast cells over 18 h (Figure 2.5a). Monotherapy with DDC⁻ and Cu^{2+} showed 70 and 94% fibroblast viability, respectively. Treatment with DDC- Cu^{2+} resulted in 75% fibroblast viability, showing no difference compared to DDC⁻ monotherapy.

2.1.5.8 Toxicity and efficacy of DDC- Cu^{2+} *in vivo* using *Galleria mellonella* larvae

To investigate potential toxic treatment effects *in vivo*, *G. mellonella* larvae were injected with DDC⁻, Cu^{2+} , DDC- Cu^{2+} or vehicle control (saline) and the survival was monitored over 4 days. DDC⁻, Cu^{2+} and DDC- Cu^{2+} showed similar survival rates as the vehicle control, indicating no treatment toxicity in *G. mellonella* (Figure 2.5b).

To assess the antimicrobial activity of DDC- Cu^{2+} *in vivo*, the survival of MRSA- or *S. epidermidis*-infected *G. mellonella* was examined over 4 days. In infected larvae, treatment with DDC⁻ or Cu^{2+} resulted in a poor survival rate, similar to the vehicle control for both MRSA- and *S. epidermidis*-infected *G. mellonella* ($p > 0.05$; Figure 2.5c,d, respectively). However, MRSA-infected and DDC- Cu^{2+} treated larvae, displayed a significantly higher survival rate of 87% (26/30 larvae) compared to MRSA-infected, vehicle control larvae that showed 47% survival (14/30 larvae, $p = 0.0004$; Figure 2.5c). Moreover, the survival rate of MRSA-infected, DDC- Cu^{2+} treated larvae was significantly higher compared to treatment with DDC⁻ alone (9/30 larvae; $p = 0.0003$) or Cu^{2+} alone (14/30 larvae; $p = 0.0003$). Similar results were found in *S. epidermidis*-infected *G. mellonella*, which showed a significantly higher survival rate of 80% (24/30 larvae) for *S. epidermidis*-infected, DDC- Cu^{2+} treated larvae compared to 47% survival (14/30 larvae) for *S. epidermidis*-infected, vehicle control larvae ($p = 0.0152$; Figure 2.5d). Survival of *S. epidermidis*-infected, DDC- Cu^{2+} treated *G. mellonella* (26/30 larvae) was also significantly higher compared to mono treatment with DDC⁻ (15/30 larvae; $p = 0.0152$) or Cu^{2+} (9/30 larvae; $p = 0.0003$).

2 Antibacterial activity of diethyldithiocarbamate and copper ions

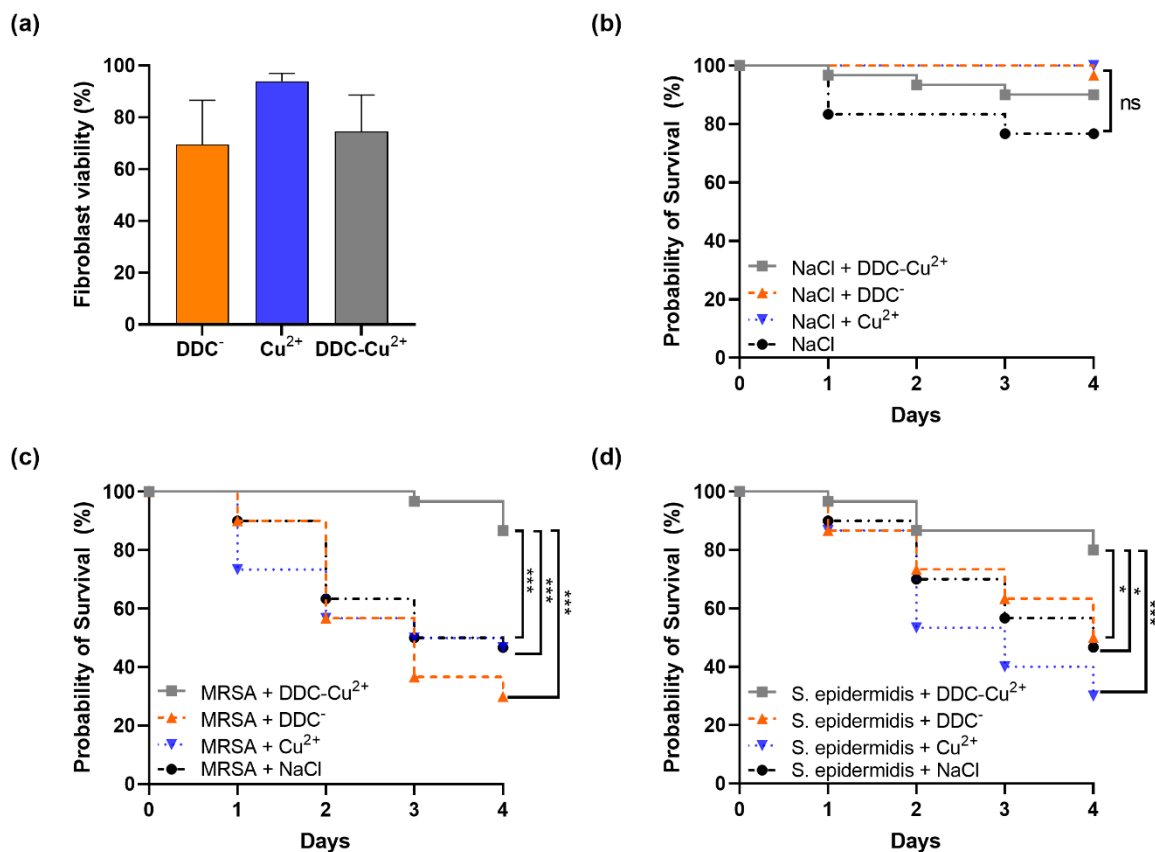


Figure 2.5: Effect of diethyldithiocarbamate [DDC⁻; orange; 8 µg/ml (a), 6.4 mg/kg (b–d)], Cu²⁺ [blue; 32 µg/ml (a), 25.6 mg/kg (b–d)] and DDC-Cu²⁺ (grey) on (a) fibroblast viability ($n = 3$), on (b) probability of *Galleria mellonella* survival (30/group; $n = 120$), on the probability of survival of *Galleria mellonella* infected with (c) MRSA Mu50 (30/group; $n = 120$), and (d) infected with *S. epidermidis* ATCC 35984 (30/group; $n = 120$; ns = not significant; * $p < 0.05$; *** $p < 0.001$).

2.1.6 Discussion

DDC⁻ is the metabolite of disulfiram, an FDA-approved drug for the oral treatment of chronic alcoholism, that has been previously investigated for its activity against fungi [190,192], parasites [177,300] and bacteria [194,196-198,221]. In the current study, DDC⁻ was repurposed and combined with Cu²⁺ for pre-clinical validation as a novel antibacterial treatment. Confirming previous results, DDC⁻ showed limited antibacterial activity against *S. aureus* and *S. epidermidis*, with MICs ranging from 16 to above 32 µg/ml and no growth inhibition of Gram-negative bacteria with MICs above 64 µg/ml. The lack of antibacterial activity of DDC⁻ against *E. coli* and *P. aeruginosa* was explained by the elevated presence of glutathione in Gram-negative bacteria. Cellular glutathione interacts with DDC⁻ and disulfiram by thiol-disulphide exchange reaction [196,198]. While monotherapy with disulfiram showed antibacterial and antibiofilm activity against *S. aureus* *in vitro* and *in vivo* and synergised with multiple antibiotics [148,198], these results were not observed with the *in vivo* formed metabolites of disulfiram [196]. As disulfiram is hypothesised to form disulphides with thiophilic residues of bacterial cofactors, metabolites, and enzymes [197,198], the lack of antibacterial activity of DDC⁻ and other metabolites can be explained by lack of thiol-disulphide exchange. In addition, disulfiram and DDC⁻ differentiate in their chemical and physical properties [360]. While disulfiram shows poor water solubility and physiological instability, therefore limiting local clinical applications [301], DDC⁻ is highly water

soluble [360], a labile molecule and a very strong metal chelator [164]. Specifically, Cu^{2+} was investigated, as disulfiram dissociates in the presence of Cu^{2+} , to form DDC^- , which chelates the metal ion and forms the stable $\text{Cu}(\text{DDC})_2$ complex that can be visualised by a colour change [221] and has been shown to result in anticancer activity [368].

Dalecki, *et al.* [221] were the first to reveal that disulfiram and DDC^- displayed antimycobacterial effects only in the presence of Cu^{2+} , as the presence of iron and zinc ions did not increase the antimicrobial activity of DDC^- against *Mycobacterium tuberculosis*. In addition, 90% of *Mycobacterium tuberculosis* inhibition occurred with 0.3 μM disulfiram, equivalent to 0.6 μM DDC^- and 0.3 μM Cu^{2+} , which is consistent with the molar ratio of 2:1 and consequently the formation of the $\text{Cu}(\text{DDC})_2$ complex [221]. Based on these results, Saputo, *et al.* [225] investigated the effect of disulfiram with Cu^{2+} on *Streptococcus mutans* and observed a reduction of disulfiram MIC from 16 $\mu\text{g}/\text{ml}$ to 4 $\mu\text{g}/\text{ml}$ (equivalent to 8 $\mu\text{g}/\text{ml}$ DDC^-) in the presence of 106.6 $\mu\text{g}/\text{ml}$ Cu^{2+} . The concentration of disulfiram required to inhibit *S. mutans* biofilm formation was even lower with 2 $\mu\text{g}/\text{ml}$ (equivalent to 4 $\mu\text{g}/\text{ml}$ DDC^-) in the presence of 106.6 $\mu\text{g}/\text{ml}$ Cu^{2+} , resulting in synergistic effects of disulfiram and Cu^{2+} against both the planktonic and biofilm forms. We obtained comparable results against *S. aureus* and *S. epidermidis*, with concentrations as low as 0.5 $\mu\text{g}/\text{ml}$ DDC^- and 2 $\mu\text{g}/\text{ml}$ Cu^{2+} against planktonic MRSA Mu50 and 4 $\mu\text{g}/\text{ml}$ DDC^- and 16 $\mu\text{g}/\text{ml}$ Cu^{2+} against biofilm MRSA Mu50, respectively, reaching synergistic effects in both forms. In contrast to the concentrations required for the antimycobacterial activity, the Cu^{2+} concentrations necessary to enhance the activity of DDC^- against *S. mutans*, *S. aureus* and *S. epidermidis* exceeded the DDC^- concentration. This concentration-dependent antibacterial activity was also observed by Menghani, *et al.* [222] against *Streptococcus pneumoniae*.

The concentrations of DDC^- and Cu^{2+} play an important role in the proposed mode of action for the antibacterial activity of DDC^- - Cu^{2+} . The mechanism of DDC^- can in part be explained by inhibition of the *S. aureus* carbonic anhydrase [214] and the chelation and extraction of required metal cofactors, including Cu^{2+} from metallo-enzymes, such as superoxide dismutase, rendering bacteria more susceptible to oxidative stress [196]. In addition, at high levels Cu^{2+} is toxic by the generation of reactive oxygen species through the $\text{Cu}^+/\text{Cu}^{2+}$ redox cycle and by competing with other metals at the enzymatic binding sites, leading to the inactivation and oxidation of free thiol groups of various proteins [369,370]. Therefore, bacteria have developed mechanisms to regulate the intracellular copper concentration and to evade copper induced toxicity, staphylococci have efflux systems in form of a P1-type ATPase transporter, copper-binding chaperones and copper-responsive regulators [371], explaining the low antimicrobial activity of Cu^{2+} with a MIC above 128 $\mu\text{g}/\text{ml}$.

To explain the mode of action behind the antimycobacterial activity of DDC^- and Cu^{2+} , Dalecki, *et al.* [221] proposed a Trojan Horse model, where the $\text{Cu}(\text{DDC})_2$ complex transports Cu^{2+} into the cytoplasm, thereby protecting Cu^{2+} from the bacterial copper resistance mechanisms, which in turn, allows access to targets that usually are not available to free Cu^{2+} [221]. However, in the present study the concentrations closest to corresponding to the $\text{Cu}(\text{DDC})_2$ complex, 8 $\mu\text{g}/\text{ml}$ DDC^- with 4 $\mu\text{g}/\text{ml}$ Cu^{2+} and 32 $\mu\text{g}/\text{ml}$ DDC^- with 16 $\mu\text{g}/\text{ml}$ Cu^{2+} , resulted in less than 25% *S. aureus* and *S. epidermidis* biofilm killing. Therefore, the antibiofilm activity of DDC^- and Cu^{2+} against *S. aureus* and *S. epidermidis* could not exclusively be associated to the $\text{Cu}(\text{DDC})_2$ -complex. The lowest concentration of the mix leading to a statistical increase in *S. aureus* and *S. epidermidis* biofilm killing compared to monotherapy with Cu^{2+} was 8 $\mu\text{g}/\text{ml}$ DDC^- in combination with 32 $\mu\text{g}/\text{ml}$ Cu^{2+} . Hence, the antibacterial activity of DDC^- - Cu^{2+} against *S. aureus* and *S. epidermidis* seems to be based on the formation of the $\text{Cu}(\text{DDC})_2$ complex and an excess of free Cu^{2+} . Based on these results,

we hypothesize that the $\text{Cu}(\text{DDC})_2$ complex inhibits at least one of the copper homeostasis components such as the efflux transporter, allowing for the additional Cu^{2+} to accumulate within the bacteria and cause copper induced toxicity (Figure 2.6). In addition, the extensive inhibition of MRSA biofilm attachment and aggregation by DDC-Cu^{2+} observed with the xCELLigence and the Bioflux systems depended on the combination of DDC^- and Cu^{2+} and can be caused by excess Cu^{2+} that represses the expression of positive biofilm formation regulators, such as *agr* and *sae* [369].

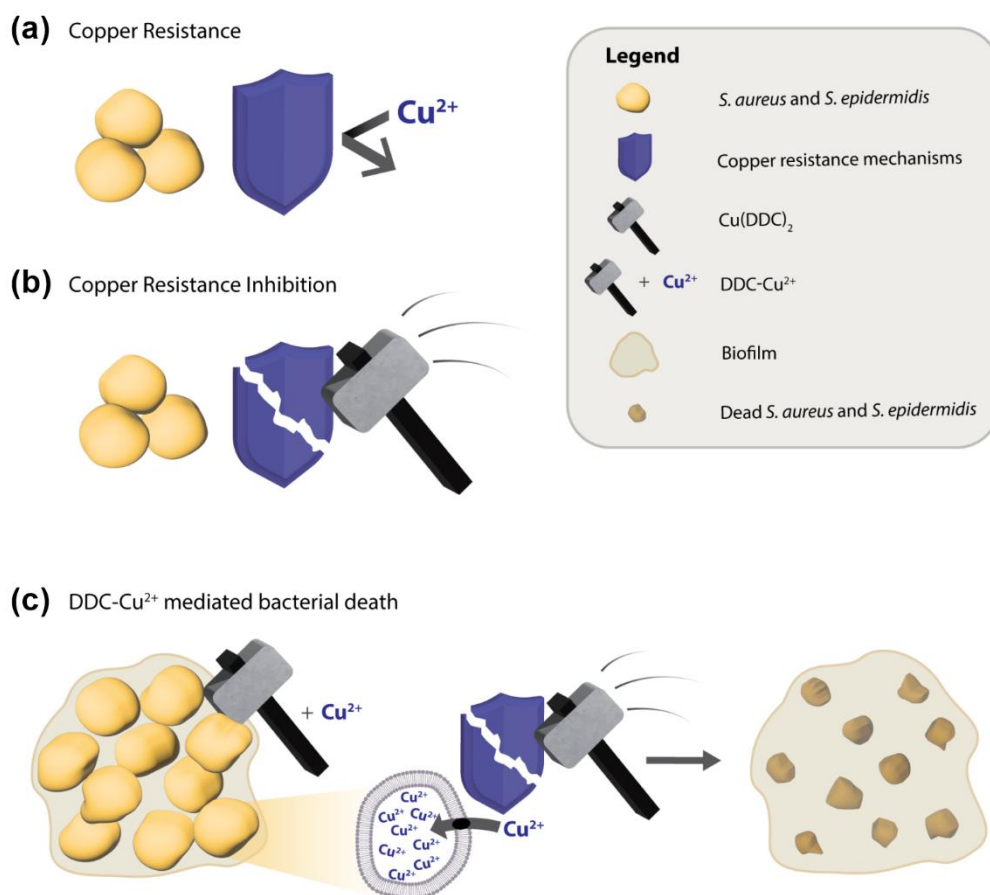


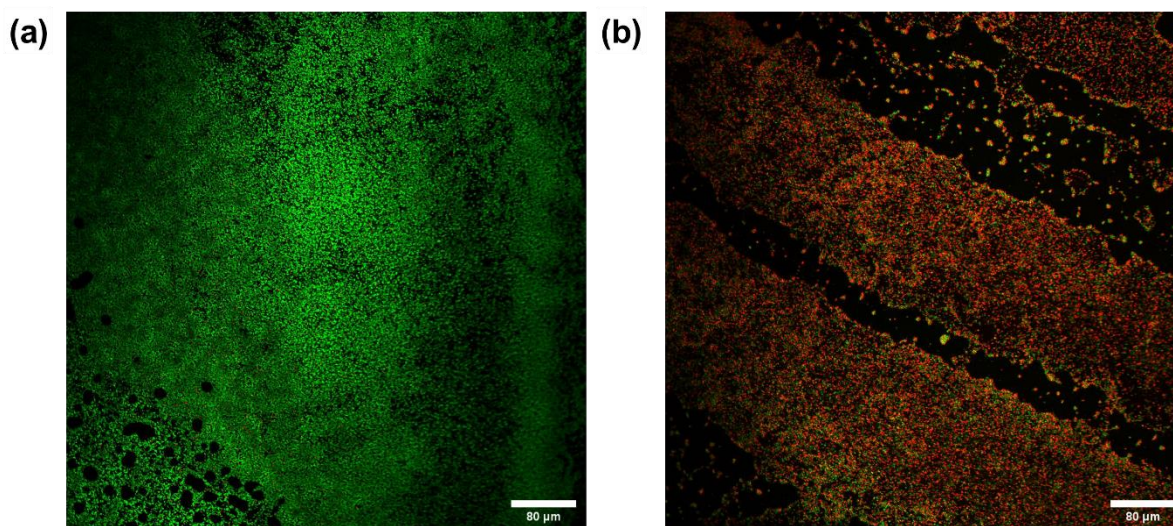
Figure 2.6: Putative diethyldithiocarbamate and copper mode of action against *S. aureus* and *S. epidermidis*. **(a)** The antibacterial activity of Cu^{2+} is limited by copper resistance mechanisms of bacteria. **(b)** The $\text{Cu}(\text{DDC})_2$ complex inhibits the bacterial copper resistance mechanism but does not kill bacteria. **(c)** The combination of $\text{Cu}(\text{DDC})_2$ complex and excessive Cu^{2+} (called DDC-Cu^{2+}) effectively kills bacteria, as the $\text{Cu}(\text{DDC})_2$ complex inhibits the copper resistance mechanisms, allowing for the excess Cu^{2+} to increase copper induced toxicity.

While the DDC-Cu^{2+} combination of 8 $\mu\text{g/ml}$ DDC^- and 32 $\mu\text{g/ml}$ Cu^{2+} inhibited planktonic *S. aureus* and *S. epidermidis* growth and biofilm formation, the same concentrations showed low cytotoxic effects against fibroblasts. As antimicrobial and cytotoxic results obtained *in vitro* do not always accurately predict activity under *in vivo* conditions [372], both the antibacterial activity and the toxicity of DDC-Cu^{2+} was investigated using the *G. mellonella* model. These larvae have been shown to be good models to assess the safety and efficacy of antimicrobial agents against *S. aureus* [372-374]. The high survival rate of uninfected, treated larvae confirmed the non-toxicity of DDC-Cu^{2+} and the significant increase of survival of MRSA- and *S. epidermidis*-infected, DDC-Cu^{2+} treated *G. mellonella* confirmed the *in vitro* antibacterial activity. To the best of our knowledge,

this is the first study to report the antibacterial activity and non-toxicity of DDC⁻ in combination with Cu²⁺ in the *G. mellonella* model. The promising results obtained with the *G. mellonella* model pre-screening experiment increases the confidence in the performance of Cu(DDC)₂ and excess Cu²⁺ to progress to preclinical mammalian models. A pharmaceutical development of the DDC-Cu²⁺ combination is ongoing to provide a drug delivery platform for the treatment of infected wounds and for surgical applications. A DDC-Cu²⁺ formulation has potential to synergistically enhance standard-of-care with oral or topical antibiotics and reduce the pressure on resistance development.

In conclusion, the combination of DDC-Cu²⁺ showed considerable *in vitro* antimicrobial activity against planktonic and biofilm cultures of *S. aureus* and *S. epidermidis*. By enhancing multiple antibiotic classes, preventing biofilm formation, showing non-toxicity and antibacterial activity *in vivo*, the DDC-Cu²⁺ combination represents an effective novel treatment strategy to control *S. aureus* and *S. epidermidis* biofilms. Ongoing studies are focused on developing drug delivery platforms containing the DDC-Cu²⁺ combination for clinical application and to determine whether similar safety and antimicrobial efficacy can be observed in other *in vivo* models of infection.

2.1.7 Supplementary files



Supplementary Figure S2.1: Confocal microscopy images of stained MRSA Mu50 biofilms with LIVE/DEAD BacLight staining after treatment with 8 µg/ml diethyldithiocarbamate and 32 µg/ml Cu²⁺. Confocal microscopy images results: green = viable bacteria; red = dead bacteria. **(a)** Untreated MRSA Mu50 biofilm at 20 ×. **(b)** MRSA Mu50 biofilm after treatment with DDC-Cu²⁺ at 20 ×. Scale bar represents 80 µm.

Supplementary File S2.2:

<https://www.frontiersin.org/articles/10.3389/fmicb.2022.999893/full#supplementary-material>. Video footage of MRSA Mu50 biofilm formation over 24 h when exposed to constant nutrient flow or when nutrient flow is supplemented with a combination of diethyldithiocarbamate and Cu²⁺ combination (DDC-Cu²⁺) using the Bioflux system. Scale bar represents 50 µm, 8 FPS corresponding to 2 h/s.

2.2 Effect of $\text{Cu}(\text{DDC})_2 + \text{Cu}^{2+}$ on biofilm dispersal

The combination of $\text{Cu}(\text{DDC})_2 + \text{Cu}^{2+}$ prevented bacterial attachment, bacterial aggregation, and reduced biofilm viability (see Section 2.1.5). Biofilm viability was assessed with the resazurin assay, which measures if cells are metabolically active after treatment exposure as an indication for viability. However, the resazurin assay does not distinguish between dead and metabolically inactive bacteria, such as persisters, and provides no information on the structure of the biofilm [375]. Therefore, microscopy images of live/dead stained biofilms treated with $\text{Cu}(\text{DDC})_2 + \text{Cu}^{2+}$ were obtained, which showed a significant increase in red (i.e., dead) bacteria. Both dyes, SYTO 9 (green dye) and propidium iodide (red dye), intercalate with nucleic acid but differ in their ability to penetrate membranes. While SYTO 9 can cross intact bacterial membranes, propidium iodide can only penetrate bacteria with damaged membranes [376]. Interpreting results from both the resazurin assay and microscopy, bacterial death following $\text{Cu}(\text{DDC})_2 + \text{Cu}^{2+}$ treatment can be assumed based on low metabolic activity and the disruption of bacterial membranes. The presence of numerous red bacteria in the microscopy images suggest that bacteria remain within the biofilm and the biofilm is not disrupted nor dislocated by treatment with $\text{Cu}(\text{DDC})_2 + \text{Cu}^{2+}$. Consequently, the effect of DDC^- , Cu^{2+} and the combination on biofilm dispersal was investigated.

Biofilm disruption by antibacterial agents can be measured by bacterial detachment [377]. Therefore, the xCELLigence RTCA system was used to measure changes in impedance of MRSA Mu50 biofilm treated with $\text{Cu}(\text{DDC})_2 + \text{Cu}^{2+}$. Baselines, compounds, and bacterial suspension were prepared as described in Chapter 2.1.4.6 with minor modifications. Two hundred μl of a 1:4 (v/v) dilution of the MRSA Mu50 bacterial suspension (OD_{600} 0.4) in nutrient broth was added to each well and the impedance measured during bacterial attachment and biofilm growth in an incubator at 37 °C. After 41 h, 100 μl of nutrient broth were removed and 100 μl of fresh media (untreated control), 8 $\mu\text{g}/\text{ml}$ DDC^- , 32 $\mu\text{g}/\text{ml}$ Cu^{2+} , or 8 $\mu\text{g}/\text{ml}$ $\text{DDC}^- + 32 \mu\text{g}/\text{ml}$ Cu^{2+} were added. The impedance of the attached biofilm with treatment was continuously and automatically measured every 15 min for 24 h in an incubator at 37 °C. Wells containing compounds in broth were assessed simultaneously to serve as baseline for the compounds' influence on impedance.

As described in Chapter 2.1.5.5, the CI correlates with bacterial attachment. It was previously shown that disruption of biofilms by antibacterial agents resulted in a decrease of CI [377,378]. Here, the effect of $\text{Cu}(\text{DDC})_2 + \text{Cu}^{2+}$ on the attachment of MRSA Mu50 biofilm was observed using the xCELLigence RTCA system (Figure 2.7 **Figure 2.7**). During the first 41 h, the CI rose quickly in all groups, as MRSA Mu50 was left untreated to enable bacterial attachment and biofilm formation. Then the biofilm was exposed to different treatments for 24 h. When MRSA Mu50 biofilm was exposed to fresh media or treated with DDC^- , the CI continued to steadily increase, suggesting bacterial growth and consequently additional bacterial attachment. When treated with Cu^{2+} , the CI remained constant, indicating no further bacterial attachment and no dislocation of already attached bacteria. In contrast, the CI decreased within the first 3 h when MRSA Mu50 biofilm was treated with $\text{Cu}(\text{DDC})_2 + \text{Cu}^{2+}$ and then remained at a constant level. As the CI reduction was minor (CI: 0.467 at 41 h; CI: 0.363 at 44 h), only few bacteria were detached from the gold electrodes at the bottom of the well, suggesting that the biofilm structure remained mostly undamaged.

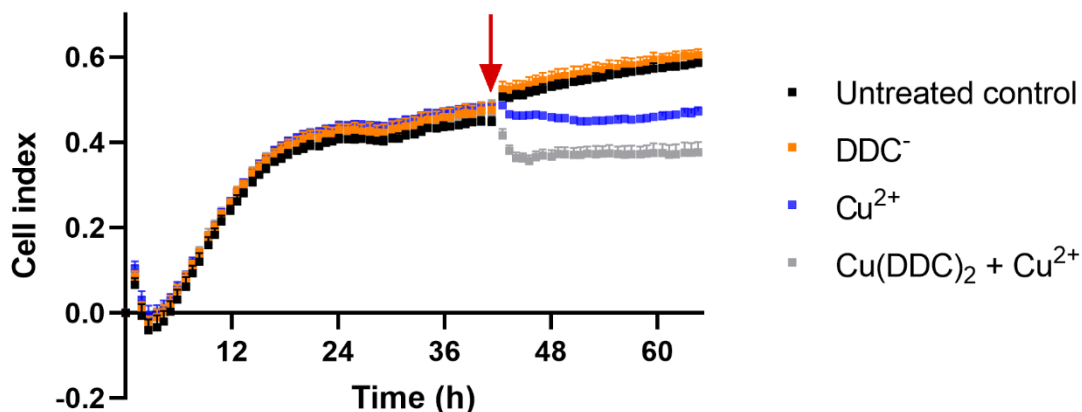


Figure 2.7: Effect of 8 $\mu\text{g}/\text{ml}$ diethyldithiocarbamate (DDC^- ; orange), 32 $\mu\text{g}/\text{ml}$ Cu^{2+} (blue) and a combination of DDC^- and Cu^{2+} ($\text{Cu}(\text{DDC})_2 + \text{Cu}^{2+}$; 8 $\mu\text{g}/\text{ml}$ $\text{DDC}^- + 32 \mu\text{g}/\text{ml}$ Cu^{2+} ; grey) on the cell index of MRSA Mu50 biofilms. Bacterial attachment and biofilm growth was measured for 41 h. Treatment was added (red arrow) to the biofilm and the impedance measured for further 24 h. Data are expressed as mean \pm SD ($n=3$).

As treatment with $\text{Cu}(\text{DDC})_2 + \text{Cu}^{2+}$ did not result in biofilm disruption, the antibiofilm activity of the combination is based on inhibition of biofilm formation and reduction of biofilm viability. However, the bacterial detachment was only assessed for MRSA Mu50 biofilms and needs to be investigated for *S. epidermidis* biofilms, as the biofilm composition and processes for biofilm disruption can differ between the species [379]. Furthermore, these results should be confirmed by quantifying the total biomass using crystal violet staining [380].

In the following chapters, the combination of $\text{Cu}(\text{DDC})_2 + \text{Cu}^{2+}$ optimised for an application in SSIs is described. The concentrations of DDC^- and Cu^{2+} were thus far expressed in $\mu\text{g}/\text{ml}$ and will be expressed in μM in the next chapters as the protocol for preparation and quantification of liposomes is based on concentrations expressed in molar. Consequently, 8 $\mu\text{g}/\text{ml}$ DDC^- correspond to 35 μM DDC^- , and 32 $\mu\text{g}/\text{ml}$ Cu^{2+} correspond to 128 μM Cu^{2+} .

3 Assessing $\text{Cu}(\text{DDC})_2$ + Cu^{2+} for surgical site infections

3.1 Publication: “*In vitro* and *in vivo* evaluation of diethyldithiocarbamate with copper ions and its liposomal formulation for the treatment of *Staphylococcus aureus* and *Staphylococcus epidermidis* biofilms”

Statement of authorship

Title of Paper	<i>In vitro</i> and <i>in vivo</i> evaluation of diethyldithiocarbamate with copper ions and its liposomal formulation for the treatment of <i>Staphylococcus aureus</i> and <i>Staphylococcus epidermidis</i> biofilms		
Publication Status	<input type="checkbox"/> Published	<input checked="" type="checkbox"/> Submitted for Publication	
	<input type="checkbox"/> Accepted for Publication	<input type="checkbox"/> Unpublished and Unsubmitted work written in a manuscript style	
Publication Details	Kaul L, Abdo AI, Coenye T, Swift S, Zannettino ACW, Süß R & Richter K. <i>In vitro</i> and <i>in vivo</i> evaluation of diethyldithiocarbamate with copper ions and its liposomal formulation for the treatment of <i>Staphylococcus aureus</i> and <i>Staphylococcus epidermidis</i> biofilms. Submitted to Biofilm on 23.01.2023 and currently under review.		

Principal author

Name of Principal author	Laurine Kaul		
Contribution to the Paper	Conceptualisation of the project, development of methods, investigation, formal analysis of data, writing – original draft preparation, corresponding author		
Overall percentage (%)	75 %		
Certification	This paper reports on original research I conducted during the period of my Higher Degree by Research candidature and is not subject to any obligations or contractual agreements with a third party that would constrain its inclusion in this thesis. I am the primary author of this paper.		
Signature		Date	08.02.2023

Co-author

By signing the Statement of Authorship, each author certifies that:

- i. The candidate’s stated contribution to the publication is accurate (as detailed above).
- ii. Permission is granted for the candidate to include the publication in the thesis; and
- iii. The sum of all co-author contributions is equal to 100% less the candidate’s stated contribution.

3 Assessing $\text{Cu}(\text{DDC})_2 + \text{Cu}^{2+}$ for surgical site infections

Name of Co-Author	Adrian Abdo		
Contribution to the Paper	Analysis of data, review and editing of manuscript		
Signature		Date	08.02.2023

Name of Co-Author	Tom Coenye		
Contribution to the Paper	Methodology and technical assistance, review and editing of manuscript		
Signature		Date	16.02.2023

Name of Co-Author	Simon Swift		
Contribution to the Paper	Methodology and technical assistance, review and editing of manuscript		
Signature	Simon Sv	Digitally signed by Simon Swift Date: 2023.02.15 13:09:41 +03'00'	Date

Name of Co-Author	Andrew Zannettino		
Contribution to the Paper	Supervision, review and editing of manuscript		
Signature		Date	15/02/23

Name of Co-Author	Regine Süß		
Contribution to the Paper	Conceptualisation of the project, supervision, review and editing of manuscript		
Signature		Date	15/2/2023

Name of Co-Author	Katharina Richter		
Contribution to the Paper	Conceptualisation of the project, supervision, review and editing of manuscript		
Signature		Date	8/2/23

The manuscript entitled “*In vitro* and *in vivo* evaluation of diethyldithiocarbamate with copper ions and its liposomal formulation for the treatment of *Staphylococcus aureus* and *Staphylococcus epidermidis* biofilms” was published on 17th May 2023 in the journal Biofilm.

3.1.1 Publication title page



In vitro and *in vivo* evaluation of diethyldithiocarbamate with copper ions and its liposomal formulation for the treatment of *Staphylococcus aureus* and *Staphylococcus epidermidis* biofilms

Laurine Kaul^{a,b,c,*}, Adrian I. Abdo^{a,c}, Tom Coenye^d, Simon Swift^e, Andrew Zannettino^{c,f,g}, Regine Süß^{b,1}, Katharina Richter^{a,c,h,1}

^a Richter Lab, Department of Surgery, Basil Hetzel Institute for Translational Health Research, University of Adelaide, 37 Woodville Road, Adelaide, SA, 5011, Australia

^b Institute of Pharmaceutical Sciences, Department of Pharmaceutics, University of Freiburg, Sarnerstr. 5, 79104, Freiburg, Germany

^c Adelaide Medical School, Faculty of Health and Medical Sciences, University of Adelaide, 4 North Terrace, Adelaide, SA, 5000, Australia

^d Laboratory of Pharmaceutical Microbiology, Ghent University, Omergaansesteeg 460, 9000, Ghent, Belgium

^e Department of Molecular Medicine and Pathology, University of Auckland, 85 Park Road, Grafton, Auckland, 1023, New Zealand

^f Precision Cancer Medicine Theme, South Australian Health & Medical Research Institute, North Terrace, Adelaide, SA, Australia

^g Central Adelaide Local Health Network, Adelaide, Australia

^h Institute for Photonics and Advanced Sensing, University of Adelaide, Adelaide, Australia

ARTICLE INFO

Keywords:

Biofilms
Surgical site infections
Diethyldithiocarbamate
Copper ions
Liposomes
Staphylococcus aureus
Staphylococcus epidermidis

ABSTRACT

Surgical site infections (SSIs) are mainly caused by *Staphylococcus aureus* (*S. aureus*) and *Staphylococcus epidermidis* (*S. epidermidis*) biofilms. Biofilms are aggregates of bacteria embedded in a self-produced matrix that offers protection against antibiotics and promotes the spread of antibiotic-resistance in bacteria. Consequently, antibiotic treatment frequently fails, resulting in the need for alternative therapies. The present study describes the *in vitro* efficacy of the $\text{Cu}(\text{DDC})_2$ complex (2:1 M ratio of diethyldithiocarbamate (DDC^-) and Cu^{2+}) with additional Cu^{2+} against *S. aureus* and *S. epidermidis* biofilms in models mimicking SSIs and *in vitro* antibacterial activity of a liposomal $\text{Cu}(\text{DDC})_2 + \text{Cu}^{2+}$ formulation. The *in vitro* activity on *S. aureus* and *S. epidermidis* biofilms grown on two hernia mesh materials and in a wound model was determined by colony forming unit (CFU) counting. Cu^{2+} -liposomes and $\text{Cu}(\text{DDC})_2$ -liposomes were prepared, and their antibacterial activity was assessed *in vitro* using the alamarBlue assay and CFU counting and *in vivo* using a *Galleria mellonella* infection model. The combination of 35 μM DDC^- and 128 μM Cu^{2+} inhibited *S. aureus* and *S. epidermidis* biofilms on meshes and in a wound infection model. $\text{Cu}(\text{DDC})_2$ -liposomes + free Cu^{2+} displayed similar antibiofilm activity to free $\text{Cu}(\text{DDC})_2 + \text{Cu}^{2+}$, and significantly increased the survival of *S. epidermidis*-infected larvae. Whilst $\text{Cu}(\text{DDC})_2 + \text{Cu}^{2+}$ showed substantial antibiofilm activity *in vitro* against clinically relevant biofilms, its application in mammalian *in vivo* models is limited by solubility. The liposomal $\text{Cu}(\text{DDC})_2 + \text{Cu}^{2+}$ formulation showed antibiofilm activity *in vitro* and antibacterial activity and low toxicity in *G. mellonella*, making it a suitable water-soluble formulation for future application on infected wounds in animal trials.

1. Introduction

Surgical site infections (SSI) are amongst the most common surgery-associated infections and occur in 1.5–20% of surgeries, depending on the nature of the surgery and country in which it is performed [1]. SSIs develop at the organ/tissue site of surgery [2] and can range from

wound or implant infections to organ infections [3]. Following a surgical procedure, such as hernia mesh repair [4], infections can affect the incision site (from superficial to deep tissue), implanted material and any part of the anatomy that was exposed or manipulated during surgery [5–7]. Consequently, SSIs represent a significant burden, by increasing patient morbidity and mortality, and adding additional cost to health

* Corresponding author. Richter Lab, Department of Surgery, Basil Hetzel Institute for Translational Health Research, University of Adelaide, 37 Woodville Road, Adelaide, SA, 5011, Australia.

E-mail address: laurine.kaul@pharmazie.uni-freiburg.de (L. Kaul).

¹ RS and KR contributed equally to this paper.

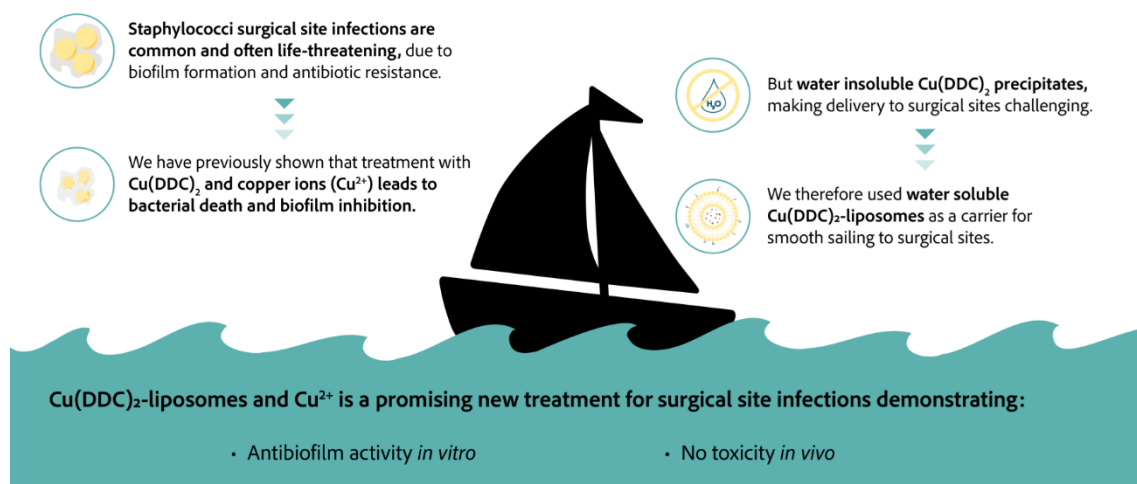
<https://doi.org/10.1016/j.biofilm.2023.100130>

Received 22 January 2023; Received in revised form 27 April 2023; Accepted 16 May 2023

Available online 17 May 2023

2590-2075/© 2023 The Authors. Published by Elsevier B.V. This is an open access article under the CC BY license (<http://creativecommons.org/licenses/by/4.0/>).

3.1.2 Graphical abstract



3.1.3 Abstract

SSIs are mainly caused by *S. aureus* and *S. epidermidis* biofilms. Biofilms are aggregates of bacteria embedded in a self-produced matrix that offers protection against antibiotics and promotes the spread of antibiotic-resistance in bacteria. Consequently, antibiotic treatment frequently fails, resulting in the need for alternative therapies. The present study describes the *in vitro* efficacy of the Cu(DDC)_2 complex (2:1 M ratio of DDC^- and Cu^{2+}) with additional Cu^{2+} against *S. aureus* and *S. epidermidis* biofilms in models mimicking SSIs and antibacterial activity of a liposomal $\text{Cu(DDC)}_2 + \text{Cu}^{2+}$ formulation. The *in vitro* activity on *S. aureus* and *S. epidermidis* biofilms grown on two hernia mesh materials and in a wound model was determined by colony forming unit (CFU) counting. Cu^{2+} -liposomes and Cu(DDC)_2 -liposomes were prepared, and their antibacterial activity was assessed *in vitro* using the alamarBlue assay and CFU counting and *in vivo* using a *Galleria mellonella* infection model. The combination of $35 \mu\text{M}$ DDC^- and $128 \mu\text{M}$ Cu^{2+} inhibited *S. aureus* and *S. epidermidis* biofilms on meshes and in a wound infection model. Cu(DDC)_2 -liposomes + free Cu^{2+} displayed similar antibiofilm activity to free $\text{Cu(DDC)}_2 + \text{Cu}^{2+}$, and significantly increased the survival of *S. epidermidis*-infected larvae. Whilst $\text{Cu(DDC)}_2 + \text{Cu}^{2+}$ showed substantial antibiofilm activity *in vitro* against clinically relevant biofilms, its application in mammalian *in vivo* models is limited by solubility. The liposomal $\text{Cu(DDC)}_2 + \text{Cu}^{2+}$ formulation showed antibiofilm activity *in vitro* and antibacterial activity and low toxicity *in vivo*, making it a suitable water-soluble formulation for future application on infected wounds in animal trials.

3.1.4 Introduction

SSI are amongst the most common surgery-associated infections and occur in 1.5-20% of surgeries, depending on the nature of the surgery and country in which it is performed [15]. SSIs develop at the organ/tissue site of surgery [11] and can range from wound or implant infections to organ infections [8]. Following a surgical procedure, such as hernia mesh repair [16], infections can affect the incision site (from superficial to deep tissue), implanted material and any part of the anatomy that was exposed or manipulated during surgery [2,4,6]. Consequently, SSIs represent a significant burden, by increasing patient morbidity and mortality, and adding additional cost to health systems [2,8,381].

The most common pathogens associated with SSIs are *S. aureus* and coagulase negative staphylococci, including *S. epidermidis*, which are natural components of the respiratory tract and skin microbiota, respectively [332]. Therefore, prevention of SSIs requires pre-operative preparations of the surgical site and antibiotic prophylaxis [381]. If an infection is detected, the routine treatment relies on additional antibiotic therapy [30,382]. However, over the last 2 decades, the antibiotic misuse and overuse has promoted the emergence of resistant strains, such as MRSA. The situation is exacerbated by biofilm infections, which are frequently staphylococcal, that offer antibiotic tolerance [21,383]. Biofilms are aggregates of bacteria embedded in a protective matrix, which enables bacteria to persist in hostile conditions, communicate with each other and become highly tolerant to antibiotics [31]. In comparison to planktonic forms of bacteria, biofilm bacteria require 10 to 1000-fold higher concentrations of antibiotics to be eradicated [52]. This is a major concern, as biofilms are present in over 80% of SSIs and are a major cause of delayed wound healing [30]. In addition, patient mortality is increased by 2 to 11-fold in MRSA-associated SSIs, compared to susceptible *S. aureus* associated SSIs and surgeries without infections [28]. Therefore, there is an unmet need for new antimicrobial agents targeting MRSA and *S. epidermidis* biofilms to prevent and treat SSIs.

DDC⁻ is a metabolite of disulfiram, a drug used for the treatment of chronic alcoholism [157], that is being repurposed for the treatment of cancer (Clinicaltrials.gov Identifier: NCT04234022, NCT05210374) and infections caused by parasites [174,176,384], viruses [359], fungi [190,192,385] and bacteria [166,212,216,221]. The anticancer and antibacterial activity of DDC⁻ is associated with the formation of complexes with metal ions, with copper ions (Cu^{2+}) being the most effective [167,221,222,386]. The combination of DDC⁻ and Cu^{2+} was antibacterial against *Mycobacterium tuberculosis* [221], *Streptococcus pneumoniae* [222] and was previously extended to planktonic *S. aureus* and *S. epidermidis* and their biofilms [387]. At a concentration of 35 μM DDC⁻ and 128 μM Cu^{2+} , the combination inhibited multiple steps in the biofilm formation cycle, reduced *S. aureus* and *S. epidermidis* biofilm viability and showed high fibroblast cell viability *in vitro*. These concentrations correspond to the instant formation of the $\text{Cu}(\text{DDC})_2$ complex [2 mol DDC⁻:1 mol Cu^{2+}] and additional Cu^{2+} , and displayed *in vivo* efficacy and non-toxicity in an invertebrate model [387].

However, the antibacterial activity of 35 μM DDC⁻ and 128 μM Cu^{2+} was only observed on biofilms grown in a microtiter well plate over 24 h [387] and can alter when exposed to biofilms grown over multiple days or in conditions similar to SSIs [388]. In addition, the $\text{Cu}(\text{DDC})_2$ complex is insoluble (<0.1 mg/ml) in water, limiting its practicality in the clinical setting [223]. This necessitates the development of a pharmaceutical formulation for optimal drug delivery to infection sites and improved antibacterial efficacy. To improve the solubility of $\text{Cu}(\text{DDC})_2$, nanoparticles including liposomal formulations of $\text{Cu}(\text{DDC})_2$ have been developed and successfully used as therapeutically active agents against cancer cells [168,223,249,250,389], with enhanced activity against breast cancer cells [230], glioblastoma [282] and neuroblastoma cells [228].

Inspired by this, our aim was to evaluate the antibacterial properties of 35 μM DDC⁻ and 128 μM Cu^{2+} ($\text{Cu}(\text{DDC})_2 + \text{Cu}^{2+}$) in biofilm models mimicking SSIs and to develop an appropriate drug delivery vehicle for $\text{Cu}(\text{DDC})_2$ to enable clinical application of the combination. Thus, this study advances our previous knowledge by presenting, for the first time, the antibiofilm activity of $\text{Cu}(\text{DDC})_2 + \text{Cu}^{2+}$ against *S. aureus* and *S. epidermidis* in an *in vitro* implant and wound infection

model. Furthermore, we have validated the non-toxicity and efficacy of the liposomal $\text{Cu}(\text{DDC})_2 + \text{Cu}^{2+}$ formulation *in vivo* using a *Galleria mellonella* infection model.

3.1.5 Materials and methods

3.1.5.1 Bacterial strains, mesh materials and chemicals

S. aureus ATCC 6538, *S. aureus* ATCC 700699 (also known as MRSA Mu50) and *S. epidermidis* ATCC 35984 were purchased from the American Type Culture Collection (Manassas, VA, USA). Bacteria were inoculated at colony forming unit (CFU)/ml or optical density at 600 nm (OD_{600}) values stated after dilution of an overnight culture grown in tryptone soya broth (TSB) or nutrient broth (Thermo Fisher Scientific, Waltham, MA, USA) at 37 °C with shaking at 180 rpm. Tryptone soya agar (TSA) was prepared by adding 1.5% agar bacteriological (Thermo Fisher Scientific). The hernia meshes Parietex Hydrophilic 2-Dimensional mesh (polyester), Parietene Lightweight monofilament polypropylene mesh (polypropylene) were donated by Covidien (Dublin, Ireland). The saturated phospholipids 1,2-distearoyl-sn-glycero-3-phosphocholine (DSPC) and 1,2-distearoyl-sn-glycero-3-phosphoethanolamine-N-[methoxy(polyethylene glycerol)-2000] (DSPE-mPEG2000) were donated by Lipoid GmbH (Ludwigshafen, Germany). Unless stated otherwise, all chemicals, materials, media, and supplements were purchased from Sigma-Aldrich (Steinheim, Germany).

3.1.5.2 Biofilm formation on hernia meshes

Round coupons (1.5 cm diameter) of polyester and polypropylene meshes were placed in a 12-well plate and immersed in 2 ml of a bacterial suspension (2×10^6 CFU/ml) of *S. aureus* ATCC 6538, MRSA Mu50 or *S. epidermidis* ATCC 35984 in TSB and incubated at 37 °C on a rotating platform at 70 rpm (3D Gyrotory Mixer; Ratek Instruments, Boronia, Australia). After 24 h incubation, meshes with attached bacteria were washed by immersing the meshes into 3 ml 0.9% (w/v) saline for 30 s at room temperature, three times consecutively, and placed into fresh TSB. Following another 72 h incubation, the meshes were washed, as previously described with 0.9% saline, to remove loosely attached cells and placed into TSB solutions containing 35 μM DDC⁻ + 128 μM Cu^{2+} . Control wells contained TSB alone (untreated control). Following 24 h treatment incubation at 37 °C on a rotating platform (70 rpm), a third washing step was performed prior to CFU counting or imaging of the coupons.

For CFU counting, meshes were collected in 10 ml 0.9% saline and biofilms were extracted from the mesh and disrupted by a series of vortexing (5 min, maximum speed, VM1 Vortex Mixer, Ratek Instruments Pty Ltd, Victoria, Australia) and sonication (15 min, Soniclean 80TD, Pulse swept power 60 W, Soniclean Pty Ltd, South Australia, Australia), prior to serial dilution and plating on TSA. CFU were counted following 24 h incubation at 37 °C. For imaging, the last washing step was performed with phosphate buffered saline. Meshes were covered and incubated with a 1:500 (v/v) dilution of LIVE/DEAD BacLight staining (1:1 mix of SYTO 9/propidium iodide; Life Technologies, Scoresby, Australia) in TSB for 20 min in the dark and imaged using the Olympus FV1000 Live cell imaging system (Olympus, Shinjuku, Japan) and a 20 \times /0.5W objective. Quantitation of live/dead cells was performed using ImageJ software (NIH, Bethesda, MA, USA). Briefly, the contrast/brightness was adjusted globally to images to minimize background before setting a threshold to highlight cells for automated counting.

3.1.5.3 *In vitro* wound model

An artificial dermis made of collagen (Corning, NY, USA) and hyaluronic acid (1.20 to 1.80 MDa; Lifecore Biomedical, MN, USA) was prepared as previously described by Brackman, *et al.* [390]. According to established protocols [391], freeze-dried bovine plasma was rehydrated in 10 ml 0.9% saline, 19 ml Bolton broth (LabM, Lancashire, UK), 1 ml freeze-thaw laked horse blood (Biotrading, Mijdrecht, Netherlands) and 20 μl heparin 100 IU. An artificial dermis was placed in each well of a 24-well plate and soaked with 1 ml of this mixture. Then, an overnight culture of MRSA Mu50 or *S. epidermidis* ATCC 35984 in TSB adjusted to an OD_{600} 0.1, was diluted 1:100 (v/v) in 0.9% saline, 10 μl were added on top of each dermis (equal to 10^4 CFU/well) and incubated statically at 37 °C for 24 h. Following biofilm formation, 1 ml of 35 μM $\text{DDC}^- + 128 \mu\text{M}$ Cu^{2+} in TSB was added. Controls included biofilms exposed to TSB (untreated control). After 24 h treatment exposure, each dermis was placed in 10 ml of 0.9% saline, and biofilms were extracted from the dermis and disrupted by three consecutive vortexing and sonication cycles for 30 s each. After serial dilution, plating on TSA and incubation at 37 °C for 24 h, CFU were counted to determine antibiofilm activity.

3.1.5.4 Liposomal preparation

Cu^{2+} -liposomes and $\text{Cu}(\text{DDC})_2$ -liposomes composed of DSPC:Chol:DSPE-mPEG₂₀₀₀ [50:45:5 M ratio] were produced and characterised according to Hartwig, *et al.* [228]. Briefly, lipid films were prepared with the thin film hydration method and hydrated with an aqueous Cu^{2+} solution (150 mM) to obtain a lipid concentration of 40 mM. Subsequently, the Cu^{2+} -lipid mix was extruded for 41 passages through an 80 nm pore-sized polycarbonate membrane (GE Healthcare Life Science, Marlborough, MA, USA) at 65 °C. Separation of non-encapsulated Cu^{2+} from Cu^{2+} -liposomes was achieved by size exclusion chromatography with a Sephadex G-50 Fine (GE Healthcare Life Science) column equilibrated with an EDTA containing sucrose buffer (300 mM sucrose, 20 mM HEPES, 30 mM EDTA, pH 7.4). Buffer exchange to an EDTA-free sucrose buffer (300 mM sucrose, 20 mM HEPES, pH 7.4) was performed through three centrifugation steps ($3000 \times g$, room temperature, 1.5 h) using Vivaspin® Turbo 4 filtration units (100 kDa MWCO; Sartorius AG, Göttingen, Germany), followed by Cu^{2+} -liposomes collection.

$\text{Cu}(\text{DDC})_2$ -liposomes were prepared by complexation of DDC^- with the liposomal encapsulated Cu^{2+} at 25 °C/300 rpm (Thermomixer comfort, Eppendorf, Hamburg, Germany) for 10 min. Excess of DDC^- was removed by three centrifugation steps ($3000 \times g$, room temperature, 45 min) with EDTA-free sucrose buffer. Non-incorporated $\text{Cu}(\text{DDC})_2$ precipitated and was separated from the $\text{Cu}(\text{DDC})_2$ -liposomes by prefiltration through a 0.45 μm cellulose acetate filter (VWR International, Radnor, PA, USA) before and after the centrifugation steps.

Cu^{2+} -liposomes and $\text{Cu}(\text{DDC})_2$ -liposomes were stored at 4–6 °C for up to 3 months and were sterile filtered under aseptic conditions through a 0.2 μm cellulose acetate filter (VWR International) before use. As previously described by Hartwig, *et al.* [228], the hydrodynamic diameter (d_h) and the polydispersity index (PDI) were measured via DLS (ZetaPals, Brookhaven Instruments Corporation, Holtsville, NY, USA) and encapsulated Cu^{2+} concentrations were determined by measuring absorbance of complexed Cu^{2+} with DDC^- in methanol at a wavelength of $\lambda_{max} = 435$ nm with a GENESYS 10S UV-Vis spectrophotometer (Thermo Fisher Scientific). Liposomes were used in biofilm challenge experiments to provide the equivalent of 35 μM DDC^- and/or 128 μM Cu^{2+} .

3.1.5.5 Antibacterial activity of liposomes

Overnight cultures of MRSA Mu50 and *S. epidermidis* 35984 in nutrient broth were adjusted to an OD₆₀₀ 0.5 and further 1:15 (v/v) diluted in nutrient broth. Black-walled 96-well microtiter plates (Greiner Bio-one, Frickenhausen, Germany) were inoculated with 100 µl bacterial suspension and incubated for 24 h at 37 °C on a rotating platform at 70 rpm. The biofilm was rinsed with 0.9% saline, exposed to 100 µl of Cu(DDC)₂-liposomes, Cu²⁺-liposomes, [Cu(DDC)₂-liposomes + Cu²⁺-liposomes], [Cu(DDC)₂-liposomes + free Cu²⁺] or 35 µM DDC⁻ + 128 µM Cu²⁺ and further incubated for 24 h under the same conditions. The treatments were removed, and the biofilm rinsed with 0.9% saline, before viability was detected by either measurement of metabolic activity with the alamarBlue assay or CFU counting.

The alamarBlue assay was performed according to Richter, *et al.* [363] and rinsed biofilms were incubated with a 10% (v/v) alamarBlue™ Cell Viability Reagent (Thermo Fisher Scientific) solution in nutrient broth. The fluorescence was measured hourly on a TECAN Spark plate reader (Männedorf, Switzerland) at $\lambda_{excitation} = 530 \text{ nm} / \lambda_{emission} = 590 \text{ nm}$ until maximum fluorescence was reached, then viability was calculated using Equation 3.1. Antibiofilm activity of the different treatments was determined as percentage of biofilm viability, where the fluorescence intensity of treated and untreated biofilms is represented by I_{treated} and I_{untreated}, respectively and I_{blank} represents the background fluorescence of the 10% (v/v) alamarBlue solution [363].

$$\% \text{ Biofilm viability} = \left(\frac{I_{\text{treated}} - I_{\text{blank}}}{I_{\text{untreated}} - I_{\text{blank}}} \right) \times 100 \quad (3.1)$$

CFU counting was performed according to Van den Driessche, *et al.* [392] and 100 µl of 0.9% saline were added to each rinsed biofilm. To disrupt the biofilm, the plates were shaken at 150 rpm and sonicated (5 min each), and the content of each well was collected separately. This process was repeated twice to extract all biofilms cells and serial dilutions of these suspensions were plated on TSA and incubated at 37 °C for 24 h, prior to CFU counting.

3.1.5.6 *In vivo* cytotoxicity and antibacterial activity

Galleria mellonella (*G. mellonella*) larvae (Angel-Zentrum, Freiburg, Germany) were used on the day of receipt and 30 larvae were assigned to each treatment group. Larvae were injected in the last left proleg with micro-fine (30 gauge) needle insulin syringes (BD, Franklin Lakes, NJ, USA). Four control groups were included, (i) not-injected larvae (uninfected, untreated control), (ii) larvae injected with 0.9% saline (uninfected, vehicle control), (iii) larvae injected with treatment (uninfected, treated control to determine toxicity) and (iv) larvae injected with a bacterial suspension and 0.9% saline (infected, vehicle control). To determine treatment efficacy, larvae were injected with a *S. epidermidis* ATCC 35984 suspension (OD₆₀₀ 0.05) in nutrient broth and with Cu(DDC)₂-liposomes, Cu²⁺-liposomes, [Cu(DDC)₂-liposomes + Cu²⁺-liposomes] or [Cu(DDC)₂-liposomes + free Cu²⁺]. Considering the dilution factor within the larvae, the concentrations of the liposomal formulations were increased 10-fold compared to the concentrations used *in vitro*. A total volume of 20 µl was injected comprising treatment or 0.9% saline in a 1:1 mix with a bacterial suspension in nutrient broth. Larvae were housed in petri dishes in the dark at 37 °C and the larvae survival was monitored daily over 4 days.

3.1.5.7 Statistical analysis

Results were statistically analysed using GraphPad Prism version 9.00 for Windows (GraphPad Software, CA, USA) and statistical significance was determined with an $\alpha = 0.05$. All experiments were carried out at least in triplicate. Parametric data are represented by the mean \pm standard

deviation (SD), which was analysed using paired 2-tailed t-tests, one-way analysis of variance (ANOVA) with Dunnett's multiple comparison test for finding differences between treatment groups and untreated controls and two-way ANOVA with Šidák's multiple comparison tests, as described in the figure legends. *G. mellonella* survival data was analysed using Kaplan-Meier survival curves with significant differences between groups determined by log-rank test, significance was Bonferroni-Holm-corrected for multiple comparisons.

3.1.6 Results

3.1.6.1 Treatment of biofilms on hernia mesh materials

When we consider the antibacterial properties of $\text{Cu}(\text{DDC})_2 + \text{Cu}^{2+}$ observed in microtiter plates possibly not correlating with complex biofilms present in SSIs [388], we used two biofilm models mimicking SSIs to further investigate the antibiofilm activity of $35 \mu\text{M DDC}^- + 128 \mu\text{M Cu}^{2+}$ *in vitro*. These models are based on an implant infection and a wound infection.

As an example of SSI on an implant, we investigated the biofilm formation of *S. aureus* and *S. epidermidis* on two commonly used, commercially available, hernia mesh materials and the ability of $\text{Cu}(\text{DDC})_2 + \text{Cu}^{2+}$ to reduce the bacterial load on these meshes. *S. aureus* ATCC 6538, MRSA Mu50 and *S. epidermidis* ATCC 35984 formed extensive biofilms during 96 h batch incubations on polyester and polypropylene mesh material with $\log(\text{CFU}/\text{mesh})$ values ranging from 7.21 to 8.91 (Figure 3.1). The imaging of *S. aureus* ATCC 6538 biofilms on polyester meshes showed a multifilament mesh structure, exhibiting niches for bacteria to attach (Figure 3.1d, top left). In contrast, the mono filaments of the polypropylene mesh were surrounded by *S. aureus* ATCC 6538 biofilms (Figure 3.1d, top right). Studies suggest that staphylococci biofilms on hernia meshes may be associated with hernia repair failure and contribute to mesh shrinkage, chronic pain or hernia recurrence [67], and there may be an association between mesh porosity and the formation of biofilms [76].

When treated with $35 \mu\text{M DDC}^- + 128 \mu\text{M Cu}^{2+}$, viability of *S. aureus* ATCC 6538 in biofilms was reduced on polyester and polypropylene meshes (Figure 3.1a). Similar results were observed in MRSA Mu50 (Figure 3.1b) and *S. epidermidis* ATCC 35984 (Figure 3.1c) biofilms \log_{10} reduction on polyester meshes and polypropylene meshes. The *S. aureus* ATCC 6538 and MRSA Mu50 \log_{10} reduction was higher on polypropylene meshes compared to polyester meshes. This could be due to multifilament meshes forming denser biofilms than monofilament meshes because of the increased surface and presence of niches [75]. In addition, the highly hydrophobic $\text{Cu}(\text{DDC})_2$ complex that is formed instantly when DDC^- and Cu^{2+} are mixed, might not reach the bacteria embedded in the niches of the multifilament mesh.

The imaging of $\text{Cu}(\text{DDC})_2 + \text{Cu}^{2+}$ treated *S. aureus* ATCC 6538 (Figure 3.1d, bottom left) confirmed a substantial number of bacteria in the niches formed by the intertwined filaments but showed mostly dead bacteria (red) on the polyester mesh and was associated with CFU reduction. In contrast, the *S. aureus* ATCC 6538 biofilm that previously surrounded the polypropylene filaments was in parts removed during washing steps, resulting in only few dead bacteria (red) imaged (Figure 3.1d bottom right). We quantified the viability based on the percentage of green and red fluorescent cells, which showed the viability was reduced when treated with $\text{Cu}(\text{DDC})_2 + \text{Cu}^{2+}$ compared to the untreated control on polyester and polypropylene meshes (Supplementary Figure S3.1). However, significant background was present due to autofluorescence of the polyester and polypropylene that compose the meshes, which significantly affected automated counting of live and dead cells. This was unavoidable since further background removal would eliminate valid signal from the analysis.

Therefore, the microscopy images visually complement the quantitative assessment of \log_{10} reduction of bacteria due to $\text{Cu}(\text{DDC})_2 + \text{Cu}^{2+}$. As the overall successful salvage rate of infected meshes can be as low as 10% and be inferior for infected polyester mesh compared to polypropylene mesh [16], the substantial \log_{10} reduction of $\text{Cu}(\text{DDC})_2 + \text{Cu}^{2+}$ on both mesh material highlights the combination as a promising treatment approach for infected hernia meshes.

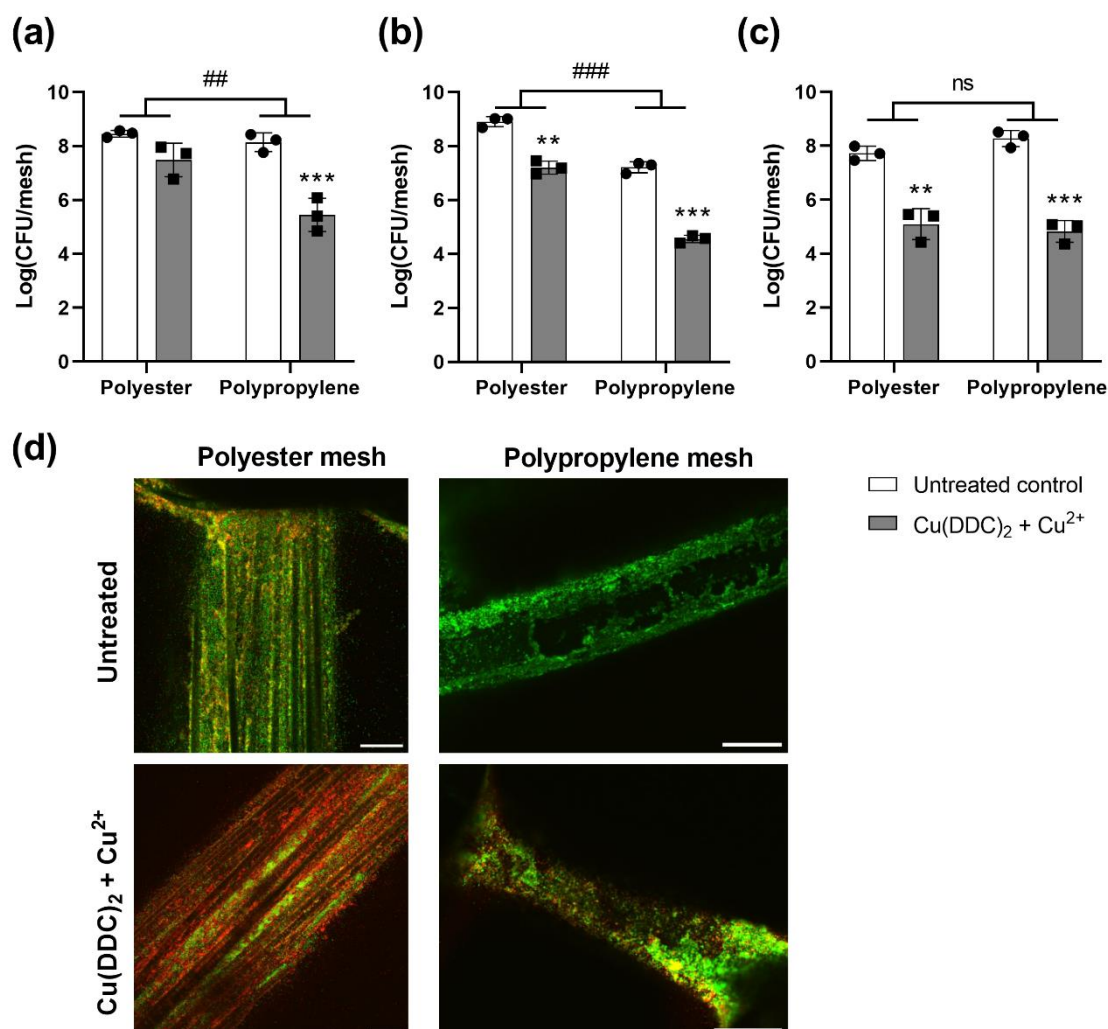


Figure 3.1: Effect of 35 μM diethyldithiocarbamate (DDC-) + 128 μM Cu^{2+} (grey; $\text{Cu}(\text{DDC})_2 + \text{Cu}^{2+}$) on biofilms grown on hernia mesh material. \log_{10} colony forming units (CFU) of (a) *S. aureus* ATCC 6538, (b) MRSA Mu50 and (c) *S. epidermidis* ATCC 35984 biofilms grown on Parietex Hydrophilic 2-Dimensional (polyester) or on Parietene Lightweight monofilament polypropylene (polypropylene) meshes compared to untreated control (white; $n=3$; mean \pm SD; 2-way ANOVA: ** $p < 0.01$, *** $p < 0.001$ indicate significant differences between $\text{Cu}(\text{DDC})_2 + \text{Cu}^{2+}$ and untreated control by Šidák's multiple comparison test; ## $p < 0.01$, ### $p < 0.001$ indicate significant differences between the polyester and the polypropylene mesh; ns=not significant). (d) To visually illustrate the quantitative culture-based cell-viability data, the effect of $\text{Cu}(\text{DDC})_2 + \text{Cu}^{2+}$ on *S. aureus* ATCC 6538 biofilms were investigated using confocal microscopy of LIVE/DEAD BacLight stained meshes. Confocal microscopy images result: green = viable bacteria; red = dead bacteria. Z-stack images taken with a 20 \times /0.5W objective are representative of three independent experiments. Scalebar indicated on bottom-right of images correspond to 75 μm .

3.1.6.2 Efficacy in an *in vitro* wound model

As second *in vitro* SSI model, the artificial dermis model was chosen, as it closely resembles a chronic wound infection with similar nutritional conditions found in wound exudate and a dermis-like scaffold based on hyaluronic acid and collagen on which bacteria can attach and form biofilms [390,393]. Here, MRSA Mu50 and *S. epidermidis* ATCC 35984 biofilms were grown on an artificial

dermis and exposed to $35 \mu\text{M DDC}^- + 128 \mu\text{M Cu}^{2+}$ (Figure 3.2). The combination of $\text{Cu}(\text{DDC})_2 + \text{Cu}^{2+}$ demonstrated a significant biofilm reduction in MRSA Mu50 and in *S. epidermidis* ATCC 35984 biofilms (Figure 3.2a). While the \log_{10} reduction was smaller compared to the mesh attachment model for both MRSA and *S. epidermidis* biofilms, $\text{Cu}(\text{DDC})_2 + \text{Cu}^{2+}$ exposure still visually reduced the biofilms on the artificial dermis (Figure 3.2b) and resulted in 97.2% and 81.5% MRSA Mu50 and *S. epidermidis* ATCC 35984 reduction, respectively, despite nutrient rich *in vivo*-like conditions. We propose three explanations for a reduced exposure of $\text{Cu}(\text{DDC})_2 + \text{Cu}^{2+}$ with the biofilm on the artificial dermis.

Firstly, when DDC^- and Cu^{2+} solutions are mixed, the water insoluble $\text{Cu}(\text{DDC})_2$ complex precipitates and sediments to the bottom of the well [394]. In previous biofilm experiments, including the biofilm on mesh material, biofilms were grown or placed at the bottom of wells, allowing for precipitated $\text{Cu}(\text{DDC})_2$ to sediment onto and interact with the biofilms, while excess Cu^{2+} was available in solution. In the wound model, biofilms are formed on top of the artificial dermis at the air-liquid interface (Figure 3.2b). Therefore, when exposed to $\text{Cu}(\text{DDC})_2 + \text{Cu}^{2+}$, limited amount of $\text{Cu}(\text{DDC})_2$ would precipitate onto the biofilm on the artificial dermis, while the remaining $\text{Cu}(\text{DDC})_2$ might interact with the hydrophobic collagen or simply sediment to the bottom of the well. Secondly, Cu^{2+} was shown to increase cross-linking of collagen in a concentration dependent matter [395], which can result in a reduced availability of Cu^{2+} for the antibiofilm activity. Lastly, DDC^- can be degraded to diethylamine and carbon sulphide in the presence of blood, due to the presence of plasma proteins and may therefore not be available to form the $\text{Cu}(\text{DDC})_2$ complex [160]. Similar effects of the microenvironmental conditions in the artificial dermis model on the antibiofilm activity of antimicrobial agents were reported [391,393,396]. For example, Grassi, *et al.* [393] observed inferior biofilm inhibition by antimicrobial peptides in the artificial dermis model compared to a 3D lung epithelial model due to the presence of blood and proposed the development of nanocarriers as drug delivery vehicle [397]. Consequently, to increase water solubility of $\text{Cu}(\text{DDC})_2$, prevent $\text{Cu}(\text{DDC})_2$ sedimentation and protect DDC^- from degradation, Cu^{2+} and $\text{Cu}(\text{DDC})_2$ were incorporated into PEGylated liposomes.

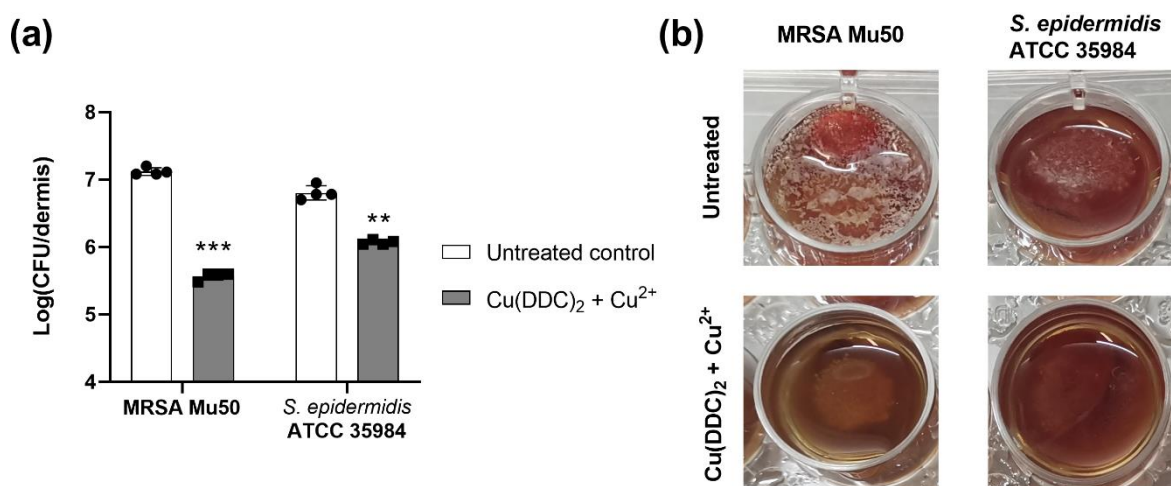


Figure 3.2: Effect of $35 \mu\text{M diethyldithiocarbamate (DDC}^-) + 128 \mu\text{M Cu}^{2+}$ on MRSA Mu50 and *S. epidermidis* ATCC 35984 biofilms grown on an artificial dermis compared to the untreated control. **(a)** Log(CFU/dermis) of untreated biofilms (white) and biofilms treated with $\text{Cu}(\text{DDC})_2 + \text{Cu}^{2+}$ (grey; $n=4$; mean \pm SD; paired 2-tailed t-tests: ** $p < 0.01$, *** $p < 0.001$). **(b)** Representative images of MRSA Mu50 (left) and *S. epidermidis* ATCC 35984 (right) biofilms when untreated (top) or treated with $\text{Cu}(\text{DDC})_2 + \text{Cu}^{2+}$ (bottom).

3.1.6.3 Characterisation of Cu²⁺-liposomes and Cu(DDC)₂-liposomes

PEGylated Cu²⁺-liposomes and Cu(DDC)₂-liposomes were prepared and characterised according to Hartwig, *et al.* [228]. The size, expressed as the d_h , and the PDI were determined for Cu²⁺-liposomes and Cu(DDC)₂-liposomes (Figure 3.3) and were similar to previously reported values [228]. The size of both the Cu²⁺-liposomes and the Cu(DDC)₂-liposomes were below 200 nm, allowing for sterile filtration and excluding the presence of large aggregates and extra-liposomal Cu(DDC)₂ [228]. In addition, the PDI of Cu²⁺-liposomes and Cu(DDC)₂-liposomes was below 0.2, indicating a homogenous population of liposomes [266,398], which has previously been confirmed by imaging of mostly unilamellar vesicles in cryo-EM images [223,228]. The production of Cu(DDC)₂-liposomes is based on DDC⁻ diffusing through the membrane of Cu²⁺-liposomes and forming the insoluble Cu(DDC)₂ complex within the liposomes, which is characterised by the colour change [394]. In addition, Wehbe, *et al.* [223] showed that the amount of Cu(DDC)₂ in liposomes correlates with the amount of Cu²⁺ in liposomes by comparing Cu²⁺ to lipid ratio to Cu(DDC)₂ to lipid ratio. Therefore, it can be assumed that both liposomes have the same lipid constitution and consequently a similar amount of PEG polymers per liposome. Based on this assumption, the different sizes of the liposomes and the homogenous vesicle population, the PEGylation of Cu²⁺-liposomes would be denser compared to Cu(DDC)₂-liposomes (Figure 3.3).

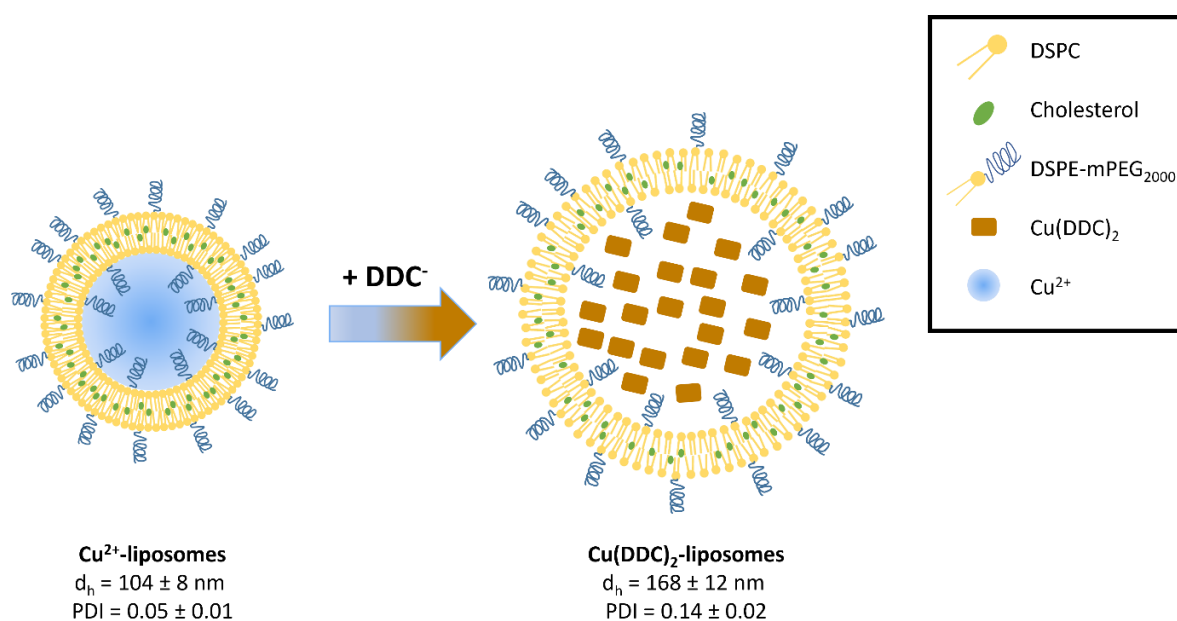


Figure 3.3: Schematic illustration of Cu²⁺-liposomes and Cu(DDC)₂-liposomes. Diethyldithiocarbamate (DDC⁻) diffuses through the membrane of the smaller Cu²⁺-liposomes and binds the encapsulated Cu²⁺ to form the water insoluble Cu(DDC)₂. The trapped Cu(DDC)₂ accumulates within the liposome, resulting in an increase in size. DSPC = 1,2-distearoyl-sn-glycero-3-phosphocholine; DSPE-mPEG₂₀₀₀ = 1,2-distearoyl-sn-glycero-3-phosphoethanolamine-N-[methoxy(polyethylene glycol)-2000]; d_h = hydrodynamic diameter; PDI = polydispersity index (n=15; mean \pm SD).

3.1.6.4 Antibiofilm activity of liposomal Cu(DDC)₂ + Cu²⁺

The liposomes were assessed for their activity against MRSA Mu50 and *S. epidermidis* ATCC 35984 biofilms (Figure 3.4). As a fast and high throughput method [392], the alamarBlue assay was first performed to determine antibiofilm activity of the liposomal formulations (Figure 3.4a). Treatment with Cu²⁺-liposomes or Cu(DDC)₂-liposomes showed no activity against MRSA Mu50 and *S. epidermidis* ATCC 35984 biofilms. Similar to the effects of free Cu²⁺ and Cu(DDC)₂ on MRSA and *S. epidermidis* biofilms [387], Cu²⁺-liposomes and Cu(DDC)₂-liposomes concentrations up to

a 4-fold increase did not inhibit biofilm viability (data not shown). The combination of [$\text{Cu}(\text{DDC})_2$ -liposomes + Cu^{2+} -liposomes] also showed no antibiofilm activity against MRSA Mu50 and *S. epidermidis* ATCC 35984. This could be a result of the $\text{Cu}(\text{DDC})_2$ -liposomes, the Cu^{2+} -liposomes or both liposomes not releasing their content extracellularly or, following bacterial uptake, intracellularly. However, cellular uptake of PEGylated $\text{Cu}(\text{DDC})_2$ -liposomes were observed in LS cells after 6 h incubation [228], which suggest bacterial uptake of the $\text{Cu}(\text{DDC})_2$ -liposomes. Notably, when $\text{Cu}(\text{DDC})_2$ -liposomes were investigated in combination with free Cu^{2+} [$\text{Cu}(\text{DDC})_2$ -liposomes + free Cu^{2+}], the biofilm viability of MRSA Mu50 and *S. epidermidis* ATCC 35984 was significantly reduced. This reduction in biofilm viability was similar to the activity of free $\text{Cu}(\text{DDC})_2 + \text{Cu}^{2+}$ against MRSA Mu50 and *S. epidermidis* ATCC 35984 biofilms. To further confirm these results, CFU counting was performed for treatments showing a reduction in biofilm viability with the alamarBlue assay (Figure 3.4b). Treatment with [$\text{Cu}(\text{DDC})_2$ -liposomes + free Cu^{2+}] and $\text{Cu}(\text{DDC})_2 + \text{Cu}^{2+}$ resulted in a significant MRSA Mu50 \log_{10} reduction and a significant *S. epidermidis* ATCC 35984 \log_{10} reduction. As the antibiofilm activity of [$\text{Cu}(\text{DDC})_2$ -liposomes + free Cu^{2+}] against MRSA and *S. epidermidis* was similar to free $\text{Cu}(\text{DDC})_2 + \text{Cu}^{2+}$ and treatment with free Cu^{2+} alone previously showed no antibiofilm activity against MRSA Mu50 and *S. epidermidis* ATCC 35984 at the tested concentration [387], we concluded that $\text{Cu}(\text{DDC})_2$ was released from the $\text{Cu}(\text{DDC})_2$ -liposomes, either intracellularly following bacterial uptake or extracellularly, but not the uncomplexed Cu^{2+} from the Cu^{2+} -liposomes.

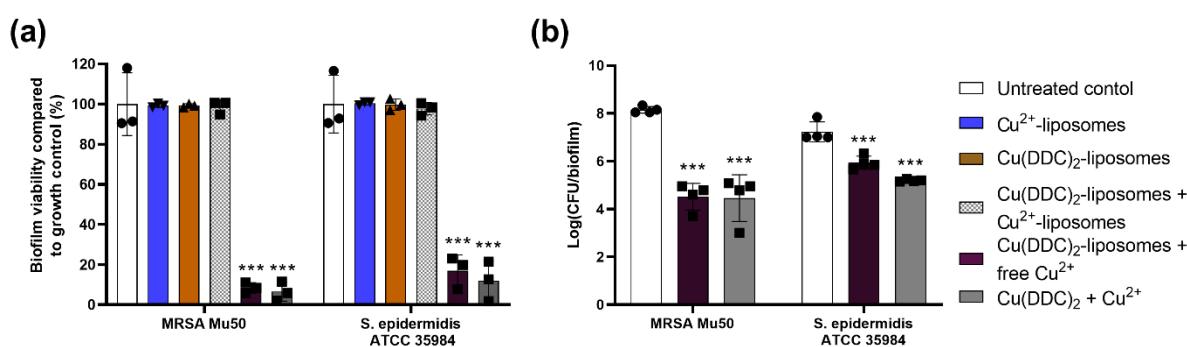


Figure 3.4: Effect of Cu^{2+} -liposomes, $\text{Cu}(\text{DDC})_2$ -liposomes, [$\text{Cu}(\text{DDC})_2$ -liposomes + Cu^{2+} -liposomes], [$\text{Cu}(\text{DDC})_2$ -liposomes + free Cu^{2+}] and $\text{Cu}(\text{DDC})_2 + \text{Cu}^{2+}$ (35 μM DDC⁻ + 128 μM Cu^{2+}) on MRSA Mu50 and *S. epidermidis* ATCC 35984 biofilm viability in comparison to the untreated control by using (a) the alamarBlue assay and (b) colony forming unit (CFU) counting. The concentrations of $\text{Cu}(\text{DDC})_2$ -liposomes and Cu^{2+} -liposomes or the combinations correspond to 35 μM diethyldithiocarbamate (DDC⁻) and/or 128 μM Cu^{2+} , respectively (n=3-4; mean \pm SD; 1-way ANOVA: *** $p < 0.001$ by Dunnett's multiple comparison tests).

Liposomes can penetrate the biofilm and release their content by fusing with the bacterial phospholipid membrane [275,399]. This interaction is dependent on biofilm properties, including bacterial species and matrix composition, and by the liposomal physicochemical properties [275]. Liposomes vary in surface charge, lipid composition, bilayer rigidity, surface modification, size and the incorporation of PEG polymers in the liposomal membrane [400,401]. As $\text{Cu}(\text{DDC})_2$ -liposomes are produced by DDC⁻ diffusion into Cu^{2+} -liposomes, it can be expected that $\text{Cu}(\text{DDC})_2$ -liposomes and Cu^{2+} -liposomes have the same lipid constitution [223] and are only different in size and membrane PEGylation density. The denser PEGylation of the Cu^{2+} -liposomes compared to the $\text{Cu}(\text{DDC})_2$ -liposomes (Figure 3.3) can present a physical barrier for Cu^{2+} -liposome interaction with bacterial membranes or biofilm matrix, and therefore, prevent the intracellular uptake of the liposomal content [400]. PEGylated liposomes were previously shown to reduce interaction with target cells [402] and limit interactions with bacterial biofilms [403]. Liposomes with a PEGylated

surface showed improved penetration of *P. aeruginosa* biofilms but reduced the affinity of liposomes to bacteria compared to non-PEGylated liposomes. The PEG modifications on the liposome surface increase hydrophilicity of liposomes which increased the affinity to biofilm matrix components, such as extracellular polymeric substance [401]. In addition, PEGylated DSPC-containing liposomes with a low surface charge and rigid bilayer reduce adsorption of the DSPC-liposomes on *S. aureus* biofilms compared to non-PEGylated liposomes [403]. To investigate if the PEG polymers are hindering adsorption of Cu^{2+} -liposomes on MRSA and *S. epidermidis* biofilms and consequently result in reduced antibiofilm activity of $[\text{Cu}(\text{DDC})_2\text{-liposomes} + \text{Cu}^{2+}\text{-liposomes}]$, the penetration of fluorescently-labelled liposomes into the biofilm should be determined using microscopical analysis [403,404] and the antibiofilm activity of non-PEGylated $[\text{Cu}(\text{DDC})_2\text{-liposomes} + \text{Cu}^{2+}\text{-liposomes}]$ should be investigated. As hydrophilic PEG polymers integration on the surface of $\text{Cu}(\text{DDC})_2\text{-liposomes}$ is necessary for superior drug to lipid ratio and improvement of colloidal stability during storage compared to non-PEGylated $\text{Cu}(\text{DDC})_2\text{-liposomes}$ [228] and $[\text{Cu}(\text{DDC})_2\text{-liposomes} + \text{free Cu}^{2+}]$ showed high antibiofilm activity against MRSA and *S. epidermidis*, incorporating $\text{Cu}(\text{DDC})_2$ into PEGylated liposomes is a water-soluble alternative for a potential application on surgical site infections.

3.1.6.5 *In vivo* toxicity and antimicrobial activity of liposomal $\text{DDC}^- + \text{Cu}^{2+}$

G. mellonella is an invertebrate infection model that is cost- and time-efficient, can mimic physiological conditions of mammals, such as temperature of 37 °C, and expresses a cellular and humoral innate immune system [405]. This immune system is capable of recognising pathogens and recruiting hemocytes to engulf pathogens and produce reactive oxygen species and antimicrobial peptides [372,406,407]. This model is in use for investigating pathogen virulence, for determining pharmacokinetic properties of antimicrobial agents and *in vivo* screening for antimicrobial activity and toxicity [372,373,408,409]. Efficacy and toxicity of antibiotics in *G. mellonella* infection models were reported to empirically support the observed effects of antibiotics in murine infection models and antibiotic susceptibility in humans [410].

To investigate potential toxic effects of the liposomes *in vivo*, *G. mellonella* larvae were exposed to liposomes and the survival was monitored over 4 days. Injection with $\text{Cu}(\text{DDC})_2\text{-liposomes}$, $\text{Cu}^{2+}\text{-liposomes}$, the combination of $[\text{Cu}(\text{DDC})_2\text{-liposomes} + \text{Cu}^{2+}\text{-liposomes}]$ and the combination of $[\text{Cu}(\text{DDC})_2\text{-liposomes} + \text{free Cu}^{2+}]$ showed similar survival rates as the vehicle control (0.9% saline) and the untreated larvae, indicating no treatment toxicity in *G. mellonella* (Figure 3.5a). Likewise, injection of free Cu^{2+} (concentration within larvae 128 μM) has been previously shown to be not toxic to *G. mellonella* larvae [387].

To assess the antimicrobial activity of $[\text{Cu}(\text{DDC})_2\text{-liposomes} + \text{Cu}^{2+}\text{-liposomes}]$ and $[\text{Cu}(\text{DDC})_2\text{-liposomes} + \text{free Cu}^{2+}]$ *in vivo*, the survival of *S. epidermidis*-infected *G. mellonella* was determined over 4 days (Figure 3.5b). In *S. epidermidis*-infected larvae, treatment with $\text{Cu}(\text{DDC})_2\text{-liposomes}$ or $\text{Cu}^{2+}\text{-liposomes}$ resulted in a low survival rate, similar to the vehicle control ($p > 0.05$). However, *S. epidermidis*-infected and $[\text{Cu}(\text{DDC})_2\text{-liposomes} + \text{Cu}^{2+}\text{-liposomes}]$ or $[\text{Cu}(\text{DDC})_2\text{-liposomes} + \text{free Cu}^{2+}]$ treated larvae showed a significantly higher survival rate compared to *S. epidermidis*-infected, saline treated larvae ($p = 0.0018$ and $p = 0.0015$, respectively). Moreover, the survival rates of both *S. epidermidis*-infected larvae treated with either $[\text{Cu}(\text{DDC})_2\text{-liposomes} + \text{Cu}^{2+}\text{-liposomes}]$ or $[\text{Cu}(\text{DDC})_2\text{-liposomes} + \text{free Cu}^{2+}]$ were significantly higher compared to treatment with $\text{Cu}(\text{DDC})_2\text{-liposomes}$ alone ($p = 0.0048$ and $p = 0.0015$, respectively) or $\text{Cu}^{2+}\text{-liposomes}$ alone ($p = 0.0203$ and $p = 0.0015$, respectively). Notably, the substantial increase in survival of the *S. epidermidis*-infected, $[\text{Cu}(\text{DDC})_2\text{-liposomes} + \text{free Cu}^{2+}]$ treated larvae showed no significant

difference to the survival rate of uninfected, untreated larvae ($p > 0.05$). While treatment with free Cu^{2+} previously showed no effect on *S. epidermidis*-infected larvae [387], treatment with $[\text{Cu}(\text{DDC})_2\text{-liposomes} + \text{free Cu}^{2+}]$ indicated efficacy against *S. epidermidis in vivo*.

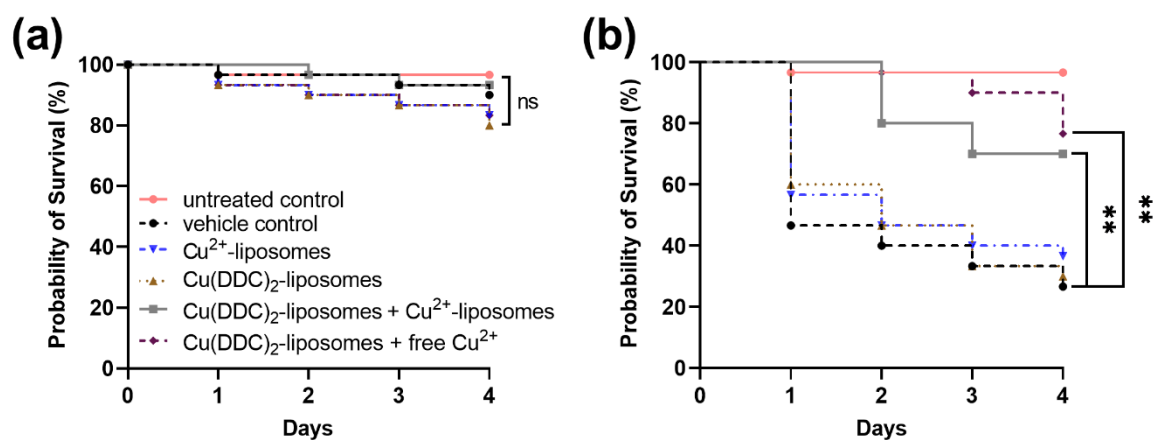


Figure 3.5: Effect of Cu^{2+} -liposomes (blue), $\text{Cu}(\text{DDC})_2$ -liposomes (brown), $[\text{Cu}(\text{DDC})_2\text{-liposomes} + \text{Cu}^{2+}\text{-liposomes}]$ (grey) and $[\text{Cu}(\text{DDC})_2\text{-liposomes} + \text{free Cu}^{2+}]$ (purple) on (a) the probability of *Galleria mellonella* survival (30/group; $n=180$; $ns = p > 0.05$) and on (b) probability of survival of *Galleria mellonella* infected with *S. epidermidis* ATCC 35984 (30/group; $n=180$; $**p < 0.01$). Vehicle = 0.9% saline (black); control = untreated, uninfected (pink). The concentrations of $\text{Cu}(\text{DDC})_2$ -liposomes and Cu^{2+} -liposomes correspond to 350 μM diethyldithiocarbamate (DDC⁻) and 1280 μM Cu^{2+} , respectively. The combination of $[\text{Cu}(\text{DDC})_2\text{-liposomes} + \text{Cu}^{2+}\text{-liposomes}]$ and $[\text{Cu}(\text{DDC})_2\text{-liposomes} + \text{free Cu}^{2+}]$ represent a ratio of [1:6.2 mol] and correspond to 350 μM DDC⁻ + 1280 μM Cu^{2+} .

Interestingly, the $[\text{Cu}(\text{DDC})_2\text{-liposomes} + \text{Cu}^{2+}\text{-liposomes}]$ combination significantly increased the survival rate of *S. epidermidis*-infected *G. mellonella* larvae, despite showing no antibiofilm activity *in vitro*. This increase in *S. epidermidis*-infected larvae survival was not significantly different to the $[\text{Cu}(\text{DDC})_2\text{-liposomes} + \text{free Cu}^{2+}]$ combination ($p > 0.05$). Consequently, the Cu^{2+} -liposomes released their content *in vivo*, rendered excess Cu^{2+} available and resulted in antibacterial activity. However, *G. mellonella* larvae were injected with bacteria and liposomes simultaneously, not allowing for *in vivo* formation of biofilms before treatment. Therefore, the *in vivo* activity of $[\text{Cu}(\text{DDC})_2\text{-liposomes} + \text{Cu}^{2+}\text{-liposomes}]$ might be limited to planktonic bacteria. In addition, survival of *S. epidermidis*-infected larvae, treated with $\text{Cu}(\text{DDC})_2$ -liposomes alone was not significantly different to the survival rate of *S. epidermidis*-infected, untreated larvae, validating previously determined effects of free $\text{Cu}(\text{DDC})_2 + \text{Cu}^{2+}$ in *S. epidermidis*-infected larvae, where excess of Cu^{2+} was crucial for antibacterial activity. Moreover, absence of toxicity of $\text{Cu}(\text{DDC})_2$ -liposomes and Cu^{2+} -liposomes in *G. mellonella* larvae are in line with previous toxicity results of free $\text{Cu}(\text{DDC})_2 + \text{Cu}^{2+}$ in *G. mellonella* and cell culture studies [387]. Consequently, the lack of toxicity and high efficacy of liposomal $\text{Cu}(\text{DDC})_2 + \text{Cu}^{2+}$ observed in the *G. mellonella* model justify progressing to a mammalian *in vivo* infection model for pharmacological testing.

3.1.7 Discussion

We previously reported antibacterial and cytotoxic results of $\text{Cu}(\text{DDC})_2 + \text{Cu}^{2+}$ against *S. aureus* and *S. epidermidis in vitro* and in *G. mellonella* larvae [387]. While the antibiofilm activity of $\text{Cu}(\text{DDC})_2 + \text{Cu}^{2+}$ was determined in an *in vitro* biofilm model that is sufficient for an initial high throughput screening of novel antimicrobial drugs [387], this model is limited by the lack of resemblance to the microenvironment present in a human wound. Specific factors, such as wound exudate, host tissue, access to nutrients, formation of a biofilm gradient, presence of multiple

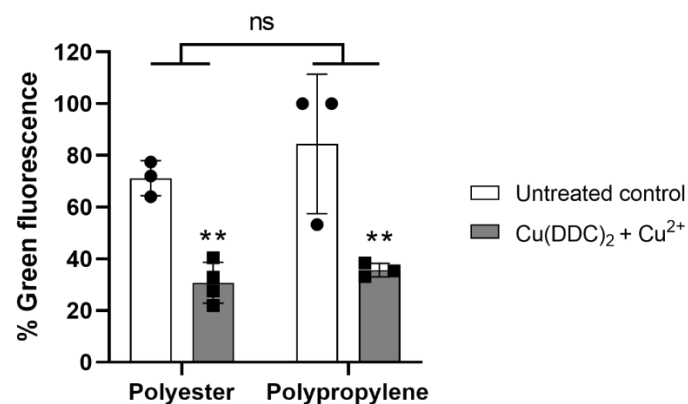
bacterial species, inflammatory responses, and the immune system, influence the progression of a biofilm infection and the wound healing process [388]. By investigating the efficacy of antimicrobial compounds in physiologically relevant *in vitro* biofilm models of surgical site infections, instabilities of the drug or interactions with wound components can be detected and addressed to increase animal study validity before progressing to costly animal studies [397]. Although $\text{Cu(DDC)}_2 + \text{Cu}^{2+}$ preserved significant antibiofilm activity in challenging host-mimicking conditions, many factors present in an infected surgical wound, such as multiple bacterial species, the inflammatory response and the immune system were not incorporated in these *in vitro* models and can alter the outcome of future *in vivo* studies. Here, the effects of $\text{Cu(DDC)}_2 + \text{Cu}^{2+}$ on biofilms of the artificial dermis assay were diminished by the low water solubility of Cu(DDC)_2 and by possible interactions with matrix components, which significantly limits the clinical application of the free compounds and shows the importance of an appropriate drug delivery system. By narrowing the gap between *in vitro* results and *in vivo* translation, we comply with the 3Rs principles by Russell and Burch [411] to improve the welfare of animals used for research.

While Cu(DDC)_2 showed *in vitro* activity against Mycobacteria [221], Streptococci [222,225], and Mycoplasma [224], the antibacterial effects have yet to be confirmed in animal models. In contrast, the research on Cu(DDC)_2 as cancer treatment has progressed to *in vivo* experiments and first clinical trials. The application of Cu(DDC)_2 in clinical trials is based on the separate oral administration of DSF and copper ions and the *in-situ* formation of Cu(DDC)_2 [162]. However, poor biostability and solubility of disulfiram and Cu(DDC)_2 often limit the treatment efficacy [160]. Alternative strategies are based on the encapsulation of Cu(DDC)_2 into nanocarrier, such as micelles [248], cyclodextrins [255], and liposomes [282,288,289]. Here, Cu^{2+} -liposomes and Cu(DDC)_2 -liposomes composed of DSPC, cholesterol and DSPE-mPEG₂₀₀₀ were investigated, as characteristics, including size, PDI, imaging, drug-to-lipid ratio and stability were described by Hartwig, *et al.* [228] and Wehbe, *et al.* [282] and freeze-drying of the liposomes enabled prolonged storage [412]. In addition, intravenous administration of 12.5 mg/kg modified PEGylated Cu(DDC)_2 -liposomes (without cholesterol) and 8 mg/kg of Cu(DDC)_2 -liposomes composed of DSPC and cholesterol were well tolerated in mice [282]. However, Wehbe, *et al.* [282] only investigated the safety of Cu(DDC)_2 -liposomes and not the combination of [Cu(DDC)_2 -liposomes + Cu^{2+} -liposomes] or [Cu(DDC)_2 -liposomes + free Cu^{2+}], which is necessary for the antibiofilm activity. Furthermore, the outcome of *in vivo* safety experiments could be altered by the different lipid composition of the PEGylated liposomes and the non-PEGylated liposomes, due to changes in circulation lifetime after intravenous administration [282]. While the non-PEGylated liposomes were not investigated because of instabilities during storage [228], the PEGylated Cu(DDC)_2 -liposomes with cholesterol were stable and showed no toxicity in *G. mellonella* at 6.4 mg/kg. *G. mellonella* larvae are a good indicator for toxicity and efficacy before progressing to mammalian studies, but the mechanisms of toxicity of the tested compounds can be altered by lack of mammal-specific metabolization processes. Therefore, the combined results of *G. mellonella* and cell assay studies are a predictor of low toxicity of antimicrobial agents but do not replace safety experiments in mammals [410,413].

3.1.8 Conclusion

The $\text{Cu}(\text{DDC})_2 + \text{Cu}^{2+}$ combination at concentrations of 35 μM $\text{DDC}^- + 128 \mu\text{M}$ Cu^{2+} reduced the bacterial load of MRSA and *S. epidermidis* biofilms in an implant and wound model *in vitro*. In addition, the low water solubility of $\text{Cu}(\text{DDC})_2$ was overcome by incorporating the agents into liposomal carriers. Liposomal $\text{Cu}(\text{DDC})_2 + \text{Cu}^{2+}$ showed antibiofilm activity *in vitro* against MRSA and *S. epidermidis* and *in vivo* efficacy against *S. epidermidis*, while being non-toxic. Therefore, the $\text{Cu}(\text{DDC})_2 + \text{Cu}^{2+}$ combination represents a promising treatment strategy against *S. aureus* and *S. epidermidis* biofilm infections. Future studies will investigate the safety and efficacy of liposomal $\text{Cu}(\text{DDC})_2 + \text{Cu}^{2+}$ in a mammalian model of wound infection.

3.1.9 Supplementary file



Supplementary Figure S3.1: Percentage of green fluorescence in confocal microscopy images of *S. aureus* ATCC 6538 biofilms on polyester or polypropylene meshes treated with $\text{Cu}(\text{DDC})_2 + \text{Cu}^{2+}$ (grey) compared to untreated meshes (white). Quantification of images as green and red fluorescence based on LIVE/DEAD BacLight staining (green = viable bacteria; red = dead bacteria). n=3-4; mean \pm SD; 2-way ANOVA: ** $p < 0.01$ indicate significant differences between $\text{Cu}(\text{DDC})_2 + \text{Cu}^{2+}$ and untreated control by Šidák's multiple comparison test; ns $p > 0.05$ indicate no significant differences between the polyester and the polypropylene mesh.

4 Development of an injectable gel for local delivery of Cu(DDC)₂ + Cu²⁺

4.1 Publication: “A thermosensitive, chitosan-based hydrogel as delivery system for antibacterial liposomes to surgical site infections”

Statement of authorship

Title of Paper	A thermosensitive, chitosan-based hydrogel as delivery system for antibacterial liposomes to surgical site infections		
Publication Status	<input checked="" type="checkbox"/> Published	<input type="checkbox"/> Submitted for Publication	
	<input type="checkbox"/> Accepted for Publication	<input type="checkbox"/> Unpublished and Unsubmitted work written in a manuscript style	
Publication Details	Kaul L, Grundmann CE, Köll-Weber M, Löffler H, Weiz A, Zannettino ACW, Richter K & Süß R. A Thermosensitive, Chitosan-Based Hydrogel as Delivery System for Antibacterial Liposomes to Surgical Site Infections. <i>Pharmaceutics</i> . 2022;14(12); doi:10.3390/pharmaceutics14122841.		

Principal author

Name of Principal author	Laurine Kaul		
Contribution to the Paper	Conceptualisation of the project, development of methods, investigation, formal analysis of data, writing – original draft preparation, corresponding author		
Overall percentage (%)	75 %		
Certification	This paper reports on original research I conducted during the period of my Higher Degree by Research candidature and is not subject to any obligations or contractual agreements with a third party that would constrain its inclusion in this thesis. I am the primary author of this paper.		
Signature		Date	08.02.2023

Co-author

By signing the Statement of Authorship, each author certifies that:

- i. The candidate's stated contribution to the publication is accurate (as detailed above).
- ii. Permission is granted for the candidate to include the publication in the thesis; and
- iii. The sum of all co-author contributions is equal to 100% less the candidate's stated contribution.

4 Development of an injectable gel for local delivery of $\text{Cu}(\text{DDC})_2 + \text{Cu}^{2+}$

Name of Co-Author	Clara E. Grundmann		
Contribution to the Paper	Methodology, review and editing of manuscript		
Signature		Date	14.02.2023

Name of Co-Author	Monika Köll-Weber		
Contribution to the Paper	Methodology, investigation, review and editing of manuscript		
Signature		Date	18.02.2023

Name of Co-Author	Hanna Löffler		
Contribution to the Paper	Investigation		
Signature		Date	17/02/2023

Name of Co-Author	Artur Weiz		
Contribution to the Paper	Investigation		
Signature		Date	16/02/2023

Name of Co-Author	Andrew Zannettino		
Contribution to the Paper	Supervision, review and editing of manuscript		
Signature		Date	15/02/23

Name of Co-Author	Katharina Richter		
Contribution to the Paper	Supervision, conceptualisation, review and editing		
Signature		Date	8/2/23




Name of Co-Author	Regine Süß		
Contribution to the Paper	Supervision, conceptualisation, review and editing		
Signature		Date	15/2/2023

4.1.1 Publication title page



Article

A Thermosensitive, Chitosan-Based Hydrogel as Delivery System for Antibacterial Liposomes to Surgical Site Infections

Laurine Kaul^{1,2,3,*}, Clara E. Grundmann², Monika Köll-Weber² , Hanna Löffler², Artur Weiz², Andrew C. W. Zannettino^{3,4,5}, Katharina Richter^{1,3,6,†}  and Regine Süß^{2,†} 

¹ Richter Lab, Department of Surgery, Basil Hetzel Institute for Translational Health Research, University of Adelaide, 37 Woodville Rd., Adelaide, SA 5011, Australia

² Institute of Pharmaceutical Sciences, Department of Pharmaceutics, University of Freiburg, Sonnenstr. 5, 79104 Freiburg, Germany

³ Adelaide Medical School, Faculty of Health and Medical Sciences, University of Adelaide, North Terrace, Adelaide, SA 5000, Australia

⁴ Precision Cancer Medicine Theme, South Australian Health & Medical Research Institute, North Terrace, Adelaide, SA 5000, Australia

⁵ Central Adelaide Local Health Network, 1 Port Rd., Adelaide, SA 5000, Australia

⁶ Institute for Photonics and Advanced Sensing, North Terrace Campus, University of Adelaide, Adelaide, SA 5005, Australia

* Correspondence: laurine.kaul@pharmazie.uni-freiburg.de

† These authors contributed equally to this work.



Citation: Kaul, L.; Grundmann, C.E.; Köll-Weber, M.; Löffler, H.; Weiz, A.; Zannettino, A.C.W.; Richter, K.; Süß, R. A Thermosensitive, Chitosan-Based Hydrogel as Delivery System for Antibacterial Liposomes to Surgical Site Infections. *Pharmaceutics* **2022**, *14*, 2841. <https://doi.org/10.3390/pharmaceutics14122841>

Academic Editor: Anna Angela Barba

Received: 22 November 2022

Accepted: 15 December 2022

Published: 18 December 2022

Publisher's Note: MDPI stays neutral with regard to jurisdictional claims in published maps and institutional affiliations.



Copyright: © 2022 by the authors. Licensee MDPI, Basel, Switzerland. This article is an open access article distributed under the terms and conditions of the Creative Commons Attribution (CC BY) license (<https://creativecommons.org/licenses/by/4.0/>).

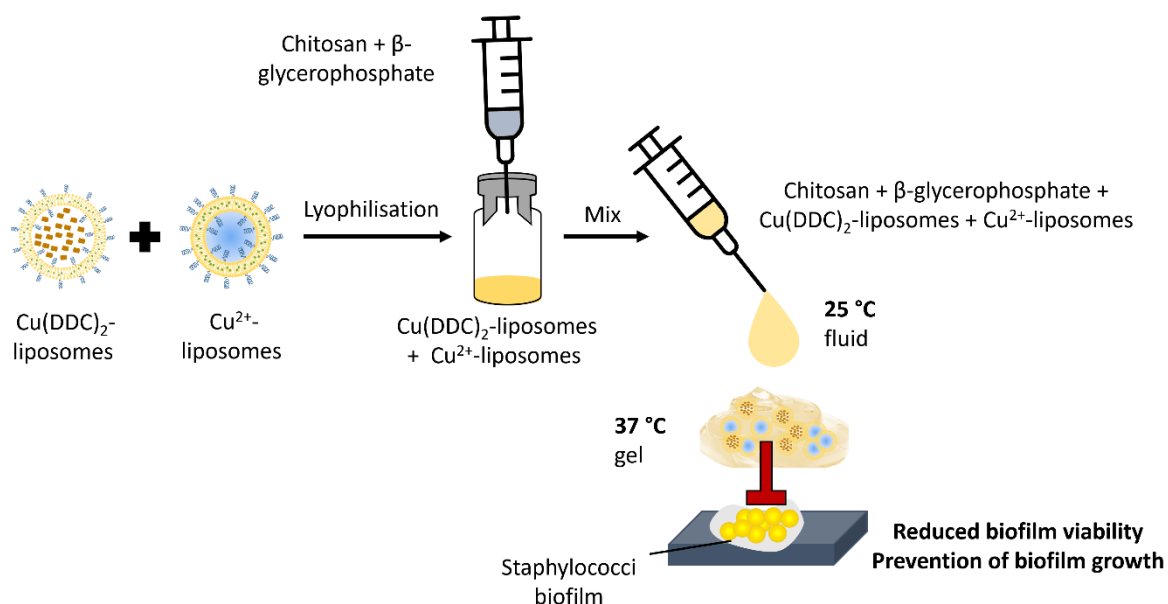
Abstract: Prophylaxis and the treatment of surgical site infections (SSIs) with antibiotics frequently fail due to the antibiotic resistance of bacteria and the ability of bacteria to reside in biofilms (i.e., bacterial clusters in a protective matrix). Therefore, alternative antibacterial treatments are required to combat biofilm infections. The combination of diethyldithiocarbamate (DDC^-) and copper ions (Cu^{2+}) exhibited antibiofilm activity against the staphylococci species associated with SSIs; however, the formation of a water-insoluble $\text{Cu}(\text{DDC})_2$ complex limits its application to SSIs. Here, we describe the development and antibiofilm activity of an injectable gel containing a liposomal formulation of $\text{Cu}(\text{DDC})_2$ and Cu^{2+} (lipogel). Lyophilized liposomes were incorporated into a mixture of chitosan (CS) and beta-glycerophosphate (βGP), and the thermosensitive gelling properties of CS- βGP and the lipogel were determined. The liposomes remained stable after lyophilization over six months at 4–6 °C and –20 °C. The sol-gel transition of the gel and lipogel occurred between 33 and 39 °C, independently of sterilization or storage at –20 °C. CS- βGP is biocompatible and the liposomes were released over time. The lipogel prevented biofilm formation over 2 days and killed 98.7% of the methicillin-resistant *Staphylococcus aureus* and 99.9% of the *Staphylococcus epidermidis* biofilms. Therefore, the lipogel is a promising new prophylaxis and treatment strategy for local application to SSIs.

Keywords: diethyldithiocarbamate; copper ions; liposomes; chitosan; beta-glycerophosphate; surgical site infections; drug delivery; thermosensitive gel; biofilms

1. Introduction

Surgical site infections (SSIs) are amongst the most serious complications following a surgical procedure [1] and affect up to 20% of surgeries [2]. Biofilm-forming bacteria, such as *Staphylococcus aureus* (*S. aureus*) and *Staphylococcus epidermidis* (*S. epidermidis*), are the major pathogens associated with SSIs [3], and the presence of biofilms has been reported in over 80% of SSIs [4]. Biofilms are communities of bacteria embedded in a self-produced matrix, which offers protection from the immune system and antibiotics [5]. Consequently, biofilms require higher antibiotic concentrations to control bacterial growth compared to single bacteria [6]. However, the administration of high antibiotic concentrations or administration over a prolonged period can result in toxic adverse effects [7]. In addition, traditional

4.1.2 Graphical abstract



4.1.3 Abstract

Prophylaxis and the treatment of SSIs with antibiotics frequently fail due to the antibiotic resistance of bacteria and the ability of bacteria to reside in biofilms (i.e., bacterial clusters in a protective matrix). Therefore, alternative antibacterial treatments are required to combat biofilm infections. The combination of DDC^- and Cu^{2+} exhibited antibiofilm activity against the staphylococci species associated with SSIs; however, the formation of a water-insoluble $\text{Cu}(\text{DDC})_2$ complex limits its application to SSIs. Here, we describe the development and antibiofilm activity of an injectable gel containing a liposomal formulation of $\text{Cu}(\text{DDC})_2$ and Cu^{2+} (lipogel). Lyophilised liposomes were incorporated into a mixture of chitosan (CS) and beta-glycerophosphate (βGP), and the thermosensitive gelling properties of CS- βGP and the lipogel were determined. The liposomes remained stable after lyophilisation over six months at $4\text{--}6^\circ\text{C}$ and -20°C . The sol-gel transition of the gel and lipogel occurred between 33 and 39°C , independently of sterilisation or storage at -20°C . CS- βGP is biocompatible and the liposomes were released over time. The lipogel prevented biofilm formation over 2 days and killed 98.7% of the methicillin-resistant *Staphylococcus aureus* and 99.9% of the *Staphylococcus epidermidis* biofilms. Therefore, the lipogel is a promising new prophylaxis and treatment strategy for local application to SSIs.

4.1.4 Introduction

SSIs are amongst the most serious complications following a surgical procedure [2] and affect up to 20% of surgeries [6]. Biofilm-forming bacteria, such as *S. aureus* and *S. epidermidis*, are the major pathogens associated with SSIs [11], and the presence of biofilms has been reported in over 80% of SSIs [333]. Biofilms are communities of bacteria embedded in a self-produced matrix, which offers protection from the immune system and antibiotics [31]. Consequently, biofilms require higher antibiotic concentrations to control bacterial growth compared to single bacteria [32]. However, the administration of high antibiotic concentrations or administration over a prolonged period can result in toxic adverse effects [331]. In addition, traditional antibiotics that play an

important role in both the prevention [11] and the treatment of SSIs [30] increasingly fail to prevent or cure SSIs due to the rise in antibiotic-resistant bacteria [28]. Therefore, identifying antibacterial agents with activity against antibiotic-resistant bacteria, such as MRSA, and their biofilms is imperative.

We previously demonstrated the antibacterial activity of a combination treatment, comprising DDC^- and Cu^{2+} , against *S. aureus*, MRSA, and *S. epidermidis* *in vitro* and *in vivo* [387]. In addition, we showed that there was no toxicity in both *in vitro* cell cultures and an invertebrate *in vivo* model [387]. When DDC^- and Cu^{2+} are mixed, a water-insoluble $\text{Cu}(\text{DDC})_2$ complex (2:1 molar ratio of DDC^- and Cu^{2+}) is instantly formed [223]. The on-site mixing of DDC^- and Cu^{2+} can be performed for pre-clinical studies, but it is not suitable for clinical use [282]. Therefore, multiple carriers have recently been developed to solubilise $\text{Cu}(\text{DDC})_2$, including nanocomplexes [229,230], nanocrystals [250], biohybrid nanoparticles [254], and liposomes [223,228,263,282,288]. As $\text{Cu}(\text{DDC})_2$ exhibits activity against cancer cells [166], these nanovesicles were developed and investigated as an anti-cancer treatment, but they can be used for drug delivery in various diseases, such as infections.

Wehbe, *et al.* [223] developed liposomes containing an aqueous Cu^{2+} core, which was then loaded with DDC^- . DDC^- diffuses through the lipid bilayer and is trapped within the liposomes when the insoluble $\text{Cu}(\text{DDC})_2$ complex is formed. Hartwig, *et al.* [228] further optimised this development process and analysed colloidal stability and drug retention during storage. As the antibacterial activity of DDC^- and Cu^{2+} is based on the presence of $\text{Cu}(\text{DDC})_2$ and an excess of Cu^{2+} [387], a mix of Cu^{2+} -liposomes and $\text{Cu}(\text{DDC})_2$ -liposomes can be used. While this liposomal dispersion might be applied to superficial surgical wounds, a local application to other surgical sites, such as an implant, would be less effective. Therefore, the present study focused on the development of an *in situ*-forming depot to facilitate injection at the surgical site and control the release of antibacterial agents.

A thermally induced gelling system comprising chitosan (CS), a naturally occurring polysaccharide, and beta-glycerophosphate (βGP) was investigated by Chenite, *et al.* [414]. The authors showed that CS- βGP can be administered to the body via injection as it is liquid at room temperature and forms a gel *in situ* at body temperature [414]. Consequently, CS- βGP has been used as a drug delivery platform for nasal, ocular, vaginal, lung, and dermal delivery [310], and a broad range of treatments have been incorporated into CS- βGP , including vaccines [415], insulin [416], anticancer drugs [320,417,418], anti-inflammatory drugs [318], antibiotics [323,324,331], and cells for tissue engineering [310,313,419]. To overcome unfavourable pharmacokinetic profiles and non-ideal properties of the drugs and to prolong or delay drug release from the gel, the drugs can be loaded into liposomes prior to CS- βGP incorporation (lipogel) [314,327,328,417,420]. However, CS- βGP as a drug delivery system for SSIs was only investigated for the antibiotic vancomycin [331], and an application of the gel against biofilms was only evaluated with incorporated zinc oxide nanoparticles against *Porphyromonas gingivalis* for peri-implant infection [321]. In addition, the development of a gel for the local delivery of DDC^- and Cu^{2+} has not yet been proposed.

The objective of the present study was to prepare and characterise *in situ*-forming lipogels containing the antibacterial agents DDC^- and Cu^{2+} , which showed antibiofilm activity against *S. aureus* and *S. epidermidis*. To improve stability and incorporation into the hydrogel, the effect of lyophilisation on colloidal stability and the storage of Cu^{2+} -liposomes and $\text{Cu}(\text{DDC})_2$ -liposomes was evaluated. For the preparation of an *in situ* thermosensitive hydrogel, CS- βGP was sterilised and used as a carrier for Cu^{2+} -liposomes and $\text{Cu}(\text{DDC})_2$ -liposomes. Changes in the rheological behaviours of the hydrogel, including gelation temperature, gelation time, and gel strength, caused

by the addition of liposomes were evaluated. The *in vitro* release of liposomes was estimated by diffusion assay and weight loss measurements and through the antibacterial and antibiofilm activity against MRSA and *S. epidermidis*.

4.1.5 Materials and methods

4.1.5.1 Bacterial strains, cell cultures, materials, and chemicals

S. epidermidis ATCC 35984 and *S. aureus* ATCC 700699 (also known as MRSA Mu50) were purchased from the American Type Culture Collection (Manassas, VA, USA). Single colonies were dissolved in 0.9% NaCl, adjusted to 0.5 McFarland units, and further 1:1000 (v/v) diluted in tryptone soya broth (TSB, Thermo Fisher Scientific, Waltham, MA, USA). Bacteria were grown in an incubator at 37 °C under aerobic conditions. Tryptone soya agar (TSA) was prepared by adding 1.5% agar bacteriological (Thermo Fisher Scientific) before steam sterilisation. A10 phosphate buffer and B trace solution were prepared according to Rybtke, *et al.* [421]. Prior to steam sterilisation, B trace solution was supplemented with 1.5% agar bacteriological and 0.5% Bacto™ Proteose Peptone (Thermo Fisher Scientific). The final AB trace agar contained 90% B trace agar, 10% sterile filtered A10 phosphate buffer, and 0.5% glucose. Cell culture studies were conducted using control human fibroblast cells (GM00038) obtained from the Coriell Institute for Medical Research (Camden, NJ, USA). The normal human skin fibroblast cell line was cultured in Eagle's minimum essential medium with Earle's salts and non-essential amino acids supplemented with 15% (v/v) foetal bovine serum (Biochrom, Berlin, Germany) and 2.2 g/l sodium bicarbonate and cultivated in cell culture flasks in an incubator at 37 °C with 5% CO₂. The lipids for the liposome production included 1,2-distearoyl-sn-glycero-3-phosphocholine (DSPC) and 1,2-distearoyl-sn-glycero-3-phosphoethanolamine-N-[methoxy(polyethylene glycerol)-2000] (DSPE-mPEG₂₀₀₀), which were generously donated by Lipoid GmbH (Ludwigshafen, Germany), and the cholesterol (Chol) was purchased from Sigma-Aldrich (Steinheim, Germany). Unless stated otherwise, all the chemicals, materials, media, and supplements were purchased from Sigma-Aldrich.

4.1.5.2 Preparation of liposomes

Cu²⁺-liposomes and Cu(DDC)₂-liposomes composed of DSPC:Chol:DSPE-mPEG₂₀₀₀ (50:45:5, molar ratio) were prepared by the thin-film hydration method described by Hartwig, *et al.* [228]. Briefly, the lipids were dissolved in chloroform and evaporated to dryness by rotation under reduced pressure at 65 °C using a rotary evaporator (Vacuubrand, Wertheim and VWR, Darmstadt, Germany). The film was then hydrated in a 150 mM CuSO₄ aqueous solution. The liposomes (40 mM total lipid) were extruded at 65 °C through a 0.08 µm polycarbonate membrane (GE Healthcare Life Science, Marlborough, MA, USA) by a 1 ml Liposofast extruder (Avestin, Ottawa, ON, Canada). Unentrapped Cu²⁺ was removed by passage over a Sephadex™ G-50 Fine (GE Healthcare Life Science) column with an EDTA-containing sucrose buffer (300 mM sucrose, 20 mM HEPES, 30 mM EDTA, pH 7.4). Cu²⁺-liposomes were collected following a buffer exchange to an EDTA-free sucrose buffer (SH: 300 mM sucrose, 20 mM HEPES, pH 7.4) by 3 centrifugation steps (3000 × g, ambient temperature, 1.5 h per step), using Vivaspin® Turbo 4 filtration units (100 kDa MWCO; Sartorius AG, Göttingen, Germany).

Cu(DDC)₂-liposomes were prepared by incubation of Cu²⁺-liposomes with 70 mM DDC⁻ in water at 25 °C and mixed at 300 rpm for 10 min using a Thermomixer comfort (Eppendorf, Hamburg, Germany), allowing the DDC⁻ to pass the liposomal membrane and to complex with the entrapped Cu²⁺. Following a filtration step with a 0.45 µm cellulose acetate filter (VWR International, Radnor, PA, USA) to remove non-encapsulated Cu(DDC)₂, excess DDC⁻ was removed during

3 centrifugation steps ($3000 \times g$, ambient temperature, 45 min per step), using Vivaspin® Turbo 4 filtration units (100 kDa MWCO). Before use, the Cu^{2+} -liposomes and $\text{Cu}(\text{DDC})_2$ -liposomes were sterile filtered with a $0.2 \mu\text{m}$ cellulose acetate filter (VWR International) and characterised according to Hartwig, *et al.* [228].

4.1.5.3 Liposome characterisation

Size and polydispersity index

The size, expressed as hydrodynamic diameter (d_h), and the polydispersity index (PDI) were measured via dynamic light scattering (DLS, ZetaPals, Brookhaven Instruments Corporation, Holtsville, NY, USA). A 1:200 (v/v) dilution of Cu^{2+} -liposomes and a 1.5:1000 (v/v) dilution of $\text{Cu}(\text{DDC})_2$ -liposomes in SH buffer (viscosity: $1.213 \text{ mPa}\cdot\text{s}$; refractive index: 1.345) were used for size and polydispersity analyses.

Quantification of encapsulated Cu^{2+}

The encapsulated Cu^{2+} of the Cu^{2+} -liposomes and $\text{Cu}(\text{DDC})_2$ -liposomes was quantitated via spectrophotometry. The absorbance of Cu^{2+} as the $\text{Cu}(\text{DDC})_2$ complex was measured at $\lambda = 435 \text{ nm}$ with a GENESYS 10S UV-Vis spectrophotometer (Thermo Fisher Scientific). The Cu^{2+} -liposomes or $\text{Cu}(\text{DDC})_2$ -liposomes were 1:10 (v/v) mixed with methanol (HPLC grade, Carl Roth, Karlsruhe, Germany), and 1 ml of the mix was measured in a 1.5 ml semi-micro polymethyl methacrylate cuvette (Brand GmbH + Co, Wertheim, Germany). Methanol disrupts the liposomal membrane and solubilises the $\text{Cu}(\text{DDC})_2$ complex. For quantitation of the Cu^{2+} -liposomes, methanol was supplemented with an excess of DDC^- ($70 \mu\text{M}$) to complex all the Cu^{2+} to $\text{Cu}(\text{DDC})_2$. The measured $\text{Cu}(\text{DDC})_2$ absorbance was quantitated by the linear least square regression analysis of a calibration curve, based on standard aqueous Cu^{2+} solutions ($0.15\text{--}1 \text{ mM}$) in $70 \mu\text{M}$ DDC^- in methanol. All the liposomal concentrations are expressed as Cu^{2+} concentrations. The $\text{Cu}(\text{DDC})_2$ -liposomes + Cu^{2+} -liposomes were mixed in a 1:6.2 molar ratio of $\text{Cu}(\text{DDC})_2$ -liposomes to Cu^{2+} -liposomes.

4.1.5.4 Lyophilisation of liposomes

The lyophilisation cycle was designed based on the glass transition of the maximally freeze-concentrated amorphous phase (T_g') of the SH buffer. The lyophilisation was conducted using the Alpha 2-4 freeze dryer (Martin Christ GmbH, Osterode am Harz, Germany) with the settings described in Table 4.1. Prior to lyophilisation, the Cu^{2+} -liposomes, $\text{Cu}(\text{DDC})_2$ -liposomes, or a mix of both were diluted to a Cu^{2+} concentration of $600 \mu\text{M}$ in SH buffer, placed in glass vials, and frozen at $-80 \text{ }^\circ\text{C}$ for 12 h. The primary drying temperature of $-45 \text{ }^\circ\text{C}$ was selected as approximately $10 \text{ }^\circ\text{C}$ below the T_g' of the SH buffer [422]. Following the end of the secondary drying, the glass vials were sealed and stored at $-20 \text{ }^\circ\text{C}$.

Table 4.1: Parameters for the lyophilisation process of $\text{Cu}(\text{DDC})_2$ -liposomes and/or Cu^{2+} -liposomes.

Parameters	Freezing	Primary drying	Secondary drying	
			First step	Second step
Temperature ($^\circ\text{C}$)	-80	-45	0	25
Pressure (mbar)	-	0.07	0.001	0.001
Time (h)	12	42	3	3

To investigate the potential effects of the lyophilisation process on the Cu^{2+} -liposome and $\text{Cu}(\text{DDC})_2$ -liposome stability, the d_h and PDI were determined following the rehydration of the lyophilisate with ultrapure water (Milli-Q system, Merck, Darmstadt, Germany; Figure 4.1). To investigate the percentage of retained Cu^{2+} or $\text{Cu}(\text{DDC})_2$ within the liposomes, the Cu^{2+} concentrations were measured using UV-Vis, as described in Section 4.1.5.3. Following rehydration, the total Cu^{2+} concentration (encapsulated and non-encapsulated, $C_{[\text{total}]}$) was measured. The intact Cu^{2+} -liposomes were then separated from the leaked non-liposomal Cu^{2+} by centrifugation ($3000 \times g$, room temperature, 10 min) using Vivaspin® Turbo 4 filtration units, and the intact $\text{Cu}(\text{DDC})_2$ -liposomes were separated from the non-liposomal $\text{Cu}(\text{DDC})_2$ by surface area filtration ($0.2 \mu\text{m}$ cellulose acetate filter). Following the filtration step, the Cu^{2+} concentrations of separated non-liposomal Cu^{2+} ($C_{[\text{Cu}^{2+}]}$) and liposomal $\text{Cu}(\text{DDC})_2$ -liposomes ($C_{[\text{Cu}(\text{DDC})_2\text{-liposome}]}$) were measured. The percentage of retained encapsulated Cu^{2+} in the Cu^{2+} -liposomes was calculated according to Equation 4.1, and the percentage of retained encapsulated $\text{Cu}(\text{DDC})_2$ in the $\text{Cu}(\text{DDC})_2$ -liposomes was calculated according to Equation 4.2.

$$\% \text{ Retained } \text{Cu}^{2+} \text{ within liposome} = \frac{C_{[\text{total}]} - C_{[\text{Cu}^{2+}]}}{C_{[\text{total}]}} \times 100 \quad (4.1)$$

$$\% \text{ Retained } \text{Cu}(\text{DDC})_2 \text{ within liposome} = \frac{C_{[\text{Cu}(\text{DDC})_2\text{-liposome}]}}{C_{[\text{total}]}} \times 100 \quad (4.2)$$

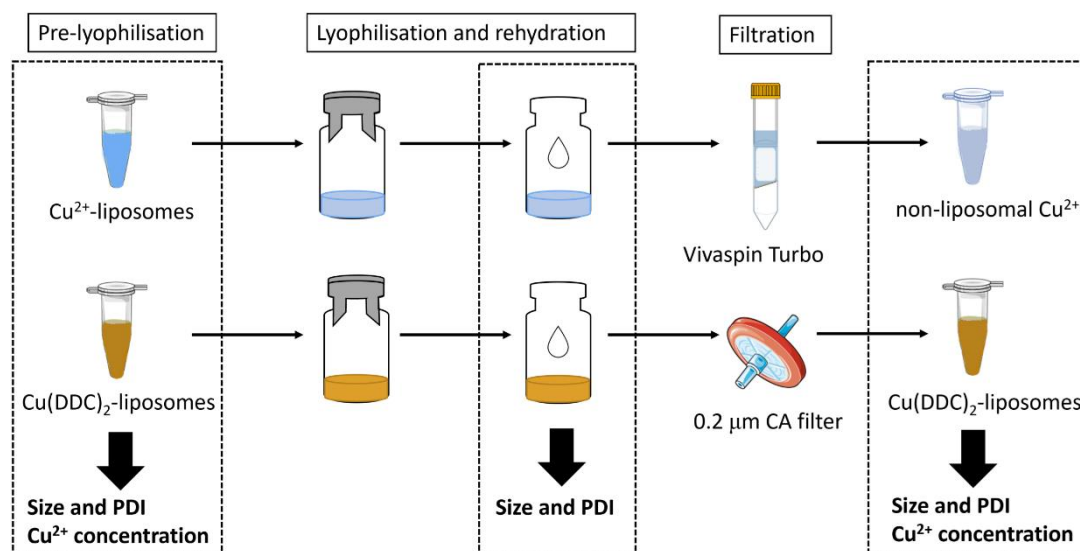


Figure 4.1: Experimental procedure of characterisation steps prior and following the lyophilisation process. The filtration step separated non-encapsulated Cu^{2+} and $\text{Cu}(\text{DDC})_2$. Hydrodynamic diameter and polydispersity index were determined prior to lyophilisation, after rehydration and following filtration. Total Cu^{2+} concentrations were determined after rehydration, while Cu^{2+} concentrations of separated non-encapsulated Cu^{2+} and $\text{Cu}(\text{DDC})_2$ -liposomes were determined following filtration and were used to calculate drug retention (%). CA = cellulose acetate.

4.1.5.5 Stability of lyophilised liposomes

For storage stability studies, aliquots of lyophilised Cu^{2+} -liposomes and $\text{Cu}(\text{DDC})_2$ -liposomes were kept at either $4\text{--}6 \text{ }^\circ\text{C}$ or $-20 \text{ }^\circ\text{C}$ for up to 168 days (approximately 6 months). At the indicated time points, lyophilised liposomes were resuspended with the amount of water removed during the lyophilisation process, characterised by DLS, and the percentage of retained Cu^{2+} or $\text{Cu}(\text{DDC})_2$ within the liposomes was determined according to Section 4.1.5.4.

4.1.5.6 Preparation of hydrogel

Chitosan (CS; 95% deacetylation; molecular weight 100–250 kDa; Heppel Medical Chitosan GmbH, Halle, Germany) was dissolved in 0.15 M acetic acid solution (2% w/v) under stirring and stored at 4 °C. To prepare the gel, ice-cold β GP (13% w/v) was added dropwise to the CS solution up to a final molar ratio of 1:4.88 of CS to β GP and stirred in an ice bath for 15 min. The CS- β GP mix with a pH of 7.15 ± 0.17 (pH meter CG 843 P, Schott, Mainz, Germany) was either directly aliquoted and stored at -20 °C or, following a 10 min rest period in the ice bath without stirring, directly used for experiments. Following storage at -20 °C, the CS- β GP mix was thawed at ambient temperature and directly used for experiments. For the use of the CS- β GP mix under aseptic conditions, the CS solution was exposed to ultraviolet light for 20 min, and the β GP was sterile filtered through a 0.2 μm cellulose acetate membrane (sterile CS- β GP). To incorporate the liposomes, the lyophilised liposomes were resuspended in thawed or freshly prepared CS- β GP.

4.1.5.7 Rheological measurements

The rheological tests were conducted with a Kinexus Lab+ rotational rheometer (Malvern Instruments, Malvern, UK), using a cone/plate geometry (CP1/40; PLS40) with a gap of 23 μm . The storage modulus (G') and loss modulus (G'') of the samples were measured within the linear viscoelastic range at a constant strain amplitude of 5% and a constant frequency of 0.5 Hz. The CS- β GP mixture (600 μl) was placed on the sample holder at 15 °C and sealed with a viscous paraffin solution to prevent sample evaporation during the measurement. The temperature sweep was performed from 15 to 45 °C with a heating rate of 2 °C/min. The time sweep was performed over 500 s and simulated an injection into the human body. The temperature was increased at a maximum heating rate from 15 to 37 °C for over 75 s; then, the temperature was held at 37 °C for the remaining time. The sol-gel transition temperature and time were defined as the intersection of the G' and G'' curves. Considering that the strength of hydrogels can be evaluated in terms of the behaviour of G' and G'' at low frequencies [311], a frequency sweep over the range of 0.1–10 Hz was performed following the time sweep at 37 °C. The effect of sterilisation, storage at -20 °C, and the incorporation of liposomes was investigated. The liposomes were added at Cu^{2+} concentrations of 128 μM .

4.1.5.8 Cytotoxicity of the gel

The human dermal fibroblast cells were seeded in the wells of the appropriate plate and incubated for 24 h. Following media renewal, the fibroblasts were exposed to either gel or supernatant over 24 h, as specified below. The fibroblast viability was assessed with the CellTiter-Glo[®] Luminescent Viability Assay (Promega Corporation, Fitchburg, WI, USA) according to the manufacturer's instructions, and luminescence was measured on a FLx800[™] Multi-Detection Microplate Reader (BioTek Instruments, Winooski, VT, USA). The percentage of fibroblast viability was calculated using Equation 4.3 with the luminescence intensity of the treated and untreated fibroblasts, represented by $I_{\text{treatment}}$ and $I_{\text{untreated}}$, respectively, and I_{blank} , representing the background luminescence of the cell medium.

$$\% \text{ Fibroblast viability} = \left(\frac{I_{\text{treatment}} - I_{\text{blank}}}{I_{\text{untreated}} - I_{\text{blank}}} \right) \times 100 \quad (4.3)$$

The cut-off for designating the treatment as non-toxic was determined according to ISO norm 10993-5:2009(E) with the direct contact method as viabilities exceeding 70%.

CS-βGP gel covering fibroblast cells

In a 12-well plate, 6×10^5 cells in 1.5 ml culture medium were seeded in each well and incubated for 24 h to allow attachment. Then, the fibroblast cells were covered with 250 or 500 μl sterile CS-βGP gel in the presence of 1 ml media for 24 h.

Fibroblast cells exposed to released components of CS-βGP gel

In a black 96-well plate, 5×10^4 cells in 200 μl culture medium were seeded in each well and incubated for 24 h. The cells were treated with a mix of 200 μl media and 100 μl of 0.9% NaCl, previously incubated with CS-βGP for 0, 6, 24, or 72 h, as described in Section 4.1.5.9.

4.1.5.9 Effect of release liposomes from CS-βGP gel on fibroblast cell viability

The release of Cu^{2+} -liposomes and $\text{Cu}(\text{DDC})_2$ -liposomes from the respective lipogels was assessed by investigating the effect of the released liposomes on human dermal fibroblast cell viability. In a 96-well plate, lyophilised liposomes equivalent to 770 μM Cu^{2+} -liposomes or 14 μM $\text{Cu}(\text{DDC})_2$ -liposomes (based on Cu^{2+} concentrations) were incorporated into 100 μl of thawed CS-βGP mix. The solution containing liposomes and CS-βGP was heated to 37 °C for 5 min using the Thermomixer comfort to enable gel formation, then covered with 100 μl release media (0.9% NaCl). Following incubation on an orbital shaker at 37 °C and 500 rpm for 0, 4, 6, 24, and 72 h for the Cu^{2+} -liposomes incorporated in the CS-βGP gel (Cu^{2+} -lipogel) and 0, 0.5, 1, 2, 4, 6, 24, and 72 h for the $\text{Cu}(\text{DDC})_2$ -liposomes incorporated in the CS-βGP gel ($\text{Cu}(\text{DDC})_2$ -lipogel), 100 μl of release media was transferred onto the fibroblast cells (5×10^4 in 200 μl culture medium, incubated at 37 °C in 5% CO_2 for 24 h) in a black 96-well plate. The fibroblast cells were exposed to the release media for 24 h at 37 °C, 5% CO_2 . The controls were incubated for 0.5, 24, and 72 h and included (i) CS-βGP gel (see Section 4.1.5.8; 0% release); (ii) Cu^{2+} -liposomes or $\text{Cu}(\text{DDC})_2$ -liposomes in release media (100% liposomal release); and (iii) unencapsulated Cu^{2+} or $\text{Cu}(\text{DDC})_2$ in release media (100% non-liposomal release). Based on the changes observed after 24 h of incubation of the $\text{Cu}(\text{DDC})_2$ -liposomes in release media, an additional measurement was taken after 6 h. The fibroblast viability was determined as described in Section 4.1.5.8.

4.1.5.10 Weight loss over time

The weight loss of the CS-βGP gel or the CS-βGP gel with incorporated $\text{Cu}(\text{DDC})_2$ -liposomes + Cu^{2+} -liposomes ($\text{Cu}(\text{DDC})_2$ + Cu^{2+} -lipogel), either freshly prepared or stored at -20 °C, was determined over 49 days. The gels were prepared by pouring 1 ml of CS-βGP solution into transwell inserts (polyester, pore size 3 μm, whose tares are known; Corning, Kaiserslautern, Germany), weighed (gel initial weight, W_i), placed in a 6-well plate, and heated to 37 °C in an incubator. The system consisting of the gel and the transwell insert was kept at 37 °C over a timeframe of 5 weeks, and each system was weighed at given time intervals (gel weight at timepoint t, W_t). The percentage of weight loss at the timepoint t was calculated using Equation 4.4.

$$\% \text{ Weight loss} = \left(1 - \frac{W_t}{W_i}\right) \times 100 \quad (4.4)$$

4.1.5.11 Antibiofilm activity of gel

The antibiofilm activity of the $\text{Cu}(\text{DDC})_2$ + Cu^{2+} -lipogel was determined as described by Richter, *et al.* [391]. Each side of the polycarbonate membranes with a 100 nm pore size (Whatman, GE Healthcare, Little Chalfont, UK) was exposed to UV light for 10 min prior to use. Up to 4 membranes were placed on a TSA plate, and each was inoculated with 1 μl of MRSA Mu50 or

S. epidermidis ATCC 35984 suspension (equivalent to 1×10^5 colony-forming units (CFU)/ml). To determine the prevention of biofilm growth, the bacteria were exposed to 200 μl $\text{Cu}(\text{DDC})_2 + \text{Cu}^{2+}$ -lipogel 10 min after inoculation and incubated for 48 h. To determine the biofilm killing of $\text{Cu}(\text{DDC})_2 + \text{Cu}^{2+}$ -lipogel, the bacterial suspension was first incubated for 24 h for MRSA Mu50 and 48 h for *S. epidermidis* ATCC 35984, to allow biofilm formation. The membranes were then transferred onto a 12-well plate containing 2 ml AB trace agar, and the biofilms were exposed to 500 μl $\text{Cu}(\text{DDC})_2 + \text{Cu}^{2+}$ -lipogel for 4 days. The membranes were transferred into new wells containing fresh AB trace agar after 2 days. Finally, the bacteria were recovered from the membranes in 10 ml 0.9% NaCl by vortexing–sonication–vortexing (1-15-1 min), diluted, and plated on TSA for CFU counting. The controls included untreated bacteria and CS- β GP gel. $\text{Cu}(\text{DDC})_2 + \text{Cu}^{2+}$ -lipogel and CS- β GP gel were applied in liquid form and formed a gel on the membrane during the incubation period at 37 °C in the incubator.

4.1.5.12 Statistical analysis

All experiments were conducted at least in triplicate, and the results were statistically analysed using GraphPad Prism version 9.4.1 for Windows (GraphPad Software, San Diego, CA, USA), and the statistical significance was set with an $\alpha = 0.05$. The parametric data are represented by the mean \pm standard deviation (SD), which was analysed using one-way ANOVA with Dunnett's or Tukey's multiple comparison test, as described in the figure legend.

4.1.6 Results and discussion

4.1.6.1 Cu^{2+} -liposomes and $\text{Cu}(\text{DDC})_2$ -liposomes are stable following lyophilisation

As PEGylated $\text{Cu}(\text{DDC})_2$ -liposomes are only stable at 4–6 °C for up to 3 months [228], the $\text{Cu}(\text{DDC})_2$ -liposomes and Cu^{2+} -liposomes were lyophilised to increase storage stability and to facilitate incorporation into the drug delivery platforms. However, the physical structure of liposomes can alter during the lyophilisation process, and this can lead to drug leakage. During the freezing process, the formation of ice crystals within the liposome or in the external aqueous phase can rupture the lipid bilayer. In addition, the aggregation or fusion of liposomes during the drying process can result in a size increase [422,423]. Therefore, the d_h and PDI were measured before lyophilisation, after rehydration, and following filtration for both the Cu^{2+} -liposomes and the $\text{Cu}(\text{DDC})_2$ -liposomes. The quantification of the encapsulated drug was calculated by measuring the Cu^{2+} concentration prior to lyophilisation (i.e., 100% control) and following filtration (Figure 4.1).

After rehydration, the size and PDI of the Cu^{2+} -liposomes were slightly increased (d_h : 123 nm; PDI: 0.06) compared to pre-lyophilisation (d_h : 110 nm; PDI: 0.05) but were restored following filtration (d_h : 115 nm; PDI: 0.06; Figure 4.2a). Similar results were observed in the lyophilised $\text{Cu}(\text{DDC})_2$ -liposomes, with a small increase after rehydration (d_h : 183 nm; PDI: 0.15) compared to pre-lyophilisation (d_h : 174 nm; PDI: 0.14) and following filtration (d_h : 170 nm; PDI: 0.13; Figure 4.2b). The pre-lyophilisation size and PDI of the Cu^{2+} -liposomes and $\text{Cu}(\text{DDC})_2$ -liposomes are in accord with previously reported values [228]. In addition, Wehbe, *et al.* [223] observed that the size determined using DLS was comparable to the vesicle size estimated by cryogenic electron microscopy (cryo-EM). The population of the liposomes was homogenous as the PDI of the Cu^{2+} -liposomes and $\text{Cu}(\text{DDC})_2$ -liposomes was below 0.2 prior to lyophilisation and following rehydration [398]. Moreover, the Cu^{2+} retention was 72.3% for the Cu^{2+} -liposomes, and the $\text{Cu}(\text{DDC})_2$ retention was 72.7% for the $\text{Cu}(\text{DDC})_2$ -liposomes (Figure 4.2c). The change in d_h and PDI was not significantly different ($p > 0.05$), which may be associated with the use of sucrose as a lyoprotectant. Sucrose can help to maintain the integrity of liposomes during the lyophilisation

process by replacing the water molecules between the phospholipid groups. Consequently, the risk of ice crystal formation is minimised, and lipid distribution is maintained in the dry space to prevent packing defects [422,424,425]. However, the leakage of Cu^{2+} and $\text{Cu}(\text{DDC})_2$ indicated a possible rearrangement or the collapse of some liposomes. Wessman, *et al.* [426] investigated the lyophilisation of similar liposomes containing DSPC:Chol:DSPE-PEG₅₀₀₀ with the lyoprotectant lactose and the effect of osmotic stress on the liposomes. They showed a similar increase in size distribution after freeze-drying and subsequent rehydration but observed a large population of double or multi-lamellar liposomes and an increase in interbilayer distance using cryo-EM, which might be the result of an osmotic imbalance of the lyoprotectant [426]. While imaging of the Cu^{2+} -liposomes and $\text{Cu}(\text{DDC})_2$ -liposomes with cryo-EM previously showed mostly unilamellar vesicles [223], imaging of the liposomes following rehydration can determine changes in the lamellarity and morphology of the liposomes caused by the lyophilisation process. The addition of sucrose within the liposomes can prevent the osmotic stress on the outer bilayer and can therefore reduce drug leakage [424]. Moreover, another lyoprotectant can be used, such as other disaccharides or oligosaccharides [425]. Here, sucrose was used as a lyoprotectant as it is part of the buffer solution used for the preparation of the liposomes.

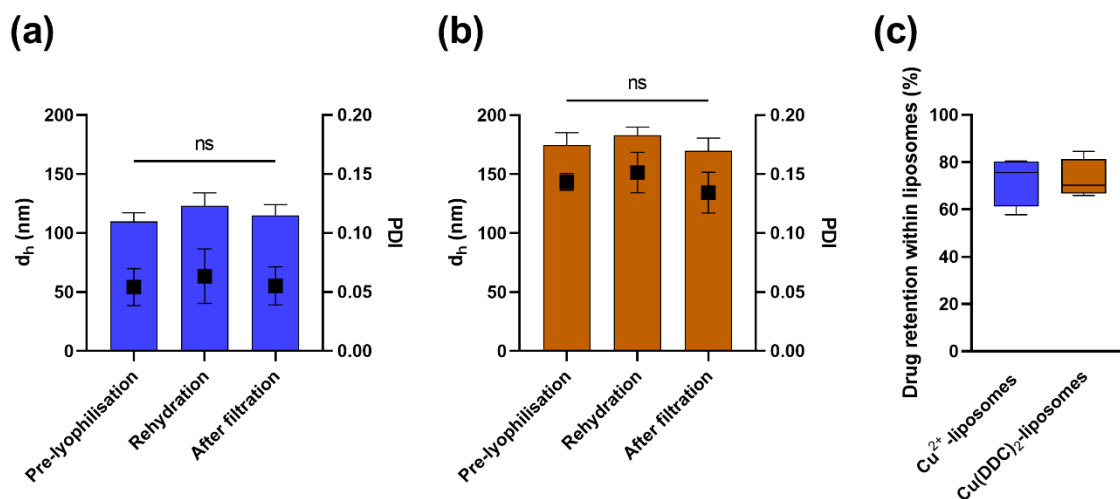
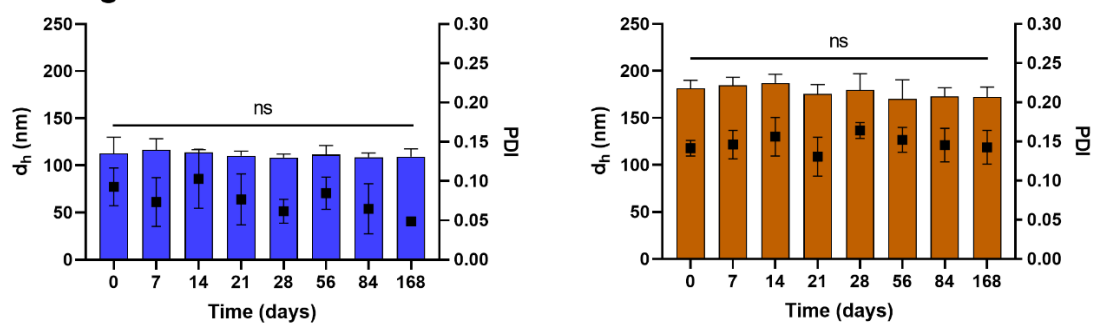


Figure 4.2: Effect of the lyophilisation processes on Cu^{2+} -liposomes (blue) and $\text{Cu}(\text{DDC})_2$ -liposomes (brown) characteristics. Hydrodynamic diameter (d_h ; bars) and polydispersity index (PDI; squares) of (a) Cu^{2+} -liposomes and (b) $\text{Cu}(\text{DDC})_2$ -liposomes prior to lyophilisation, when rehydrated and following filtration. (c) Drug (Cu^{2+} or $\text{Cu}(\text{DDC})_2$) retention within Cu^{2+} -liposomes or $\text{Cu}(\text{DDC})_2$ -liposomes after lyophilisation. Data are expressed as the mean \pm standard deviation ($n = 4$; repeated measures 1-way ANOVA: ns = not significant $p > 0.05$).

4.1.6.2 Lyophilised liposomes are stable over 6 months

The colloidal stability of the lyophilised Cu^{2+} -liposomes and $\text{Cu}(\text{DDC})_2$ -liposomes following storage at 4–6 °C (Figure 4.3a) or –20 °C (Figure 4.3b) was determined by changes in the d_h and PDI. The Cu^{2+} -liposomes and $\text{Cu}(\text{DDC})_2$ -liposomes stored at 4–6 °C and –20 °C over 6 months (168 days) showed no significant difference in d_h and PDI ($p > 0.05$). Additionally, the percentage of Cu^{2+} retained within the Cu^{2+} -liposomes and the $\text{Cu}(\text{DDC})_2$ retained within the $\text{Cu}(\text{DDC})_2$ -liposomes were not reduced after storage at 4–6 °C (Figure 4.4a) or –20 °C (Figure 4.4b) for up to 6 months, with 68.0% and 73.6% Cu^{2+} retention in the Cu^{2+} -liposomes, respectively, and 67.6% and 70.1% $\text{Cu}(\text{DDC})_2$ retention in the $\text{Cu}(\text{DDC})_2$ -liposomes, respectively. Therefore, the lyophilised Cu^{2+} -liposomes and $\text{Cu}(\text{DDC})_2$ -liposomes can be stored at 4–6 °C and –20 °C without significant changes in size and PDI and without drug leakage.

(a) Storage at 4-6 °C



(b) Storage at -20 °C

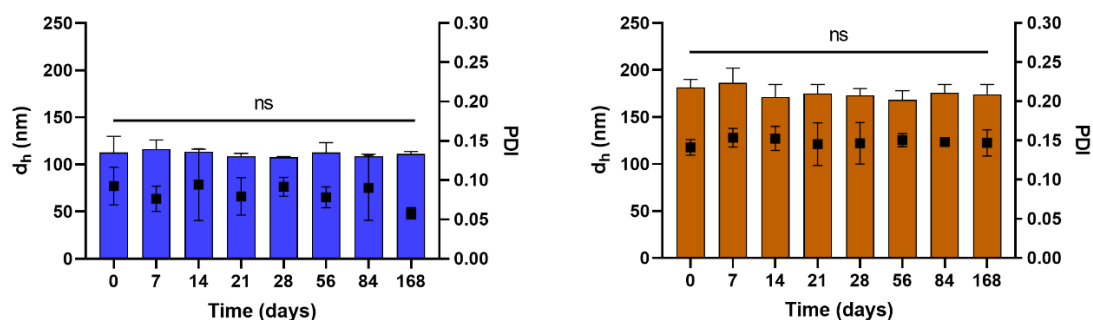


Figure 4.3: Colloidal stability analysis of rehydrated Cu^{2+} -liposomes (blue) and $\text{Cu}(\text{DDC})_2$ -liposomes (brown) after storage in lyophilised form at (a) 4–6 °C and (b) –20 °C. Aliquots of lyophilised Cu^{2+} -liposomes and $\text{Cu}(\text{DDC})_2$ -liposomes were stored for up to 168 days and resuspended, and the hydrodynamic diameter (d_h ; bars) and polydispersity index (PDI; squares) were determined via dynamic light scattering. Data are expressed as the mean \pm standard deviation ($n = 3$; 1-way ANOVA with Dunnett’s multiple comparison test, ns = not significant $p > 0.05$).

Low storage temperatures facilitate the subsequent incorporation of the liposomes into the CS- β GP mix, which was either freshly prepared at 4 °C or stored at –20 °C. It was previously stated that the storage temperature should be at least 50 °C below the glass transition temperature [423], which is between 65 and 77 °C for sucrose [422]. Therefore, the storage temperatures of –20 °C and 4–6 °C are in line with these recommendations.

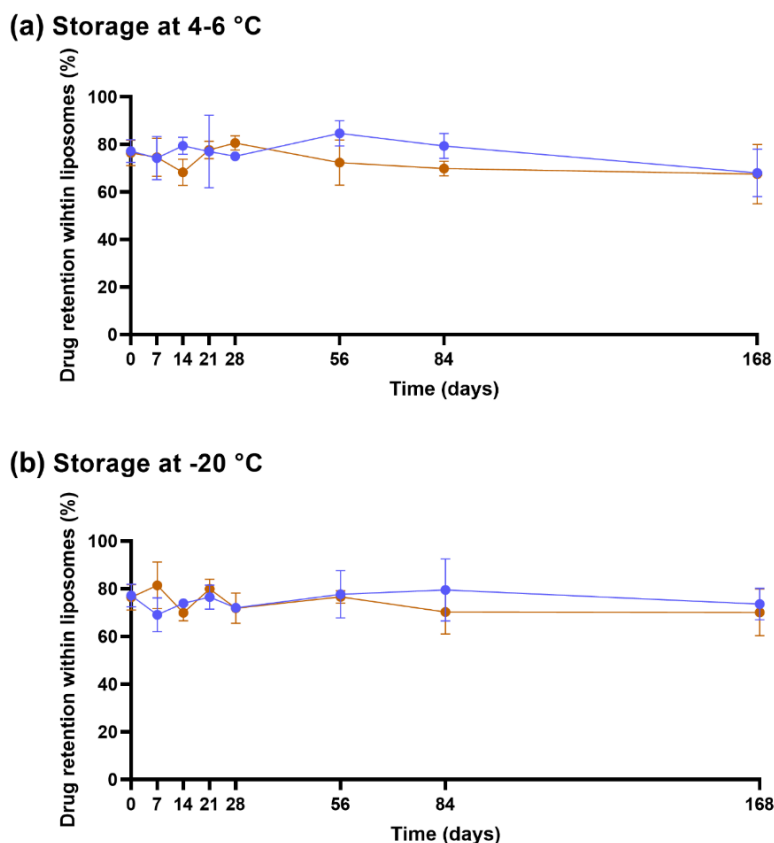


Figure 4.4: Retention of Cu²⁺ in Cu²⁺-liposomes (blue) and Cu(DDC)₂ in Cu(DDC)₂-liposomes (brown) following storage of the lyophilised liposomes at 4–6 °C or –20 °C. Aliquots of lyophilised Cu²⁺-liposomes and Cu(DDC)₂-liposomes were stored at (a) 4–6 °C or (b) –20 °C for up to 168 days. Cu²⁺-liposomes and Cu(DDC)₂-liposomes were resuspended and filtered after predetermined storage times. Cu²⁺ concentrations of Cu²⁺-liposomes and Cu(DDC)₂-liposomes were determined before and after the filtration step. A reduction in Cu²⁺ concentration indicated Cu²⁺ or Cu(DDC)₂ leakage from liposomes. Data are expressed as the mean ± standard deviation (n = 3).

4.1.6.3 The sol-gel transition of CS-βGP is temperature sensitive

The thermosensitive properties of CS-βGP (i.e., the transition from sol to gel) were measured at different temperatures by rheological measurements. While body temperature in a healthy human is around 37 °C, the temperature can drop during long surgical procedures but should not be lower than 36 °C [427]. Therefore, sol-gel transition temperatures of CS-βGP should not exceed 36–37 °C. While the sol-gel transition temperature and time differed between the tested CS-βGP mixes, all the rheological curves exhibited viscoelastic properties. Figure 4.5 displays the representative curves of a temperature sweep (Figure 4.5a) and a time sweep (Figure 4.5b) of CS-βGP stored at –20 °C. Both rheological measurements started at a temperature of 15 °C with $G' < G''$, corresponding to higher viscous properties compared to elastic properties, resulting in a liquid form of the thawed CS-βGP. In Figure 4.5a, the temperature was increased from 15 °C to 45 °C over 15 min, resulting in a steady increase in G' , while G'' slightly decreased. At 40.0 °C, $G' > G''$, indicating the sol-gel transition and consequent formation of CS-βGP gel. Following the sol-gel transition and until reaching 45 °C, the difference between G' and G'' continuously increased. Moreover, the sol-gel transition time was determined when the temperature was increased from 15 to 37 °C in 75 s (maximum heating rate) and maintained at 37 °C for 425 s, mimicking an injection into the human body (Figure 4.5b). While with $G' < G''$ at 15 °C, the rapid rise in temperature resulted in an increase in G' , while G'' remained constant. After a total time of 125 s or 50 s after reaching 37 °C, $G' > G''$, indicating the sol-gel transition and the formation of CS-βGP gel.

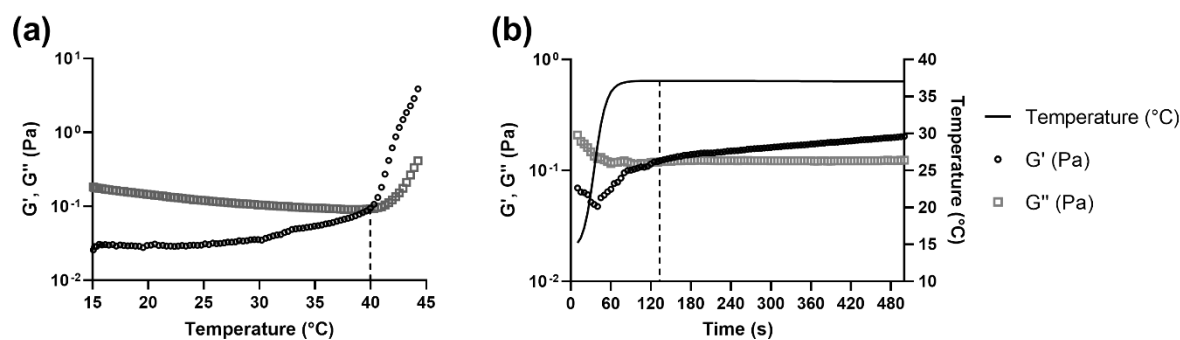


Figure 4.5: Representative rheological curves of temperature- and time-dependent sol-gel transition of sterilised chitosan with β -glycerophosphate (molar ratio 1:4.88) stored at -20 °C. Measurement of the storage modulus (G') and loss modulus (G'') during a (a) temperature sweep and (b) over time when simulating an injection (temperature rises from 15 to 37 °C in 75 s). The dotted lines represent the temperature and/or time at the sol-gel transition.

As described in Table 4.2, the sol-gel transition of non-sterilised CS- β GP, sterilised CS- β GP, Cu^{2+} -lipogel, and $\text{Cu}(\text{DDC})_2 + \text{Cu}^{2+}$ -lipogel was below body temperature and showed negligible differences in temperatures, ranging from 33.3 to 35.3 °C. Similarly to the results of the temperature sweep, the sol-gel transition times of sterilised CS- β GP, the Cu^{2+} -lipogels, and the $\text{Cu}(\text{DDC})_2 + \text{Cu}^{2+}$ -lipogels were equal to or below the 75 s required to reach 37 °C. In contrast, the $\text{Cu}(\text{DDC})_2$ -lipogels, thawed CS- β GP, and thawed $\text{Cu}(\text{DDC})_2 + \text{Cu}^{2+}$ -lipogels increased the sol-gel transition temperatures above body temperature, with temperatures ranging from 37.9 to 39.2 °C. However, these mixes resulted in a sol-gel transition over time when held at 37 °C. The $\text{Cu}(\text{DDC})_2$ -lipogels showed the longest sol-gel transition time, with a total of 330 s and 255 s once reaching 37 °C. The sol-gel transition times of the thawed CS- β GP and thawed $\text{Cu}(\text{DDC})_2 + \text{Cu}^{2+}$ -lipogels were 90 s and 118 s, respectively, corresponding to 15 s and 43 s after reaching 37 °C, respectively.

Table 4.2: Sol-gel transition temperature (°C) and time (s) of chitosan with β -glycerophosphate (CS- β GP; molar ratio 1:4.88). The sol-gel transition temperature and time were determined by rheological measurements of a temperature sweep and a time sweep mimicking an injection, respectively. During the temperature sweep, the temperature was increased from 15 to 45 °C at a rate of 2 °C/min. During the time sweep, the temperature was increased from 15 °C to 37 °C at maximum heating rate (within 75 s, mimicking an injection), and the time until sol-gel transition was either measured as total time (start point 15 °C) or time at 37 °C (start point 37 °C). ND = not determined; NR = 37 °C not reached. Data are expressed as mean \pm standard deviation ($n = 3-4$).

CS- β GP mix	Sterile	+ Cu^{2+} -liposomes	+ $\text{Cu}(\text{DDC})_2$ -liposomes	Temperature (°C) \pm SD	Total time (s) \pm SD	Time (s) at 37 °C
Freshly prepared	-	-	-	35.3 \pm 3.1	ND	ND
	+	-	-	34.2 \pm 2.9	68 \pm 16	NR
	+	+	-	34.8 \pm 0.5	70 \pm 4	NR
	+	-	+	38.8 \pm 1.5	330 \pm 144	255
	+	+	+	33.3 \pm 2.6	75 \pm 14	NR
stored at -20 °C	+	-	-	39.2 \pm 1.0	90 \pm 25	15
	+	+	+	37.9 \pm 3.3	118 \pm 50	43

The sterilisation process of CS- β GP only slightly reduced the sol-gel transition temperature compared to non-sterilised CS- β GP, which could be the result of minor CS polymer degradation. It was previously determined that the sterilisation of CS and β GP should be performed separately as terminal sterilisation of the temperature sensitive CS- β GP is impossible with methods relying on steam or dry heat. Sterile filtration of the gel is not possible due to viscosity, and sterilisation with

gamma radiation causes degradation of the CS polymer chains. The most common sterilisation processes involve sterile filtration of the β GP solution and steam sterilisation of the CS powder in water and the dissolving of CS by adding acetic acid [428]. However, this sterilisation process of CS resulted in sol-gel transition temperatures around 15 °C (Supplementary Figure S4.1), which could be a result of direct damage to the CS polymers [310]. While heat sterilising the CS powder prior to solubilisation was suggested to be a suitable sterilisation method, contradictory results were reported [429]. In contrast to the literature reporting degradation of the CS polymer under ultraviolet light [428], we successfully sterilised the CS solution using ultraviolet light.

The differences in the sol-gel transition temperatures and times, caused by the storage conditions or the incorporation of liposomes, can be associated with changes in the mechanisms behind the formation of the thermosensitive gel. The mechanisms for the formation of the CS- β GP gel were previously described by Saravanan, *et al.* [313]. The addition of β GP to the acidic CS solution results in the pH increasing to a physiological range. The phosphate groups of the β GP are attracted through electrostatic forces to the amino groups of CS, resulting in a protective layer of water molecules around the CS polymers. Due to this protective layer, the CS- β GP remains in solution at low temperatures. However, when temperatures are increased, the water molecules are scattered, resulting in hydrophobic interactions of the CS polymers and, consequently, in the formation of a gel [313]. A CS- β GP gel of similar composition and with comparable thermosensitive properties was previously determined to not be thermo-reversible by showing no sol-gel-sol reversibility with decreasing temperatures [317].

Adding Cu^{2+} -liposomes did not affect the sol-gel transition temperature and time, however, adding $\text{Cu}(\text{DDC})_2$ -liposomes increased the temperature above 37 °C. As both liposomes contain the same lipids [228,282], the difference cannot be attributed to liposome charge but can be a result of size difference. As the d_h of $\text{Cu}(\text{DDC})_2$ -liposomes is larger compared to Cu^{2+} -liposomes, liposome interference with CS cross-linking can occur [420]. The incorporation of $\text{Cu}(\text{DDC})_2$ -liposomes + Cu^{2+} -liposomes did not change the sol-gel transition time, which can be explained by the molar ratio of the combination, consisting of a higher amount of Cu^{2+} -liposomes compared to $\text{Cu}(\text{DDC})_2$ -liposomes. This could be verified by determining the sol-gel transition time of the lipogels containing different concentrations of $\text{Cu}(\text{DDC})_2$ -liposomes. Furthermore, the resuspension of the lyophilised liposomes in CS- β GP could affect the size and morphology of the liposomes or lead to liposomal aggregation, which should be visually assessed by cryo-EM [430]. CS can coat liposomes by forming polymeric layers that modify the liposomal surface and lead to an increase in liposome size [431].

The CS- β GP was stored at -20 °C as storage at 4–6 °C was previously reported to result in sol-gel transition over time when using CS with a high degree of deacetylation [428]. After storage of the CS- β GP at -20 °C, the thawed preparation was liquid, the sol-gel transition temperature was above body temperature, and the sol-gel transition time at 37 °C increased compared to the freshly prepared CS- β GP. We suggest that during the freezing process, the water molecules that formed the protective layer crystallised, which reduced the space between the CS polymers by disrupting the electrostatic attraction between CS and β GP. This was previously observed in a CS solution with NaCl, which showed an increased positive charge following a freeze–thawing cycle to -20 °C and a more concentrated CS solution [432]. In addition, the reduced space between polymer chains after freezing was also reported as the base of CS cryogels [433]. Consequently, following the thawing process, the interaction between CS and β GP and the protective hydration layer need to be restored,

which is further hindered by the proximity of the CS polymers. Once restored, the hydrophobic interactions of the CS polymer can lead to the gel formation with increasing temperature.

Based on the viscoelastic properties determined using rheological measurements, the CS- β GP system is closer to a liquid than to a solid form at ambient temperature. To guarantee an effortless application at the surgical site, the formulation should be prepared (i.e., thawed and/or mixed with liposomes) and administered as a fluid at temperatures below 33 °C. Once injected at the site of action, the physiological temperature induces the formation of the $\text{Cu}(\text{DDC})_2 + \text{Cu}^{2+}$ -lipogel within one minute to prolong drug exposure.

4.1.6.4 Mechanical strength of CS- β GP gel

The gel strength was measured by observing G' and G'' over a frequency sweep (Figure 4.6). The strong gel behaviour of CS- β GP gels can be attributed to $G' \gg G''$ [428] and an intact gel structure to G' and G'' remaining almost parallel to each other over the whole frequency range. The disruptions of the CS interactions and the breaking up of the gel structure result in changes in G' and G'' , such as a decrease in G' while G'' remains constant [311,312]. In Figure 4.6a, a representative curve of CS- β GP gel at 37 °C shows that $G' > G''$ and both properties remained parallel to each other, indicating a gel-like behaviour. To determine the effect of sterilisation, storage at -20 °C, and the incorporation of liposomes on the gel strength, the ratio of G'/G'' was observed with increased frequency (Figure 4.6b). While the G'/G'' ratio of the $\text{Cu}(\text{DDC})_2$ -lipogel was reduced with increasing frequency, indicating a destabilisation of the gel structure, CS- β GP, sterile CS- β GP, -20 °C stored CS- β GP, the Cu^{2+} -lipogels, and the $\text{Cu}(\text{DDC})_2 + \text{Cu}^{2+}$ -lipogels remained constant, suggesting a stable gel structure up to 10 Hz. The destabilisation of the gel structure through incorporation of $\text{Cu}(\text{DDC})_2$ -liposomes and the increased sol-gel transition temperature and time further suggest the interference of $\text{Cu}(\text{DDC})_2$ -liposomes with the cross-linking of CS polymers. To characterise the gel and lipogel, scanning electron microscopy can be used to investigate the pore size of the CS- β GP structure and to visualise the liposomes in the gel [417,434].

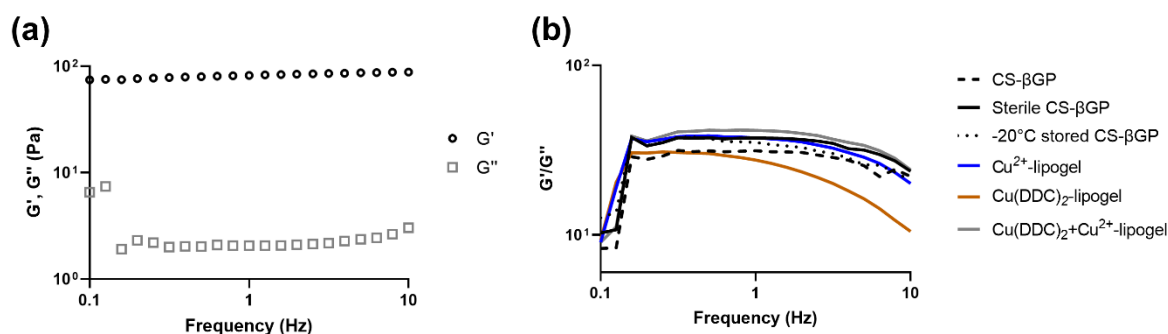


Figure 4.6: Frequency sweep (0.1–10 Hz) of chitosan with β -glycerophosphate (CS- β GP) gels and lipogels at 37 °C. (a) Representative curve of storage modulus (G') and loss modulus (G'') of sterile CS- β GP gel and (b) ratio of G'/G'' of CS- β GP gels exposed to sterilisation procedures, stored at -20 °C or with incorporated liposomes. Data are expressed as mean ($n = 3$).

4.1.6.5 CS- β GP is biocompatible

CS is a non-toxic, biodegradable, and biocompatible polymer approved by the FDA. Similarly, β GP, which is found naturally in the body, has been approved by the FDA for intravenous administration for the treatment of phosphate metabolism imbalances [310]. To determine the effect of CS- β GP on human cells, the human dermal fibroblast cells were covered with CS- β GP (Figure 4.7a). The

CS- β GP showed negligible cytotoxic effects, with over 70% fibroblast viability. A slight fibroblast viability reduction from 89.0% to 74.1% was observed with the increasing amount of CS- β GP, which can be explained by the limited access of the fibroblast cells to oxygen and nutrients *in vitro* [435]. To assess the effect of the components released from the CS- β GP on human cells, the CS- β GP was incubated for up to 72 h with 0.9% NaCl, before the supernatant was transferred onto the fibroblast cells and incubated for 24 h (Figure 4.7b). The fibroblast viability remained above 70%, indicating no toxicity of components released from the gel over 72 h. The cytotoxicity of CS- β GP was previously observed to be dependent on the deacetylation degree of CS, the solvent used to dissolve CS, and the β GP concentrations. Therefore, the biocompatibility of CS- β GP can be explained by the high deacetylation degree of CS [436] and the use of acetic acid to dissolve CS [437] and on β GP concentrations below 15% or 1.115 M [428,438,439].

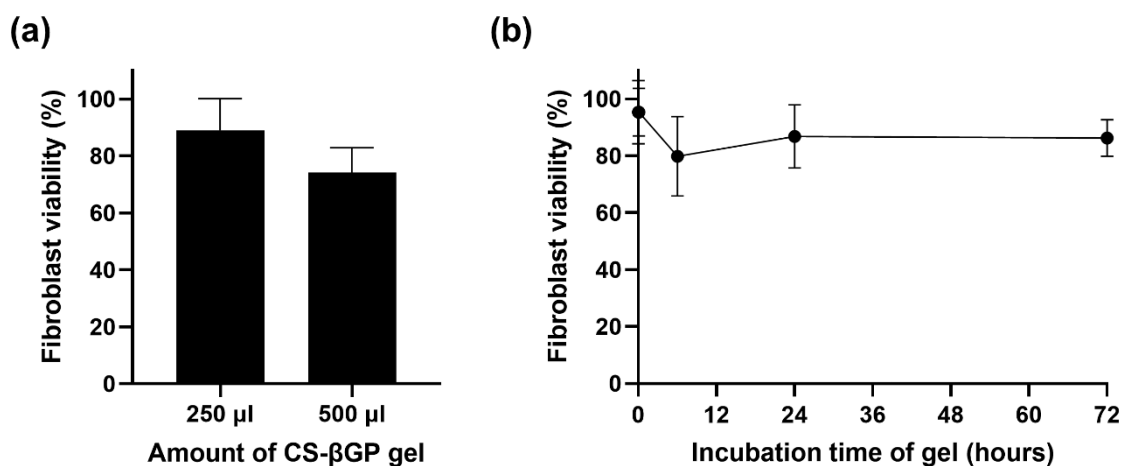


Figure 4.7: Effect of sterile chitosan with β -glycerophosphate (CS- β GP) on human dermal fibroblast cell viability. (a) Fibroblast cells were covered with 250 μ L or 500 μ L of sterile CS- β GP for 24 h. (b) Fibroblast cells were treated for 24 h with 0.9% NaCl previously incubated with sterile CS- β GP gel for up to 72 h to observe unwanted cytotoxic effect of components released from the gel. Fibroblast viability was measured using the CellTiter-Glo viability assay. Data are expressed as mean \pm standard deviation ($n = 3$).

4.1.6.6 Released liposomes from CS- β GP gel affect fibroblast viability

Pharmaceutical drug release assays for gel formulation typically require big volumes of release media, and therefore, they require either very sensitive quantitative methods or high concentrations of compounds [440]. The quantification of the Cu²⁺-liposomes and Cu(DDC)₂-liposomes was performed by measuring the Cu(DDC)₂ complex absorbance with UV spectrophotometry. However, the antibacterial concentration of Cu(DDC)₂ + Cu²⁺ is 128 μ M [387], and the detection limit of this method is 100 μ M Cu²⁺, rendering the detection of small concentrations challenging. Therefore, the release of Cu²⁺-liposomes and Cu(DDC)₂-liposomes from the respective lipogels over time was investigated by measuring the effect of released liposomes on fibroblast viability. The lipogels were incubated with 0.9% NaCl for up to 72 h; the release medium was then transferred onto fibroblast cells and incubated for 24 h; then, the fibroblast viability was measured (Figure 4.8a).

4 Development of an injectable gel for local delivery of $\text{Cu}(\text{DDC})_2 + \text{Cu}^{2+}$

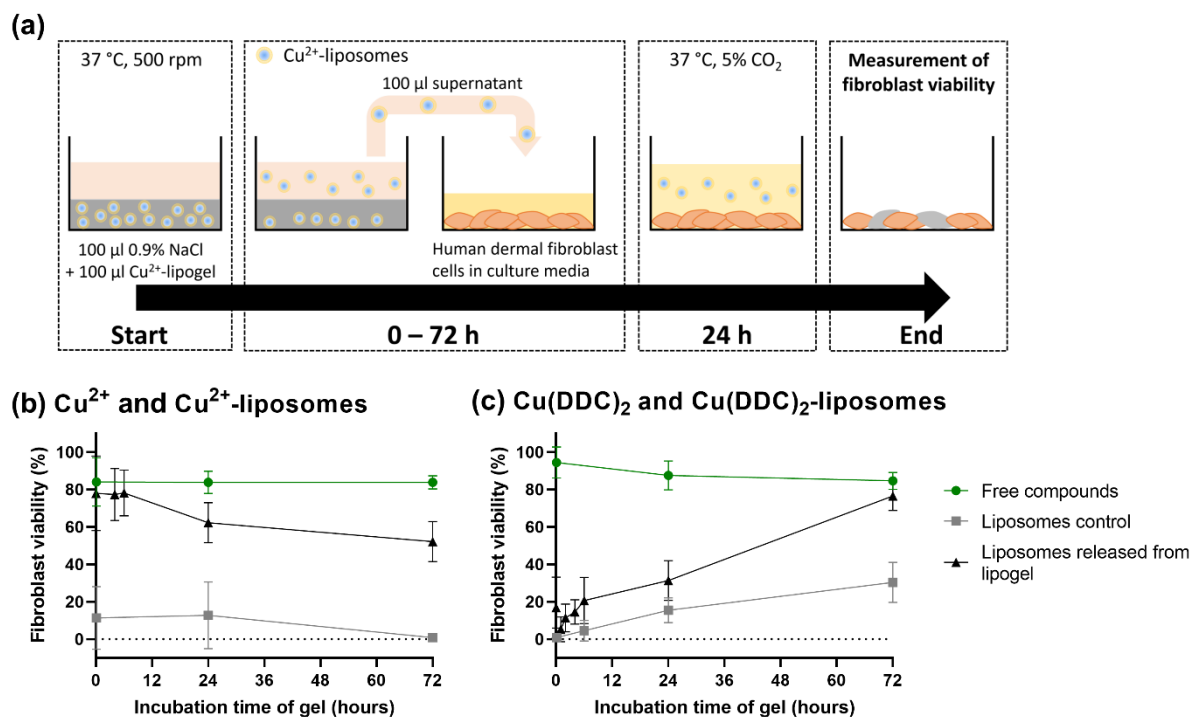


Figure 4.8: Effect on human dermal fibroblast cell viability of liposomes released from sterile chitosan with β -glycerophosphate (CS- β GP) gel over 72 h. **(a)** Experimental procedure exemplified with release of Cu^{2+} -liposomes from the Cu^{2+} -lipogel over 72 h. Cu^{2+} -lipogel was covered with release media and incubated at 37 °C and 500 rpm. After predetermined timepoints, the supernatant was transferred onto human dermal fibroblast cells. Following 24 h incubation, fibroblast viability was measured using CellTiter-Glo viability assay. **(b)** Effect on fibroblast viability of released Cu^{2+} -liposomes from Cu^{2+} -lipogel over time. Controls include the effect of free Cu^{2+} incubated with sterile CS- β GP gel (corresponding to 100% released non-liposomal Cu^{2+}) and of Cu^{2+} -liposomes incubated with sterile CS- β GP (corresponding to 100% released Cu^{2+} -liposomes). **(c)** Effect on fibroblast viability of released $\text{Cu}(\text{DDC})_2$ -liposomes from $\text{Cu}(\text{DDC})_2$ -lipogel over time. Controls include the effect of free $\text{Cu}(\text{DDC})_2$ incubated with sterile CS- β GP (corresponding to 100% released non-liposomal $\text{Cu}(\text{DDC})_2$) and of $\text{Cu}(\text{DDC})_2$ -liposomes incubated with sterile CS- β GP (corresponding to 100% released $\text{Cu}(\text{DDC})_2$ -liposomes). Data are expressed as mean \pm standard deviation ($n = 3$).

When the fibroblast cells were incubated with the release media containing free Cu^{2+} , the viability remained at approximately 84% over 72 h (Figure 4.8b), which indicated no toxicity and was similar to the effect of CS- β GP gel alone (Figure 4.7b). In contrast, the fibroblast cells incubated with supernatant containing the same concentration of Cu^{2+} -liposomes resulted in reduced fibroblast viability, ranging from 1 to 13%, thereby permitting a distinction between the effect on the fibroblast viability of released free Cu^{2+} and of released Cu^{2+} -liposomes. The difference in fibroblast viability can be associated with free Cu^{2+} interacting with components of the gel, such as CS [441] and therefore a lower Cu^{2+} concentration being transferred onto the fibroblast cells. In addition, no changes in fibroblast viability were observed over time when exposed to Cu^{2+} -liposomes, suggesting the stability of Cu^{2+} -liposomes and no leakage over 72 h at 37 °C. The Cu^{2+} -lipogels showed no effect of Cu^{2+} -liposomes in the first 6 h, with fibroblast viability remaining at approximately 78%, indicating no release of Cu^{2+} -liposomes. However, following the incubation of the lipogel for 24 and 72 h, the fibroblast viability was reduced to 62% and 52%, respectively, indicating a release of Cu^{2+} -liposomes from the gel. Therefore, we assume that Cu^{2+} -liposomes were not released within the first 6 h and then were slowly released from the gel, reaching concentrations corresponding to approximately 50% fibroblast viability after 72 h incubation (Figure 4.8b).

The same experiment was performed with the $\text{Cu}(\text{DDC})_2$ -lipogels (Figure 4.8c). When the fibroblasts were incubated with release media containing free $\text{Cu}(\text{DDC})_2$, the viability remained

between 85 and 95% over 72 h. Due to the low water solubility of $\text{Cu}(\text{DDC})_2$, the complex can sediment into the gel structure or to the surface of the well and fail to be transferred with the supernatant onto the fibroblast cells. In addition, the bioavailability of precipitated substances for cellular uptake is reduced [442]. In contrast, when the fibroblast cells were exposed to the $\text{Cu}(\text{DDC})_2$ -liposomes, the viability was reduced to 2% and 5% after 0.5 and 6 h, respectively, before increasing to 15% and 30% after 24 and 72 h, respectively. This indicates that the $\text{Cu}(\text{DDC})_2$ -liposomes were not stable over 72 h and that water-insoluble $\text{Cu}(\text{DDC})_2$ leaked from the liposomes. Leaked $\text{Cu}(\text{DDC})_2$ sedimented and was not transferred onto the fibroblast cells with the release media, resulting in increased fibroblast viability compared to the intact $\text{Cu}(\text{DDC})_2$ -liposomes. The release media of the $\text{Cu}(\text{DDC})_2$ -lipogels showed fibroblast viability below 21% within the first 6 h, suggesting an instant release of the $\text{Cu}(\text{DDC})_2$ -liposomes from the gel. Similar to the $\text{Cu}(\text{DDC})_2$ -liposome control, the fibroblast viability increased after 24 h and 72 h, reaching 31% and 77%, respectively, and correlating with the $\text{Cu}(\text{DDC})_2$ -liposomes being unstable. Therefore, the effect on the fibroblast viability indicated a release of $\text{Cu}(\text{DDC})_2$ -liposomes within the first 0.5 h and unstable $\text{Cu}(\text{DDC})_2$ -liposomes after 24 h.

The effect of the release media incubated with the lipogel on fibroblast viability can be associated with the release of Cu^{2+} -liposomes and $\text{Cu}(\text{DDC})_2$ -liposomes, but this is an indirect assessment of the liposomal release behaviour from the lipogel. The integrity of the liposomes released from the gel should be verified by cryo-transmission electron microscopy [282]. As the release media was not replaced to investigate the effect on the fibroblast viability of the accumulated release of $\text{Cu}(\text{DDC})_2$ -liposomes or Cu^{2+} -liposomes, the concentration in the release media and the concentration remaining in the gel could reach equilibrium. This could potentially mask the further release of Cu^{2+} -liposomes which would otherwise have occurred. This should not be the case for $\text{Cu}(\text{DDC})_2$ -liposome release, as the leakage of insoluble $\text{Cu}(\text{DDC})_2$ from the liposome would create a new concentration gradient for further release of $\text{Cu}(\text{DDC})_2$ -liposomes. In addition, the effects of hydrophobic $\text{Cu}(\text{DDC})_2$ being released from the liposomes on the CS–CS hydrophobic interactions and the potential of Cu^{2+} to chelate CS, thereby producing gel matrices [441] and altering the CS- β GP, were not investigated. While smaller particles are expected to diffuse faster than more voluminous particles [314], the interference of $\text{Cu}(\text{DDC})_2$ -liposomes with the gel matrix, which also caused the increased sol-gel transition temperature and the reduced gel strength, could explain the burst release. In addition, liposome release cannot only be attributed to diffusion processes, but might also be a result of erosion and water escaping the gel structure [417].

4.1.6.7 Weight loss of CS- β GP gel and $\text{Cu}(\text{DDC})_2$ + Cu^{2+} -lipogel over time

Typically, an erosion assay is performed in a solution containing lysozyme to mimic the enzymes present in physiological fluids in order to assess degradability of the gel over time [443]. However, as the antibacterial assays are performed without the presence of liquid, we measured the weight loss to show a release of the liposomes under dry conditions. The percentage weight losses of the CS- β GP gels and lipogels over time are described in Figure 4.9a for freshly prepared gels and Figure 4.9b for CS- β GP stored at $-20\text{ }^\circ\text{C}$. One-phase association kinetics was observed independently of the storage conditions and incorporation of liposomes. All the gels reached a plateau after 21 days, and the weight loss remained constant until day 49. In addition, 50% weight loss was reached for all the gels within a range of 2.6 to 3.9 days. The CS- β GP stored at $-20\text{ }^\circ\text{C}$ reached 50% weight loss in a smaller time period compared to the freshly prepared gel (-0.8 days without liposomes and -1.1 days with liposomes) and the incorporation of liposomes also slightly reduced the time until 50% weight loss compared to the gels without liposomes (-0.3 days in fresh gels and -0.5 days in

–20 °C stored). This was also observed by the increased rate constants of the lipogels compared to the rate constants of the CS- β GP gels without liposomes (Table 4.3). While most of the weight loss can be attributed to water escaping the gel, the increased rate constant of the lipogels suggest that the liposomes are released with the water from the gel structure. This can be confirmed by measuring the Cu^{2+} concentration of the released water or by determining the antibacterial activity of the lipogel under similar conditions.

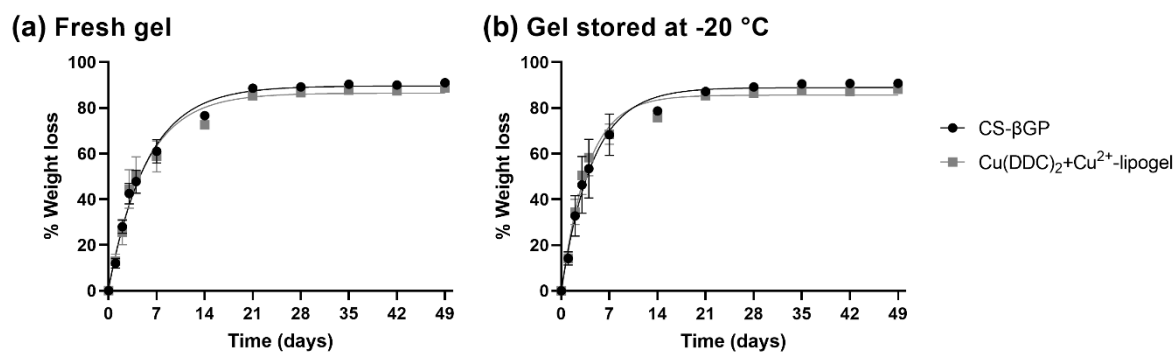


Figure 4.9: Non-linear fit of the percentage of accumulated weight loss over 49 days at 37 °C of chitosan with β -glycerophosphate (CS- β GP) gel and $\text{Cu}(\text{DDC})_2 + \text{Cu}^{2+}$ -lipogel. Weight loss of (a) freshly prepared gels or (b) gels based on CS- β GP stored at –20 °C. Data are expressed as mean \pm standard deviation ($n = 3$).

Table 4.3: Mean time until 50% of weight loss and rate constant based on non-linear fit of weight loss over 49 days at 37 °C of chitosan with β -glycerophosphate (CS- β GP) gel or –20 °C stored CS- β GP gel, alone or as $\text{Cu}(\text{DDC})_2 + \text{Cu}^{2+}$ -lipogel. Data are expressed as mean with 95% confidence interval (95% CI; $n = 3$).

CS- β GP gel	+ $\text{Cu}(\text{DDC})_2$ -liposomes + Cu^{2+} -liposomes	Mean time until 50% weight loss [95% CI] (Days)	Rate constant [95% CI] (1/Days)	R^2
fresh	–	3.9 [3.5 to 4.4]	0.18 [0.16 to 0.20]	0.988
	+	3.7 [3.1 to 4.5]	0.19 [0.15 to 0.22]	0.972
–20 °C	–	3.1 [2.6 to 3.8]	0.22 [0.18 to 0.26]	0.966
	+	2.6 [2.3 to 3.1]	0.26 [0.23 to 0.30]	0.975

4.1.6.8 Antibiofilm activity of $\text{Cu}(\text{DDC})_2 + \text{Cu}^{2+}$ -lipogel

The lipogels were investigated for the prevention of MRSA Mu50 and *S. epidermidis* ATCC 35984 biofilm growth (Figure 4.10a) and the inhibition of formed biofilms (Figure 4.10b). The concentrations were chosen based on the weight loss assay as the gel was not in contact with any fluid; therefore, the estimated release behaviour (Section 4.1.6.6) might not correlate with the release under dry conditions. The optimal concentration was previously determined to be a 1:6.2 molar ratio of $\text{Cu}(\text{DDC})_2$ to Cu^{2+} with a total Cu^{2+} concentration of 128 μM [387]. Under the assumption that during weight loss, the liposomes are released from the gel, 30% and 50% of liposomes would be available after 2 days and 3–4 days, respectively. Therefore, we chose to investigate the lipogels containing 256 μM (128 μM after 3–4 days) and 512 μM (256 μM after 3–4 days) $\text{Cu}(\text{DDC})_2 + \text{Cu}^{2+}$.

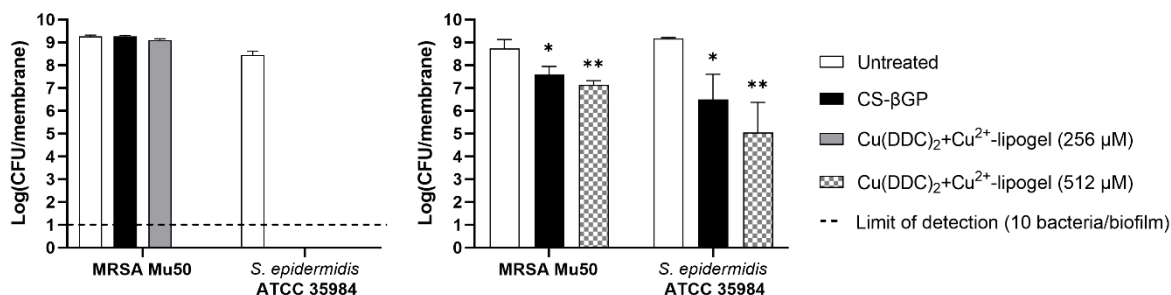


Figure 4.10: Effect of Cu(DDC)₂+Cu²⁺-lipogel on colony-forming units (CFUs) of MRSA Mu50 and *S. epidermidis* ATCC 35984. Log(CFU/membrane) in (a) prevention of biofilm formation assay over 2 days and (b) biofilm treatment over 4 days. Missing bars represent no bacterial detection (below limit of detection; dashed line). Concentrations of Cu(DDC)₂-liposomes + Cu²⁺-liposomes correspond to the total Cu²⁺ concentration and are based on a 1:6.2 molar ratio of Cu(DDC)₂-liposomes to Cu²⁺-liposomes. Data are expressed as geometric mean ± standard deviation (n = 3; 1-way ANOVA with Tukey's multiple comparison test, **p* < 0.05, ***p* < 0.01). CS-βGP = chitosan with β-glycerophosphate.

The exposure to CS-βGP and 256 μM Cu(DDC)₂+Cu²⁺-lipogel did not prevent MRSA Mu50 biofilm formation over 2 days (log₁₀ 9.3 and 9.1 CFU/membrane, respectively) compared to the untreated control (log₁₀ 9.3 CFU/membrane, *p* > 0.05). In contrast, no MRSA Mu50 bacteria were detected when exposed to 512 μM Cu(DDC)₂+Cu²⁺-lipogel. Therefore, we observed no antibacterial activity of the CS-βGP gel and prevention of biofilm growth by the lipogels in a concentration-dependent manner. The 256 μM Cu(DDC)₂+Cu²⁺-lipogel did not prevent biofilm growth, which can be explained by the amount of liposomes released from the gel over 2 days based on the weight loss assay (Figure 4.9b). As only 30% of the liposomes, corresponding to approximately 80 μM, would be released after 2 days, the minimum concentration for the biofilm prevention of 128 μM Cu(DDC)₂ + Cu²⁺ would not be reached. In contrast, the 512 μM Cu(DDC)₂+Cu²⁺-lipogel, which would release approximately 150 μM after 2 days, reached the minimum liposome concentration needed for antibacterial activity to prevent biofilm growth. Consequently, the antibacterial activity is associated with the release of liposomes from the gel, which confirms the hypothesis that under the condition of the weight loss assay, the liposomes are released from the gel structure with water.

When *S. epidermidis* ATCC 35984 was exposed to CS-βGP alone, no bacteria were detected after 2 days, suggesting the antibacterial activity of CS-βGP against *S. epidermidis* specifically. As *S. epidermidis* is a facultative anaerobe, the observed eradication of bacteria cannot be linked to the limited oxygen supply, which can even promote biofilm formation by enhancing the production of cell-adhesion and cell-promoting molecules [444]. CS-βGP mixes based on different concentrations, with α,βGP or with chitosan derivatives previously inhibited *Porphyromonas gingivalis* and *S. aureus* growth [445,446] and postponed *Escherichia coli* growth [447]. The antibacterial activity of the different CS-βGP mixes was attributed to the antibacterial activity of the chitosan polymer [446-448]. For example, low molecular weight chitosan (107 kDa) at subinhibitory concentrations previously showed a significant reduction in the metabolic activity of *S. epidermidis* biofilms but not *S. aureus* biofilms [308]. In addition, Carlson, *et al.* [449] showed the microbe-specific efficacy of chitosan coatings, based on the varying cell surface charges and differences in cell wall and membrane structure. They also showed extensively reduced *S. epidermidis* biofilm formation, compared to no significantly reduced *S. aureus* biofilm formation [449]. As eradication of *S. epidermidis* was already seen with the CS-βGP, both concentrations of the Cu(DDC)₂+Cu²⁺-lipogel resulted in the same biofilm growth inhibition (Figure 4.10a).

A 512 μM $\text{Cu}(\text{DDC})_2 + \text{Cu}^{2+}$ -lipogel concentration was chosen for the biofilm experiments as this concentration achieved the bacterial eradication of planktonic MRSA Mu50 (Figure 4.10a). The MRSA Mu50 and *S. epidermidis* ATCC 35984 biofilms treated with CS- β GP resulted in statistically significant \log_{10} reduction compared to the untreated control, corresponding to 93.7% and 98.7% biofilm killing, respectively (Figure 4.10b). The treatment with 512 μM $\text{Cu}(\text{DDC})_2 + \text{Cu}^{2+}$ -lipogel also significantly reduced the MRSA Mu50 and *S. epidermidis* biofilms compared to the untreated control, with 98.2% and 99.9% biofilm killing, respectively. While no significant difference was observed between the CS- β GP gel and the $\text{Cu}(\text{DDC})_2 + \text{Cu}^{2+}$ -lipogel, the \log_{10} of the $\text{Cu}(\text{DDC})_2 + \text{Cu}^{2+}$ -lipogel was reduced compared to that of the CS- β GP gel.

Exposure to the $\text{Cu}(\text{DDC})_2 + \text{Cu}^{2+}$ -lipogel successfully prevented MRSA and *S. epidermidis* biofilm formation over 2 days but did not eradicate the pre-formed biofilms. As bacteria in biofilms can be up to 1000-fold less susceptible to antimicrobial agents compared to planktonic bacteria [52], the reduced activity of the lipogel against the biofilms can be associated with the presence of a protective matrix and a stratified profile. Colony biofilms are subject to oxygen and nutrient gradients, creating layers of bacteria in different metabolic states [450]. The reduced antibiofilm activity of the lipogel can be investigated by evaluating the penetration of the released liposomes in different layers of the biofilm using fluorescently labelled liposomes, live/dead staining of bacteria, and microscopical analysis [391,404]. To further enhance the antibiofilm activity, a CS- β GP gel containing liposomes can be combined with antibiotics. DDC⁻ and Cu^{2+} previously showed synergistic effects *in vitro* with a range of different antibiotics [387]; therefore, the antibiofilm properties of the gel in combination with antibiotics should be examined. In addition, the colony biofilm assay provides a continuous flow of nutrients through the membrane, but the effects of host matrix components, wound simulating media, a 3D biofilm gradient, and a polymicrobial biofilm were not investigated. Therefore, the antibiofilm activity of the lipogel should be examined in an *in vitro* model that mimics the wound environment of SSIs [388]. The bacterial species chosen for the prevention and antibiofilm assay were MRSA and *S. epidermidis*, as they are mostly found in SSIs. However, isolated bacterial species vary depending on the surgical procedure, and staphylococci are not typically found in gastrointestinal and urological surgeries, which are mostly caused by Gram-negative and anaerobic bacteria [7,27]. As $\text{Cu}(\text{DDC})_2 + \text{Cu}^{2+}$ previously showed no activity against Gram-negative bacteria [387], the application of the lipogel is restricted to the SSIs caused by staphylococci.

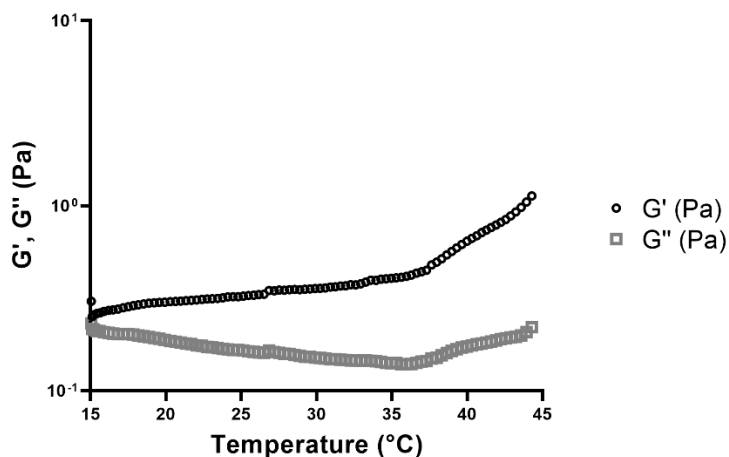
Consequently, the $\text{Cu}(\text{DDC})_2 + \text{Cu}^{2+}$ -lipogel should be further evaluated for antibiofilm activity *in vitro* and as a preventive antibacterial therapy of surgical sites *in vivo*, including surgical wounds and medical devices, such as hernia meshes and joint replacements.

4.1.7 Conclusion

A thermosensitive CS- β GP gel with incorporated DDC⁻ and Cu^{2+} was evaluated as a treatment for surgical site infections. The findings reveal that CS- β GP is an injectable and biocompatible gel, which can be stored frozen and thawed prior to use. The lyophilisation of $\text{Cu}(\text{DDC})_2$ -liposomes and Cu^{2+} -liposomes increased the storage stability and facilitated the incorporation into CS- β GP, without affecting its thermosensitive properties. Liposomes were released from the lipogel over time through diffusion processes and gel mass reduction due to weight loss, resulting in high *in vitro* antibiofilm activity against MRSA and *S. epidermidis* by preventing biofilm formation and reducing the viability of the formed biofilms. Future work will examine the *in vitro* antibiofilm

activity of the lipogel in combination with antibiotics, and *in vivo* studies will determine the efficacy and safety of the lipogel.

4.1.8 Supplementary file



Supplementary Figure S4.1: Representative rheological curves of temperature-dependent sol-gel transition of autoclaved chitosan with sterile filtered β -glycerophosphate (CS- β GP; molar ratio 1:4.88). Measurement of the storage modulus (G') and loss modulus (G'') during a temperature range.

4.2 Management of hydrogel prior to administration

4.2.1 Stability of hydrogel at -20 °C

The gelling properties of CS- β GP were previously observed to be temperature-dependent. Specifically, the sol-gel transition of CS- β GP occurred at body temperature and within one minute of reaching 37 °C. The thermosensitive properties of the gel were sustained when sterilised, loaded with a liposomal formulation of $\text{Cu}(\text{DDC})_2 + \text{Cu}^{2+}$, and stored overnight at -20 °C (Chapter 4.1.6.3). Short storage of CS- β GP at -20 °C only resulted in small changes of the sol-gel transition temperature and time but the effects of prolonged storage of CS- β GP at -20 °C on the gelling properties needed to be investigated.

Aliquots of sterilised CS- β GP were kept at -20 °C for up to 84 days (approximately 3 months). At indicated time points, CS- β GP was rapidly thawed by immersion in a water bath at 32 °C for 2 min and resting at ambient temperature for 5 min or until liquid. The thawed CS- β GP was loaded onto the rheometer and a time sweep was performed according to Chapter 4.1.5.7. The intersection of the G' and G'' curve defined the sol-gel transition temperature and time. Statistical analysis was performed using GraphPad Prism version 9.4.1 for Windows (GraphPad Software, San Diego, CA, USA). The parametric data are represented by mean \pm SD, which was analysed using one-way ANOVA with Tukey's multiple comparison test.

As displayed in Figure 4.11, the sol-gel transition time remained constant at around $68 \text{ s} \pm 20 \text{ s}$ over 56 days (approximately 2 months). After 84 days, the sol-gel-transition time increased to $183 \text{ s} \pm 124 \text{ s}$ but the rise was not statistically significant ($p > 0.05$). While the mean sol-gel transition temperature was around 36 °C after 1 day and 28 days, it was reduced to 30 °C after 7 days, 33 °C after 56 days, and 34 °C after 84 days. These non-significant variations in the temperature ($p > 0.05$) can be associated with a sol-gel transition time below 75 s, which is the minimum time required to reach 37 °C during the time sweep.

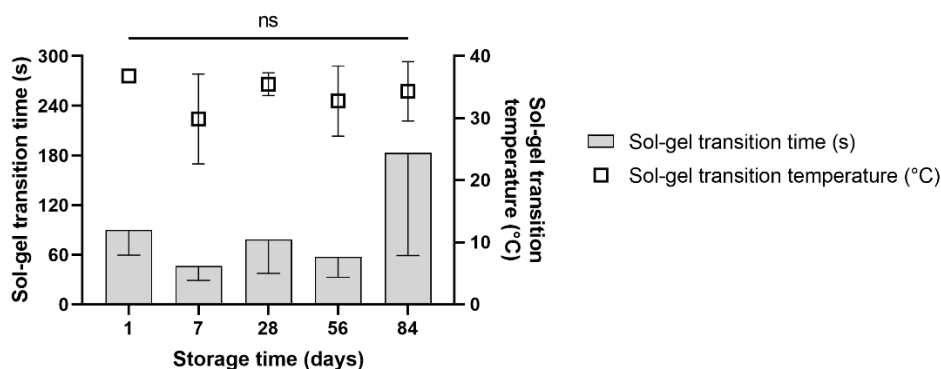


Figure 4.11: Effect of storage time at $-20\text{ }^{\circ}\text{C}$ on sol-gel transition temperature ($^{\circ}\text{C}$) and time (s) of chitosan with β -glycerophosphate (CS- β GP; molar ratio 1:4.88). The sol-gel transition temperature and time were determined by rheological measurements of a time sweep mimicking an injection. During the time sweep, the temperature was increased from $15\text{ }^{\circ}\text{C}$ to $37\text{ }^{\circ}\text{C}$ at maximum heating rate (within 75 s, mimicking an injection), and the time until sol-gel transition was measured. Data are expressed as mean \pm standard deviation ($n = 2\text{-}3$; ordinary one-way ANOVA with Tukey's multiple comparison test; ns = not significant $p > 0.05$).

The increase in sol-gel transition time of CS- β GP stored at $-20\text{ }^{\circ}\text{C}$ for 84 days could indicate changes of the physicochemical and mechanical properties of CS polymers over time. The stability of CS polymers is dependent on internal factors, such as molecular weight, deacetylation content, and moisture content, as well as external factors, such as humidity, temperature, and sterilisation. Freezing of CS- β GP mixture can impose stress on the CS structure and cause polymer degradation [429], consequently retarding the sol-gel transition. In future studies, changes in the CS- β GP gel structure as a result of CS polymer degradation during storage should be visualised using scanning electron microscopy [417,434]. Depolymerisation of CS can be investigated through changes in the absolute-molecular weight using the Langmuir Blodgett technique and atomic force microscopy [451]. Furthermore, the effect of storage beyond 3 months on the gelling properties of CS- β GP should be determined to observe a potential correlation between increased sol-gel transition time and time stored at $-20\text{ }^{\circ}\text{C}$.

In summary, storage of CS- β GP at $-20\text{ }^{\circ}\text{C}$ over 2 months showed no difference in gelling temperatures. While the sol-gel transition time slightly increased after 3 months, CS- β GP still formed a gel at physiological temperatures within 3 min. Therefore, CS- β GP can be stored at $-20\text{ }^{\circ}\text{C}$ for up to 3 months.

4.2.2 Estimated time for preparation and administration of the hydrogel

The CS- β GP gel and lipogel were developed for administration on surgical sites during operations. Therefore, the preparation and administration of the mixture should be simple and fast. The liposomes and CS- β GP need to be stored separately at $-20\text{ }^{\circ}\text{C}$ and mixed upon administration, due to instabilities of the liposomes in aqueous solutions. However, storage of the CS- β GP mixture below freezing temperatures leads to an additional step in the preparation: thawing of CS- β GP. The preparation process can be described as following:

4.2.2 Estimated time for preparation and administration of the hydrogel

- (1) Removing CS- β GP mixture and lyophilised liposomes from storage.
- (2) Thawing of CS- β GP mixture.
- (3) Injecting liquid CS- β GP into glass vial containing the lyophilised liposomes.
- (4) Gently swirling the glass vial for 1 min to disperse lyophilised liposomes.
- (5) Drawing up the CS- β GP liquid containing the liposomes in a syringe.
- (6) Administering the CS- β GP liquid containing the liposomes at the site of action.

The thawing rate is dependent on the container, the amount of frozen mixture, and the environmental temperature [452], making a prediction difficult. In addition, it was previously reported that gelling of CS- β GP can occur over time at temperatures below the physiological range [428]. Therefore, the time until sol-gel transition at ambient room temperature should be investigated in future studies to give an indication on the timeframe for preparation.

The gelling properties of freshly prepared CS- β GP and thawed CS- β GP (stored at -20 °C) over time were determined by rheological measurements by mimicking a thawing process. To simulate conditions of frozen CS- β GP exposed to room temperature, a time sweep was performed over 4 h. The temperature was increased from 3 °C to 25 °C at a heating rate of 0.15 °C/min as an estimate of the temperature within the gel during thawing; then, the temperature was held at 25 °C for the remaining time. Sample loading and adjustment of rheometer settings (cone/plate geometry, gap, constant strain amplitude and constant frequency) were performed as described in Chapter 4.1.5.7. The intersection of the G' and G'' curve defined the sol-gel transition temperature and time. As loading of CS- β GP stored at -20 °C was not possible in solid state, the mixture was rapidly thawed prior to the measurement, as described in Chapter 4.2.1.

To estimate the timeframe for preparation of the lipogel prior to administration, the sol-gel transition of freshly prepared and stored CS- β GP was evaluated when mimicking a thawing process. Figure 4.12 displays the curves of a time sweep with a slow temperature rise from 3 °C to 25 °C of fresh CS- β GP (Figure 4.12a) and CS- β GP stored at -20 °C (Figure 4.12b). As described in Chapter 4.1.6.3, when $G' < G''$ the material is in liquid form, while a gel is formed when $G' > G''$. Fresh and stored CS- β GP were fluid at 3 °C, as $G' < G''$. Despite the slowly rising temperatures, reaching 25 °C after 2.5 h, both mixtures remained in liquid form. The sol-gel transition occurred at 25 °C after 2 h 50 min 00 s (n=1) for fresh CS- β GP and 2 h 39 min 20 s (n=1) for CS- β GP stored at -20 °C.

While these measurements should be replicated at least twice in future studies, the sol-gel transition at ambient temperature appeared to occur independently of storage history. Freshly prepared and CS- β GP stored at -20 °C formed gels after more than 2.5 h and within 10-20 min of reaching 25 °C, indicating no effect of freezing and thawing of the mixture. This suggests that CS- β GP stored at -20 °C is stable in liquid form until temperatures reach 25 °C. The effect of thawing at low temperatures, such as 4 to 6 °C, on the gelling properties of CS- β GP stored at -20 °C should be investigated in the future to determine if intermediate storage in a fridge is possible.

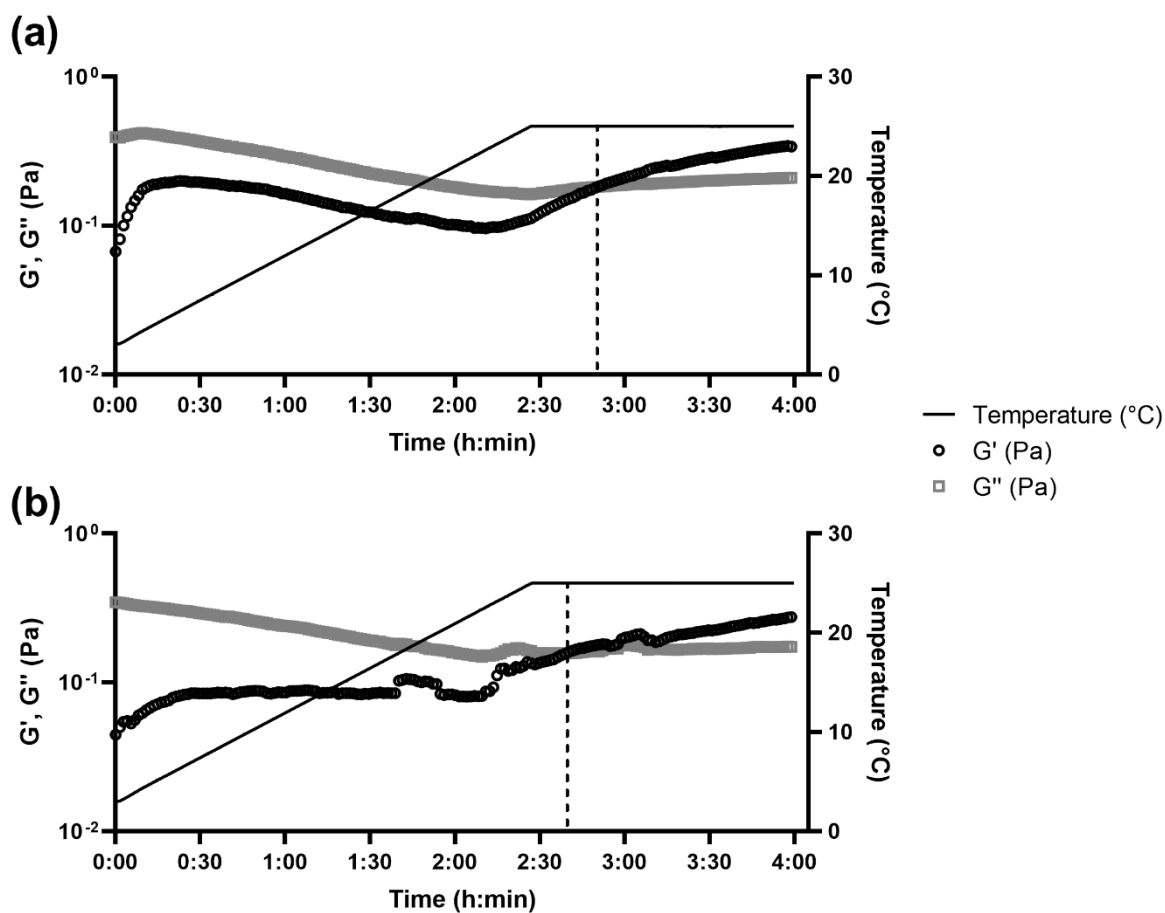


Figure 4.12: Rheological curves of temperature- and time-dependent sol-gel transition of sterilised chitosan with β -glycerophosphate (molar ratio 1:4.88). Measurement of the storage modulus (G') and loss modulus (G'') during a temperature-dependent time sweep for (a) freshly prepared gel or (b) thawed gel that was stored at -20 °C. The dotted lines represent the temperature and time at the sol-gel transition.

5 Discussion and future perspectives

5.1 DDC⁻ and Cu²⁺ as antibacterial agents

In Chapter 2, the antibacterial and antibiofilm activity of DDC⁻ against *S. aureus* and *S. epidermidis* was shown to be Cu²⁺ dependent. The optimal concentrations of the compounds were 8 µg/ml (equivalent to 35 µM) DDC⁻ combined with 32 µg/ml (equivalent to 128 µM) Cu²⁺. These concentrations corresponded to the formation of the Cu(DDC)₂ complex and an excess of Cu²⁺, which inhibited bacterial attachment and aggregation, and reduced the viability of pre-formed biofilms. Previous studies have shown that the antibacterial activity of DSF with Cu²⁺ against *M. tuberculosis* [221] and *S. mutans* [225] was associated with a reduction of DSF to DDC⁻ and the formation of the Cu(DDC)₂ complex. Furthermore, Menghani, *et al.* [222] reported Cu²⁺-dependent antibacterial activity of DDC⁻ against *S. pneumoniae*, despite no reported activity of DSF with Cu²⁺. As Haeili, *et al.* [226] showed that the antibacterial activity of DSF against MRSA is Cu²⁺-independent, the effect of water soluble DDC⁻ in the presence of Cu²⁺, instead of the water insoluble DSF, was investigated in the studies described herein.

The mechanism of action underlying the antibacterial activity of DDC⁻ in combination with Cu²⁺ remains unclear. Based on a previous hypothesis, in which Dalecki, *et al.* [221] suggested that Cu(DDC)₂ acts as “Trojan horse” against *M. tuberculosis*, they proposed that Cu(DDC)₂ inhibits bacterial copper homeostasis, resulting in an intracellular accumulation of additional Cu²⁺. Bacterial death then occurs by copper (Cu⁺ and Cu²⁺) induced bacterial toxicity, which includes oxidative stress by (i) the generation of ROS and disruption of key cellular functions, such as metabolic enzymes, (ii) interacting with thiol groups, and (iii) displacing iron from iron-sulphur clusters [369,370,453].

To confirm this theory, three approaches could be considered for future studies:

- Changes in abundance of copper detoxifying components could be measured by quantitative proteomic analysis from *S. aureus* and *S. epidermidis* cell lysates. More specifically, the levels of the copper exporting P-type ATPase CopA and copper metallochaperone CopZ could be evaluated following treatment with Cu(DDC)₂ + Cu²⁺. Under Cu²⁺-depleted conditions, basal levels of CopA and CopZ would be expected. In contrast, the levels of CopA and CopZ could be elevated following exposure to Cu²⁺ alone. Consequently, inhibition of copper resistance mechanisms by Cu(DDC)₂ + Cu²⁺ would translate to lower levels of CopA and/or CopZ compared to the Cu²⁺ levels alone [453].
- Bacterial copper concentrations could be determined via inductively coupled plasma mass spectroscopy (ICP-MS) and Phen Green™ FL assay. Cellular Cu²⁺ accumulation following Cu(DDC)₂ + Cu²⁺ treatment would result in the detection by ICP-MS of increased Cu²⁺ levels compared to the copper content of Cu²⁺ treated bacteria. While ICP-MS measures the total cellular Cu²⁺ content, the fluorescent metal sensor Phen Green™ FL would be taken up by bacteria, allowing the monitoring of the intracellular fluctuations of accessible Cu²⁺. The fluorescence would be quenched by Cu²⁺ and inversely correlated with the intracellular Cu²⁺ content. By inhibiting copper resistance mechanisms, such as metal-chaperone CopZ, through Cu(DDC)₂ + Cu²⁺, higher concentration of accessible intracellular Cu²⁺ could be detected [221,226].

- Changes in levels of proteins and virulence factors affected by copper stress-responses and the generation of ROS could be measured. For example, glyceraldehyde-3-phosphate dehydrogenase is essential for *S. aureus* glycolysis and would be inhibited by Cu^{2+} [453]. The expression or abundance of virulence factors, such as *agr* and *sae*, phenol-soluble modulins, and leukocidin-like proteins have previously been shown to be downregulated or reduced in the presence of high Cu^{2+} concentrations [369,453]. Furthermore, the generation of ROS has been shown to be closely associated with copper-induced toxicity and could be measured using the luminescent probe L-012 [454] or the fluorescent probe dichlorofluorescein [138,455]. Therefore, comparing the levels of these proteins after $\text{Cu}(\text{DDC})_2 + \text{Cu}^{2+}$ treatment with levels of much higher bactericidal Cu^{2+} concentrations and the presence of high ROS levels could provide an indication on the importance of copper-induced toxicity on bacterial cell death.

The microscopy images of MRSA and *S. epidermidis* biofilms stained with LIVE/DEAD staining suggested that treatment with $\text{Cu}(\text{DDC})_2 + \text{Cu}^{2+}$ resulted in disruption of the bacterial membrane. To investigate the damages to the bacterial membrane, caused by this combination, future experiments in which lipid vesicles mimicking *S. aureus* membranes could be investigated for leakage [352,456]. Furthermore, lipid peroxidation resulting from oxidative stress [457] could be determined using nuclear magnetic resonance or mass spectrometry coupled with liquid chromatography [458].

The genotypes of the *S. aureus* and MRSA strains should be compared to determine a potential correlation between variations in MIC and biofilm viability resulting from the presence of copper hypertolerance genes, such as *copB*, *mco*, *copL* in certain strains [459,460]. Bacteria, such as *S. aureus*, can become copper hyper-resistant by developing an additional copper efflux transporter (CopB), Cu^{2+} -dependent multicopper oxidase (MCO) and copper lipoproteins (CopL), or by mutations of the copper-sensitive operon repressor [460,461]. Therefore, gaining more knowledge about the mechanism behind the antibacterial activity of $\text{Cu}(\text{DDC})_2 + \text{Cu}^{2+}$ is important to estimate the risk of resistance development. In addition, resistance induction and single-step resistance selection should be investigated in *S. aureus* and *S. epidermidis* following treatment with $\text{Cu}(\text{DDC})_2 + \text{Cu}^{2+}$. While the resistance-inducing assay examines the development of multiple mutations, each associated with a small benefit but leading to high resistance when combined, the single step resistance selection assays could assist in identifying a single mutation that provides high drug resistance [462].

The $\text{Cu}(\text{DDC})_2 + \text{Cu}^{2+}$ combination showed synergistic and additive effects with a range of antibiotics, except for erythromycin. While the mechanism of action behind the antibacterial activity of $\text{Cu}(\text{DDC})_2 + \text{Cu}^{2+}$ could explain variations in synergistic effects between antibiotics, only one or two representatives per antibiotic class were investigated. Therefore, more antibiotics need to be investigated for synergistic effects, especially the standard of care antibiotics for prevention of SSIs, such as mupirocin, ceftazolin, and ampicillin, and for treatment of SSIs, such as rifampicin, linezolid, daptomycin, tigecycline, and sulfamethoxazole-trimethoprim [27]. By reciprocally enhancing each other's antibacterial activities, lower doses of $\text{Cu}(\text{DDC})_2 + \text{Cu}^{2+}$ and antibiotics could be administered, thereby reducing the risks for unwanted side effects. In addition, the post-antibiotic effect of $\text{Cu}(\text{DDC})_2 + \text{Cu}^{2+}$ could be investigated to minimise the dosage for therapeutic clearance and define a treatment interval for future *in vivo* and clinical experiments [148,153].

While exposure to $\text{Cu}(\text{DDC})_2 + \text{Cu}^{2+}$ resulted in high human dermal fibroblast cell viability, its effects on the viability of other cell types relevant to surgical sites, such as keratinocytes should be

investigated [388]. In addition, selective activity of Cu(DDC)₂ + Cu²⁺ against bacteria or biofilms in the presence of human cells could be determined using *in vitro* intracellular- and extracellular-infection models of *S. aureus* or *S. epidermidis* [463].

The antibiofilm activity of Cu(DDC)₂ + Cu²⁺ in microtiter plates was also demonstrated in *in vitro* biofilm models mimicking SSIs, including an infected medical device model and an artificial dermis model (Chapter 3). The high antibacterial and low cytotoxic effects of Cu(DDC)₂ + Cu²⁺ were further noted in MRSA and *S. epidermidis*-infected larvae of the greater wax moth. As the *in vitro* and *in vivo* experiments were successful, the combination of Cu(DDC)₂ + Cu²⁺ should be further investigated for safety and efficacy in mammalian *in vivo* models. However, owing to the low solubility of the Cu(DDC)₂ complex, evaluation in both pre-clinical animal and clinical studies would be limited, necessitating the development of specific formulations to enhance its bioavailability.

5.2 Liposomal formulation of Cu(DDC)₂ + Cu²⁺

In Chapter 3, the Cu(DDC)₂ + Cu²⁺ combination reduced the viability of biofilms grown on hernia meshes and on artificial dermis. However, it was assumed that the antibiofilm activity was limited, owing to the low water solubility of Cu(DDC)₂. The complex forms instantly when DDC⁻ and Cu²⁺ are mixed and sediments onto surfaces [223], rendering pre-clinical and a clinical application problematic. Therefore, a liposomal formulation of Cu²⁺ and Cu(DDC)₂ developed by Hartwig, *et al.* [228] and consisting of DSPC, Chol and DSPE-mPEG₂₀₀₀ was investigated as a water-soluble alternative. While Cu(DDC)₂-liposomes, with free Cu²⁺, showed similar antibiofilm activity against MRSA and *S. epidermidis* compared with free compounds, the combination of Cu(DDC)₂-liposomes with Cu²⁺-liposomes did not reduce biofilm viability. It was hypothesised that Cu(DDC)₂ was released from the liposomes and/or the liposomes interact with bacteria or the biofilm matrix. Furthermore, it was postulated that the dense PEG polymers surrounding Cu²⁺-liposomes stabilised the liposomes during incubation at 37 °C but prevented the release of Cu²⁺, thereby hindering the interaction of the liposomes with bacteria or biofilms over 24 h. This hypothesis was based on the smaller size of Cu²⁺-liposomes compared to Cu(DDC)₂-liposomes and the assumption that Cu²⁺-liposomes and Cu(DDC)₂-liposomes provided the same lipid bilayer constitution. This assumption was made as Cu(DDC)₂-liposomes are formed by remote loading of DDC⁻ into Cu²⁺-liposomes and the liposomal Cu(DDC)₂-to-lipid ratio was directly proportional to the liposomal Cu²⁺-to-lipid ratio [223]. To this end, future studies should define the exact lipid composition of the Cu²⁺-liposomes and Cu(DDC)₂-liposomes using the Bartlett assay [228] or through high-performance liquid chromatography [464]. Furthermore, transmission cryo-electron microscopy could be used to visualise if Cu²⁺-liposomes which remain intact over 24 h when incubated with bacteria [223,282]. Permeability and retention of fluorescently-labelled liposomes (e.g., with 0.5% dioctadecyloxycarbocyanin perchlorate) on biofilms should be investigated in a biofilm transwell model by measuring the fluorescence intensity of the suspensions above and below the biofilm in the transwell [401].

To potentiate the interaction of Cu²⁺-liposomes and Cu(DDC)₂-liposomes with bacterial cells, the coating and constitution of the lipid bilayer membrane could be adapted. Surface decoration with PEG polymers is required for stability of liposomes during storage [228] but reduces the affinity of liposomes to *S. aureus* biofilms [277] and to intracellular MRSA compared to non-PEGylated liposomes [465]. As alternatives to PEG, poly[2-(methacryloyloxy)ethyl phosphorylcholine] could be attached onto the surface of the liposomes, as previous studies have shown superior effects

against biofilms, due to improved bacterial uptake, compared to PEGylated liposomes [466]. Furthermore, the physiochemical characteristics of the liposomes could be changed by including surface charge, specific targeting, and responsiveness to stimuli. By incorporating a cationic phospholipid, such as dioleoyl-3-trimethylammonium propane, the antibiofilm effects and the retention in *S. epidermidis* and *S. aureus* biofilms could be increased [270,404,467]. This extended contact would occur via electrostatic forces between positively charged liposomes and the negatively charged bacterial membrane, which is mainly composed of anionic lipids, and negatively charged biofilm structures, such as eDNA [400,468]. As cationic liposomal formulations typically show toxic effects in human cells, cytotoxicity assays would be required to assess the benefit : risk ratio [467]. The incorporation of anionic phospholipids, such as dipalmitoyl phosphoryl glycerol sodium salt, is not recommended, due to possible interactions with Cu^{2+} ions and repulsive electrostatic forces between anionic liposomes and negatively charged bacteria that could reduce adsorption on *S. epidermidis* and *S. aureus* biofilms [404,467]. To lower the risk of adverse effects and to further increase the antibiofilm activity of liposomes, the surface of liposomes could be altered to target pathogenic surface components and increase the site-specific delivery of the antibacterial agents. *S. aureus* surface proteins, such as staphylococcal protein A, or bacterial cell components could be targeted by liposomes coated with antibodies, glycoproteins, peptides, and aptamers [278,280]. Furthermore, to improve the release of Cu^{2+} from the liposomes in the slightly acidic biofilms, pH-sensitive liposomes could be developed using dioleoyl phosphatidylethanolamine [469] and cholesteryl hemisuccinate lipid [470].

$\text{Cu}(\text{DDC})_2 + \text{Cu}^{2+}$ was incorporated into liposomes to increase the water solubility of $\text{Cu}(\text{DDC})_2$ and to protect DDC^- from degradation by blood components. Therefore, the stability of $\text{Cu}(\text{DDC})_2$ -liposomes and Cu^{2+} -liposomes should be investigated in blood serum. The liposomes could be incubated at 37 °C with a 10% foetal bovine serum solution and the particle size and Cu^{2+} or $\text{Cu}(\text{DDC})_2$ content evaluated after pre-determined time periods [290]. The protective effects of the liposomes could also prevent the development of resistance and extend the antibacterial activity of $\text{Cu}(\text{DDC})_2 + \text{Cu}^{2+}$ to Gram-negative bacteria, which could be investigated by MIC assays [361]. The lack of effects against *E. coli* or *P. aeruginosa* by the free combination was attributed to the presence of glutathione in Gram-negative bacteria that can interact with DDC^- and Cu^{2+} (Chapter 2). Therefore, the incorporation of $\text{Cu}(\text{DDC})_2 + \text{Cu}^{2+}$ into liposomes could offer protection from glutathione and render Gram-negative bacteria susceptible to this combination. However, compared to staphylococci, Gram-negative bacteria possess different copper resistance mechanisms [471] that might not be inhibited by $\text{Cu}(\text{DDC})_2 + \text{Cu}^{2+}$.

The combination of $\text{Cu}(\text{DDC})_2$ -liposomes + free Cu^{2+} and $\text{Cu}(\text{DDC})_2$ -liposomes + Cu^{2+} -liposomes showed increased survival of *S. epidermidis*-infected *G. mellonella*. The efficacy of the liposomal combination against MRSA-infected *G. mellonella* could not be assessed due to unpredictable survival rates within the controls. Larvae, purchased from commercial sources (i.e., a recreational fishing tackle shop) were subject to variations in culture and storage conditions and differences in the “age” of the larvae. While the controls of the *S. epidermidis*-infected larvae and untreated larvae were consistent, these experiments should be repeated with larvae cultured and stored under conditions suited for laboratory experiments.

Currently, the liposome production consists of thin-film hydration, extrusion, size exclusion chromatography, buffer exchange, remote loading, and filtration. This multi-step process is laborious and not easily scalable to produce large quantities of liposomes. To facilitate the production of Cu^{2+} -liposomes, the lipid film preparation and extrusion could be replaced by dual

centrifugation [472]. The production of Cu(DDC)₂-liposomes could also be performed as a one-step synthesis using a modified version of the ethanol injection method, as described by Paun, *et al.* [288]. Moreover, the lengthy lyophilisation process of the liposomes described in Chapter 4 could be shortened by determining the moment of transition from primary to secondary drying and by optimising the freezing rate. The sublimation of the last ice crystal could be determined using the Pirani gauge or the pressure increase test to measure pressure changes caused by sublimated water. Furthermore, weight changes can provide an indication on the water content. Reaching the equilibrium water content correlates with a constant weight of the material over 30 min. The freezing rate results in small or large ice crystals which were associated with the time necessary for primary or secondary drying [473].

Lastly, alternative nanovesicles for Cu(DDC)₂ could be investigated for antibacterial activity, such as Cu(DDC)₂ micelles [248,249], cyclodextrins [255], incorporated in apoferritin [254] or bovine serum albumin [253]. Here, the liposomal formulation developed by Hartwig, *et al.* [228] for neuroblastoma was repurposed as antibacterial agent against *S. aureus* and *S. epidermidis*. The liposomes are a drug delivery vesicle for both Cu(DDC)₂ and Cu²⁺ and were further embedded in an injectable gel for local delivery on SSIs.

5.3 Injectable hydrogel as drug-delivery platform for Cu(DDC)₂-liposomes and Cu²⁺-liposomes

For clinical application on surgical sites, lyophilised liposomes were incorporated into a thermosensitive gel comprising CS and βGP. As described in Chapter 4, the sterilised CS-βGP mixture could be stored at -20 °C, transitions from sol - gel within a few minutes at temperatures in the physiological range and is biocompatible. The incorporation of the liposomes into the CS-βGP mixture resulted in small changes of the sol-gel transition temperature and time but remained within the physiological range. Confirmation of the incorporation of liposomes and the structure of the CS-βGP gel could be visually assessed using scanning electron microscopy. Furthermore, the weight loss of the lipogel over time was measured to give an indication on stability, degradation, and the release of the liposomal formulation from the hydrogel. However, the weight loss assay was performed under dry conditions at 37 °C (i.e., CS-βGP gel or lipogel in transwell) and did not include physiological conditions, such as moisture, pH and enzymes [474]. Therefore, the stability and degradation of the gels should be further investigated by measuring the weight loss over time when incubated in an enzymatic solution (e.g., lysozyme in PBS, pH 7.4) [443].

For most experiments, the fluid CS-βGP mixture containing liposomes was handled using pipettes. For an application on surgical sites, the CS-βGP mixture with liposomes will be injected using a syringe. Therefore, a syringeability assay should be performed for CS-βGP mixture, with or without, liposomes to determine the appropriate needle gauge range [474]. As described by Moreira, *et al.* [475], the syringeability is determined as the percentage of expelled hydrogel solution from a syringe with a specific needle (e.g., 21G^{1/4} needle corresponding to 30 × 0.8mm) under a constant force of 50 N for 5 s. The mass of the expelled solution could be compared to the mass of the sample prior to injection and a high syringeability would be associated with accuracy of dose measurements and ease of application [475]. As the administration of the lipogel is not subcutaneous but on surgical sites or infected surgical wounds, an injectability assay to determine the force required for subcutaneous administration was not necessary [474].

The release of the liposomes from the lipogel was estimated based on the effect of the liposomes on fibroblast cell viability and on MRSA and *S. epidermidis* biofilms. The suggested release profile of Cu(DDC)₂-liposomes and Cu²⁺-liposomes from the lipogel needs to be confirmed by appropriate quantification of free or liposomal compounds. Quantification with UV spectrophotometry of released liposomes was not possible due to the small amount of lipogel investigated and drug concentrations below the limit of quantification [476]. Incorporating higher concentrations of liposomes in the lipogel can alter the stability of the liposomes and the gel structure and consequently the release profile of the lipogel. Furthermore, the lengthy liposomes production was a limiting factor for the release assay optimisation, as large amounts of lipogels could not be prepared in a timely manner. Alternative methods of quantification with a high selectivity and sensitivity for Cu²⁺ or Cu(DDC)₂ should be investigated, including graphite furnace atomic absorption spectrometry [223,389,394,441] or high-performance liquid chromatography [290]. To differentiate between the release of free Cu(DDC)₂ and Cu(DDC)₂-liposomes, unfiltered supernatant (free Cu(DDC)₂ + Cu(DDC)₂-liposomes) and filtered supernatant (Cu(DDC)₂-liposomes) should be measured and compared. Differentiation between the release of free compounds or liposomes from the lipogel could also be visually assessed by cryo-electron microscopy of the supernatant [223].

The lipogel prevented the formation of MRSA and *S. epidermidis* biofilm and reduced biofilm viability compared to CS-βGP gel. Therefore, the *in vitro* antibiofilm activity of the lipogel was associated with the release of Cu(DDC)₂-liposomes and Cu²⁺-liposomes from the gel and the antibiofilm activity of the liposomes. The effects of Cu(DDC)₂-liposomes + Cu²⁺-liposomes against MRSA and *S. epidermidis* contradicted with the lack of *in vitro* antibiofilm activity of the liposomes observed in Chapter 3. These differences could be explained by longer treatment times, liposomal changes during lyophilisation and interactions with CS polymers. While the biofilms were incubated with Cu(DDC)₂-liposomes + Cu²⁺-liposomes for 24 h in Chapter 3, the biofilms were treated with lipogels for 4 days in Chapter 4. Therefore, the antibiofilm activity of Cu(DDC)₂-liposomes + Cu²⁺-liposomes should also be investigated after 48 h or up to 72 h incubation (maximum time before the biofilm dies from nutrient depletion). Furthermore, the liposomes incorporated into the lipogel in Chapter 4 were lyophilised and compared to the liposomes analysed in Chapter 3. Previous studies have shown that the lyophilisation process can induce changes in the lamellarity and morphology of the liposomes [426], which can reduce the stability at 37 °C and promote interaction with biofilm components and bacterial membrane. Therefore, cryo-electron microscopy images of redispersed lyophilised and non-lyophilised liposomes should be analysed [223,426] and the stability of Cu²⁺-liposomes over 4 days at 37 °C investigated using dynamic light scattering [228]. Lastly, CS polymers of the hydrogel matrix can coat the liposomes and change their characteristics, such as increasing the liposomal size and exhibiting a positive charge. While liposomes coated with CS typically release encapsulated drugs in a retarded or slower manner [431], the positive charge of CS coated liposomes can promote interaction with negatively charged bacterial membrane or biofilm components [270] and the CS layer can affect the dense PEGylation at the surface of Cu²⁺-liposomes. In addition, the intrinsic antimicrobial activity of CS can synergise with Cu(DDC)₂ + Cu²⁺ enclosed in the liposomes [431,477].

While the eradication of *in vitro* formed biofilms was not possible, the reduced bacterial viability might provide the host immune system an opportunity to overcome the biofilm infection. Furthermore, the co-administration of the lipogel with standards of care antibiotics could further increase the antibiofilm activity and should be investigated *in vivo* in the future. During *in vivo* studies, wound healing properties of the lipogel should also be determined.

6 Conclusion

The aim of this project was to develop a novel antibacterial therapy for the prevention and treatment of *S. aureus* and *S. epidermidis* associated SSIs that can be applied locally at the site of infection. In this thesis, the capacity of DDC⁻ and Cu²⁺ to reduce biofilm viability, prevent biofilm formation, and synergise with antibiotics was described. This antibacterial activity, synergistic effects in combination with specific antibiotics, and the low cytotoxic effects in human cell culture make Cu(DDC)₂ + Cu²⁺ a promising agent in the fight against staphylococci biofilms. While the combination showed efficacy and no toxicity in a small invertebrate *in vivo* model, further progress into mammalian animal models was initially limited by the low water solubility of Cu(DDC)₂. Therefore, a liposomal formulation of Cu(DDC)₂ + Cu²⁺ was used as water soluble alternative, which showed similar antibiofilm activity *in vitro* as well as efficacy and safety *in vivo* compared to the free combination. Finally, a biocompatible CS-βGP hydrogel with thermosensitive properties was shown to be a suitable drug delivery system for liposomal Cu(DDC)₂ + Cu²⁺ for SSIs. The CS-βGP solution and the lyophilised Cu(DDC)₂ + Cu²⁺ liposomes can be stored at -20 °C, mixed upon thawing and directly injected onto the surgical site or the infected surgical wound. The developed injectable lipogel prevented biofilm formation and reduced biofilm viability *in vitro* by releasing liposomal Cu(DDC)₂ + Cu²⁺ over time. The pre-clinical studies demonstrated that the lipogel based on CS-βGP, containing a combination of DDC⁻ and Cu²⁺ as liposomes, represents a promising new approach for the prevention and the treatment of *S. aureus* and *S. epidermidis* associated SSIs.

7 Appendix

Publication: “The revival of dithiocarbamates: from pesticides to innovative medical treatments“

Statement of authorship

Title of Paper	The revival of dithiocarbamates: from pesticides to innovative medical treatments		
Publication Status	<input checked="" type="checkbox"/> Published	<input type="checkbox"/> Submitted for Publication	
	<input type="checkbox"/> Accepted for Publication	<input type="checkbox"/> Unpublished and Unsubmitted work written in a manuscript style	
Publication Details	Kaul L, Süß R, Zannettino A, Richter K. The revival of dithiocarbamates: from pesticides to innovative medical treatments. iScience. 2021;24(2):102092; doi:10.1016/j.isci.2021.102092.		

Principal author

Name of Principal author	Laurine Kaul		
Contribution to the Paper	Review of literature, writing of original draft		
Overall percentage (%)	85%		
Certification	This paper reports on original research I conducted during the period of my Higher Degree by Research candidature and is not subject to any obligations or contractual agreements with a third party that would constrain its inclusion in this thesis. I am the primary author of this paper.		
Signature		Date	08.02.2023

Co-author

By signing the Statement of Authorship, each author certifies that:

- i. The candidate’s stated contribution to the publication is accurate (as detailed above).
- ii. Permission is granted for the candidate to include the publication in the thesis; and
- iii. The sum of all co-author contributions is equal to 100% less the candidate’s stated contribution.

Name of Co-Author	Regine Süß		
Contribution to the Paper	Supervision, review and editing of manuscript		
Signature		Date	15/2/2023

Name of Co-Author	Andrew Zannettino		
Contribution to the Paper	Supervision, review and editing of manuscript		
Signature		Date	15/02/23

Name of Co-Author	Katharina Richter		
Contribution to the Paper	Supervision, review and editing of manuscript, corresponding author		
Signature		Date	8/2/23

Publication title page

iScience

CellPress
OPEN ACCESS

Review

The revival of dithiocarbamates: from pesticides to innovative medical treatments

Laurine Kaul,^{1,2,3} Regine Süß,² Andrew Zannettino,^{3,4,5} and Katharina Richter^{1,3,*}

SUMMARY

Dithiocarbamates (DTCs) have been used for various applications, including as hardening agents in rubber manufacturing, as fungicide in agriculture, and as medications to treat alcohol misuse disorder. The multi-faceted effects of DTCs rely mainly on metal binding abilities and a high reactivity with thiol groups. Therefore, the list of potential applications is still increasing, exemplified by the US Food and Drug Administration approval of disulfiram (Antabuse) and its metabolite diethyldithiocarbamate in clinical trials against cancer, human immunodeficiency virus, and Lyme disease, as well as new DTC-related compounds that have been synthesized to target diseases with unmet therapeutic needs. In this review, we will discuss the latest progress of DTCs as anti-cancer agents and provide a summary of the mechanisms of action. We will explain the expansion of DTCs' activity in the fields of microbiology, neurology, cardiology, and ophthalmology, thereby providing evidence for the important role and therapeutic potential of DTCs as innovative medical treatments.

INTRODUCTION

Chemical structures containing dithiocarbamates (DTCs) as functional group began their life as catalysts in the rubber vulcanization process in the early 1880s. In 1943, the first DTC derivative, nabam, was patented as fungicide for agricultural use, followed by zineb, the first DTC to be coupled with a metal. The best known DTC derivative, diethyldithiocarbamate (DDC), is the active metabolite of the anti-alcoholic drug, disulfiram (DSF) (Bala et al., 2014). Notably, DTCs have recently resurfaced as potential drug therapies, owing to (1) their ability to chelate metals and (2) their affinity for thiol groups present in human and microbial enzymes (Sauna et al., 2005; Buac et al., 2012).

To date, a small number of articles have described the emerging importance of DTCs in medicine and the potential of DSF for various biomedical applications. DSF and DDC represent interesting candidate drug therapies, as they are inexpensive and have an excellent safety record (Viola-Rhenals et al., 2018). In the past 20 years, DSF and DDC have been extensively investigated as cancer treatments, as antimicrobial agents, and for their application in cardiology and neurology. In addition, new chemical structures with DTC moieties have been synthesized and tested for their anti-cancer, antiviral, ophthalmic, and neurological applications (i.e., for the treatment of Alzheimer disease) (Figure 1).

DITHIOCARBAMATES: NEW ALLIES IN THE FIGHT AGAINST CANCER

According to the World Health Organization (WHO), in 2018, one in six deaths was caused by cancer worldwide. Cancer is broadly defined as cells that display abnormal and uncontrolled growth. Treatment options include chemotherapeutic agents that are usually associated with toxic side effects and limited therapeutic activity due to the development of drug resistances in a significant number of patients (Gillet and Gottesman, 2010). Therefore, new anti-cancer drugs that display selectivity for cancer cells without the associated development of resistance are urgently required.

Current status of research on DTC in cancer

The anti-cancer activity of DSF was first observed when an alcoholic patient showed complete remission of metastatic breast cancer when being treated with the anti-alcoholic drug DSF in 1977 (Skrott and Cvek, 2012). According to clinicaltrials.gov, DSF's anti-cancer properties have seen these agents as the subject of 21 clinical trials with the focus on metastatic breast, prostate, and pancreatic cancer; glioblastoma;

¹Richter Lab, Department of Surgery, Basil Hetzel Institute for Translational Health Research, University of Adelaide, Adelaide, SA 5011, Australia

²Department of Pharmaceutical Technology and Biopharmacy, Institute of Pharmaceutical Sciences, University of Freiburg, Freiburg 79104, Germany

³Adelaide Medical School, Faculty of Health and Medical Sciences, University of Adelaide, Adelaide, SA 5005, Australia

⁴Precision Medicine Theme, South Australian Health & Medical Research Institute, Adelaide, SA 5000, Australia

⁵Central Adelaide Local Health Network, Adelaide, SA 5011, Australia

*Correspondence: katharina.richter@adelaide.edu.au
<https://doi.org/10.1016/j.isci.2021.102092>



8 Bibliography

1. Dobson, G.P. Trauma of major surgery: A global problem that is not going away. *Int J Surg* **2020**, *81*, 47-54, doi:10.1016/j.ijsu.2020.07.017.
2. Costa, A.C.D.; Santa-Cruz, F.; Ferraz Á, A.B. What's new in infection on surgical site and antibiotic prophylaxis in surgery? *Arq Bras Cir Dig* **2021**, *33*, e1558, doi:10.1590/0102-672020200004e1558.
3. Ademuyiwa, A.O.; Hardy, P.; Runigamugabo, E.; Sodonougbo, P.; Behanzin, H.; et al. Reducing surgical site infections in low-income and middle-income countries (FALCON): A pragmatic, multicentre, stratified, randomised controlled trial. *Lancet* **2021**, *398*, 1687-99, doi:10.1016/S0140-6736(21)01548-8.
4. Mangram, A.J.; Horan, T.C.; Pearson, M.L.; Silver, L.C.; Jarvis, W.R.; et al. Guideline for prevention of surgical site infection, 1999. *Infect Control Hosp Epidemiol* **1999**, *20*, 250-80.
5. Horan, T.C.; Gaynes, R.P.; Martone, W.J.; Jarvis, W.R.; Emori, T.G. CDC definitions of nosocomial surgical site infections, 1992: A modification of CDC definitions of surgical wound infections. *Infect Control Hosp Epidemiol* **1992**, *13*, 606-8, doi:10.1016/S0196-6553(05)80201-9.
6. Owens, C.D.; Stoessel, K. Surgical site infections: Epidemiology, microbiology and prevention. *J Hosp Infect* **2008**, *70*, 3-10, doi:10.1016/S0195-6701(08)60017-1.
7. European Centre for Disease Prevention and Control. *Healthcare-associated infections: Surgical site infections*; Annual epidemiological report for 2017; ECDC: Stockholm, **2019**.
8. Andersson, R.; Søreide, K.; Ansari, D. Surgical infections and antibiotic stewardship: In need for new directions. *Scand J Surg* **2021**, *110*, 110-2, doi:10.1177/1457496919891617.
9. Piednoir, E.; Robert-Yap, J.; Baillet, P.; Lermite, E.; Christou, N. The socioeconomic impact of surgical site infections. *Front Public Health* **2021**, *9*, 712461, doi:10.3389/fpubh.2021.712461.
10. Di Marzo, F. The burden of surgical site infections: Pathophysiology and risk factors—Preoperative measures to prevent surgical site infections. In *Infections in Surgery: Prevention and Management*, Sartelli, M., Coimbra, R., Pagani, L., et al., Eds.; Springer International Publishing: Cham, **2021**; pp. 1-15.
11. World Health Organization. *Global guidelines for the prevention of surgical site infection, second edition*; WHO: Geneva, **2018**.
12. Berríos-Torres, S.I.; Umscheid, C.A.; Bratzler, D.W.; Leas, B.; Stone, E.C.; et al. Centers for disease control and prevention guideline for the prevention of surgical site infection, 2017. *JAMA Surg* **2017**, *152*, 784-91, doi:10.1001/jamasurg.2017.0904.
13. McCaffrey, N.; Scollo, M.; Dean, E.; White, S.L. What is the likely impact on surgical site infections in Australian hospitals if smoking rates are reduced? A cost analysis. *PLoS One* **2021**, *16*, e0256424, doi:10.1371/journal.pone.0256424.
14. Worth, L.J.; Bull, A.L.; Spelman, T.; Brett, J.; Richards, M.J. Diminishing surgical site infections in Australia: Time trends in infection rates, pathogens and antimicrobial resistance using a comprehensive Victorian surveillance program, 2002-2013. *Infect Control Hosp Epidemiol* **2015**, *36*, 409-16, doi:10.1017/ice.2014.70.
15. Andersen, B.M. Prevention of postoperative wound infections. In *Prevention and Control of Infections in Hospitals*, Andersen, B.M., Ed.; Springer, Cham: **2019**; pp. 377-437.
16. Wilson, R.B.; Farooque, Y. Risks and prevention of surgical site infection after hernia mesh repair and the predictive utility of ACS-NSQIP. *J Gastrointest Surg* **2022**, *26*, 950-64, doi:10.1007/s11605-022-05248-6.
17. de Lissovoy, G.; Fraeman, K.; Hutchins, V.; Murphy, D.; Song, D.; et al. Surgical site infection: Incidence and impact on hospital utilization and treatment costs. *Am J Infect Control* **2009**, *37*, 387-97, doi:10.1016/j.ajic.2008.12.010.

18. European Centre for Disease Prevention and Control. *Surveillance of surgical site infections and prevention indicators in European hospitals - HAI-Net SSI protocol, version 2.2*; ECDC: Stockholm, **2017**.
19. Ortega, G.; Rhee, D.S.; Papandria, D.J.; Yang, J.; Ibrahim, A.M.; et al. An evaluation of surgical site infections by wound classification system using the ACS-NSQIP. *J Surg Res* **2012**, *174*, 33-8, doi:10.1016/j.jss.2011.05.056.
20. Papadopoulos, A.; Machairas, N.; Tsourouflis, G.; Chouliaras, C.; Maniotti, E.; et al. Risk factors for surgical site infections in patients undergoing emergency surgery: A single-centre experience. *In Vivo* **2021**, *35*, 3569-74, doi:10.21873/invivo.12660.
21. Humphreys, H.; Becker, K.; Dohmen, P.M.; Petrosillo, N.; Spencer, M.; et al. Staphylococcus aureus and surgical site infections: Benefits of screening and decolonization before surgery. *J Hosp Infect* **2016**, *94*, 295-304, doi:10.1016/j.jhin.2016.06.011.
22. Abu Hamdeh, S.; Lytsy, B.; Ronne-Engström, E. Surgical site infections in standard neurosurgery procedures— a study of incidence, impact and potential risk factors. *Br J Neurosurg* **2014**, *28*, 270-5, doi:10.3109/02688697.2013.835376.
23. Davies, B.M.; Jones, A.; Patel, H.C. Implementation of a care bundle and evaluation of risk factors for surgical site infection in cranial neurosurgery. *Clin Neurol Neurosurg* **2016**, *144*, 121-5, doi:10.1016/j.clineuro.2016.03.025.
24. Olsen, M.A.; Lefta, M.; Dietz, J.R.; Brandt, K.E.; Aft, R.; et al. Risk factors for surgical site infection after major breast operation. *J Am Coll Surg* **2008**, *207*, 326-35, doi:10.1016/j.jamcollsurg.2008.04.021.
25. Palubicka, A.; Jaworski, R.; Wekwejt, M.; Swieczko-Zurek, B.; Pikula, M.; et al. Surgical site infection after breast surgery: A retrospective analysis of 5-year postoperative data from a single center in Poland. *Medicina (Kaunas)* **2019**, *55*, 512, doi:10.3390/medicina55090512.
26. Rubio-Perez, I.; Alvarez-Peña, E. The infected mesh: How to treat it. In *Infections in Surgery: Prevention and Management*, Sartelli, M., Coimbra, R., Pagani, L., et al., Eds.; Springer International Publishing: Cham, **2021**; pp. 55-65.
27. Hrynshyn, A.; Simões, M.; Borges, A. Biofilms in surgical site infections: Recent advances and novel prevention and eradication strategies. *Antibiotics (Basel)* **2022**, *11*, 69, doi:10.3390/antibiotics11010069.
28. Anderson, D.J.; Sexton, D.J.; Kanafani, Z.A.; Auten, G.; Kaye, K.S. Severe surgical site infection in community hospitals: Epidemiology, key procedures, and the changing prevalence of methicillin-resistant Staphylococcus aureus. *Infect Control Hosp Epidemiol* **2007**, *28*, 1047-53, doi:10.1086/520731.
29. Hoiby, N.; Ciofu, O.; Johansen, H.K.; Song, Z.J.; Moser, C.; et al. The clinical impact of bacterial biofilms. *Int J Oral Sci* **2011**, *3*, 55-65, doi:10.4248/ijos11026.
30. Percival, S.L. Importance of biofilm formation in surgical infection. *Br J Surg* **2017**, *104*, e85-e94, doi:10.1002/bjs.10433.
31. Costerton, J.W.; Stewart, P.S.; Greenberg, E.P. Bacterial biofilms: A common cause of persistent infections. *Science* **1999**, *284*, 1318-22, doi:10.1126/science.284.5418.1318
32. Kragh, K.N.; Richter, K. Introduction: Biofilms 101. In *Antibiofilm Strategies: Current and Future Applications to Prevent, Control and Eradicate Biofilms*, Richter, K., Kragh, K.N., Eds.; Springer International Publishing: Cham, **2022**; Volume 11, pp. 3-15.
33. Boudarel, H.; Mathias, J.-D.; Blaysat, B.; Grédiac, M. Towards standardized mechanical characterization of microbial biofilms: Analysis and critical review. *NPJ Biofilms Microbiomes* **2018**, *4*, 17, doi:10.1038/s41522-018-0062-5.
34. Donlan, R.M.; Costerton, J.W. Biofilms: Survival mechanisms of clinically relevant microorganisms. *Clin Microbiol Rev* **2002**, *15*, 167-93, doi:10.1128/CMR.15.2.167-193.2002.
35. Archer, N.K.; Mazaitis, M.J.; Costerton, J.W.; Leid, J.G.; Powers, M.E.; et al. Staphylococcus aureus biofilms: Properties, regulation, and roles in human disease. *Virulence* **2011**, *2*, 445-59, doi:10.4161/viru.2.5.17724.

36. Flemming, H.C.; Wingender, J.; Szewzyk, U.; Steinberg, P.; Rice, S.A.; et al. Biofilms: An emergent form of bacterial life. *Nat Rev Microbiol* **2016**, *14*, 563-75, doi:10.1038/nrmicro.2016.94.
37. Karygianni, L.; Ren, Z.; Koo, H.; Thurnheer, T. Biofilm matrixome: Extracellular components in structured microbial communities. *Trends Microbiol* **2020**, *28*, 668-81, doi:10.1016/j.tim.2020.03.016.
38. Schilcher, K.; Horswill, A.R. Staphylococcal biofilm development: Structure, regulation, and treatment strategies. *Microbiol Mol Biol Rev* **2020**, *84*, e00026-19, doi:10.1128/MMBR.00026-19.
39. Flemming, H.C.; Wingender, J. The biofilm matrix. *Nat Rev Microbiol* **2010**, *8*, 623-33, doi:10.1038/nrmicro2415.
40. Richter, K.; Van den Driessche, F.; Coenye, T. Innovative approaches to treat *Staphylococcus aureus* biofilm-related infections. *Essays Biochem* **2017**, *61*, 61-70, doi:10.1042/ebc20160056.
41. Sauer, K.; Stoodley, P.; Goeres, D.M.; Hall-Stoodley, L.; Burmølle, M.; et al. The biofilm life cycle: Expanding the conceptual model of biofilm formation. *Nat Rev Microbiol* **2022**, *20*, 608-20, doi:10.1038/s41579-022-00767-0.
42. Dunne, W.M., Jr. Bacterial adhesion: Seen any good biofilms lately? *Clin Microbiol Rev* **2002**, *15*, 155-66, doi:10.1128/CMR.15.2.155-166.2002.
43. Foster, T.J.; Geoghegan, J.A.; Ganesh, V.K.; Hook, M. Adhesion, invasion and evasion: The many functions of the surface proteins of *Staphylococcus aureus*. *Nat Rev Microbiol* **2014**, *12*, 49-62, doi:10.1038/nrmicro3161.
44. Geraci, J.; Neubauer, S.; Pöllath, C.; Hansen, U.; Rizzo, F.; et al. The *Staphylococcus aureus* extracellular matrix protein (Emp) has a fibrous structure and binds to different extracellular matrices. *Sci Rep* **2017**, *7*, 13665, doi:10.1038/s41598-017-14168-4.
45. Vazquez, V.; Liang, X.; Horndahl, J.K.; Ganesh, V.K.; Smeds, E.; et al. Fibrinogen is a ligand for the *Staphylococcus aureus* Microbial Surface Components Recognizing Adhesive Matrix Molecules (MSCRAMM) Bone Sialoprotein-binding Protein (Bbp). *J Biol Chem* **2011**, *286*, 29797-805, doi:10.1074/jbc.M110.214981.
46. O'Toole, G.; Kaplan, H.B.; Kolter, R. Biofilm formation as microbial development. *Annu Rev Microbiol* **2000**, *54*, 49-79, doi:10.1146/annurev.micro.54.1.49.
47. Brackman, G.; Coenye, T. Quorum sensing inhibitors as anti-biofilm agents. *Curr Pharm Des* **2015**, *21*, 5-11, doi:10.2174/1381612820666140905114627.
48. Lister, J.L.; Horswill, A.R. *Staphylococcus aureus* biofilms: Recent developments in biofilm dispersal. *Front Cell Infect Microbiol* **2014**, *4*, 178, doi:10.3389/fcimb.2014.00178.
49. Fleming, D.; Rumbaugh, K.P. Approaches to dispersing medical biofilms. *Microorganisms* **2017**, *5*, 15, doi:10.3390/microorganisms5020015.
50. González, J.F.; Hahn, M.M.; Gunn, J.S. Chronic biofilm-based infections: Skewing of the immune response. *Pathog Dis* **2018**, *76*, fty023, doi:10.1093/femspd/fty023.
51. Sandvik, E.L.; Borgogna, T.R.; Stewart, P.S. Antimicrobial and innate immune tolerance mechanisms in biofilms. In *Antibiofilm Strategies: Current and Future Applications to Prevent, Control and Eradicate Biofilms*, Richter, K., Kragh, K.N., Eds.; Springer International Publishing: Cham, **2022**; pp. 17-35.
52. Mah, T.F.; O'Toole, G.A. Mechanisms of biofilm resistance to antimicrobial agents. *Trends Microbiol* **2001**, *9*, 34-9, doi:10.1016/s0966-842x(00)01913-2.
53. Evans, R.C.; Holmes, C.J. Effect of vancomycin hydrochloride on *Staphylococcus epidermidis* biofilm associated with silicone elastomer. *Antimicrob Agents Chemother* **1987**, *31*, 889-94, doi:10.1128/aac.31.6.889.
54. Gristina, A.G.; Hobgood, C.D.; Webb, L.X.; Myrvik, Q.N. Adhesive colonization of biomaterials and antibiotic resistance. *Biomaterials* **1987**, *8*, 423-6, doi:10.1016/0142-9612(87)90077-9.

8 Bibliography

55. Macià, M.D.; Oliver, A. Antibiotic Resistance Development in Bacterial Biofilms. In *Antibiofilm Strategies: Current and Future Applications to Prevent, Control and Eradicate Biofilms*, Richter, K., Kragh, K.N., Eds.; Springer International Publishing: Cham, **2022**; pp. 37-58.
56. Lamret, F.; Colin, M.; Mongaret, C.; Gangloff, S.C.; Reffuveille, F. Antibiotic tolerance of *Staphylococcus aureus* biofilm in periprosthetic joint infections and antibiofilm strategies. *Antibiotics (Basel)* **2020**, *9*, 547, doi:10.3390/antibiotics9090547.
57. Le, K.Y.; Otto, M. Quorum-sensing regulation in staphylococci—an overview. *Front Microbiol* **2015**, *6*, 1174, doi:10.3389/fmicb.2015.01174.
58. Fux, C.A.; Stoodley, P.; Hall-Stoodley, L.; Costerton, J.W. Bacterial biofilms: A diagnostic and therapeutic challenge. *Expert Rev Anti Infect Ther* **2003**, *1*, 667-83, doi:10.1586/14787210.1.4.667.
59. Guo, Y.; Song, G.; Sun, M.; Wang, J.; Wang, Y. Prevalence and therapies of antibiotic-resistance in *Staphylococcus aureus*. *Front Cell Infect Microbiol* **2020**, *10*, 107, doi:10.3389/fcimb.2020.00107.
60. Edmiston, C.E., Jr.; McBain, A.J.; Roberts, C.; Leaper, D. Clinical and microbiological aspects of biofilm-associated surgical site infections. *Adv Exp Med Biol* **2015**, *830*, 47-67, doi:10.1007/978-3-319-11038-7_3.
61. Jiang, N.; Rao, F.; Xiao, J.; Yang, J.; Wang, W.; et al. Evaluation of different surgical dressings in reducing postoperative surgical site infection of a closed wound: A network meta-analysis. *Int J Surg* **2020**, *82*, 24-9, doi:10.1016/j.ijsu.2020.07.066.
62. Dumville, J.C.; Gray, T.A.; Walter, C.J.; Sharp, C.A.; Page, T.; et al. Dressings for the prevention of surgical site infection. *Cochrane Database Syst Rev* **2016**, *12*, Cd003091, doi:10.1002/14651858.CD003091.pub4.
63. Thomas, J.G.; Motlagh, H.; Povey, S.B.; Percival, S.L. The role of micro-organisms and biofilms in dysfunctional wound healing. In *Adv Wound Repair Therapies*, Farrar, D., Ed.; Woodhead Publishing: **2011**; pp. 39-76.
64. Ubbink, D.T.; Westerbos, S.J.; Nelson, E.A.; Vermeulen, H. A systematic review of topical negative pressure therapy for acute and chronic wounds. *Br J Surg* **2008**, *95*, 685-92, doi:10.1002/bjs.6238.
65. Gao, J.; Wang, Y.; Song, J.; Li, Z.; Ren, J.; et al. Negative pressure wound therapy for surgical site infections: A systematic review and meta-analysis. *J Adv Nurs* **2021**, *77*, 3980-90, doi:10.1111/jan.14876.
66. Khatoon, Z.; McTiernan, C.D.; Suuronen, E.J.; Mah, T.-F.; Alarcon, E.I. Bacterial biofilm formation on implantable devices and approaches to its treatment and prevention. *Heliyon* **2018**, *4*, e01067, doi:10.1016/j.heliyon.2018.e01067.
67. Patiniott, P.; Jacombs, A.; Kaul, L.; Hu, H.; Warner, M.; et al. Are late hernia mesh complications linked to staphylococci biofilms? *Hernia* **2022**, *26*, 1293-9, doi:10.1007/s10029-022-02583-0.
68. Agarwal, A.; Mooney, M.; Agarwal, A.G.; Jayaswal, D.; Saakyan, G.; et al. High prevalence of biofilms on retrieved implants from aseptic pseudarthrosis cases. *Spine Surg Relat Res* **2021**, *5*, 104-8, doi:10.22603/ssrr.2020-0147.
69. Kathju, S.; Nistico, L.; Melton-Kreft, R.; Lasko, L.A.; Stoodley, P. Direct demonstration of bacterial biofilms on prosthetic mesh after ventral herniorrhaphy. *Surg Infect (Larchmt)* **2015**, *16*, 45-53, doi:10.1089/sur.2014.026.
70. Wu, H.; Moser, C.; Wang, H.-Z.; Høiby, N.; Song, Z.-J. Strategies for combating bacterial biofilm infections. *Int J Oral Sci* **2014**, *7*, 1, doi:10.1038/ijos.2014.65.
71. Memar, M.Y.; Yekani, M.; Alizadeh, N.; Baghi, H.B. Hyperbaric oxygen therapy: Antimicrobial mechanisms and clinical application for infections. *Biomed Pharmacother* **2019**, *109*, 440-7, doi:10.1016/j.biopha.2018.10.142.
72. Jensen, P.Ø.; Møller, S.A.; Stjernekilde, S.; Olsen, P.; Moser, C.; et al. Hyperbaric oxygen treatment may advance the outcome of antibiotic treatment of biofilm infections. In *Antibiofilm*

- Strategies: Current and Future Applications to Prevent, Control and Eradicate Biofilms*, Richter, K., Kragh, K.N., Eds.; Springer International Publishing: Cham, **2022**; pp. 201-23.
73. Stizzo, M.; Manfredi, C.; Spirito, L.; Sciorio, C.; Romero Otero, J.; et al. Hyperbaric oxygen therapy as adjuvant treatment for surgical site infections after male-to-female gender affirmation surgery: A 10-year experience. *Andrology* **2022**, *10*, 1310-6, doi:10.1111/andr.13214.
 74. Rochford, E.T.J.; Richards, R.G.; Moriarty, T.F. Influence of material on the development of device-associated infections. *Clin Microbiol Infect* **2012**, *18*, 1162-7, doi:10.1111/j.1469-0691.2012.04002.x.
 75. Engelsman, A.F.; van der Mei, H.C.; Busscher, H.J.; Ploeg, R.J. Morphological aspects of surgical meshes as a risk factor for bacterial colonization. *Br J Surg* **2008**, *95*, 1051-9, doi:10.1002/bjs.6154.
 76. Jacombs, A.S.W.; Karatassas, A.; Klosterhalfen, B.; Richter, K.; Patiniott, P.; et al. Biofilms and effective porosity of hernia mesh: Are they silent assassins? *Hernia* **2020**, *24*, 197-204, doi:10.1007/s10029-019-02063-y.
 77. Klinge, U.; Klosterhalfen, B. Mesh implants for hernia repair: An update. *Expert Rev Med Devices* **2018**, *15*, 735-46, doi:10.1080/17434440.2018.1529565.
 78. Sarvari, R.; Naghili, B.; Agbolaghi, S.; Abbaspoor, S.; Bannazadeh Baghi, H.; et al. Organic/polymeric antibiofilm coatings for surface modification of medical devices. *Int J Polym Mater* **2022**, *72*, 867-908, doi:10.1080/00914037.2022.2066668.
 79. Shahid, A.; Aslam, B.; Muzammil, S.; Aslam, N.; Shahid, M.; et al. The prospects of antimicrobial coated medical implants. *J Appl Biomater* **2021**, *19*, 1-21, doi:10.1177/22808000211040304.
 80. Benčina, M.; Resnik, M.; Starič, P.; Junkar, I. Use of plasma technologies for antibacterial surface properties of metals. *Molecules* **2021**, *26*, 1418, doi:10.3390/molecules26051418.
 81. Mirel, S.; Pusta, A.; Moldovan, M.; Moldovan, S. Antimicrobial meshes for hernia repair: Current progress and perspectives. *J Clin Med* **2022**, *11*, 883, doi:10.3390/jcm11030883.
 82. Bohara, S.; Suthakorn, J. Surface coating of orthopedic implant to enhance the osseointegration and reduction of bacterial colonization: A review. *Biomater Res* **2022**, *26*, 26, doi:10.1186/s40824-022-00269-3.
 83. Ventola, C.L. The antibiotic resistance crisis: Part 1: Causes and threats. *Pharma Therap* **2015**, *40*, 277-83, PMID: 25859123.
 84. Beyer, P.; Paulin, S. The antibacterial research and development pipeline needs urgent solutions. *ACS Infect Dis* **2020**, *6*, 1289-91, doi:10.1021/acsinfecdis.0c00044.
 85. World Health Organization. *2021 Antibacterial agents in clinical and preclinical development: An overview and analysis*; WHO: Geneva, **2022**.
 86. Bulger, E.M.; May, A.K.; Robinson, B.R.H.; Evans, D.C.; Henry, S.; et al. A novel immune modulator for patients with necrotizing soft tissue infections (NSTI): Results of a multicenter, phase 3 randomized controlled trial of reltecimod (AB 103). *Ann Surg* **2020**, *272*, 469-78, doi:10.1097/sla.0000000000004102.
 87. DiNubile, M.J.; Parra, S.; Salomó, A.C.; Levinson, S.L. Adjunctive recombinant human plasma gelsolin for severe coronavirus disease 2019 pneumonia. *Open Forum Infect Dis* **2022**, *9*, ofac357, doi:10.1093/ofid/ofac357.
 88. Han, J.; Poma, A. Molecular targets for antibody-based anti-biofilm therapy in infective endocarditis. *Polymers (Basel)* **2022**, *14*, 3198, doi:10.3390/polym14153198.
 89. Raafat, D.; Otto, M.; Reppschläger, K.; Iqbal, J.; Holtfreter, S. Fighting *Staphylococcus aureus* Biofilms with Monoclonal Antibodies. *Trends Microbiol* **2019**, *27*, 303-22, doi:10.1016/j.tim.2018.12.009.
 90. Novotny, L.A.; Goodman, S.D.; Bakaletz, L.O. Targeting a bacterial DNABII protein with a chimeric peptide immunogen or humanised monoclonal antibody to prevent or treat recalcitrant biofilm-mediated infections. *EBioMedicine* **2020**, *59*, 102867, doi:10.1016/j.ebiom.2020.102867.

91. Schuch, R.; Khan, B.K.; Raz, A.; Rotolo, J.A.; Wittekind, M. Bacteriophage lysin CF-301, a potent antistaphylococcal biofilm agent. *Antimicrob Agents Chemother* **2017**, *61*, e02666-16, doi:10.1128/aac.02666-16.
92. Jun, S.Y.; Jung, G.M.; Yoon, S.J.; Oh, M.-D.; Choi, Y.-J.; et al. Antibacterial properties of a pre-formulated recombinant phage endolysin, SAL-1. *Int J Antimicrob Agents* **2013**, *41*, 156-61, doi:10.1016/j.ijantimicag.2012.10.011.
93. Ferry, T.; Kolenda, C.; Batailler, C.; Gustave, C.A.; Lustig, S.; et al. Phage therapy as adjuvant to conservative surgery and antibiotics to salvage patients with relapsing *S. aureus* prosthetic knee infection. *Front Med (Lausanne)* **2020**, *7*, 570572, doi:10.3389/fmed.2020.570572.
94. Kifelew, L.G.; Warner, M.S.; Morales, S.; Vaughan, L.; Woodman, R.; et al. Efficacy of phage cocktail AB-SA01 therapy in diabetic mouse wound infections caused by multidrug-resistant *Staphylococcus aureus*. *BMC Microbiol* **2020**, *20*, 204, doi:10.1186/s12866-020-01891-8.
95. Ooi, M.L.; Drilling, A.J.; Morales, S.; Fong, S.; Moraitis, S.; et al. Safety and tolerability of bacteriophage therapy for chronic rhinosinusitis due to *Staphylococcus aureus*. *JAMA Otolaryngol Head Neck Surg* **2019**, *145*, 723-9, doi:10.1001/jamaoto.2019.1191.
96. Zhu, F.C.; Zeng, H.; Li, J.X.; Wang, B.; Meng, F.Y.; et al. Evaluation of a recombinant five-antigen *Staphylococcus aureus* vaccine: The randomized, single-centre phase 1a/1b clinical trials. *Vaccine* **2022**, *40*, 3216-27, doi:10.1016/j.vaccine.2022.04.034.
97. Watson, A.; Maan, H.; Kolodkin-Gal, I.; Freund, N.T. Antibodies against biofilms: Mechanisms and applications. In *Antibiofilm Strategies: Current and Future Applications to Prevent, Control and Eradicate Biofilms*, Richter, K., Kragh, K.N., Eds.; Springer International Publishing: Cham, **2022**; pp. 263-98.
98. de Vor, L.; van Dijk, B.; van Kessel, K.; Kavanaugh, J.S.; de Haas, C.; et al. Human monoclonal antibodies against *Staphylococcus aureus* surface antigens recognize in vitro and in vivo biofilm. *Elife* **2022**, *11*, e67301, doi:10.7554/eLife.67301.
99. François, B.; Jafri, H.S.; Chastre, J.; Sánchez-García, M.; Eggimann, P.; et al. Efficacy and safety of suvatroxumab for prevention of *Staphylococcus aureus* ventilator-associated pneumonia (SAATELLITE): A multicentre, randomised, double-blind, placebo-controlled, parallel-group, phase 2 pilot trial. *Lancet Infect Dis* **2021**, *21*, 1313-23, doi:10.1016/s1473-3099(20)30995-6.
100. François, B.; Mercier, E.; Gonzalez, C.; Asehnoune, K.; Nseir, S.; et al. Safety and tolerability of a single administration of AR-301, a human monoclonal antibody, in ICU patients with severe pneumonia caused by *Staphylococcus aureus*: First-in-human trial. *Intensive Care Med* **2018**, *44*, 1787-96, doi:10.1007/s00134-018-5229-2.
101. Liao, S.; Lin, Y.; Liu, L.; Yang, S.; Lin, Y.; et al. ADAM10-a "multitasker" in sepsis: Focus on its posttranslational target. *Inflamm Res* **2022**, *72*, 395-423, doi:10.1007/s00011-022-01673-0.
102. Xiong, Y.Q.; Estellés, A.; Li, L.; Abdelhady, W.; Gonzales, R.; et al. A human biofilm-disrupting monoclonal antibody potentiates antibiotic efficacy in rodent models of both *Staphylococcus aureus* and *Acinetobacter baumannii* infections. *Antimicrob Agents Chemother* **2017**, *61*, e00904-17, doi:10.1128/aac.00904-17.
103. Estellés, A.; Woischnig, A.K.; Liu, K.; Stephenson, R.; Lomongsod, E.; et al. A high-affinity native human antibody disrupts biofilm from *Staphylococcus aureus* bacteria and potentiates antibiotic efficacy in a mouse implant infection model. *Antimicrob Agents Chemother* **2016**, *60*, 2292-301, doi:10.1128/aac.02588-15.
104. Cameron, D.R.; Valente, L.G.; Pitton, M.; Prazak, J.; Que, Y.-A. Bacteriophages for the Treatment of Biofilm-Associated Infections. In *Antibiofilm Strategies: Current and Future Applications to Prevent, Control and Eradicate Biofilms*, Richter, K., Kragh, K.N., Eds.; Springer International Publishing: Cham, **2022**; pp. 181-99.
105. Chang, C.; Yu, X.; Guo, W.; Guo, C.; Guo, X.; et al. Bacteriophage-mediated control of biofilm: A promising new dawn for the future. *Front Microbiol* **2022**, *13*, 825828, doi:10.3389/fmicb.2022.825828.
106. Plumet, L.; Ahmad-Mansour, N.; Dunyach-Remy, C.; Kissa, K.; Sotto, A.; et al. Bacteriophage therapy for *Staphylococcus aureus* infections: A review of animal models, treatments, and clinical trials. *Front Cell Infect Microbiol* **2022**, *12*, 907314, doi:10.3389/fcimb.2022.907314.

107. Morris, J.L.; Letson, H.L.; Elliott, L.; Grant, A.L.; Wilkinson, M.; et al. Evaluation of bacteriophage as an adjunct therapy for treatment of peri-prosthetic joint infection caused by *Staphylococcus aureus*. *PLoS One* **2019**, *14*, e0226574, doi:10.1371/journal.pone.0226574.
108. Ling, H.; Lou, X.; Luo, Q.; He, Z.; Sun, M.; et al. Recent advances in bacteriophage-based therapeutics: Insight into the post-antibiotic era. *Acta Pharmaceutica Sinica B* **2022**, *12*, 4348-64, doi:10.1016/j.apsb.2022.05.007.
109. Fowler, V.G., Jr.; Das, A.F.; Lipka-Diamond, J.; Schuch, R.; Pomerantz, R.; et al. Exebacase for patients with *Staphylococcus aureus* bloodstream infection and endocarditis. *J Clin Invest* **2020**, *130*, 3750-60, doi:10.1172/jci136577.
110. Ford, C.A.; Hurford, I.M.; Cassat, J.E. Antivirulence strategies for the treatment of *Staphylococcus aureus* infections: A mini review. *Front Microbiol* **2021**, *11*, 632706, doi:10.3389/fmicb.2020.632706.
111. Escajadillo, T.; Nizet, V. Pharmacological targeting of pore-forming toxins as adjunctive therapy for invasive bacterial infection. *Toxins (Basel)* **2018**, *10*, 542, doi:10.3390/toxins10120542.
112. Beavers, W.N.; Skaar, E.P. Neutrophil-generated oxidative stress and protein damage in *Staphylococcus aureus*. *Pathog Dis* **2016**, *74*, ftw060, doi:10.1093/femspd/ftw060.
113. Boero, E.; Cruz, A.R.; Pansegrau, W.; Giovani, C.; Rooijackers, S.H.M.; et al. Natural human immunity against staphylococcal protein A relies on effector functions triggered by IgG3. *Front Immunol* **2022**, *13*, 834711, doi:10.3389/fimmu.2022.834711.
114. Mahdally, N.H.; George, R.F.; Kashef, M.T.; Al-Ghobashy, M.; Murad, F.E.; et al. Staquorsin: A novel *Staphylococcus aureus* Agr-mediated quorum sensing inhibitor impairing virulence in vivo without notable resistance development. *Front Microbiol* **2021**, *12*, 700494, doi:10.3389/fmicb.2021.700494.
115. Mishra, R.; Panda, A.K.; De Mandal, S.; Shakeel, M.; Bisht, S.S.; et al. Natural anti-biofilm agents: Strategies to control biofilm-forming pathogens. *Front Microbiol* **2020**, *11*, 566325, doi:10.3389/fmicb.2020.566325.
116. Suzuki, M. Learning from nature: Naturally derived remedies. In *Antibiofilm Strategies: Current and Future Applications to Prevent, Control and Eradicate Biofilms*, Richter, K., Kragh, K.N., Eds.; Springer International Publishing: Cham, **2022**; pp. 325-50.
117. Memar, M.Y.; Saadat, Y.R.; Hejazian, S.M.; Ardalani, M.; Ahmadian, E.; et al. Probiotics action against biofilms. In *Antibiofilm Strategies: Current and Future Applications to Prevent, Control and Eradicate Biofilms*, Richter, K., Kragh, K.N., Eds.; Springer International Publishing: Cham, **2022**; pp. 99-125.
118. Bekiaridou, A.; Karlafti, E.; Oikonomou, I.M.; Ioannidis, A.; Papavramidis, T.S. Probiotics and their effect on surgical wound healing: A systematic review and new insights into the role of nanotechnology. *Nutrients* **2021**, *13*, 4265, doi:10.3390/nu13124265.
119. Hu, X.; Huang, Y.-Y.; Wang, Y.; Wang, X.; Hamblin, M.R. Antimicrobial photodynamic therapy to control clinically relevant biofilm infections. *Front Microbiol* **2018**, *9*, 1299, doi:10.3389/fmicb.2018.01299.
120. Martins Antunes de Melo, W.C.; Celiešiūtė-Germanienė, R.; Šimonis, P.; Stirkė, A. Antimicrobial photodynamic therapy (aPDT) for biofilm treatments. Possible synergy between aPDT and pulsed electric fields. *Virulence* **2021**, *12*, 2247-72, doi:10.1080/21505594.2021.1960105.
121. Parasuraman, P.; Anju, V.T.; Lal, S.B.S.; Sharan, A.; Busi, S.; et al. Synthesis and antimicrobial photodynamic effect of methylene blue conjugated carbon nanotubes on *E. coli* and *S. aureus*. *Photochem Photobiol Sci* **2019**, *18*, 563-76, doi:10.1039/c8pp00369f.
122. Buzzá, H.H.; Alves, F.; Tomé, A.J.B.; Chen, J.; Kassab, G.; et al. Porphyrin nanoemulsion for antimicrobial photodynamic therapy: Effective delivery to inactivate biofilm-related infections. *Proc Natl Acad Sci U S A* **2022**, *119*, e2216239119, doi:10.1073/pnas.2216239119.
123. Kirtane, A.R.; Verma, M.; Karandikar, P.; Furin, J.; Langer, R.; et al. Nanotechnology approaches for global infectious diseases. *Nat Nanotechnol* **2021**, *16*, 369-84, doi:10.1038/s41565-021-00866-8.

8 Bibliography

124. Pinto, R.M.; Lopes-de-Campos, D.; Martins, M.C.L.; Van Dijck, P.; Nunes, C.; et al. Impact of nanosystems in *Staphylococcus aureus* biofilms treatment. *FEMS Microbiol Rev* **2019**, *43*, 622-41, doi:10.1093/femsre/fuz021.
125. Facal Marina, P.; Kaul, L.; Mischer, N.; Richter, K. Metal-based nanoparticles for biofilm treatment and infection control: From basic research to clinical translation. In *Antibiofilm Strategies: Current and Future Applications to Prevent, Control and Eradicate Biofilms*, Richter, K., Kragh, K.N., Eds.; Springer International Publishing: Cham, **2022**; pp. 467-500.
126. Barbarossa, A.; Rosato, A.; Corbo, F.; Clodoveo, M.L.; Fracchiolla, G.; et al. Non-antibiotic drug repositioning as an alternative antimicrobial approach. *Antibiotics (Basel)* **2022**, *11*, 816, doi:10.3390/antibiotics11060816.
127. Pushpakom, S.; Iorio, F.; Eyers, P.A.; Escott, K.J.; Hopper, S.; et al. Drug repurposing: Progress, challenges and recommendations. *Nat Rev Drug Disc* **2018**, *18*, 41, doi:10.1038/nrd.2018.168.
128. Farha, M.A.; Brown, E.D. Drug repurposing for antimicrobial discovery. *Nat Microbiol* **2019**, *4*, 565-77, doi:10.1038/s41564-019-0357-1.
129. Boyd, N.K.; Teng, C.; Frei, C.R. Brief overview of approaches and challenges in new antibiotic development: A focus on drug repurposing. *Front Cell Infect Microbiol* **2021**, *11*, 684515, doi:10.3389/fcimb.2021.684515.
130. Paes Leme, R.C.; da Silva, R.B. Antimicrobial activity of non-steroidal anti-inflammatory drugs on biofilm: Current evidence and potential for drug repurposing. *Front Microbiol* **2021**, *12*, 707629, doi:10.3389/fmicb.2021.707629.
131. Abbas, H.A.; Atallah, H.; El-Sayed, M.A.; El-Ganiny, A.M. Diclofenac mitigates virulence of multidrug-resistant *Staphylococcus aureus*. *Arch Microbiol* **2020**, *202*, 2751-60, doi:10.1007/s00203-020-01992-y.
132. Hendrix, A.S.; Spoonmore, T.J.; Wilde, A.D.; Putnam, N.E.; Hammer, N.D.; et al. Repurposing the nonsteroidal anti-inflammatory drug diflunisal as an osteoprotective, antivirulence therapy for *Staphylococcus aureus* osteomyelitis. *Antimicrob Agents Chemother* **2016**, *60*, 5322-30, doi:10.1128/aac.00834-16.
133. Zhang, S.; Tang, H.; Wang, Y.; Nie, B.; Yang, H.; et al. Antibacterial and antibiofilm effects of flufenamic acid against methicillin-resistant *Staphylococcus aureus*. *Pharmacol Res* **2020**, *160*, 105067, doi:10.1016/j.phrs.2020.105067.
134. Thangamani, S.; Mohammad, H.; Abushahba, M.F.; Sobreira, T.J.; Seleem, M.N. Repurposing auranofin for the treatment of cutaneous staphylococcal infections. *Int J Antimicrob Agents* **2016**, *47*, 195-201, doi:10.1016/j.ijantimicag.2015.12.016.
135. She, P.; Li, S.; Zhou, L.; Luo, Z.; Liao, J.; et al. Insights into idarubicin antimicrobial activity against methicillin-resistant *Staphylococcus aureus*. *Virulence* **2020**, *11*, 636-51, doi:10.1080/21505594.2020.1770493.
136. Sedlmayer, F.; Woischnig, A.-K.; Unterreiner, V.; Fuchs, F.; Baeschlin, D.; et al. 5-Fluorouracil blocks quorum-sensing of biofilm-embedded methicillin-resistant *Staphylococcus aureus* in mice. *Nucleic Acids Res* **2021**, *49*, e73-e, doi:10.1093/nar/gkab251.
137. Yeo, W.-S.; Arya, R.; Kim, K.K.; Jeong, H.; Cho, K.H.; et al. The FDA-approved anti-cancer drugs, streptozotocin and floxuridine, reduce the virulence of *Staphylococcus aureus*. *Sci Rep* **2018**, *8*, 2521, doi:10.1038/s41598-018-20617-5.
138. Liu, Y.; She, P.; Xu, L.; Chen, L.; Li, Y.; et al. Antimicrobial, antibiofilm, and anti-persister activities of penfluridol against *Staphylococcus aureus*. *Front Microbiol* **2021**, *12*, 727692, doi:10.3389/fmicb.2021.727692.
139. Khayat, M.T.; Abbas, H.A.; Ibrahim, T.S.; Khayyat, A.N.; Alharbi, M.; et al. Anti-quorum sensing activities of gliptins against *Pseudomonas aeruginosa* and *Staphylococcus aureus*. *Biomedicines* **2022**, *10*, 1169, doi:10.3390/biomedicines10051169.
140. She, P.; Li, S.; Zhou, L.; Liu, Y.; Xu, L.; et al. Repurposing eltrombopag as an antimicrobial agent against methicillin-resistant *Staphylococcus aureus*. *Front Microbiol* **2021**, *12*, 790686, doi:10.3389/fmicb.2021.790686.

141. Xu, L.; She, P.; Chen, L.; Li, S.; Zhou, L.; et al. Repurposing candesartan cilexetil as antibacterial agent for MRSA infection. *Front Microbiol* **2021**, *12*, 688772, doi:10.3389/fmicb.2021.688772.
142. Sun, T.; Huang, J.; Zhang, W.; Zheng, X.; Wang, H.; et al. Simvastatin-hydroxyapatite coatings prevent biofilm formation and improve bone formation in implant-associated infections. *Bioact Mater* **2023**, *21*, 44-56, doi:10.1016/j.bioactmat.2022.07.028.
143. Zheng, J.; Shang, Y.; Wu, Y.; Zhao, Y.; Chen, Z.; et al. Loratadine inhibits *Staphylococcus aureus* virulence and biofilm formation. *iScience* **2022**, *25*, 103731, doi:10.1016/j.isci.2022.103731.
144. Li, Y.; She, P.; Xu, L.; Liu, Y.; Liu, S.; et al. Anti-hepatitis C virus drug simeprevir: A promising antimicrobial agent against MRSA. *Appl Microbiol Biotechnol* **2022**, *106*, 2689-702, doi:10.1007/s00253-022-11878-2.
145. Kaul, G.; Akhir, A.; Shukla, M.; Rawat, K.S.; Sharma, C.P.; et al. Nitazoxanide potentiates linezolid against linezolid-resistant *Staphylococcus aureus* in vitro and in vivo. *J Antimicrob Chemother* **2022**, *77*, 2456-60, doi:10.1093/jac/dkac201.
146. Mahey, N.; Tambat, R.; Chandal, N.; Verma, D.K.; Thakur, K.G.; et al. Repurposing approved drugs as fluoroquinolone potentiators to overcome efflux pump resistance in *Staphylococcus aureus*. *Microbiol Spectr* **2021**, *9*, e0095121, doi:10.1128/Spectrum.00951-21.
147. Weiss, A.; Delavenne, E.; Matias, C.; Lagler, H.; Simon, D.; et al. Topical niclosamide (ATx201) reduces *Staphylococcus aureus* colonization and increases Shannon diversity of the skin microbiome in atopic dermatitis patients in a randomized, double-blind, placebo-controlled Phase 2 trial. *Clin Transl Med* **2022**, *12*, e790, doi:10.1002/ctm2.790.
148. Thakare, R.; Shukla, M.; Kaul, G.; Dasgupta, A.; Chopra, S. Repurposing disulfiram for treatment of *Staphylococcus aureus* infections. *Int J Antimicrob Agents* **2019**, *53*, 709-15, doi:10.1016/j.ijantimicag.2019.03.024.
149. Torres, N.S.; Abercrombie, J.J.; Srinivasan, A.; Lopez-Ribot, J.L.; Ramasubramanian, A.K.; et al. Screening a commercial library of pharmacologically active small molecules against *Staphylococcus aureus* biofilms. *Antimicrob Agents Chemother* **2016**, *60*, 5663-72, doi:10.1128/aac.00377-16.
150. Rajamuthiah, R.; Fuchs, B.B.; Conery, A.L.; Kim, W.; Jayamani, E.; et al. Repurposing salicylanilide anthelmintic drugs to combat drug resistant *Staphylococcus aureus*. *PLoS One* **2015**, *10*, e0124595, doi:10.1371/journal.pone.0124595.
151. Leão, C.; Borges, A.; Simões, M. NSAIDs as a drug repurposing strategy for biofilm control. *Antibiotics (Basel)* **2020**, *9*, 591, doi:10.3390/antibiotics9090591.
152. Wei, Y.P.; Chien, J.C.; Hsiang, W.H.; Yang, S.W.; Chen, C.Y. Aspirin administration might accelerate the subsidence of periprosthetic joint infection. *Sci Rep* **2020**, *10*, 15967, doi:10.1038/s41598-020-72731-y.
153. Graziano, T.S.; Cuzzullin, M.C.; Franco, G.C.; Schwartz-Filho, H.O.; de Andrade, E.D.; et al. Statins and antimicrobial effects: Simvastatin as a potential drug against *Staphylococcus aureus* biofilm. *PLoS One* **2015**, *10*, e0128098, doi:10.1371/journal.pone.0128098.
154. Roder, C.; Thomson, M.J. Aurano-fin: Repurposing an old drug for a golden new age. *Drugs R D* **2015**, *15*, 13-20, doi:10.1007/s40268-015-0083-y.
155. Chen, H.; Yang, N.; Yu, L.; Li, J.; Zhang, H.; et al. Synergistic microbicidal effect of AUR and PEITC against *Staphylococcus aureus* skin infection. *Front Cell Infect Microbiol* **2022**, *12*, 927289, doi:10.3389/fcimb.2022.927289.
156. Kragh, H. From Disulfiram to Antabuse: The invention of a drug. *Bull Hist Chem* **2008**, *33*, 82-8.
157. Ellis, P.M.; Dronsfield, A.T. Antabuse's diamond anniversary: Still sparkling on? *Drug Alcohol Rev* **2013**, *32*, 342-4, doi:10.1111/dar.12018.
158. Wright, C.; Moore, R.D. Disulfiram treatment of alcoholism. *Am J Med* **1990**, *88*, 647-55, doi:10.1016/0002-9343(90)90534-K.

159. Yang, Q.; Yao, Y.; Li, K.; Jiao, L.; Zhu, J.; et al. An updated review of disulfiram: Molecular targets and strategies for cancer treatment. *Curr Pharm Des* **2019**, *25*, 3248-56, doi:10.2174/1381612825666190816233755.
160. Johansson, B. A review of the pharmacokinetics and pharmacodynamics of disulfiram and its metabolites. *Acta Psychiatr Scand* **1992**, *86*, 15-26, doi:10.1111/j.1600-0447.1992.tb03310.x.
161. Lee, S.A.; Elliott, J.H.; McMahon, J.; Hartogenesis, W.; Bumpus, N.N.; et al. Population pharmacokinetics and pharmacodynamics of disulfiram on inducing latent HIV-1 transcription in a phase IIb trial. *Clin Pharm Therap* **2019**, *105*, 692-702, doi:10.1002/cpt.1220.
162. Kannappan, V.; Ali, M.; Small, B.; Rajendran, G.; Elzhenni, S.; et al. Recent advances in repurposing disulfiram and disulfiram derivatives as copper-dependent anticancer agents. *Front Mol Biosci* **2021**, *8*, 741316, doi:10.3389/fmolb.2021.741316.
163. Petersen, E.N. The pharmacology and toxicology of disulfiram and its metabolites. *Acta Psychiatr Scand Suppl* **1992**, *369*, 7-13, doi:10.1111/j.1600-0447.1992.tb03309.x.
164. Butcher, K.; Kannappan, V.; Kilari, R.S.; Morris, M.R.; McConville, C.; et al. Investigation of the key chemical structures involved in the anticancer activity of disulfiram in A549 non-small cell lung cancer cell line. *BMC Cancer* **2018**, *18*, 753, doi:10.1186/s12885-018-4617-x.
165. Skrott, Z.; Cvek, B. Diethyldithiocarbamate complex with copper: The mechanism of action in cancer cells. *Mini Rev Med Chem* **2012**, *12*, 1184-92, doi:10.2174/138955712802762068.
166. Kaul, L.; Süß, R.; Zannettino, A.; Richter, K. The revival of dithiocarbamates: From pesticides to innovative medical treatments. *iScience* **2021**, *24*, 102092, doi:10.1016/j.isci.2021.102092.
167. Tawari, P.E.; Wang, Z.; Najlah, M.; Tsang, C.W.; Kannappan, V.; et al. The cytotoxic mechanisms of disulfiram and copper(ii) in cancer cells. *Toxicol Res (Camb)* **2015**, *4*, 1439-42, doi:10.1039/c5tx00210a.
168. Allensworth, J.L.; Evans, M.K.; Bertucci, F.; Aldrich, A.J.; Festa, R.A.; et al. Disulfiram (DSF) acts as a copper ionophore to induce copper-dependent oxidative stress and mediate anti-tumor efficacy in inflammatory breast cancer. *Mol Oncol* **2015**, *9*, 1155-68, doi:10.1016/j.molonc.2015.02.007.
169. Wiggins, H.L.; Wymant, J.M.; Solfa, F.; Hiscox, S.E.; Taylor, K.M.; et al. Disulfiram-induced cytotoxicity and endo-lysosomal sequestration of zinc in breast cancer cells. *Biochem Pharmacol* **2015**, *93*, 332-42, doi:10.1016/j.bcp.2014.12.014.
170. Custodio, M.M.; Sparks, J.; Long, T.E. Disulfiram: A repurposed drug in preclinical and clinical development for the treatment of infectious diseases. *Antiinfect Agents* **2022**, *20*, e040122199856, doi:10.2174/2211352520666220104104747.
171. Meneguello, J.E.; Murase, L.S.; de Souza, J.V.P.; de Oliveira, C.G.; Ghiraldi-Lopes, L.D.; et al. Systematic review of disulfiram as an antibacterial agent: What is the evidence? *Int J Antimicrob Agents* **2022**, *59*, 106578, doi:10.1016/j.ijantimicag.2022.106578.
172. Shirley, D.-A.; Sharma, I.; Warren, C.A.; Moonah, S. Drug repurposing of the alcohol abuse medication disulfiram as an anti-parasitic agent. *Front Cell Infect Microbiol* **2021**, *11*, 633194, doi:10.3389/fcimb.2021.633194.
173. Lajarin-Reinares, M.; Martinez-Esteve, E.; Pena-Rodríguez, E.; Cañellas-Santos, M.; Bulut, S.; et al. The efficacy and biopharmaceutical properties of a fixed-dose combination of disulfiram and benzyl benzoate. *Int J Mol Sci* **2022**, *23*, 10969, doi:10.3390/ijms231810969.
174. Rennar, G.A.; Gallinger, T.L.; Mäder, P.; Lange-Grünweller, K.; Haeberlein, S.; et al. Disulfiram and dithiocarbamate analogues demonstrate promising antischistosomal effects. *Eur J Med Chem* **2022**, *242*, 114641, doi:10.1016/j.ejmech.2022.114641.
175. Argüello-García, R.; Ortega-Pierres, M.G. *Giardia duodenalis* virulence - "To be, or not to be". *Curr Trop Med Rep* **2021**, *8*, 246-56, doi:10.1007/s40475-021-00248-z.
176. Almeida-Silva, J.; Menezes, D.S.; Fernandes, J.M.P.; Almeida, M.C.; Vasco-Dos-Santos, D.R.; et al. The repositioned drugs disulfiram/diethyldithiocarbamate combined to benznidazole: Searching for Chagas disease selective therapy, preventing toxicity and drug resistance. *Front Cell Infect Microbiol* **2022**, *12*, 926699, doi:10.3389/fcimb.2022.926699.

177. Khouri, R.; Novais, F.; Santana, G.; de Oliveira, C.I.; Vannier dos Santos, M.A.; et al. DETC induces leishmania parasite killing in human in vitro and murine in vivo models: A promising therapeutic alternative in leishmaniasis. *PLoS One* **2010**, *5*, e14394, doi:10.1371/journal.pone.0014394.
178. Deharo, E.; Barkan, D.; Krugliak, M.; Golenser, J.; Ginsburg, H. Potentiation of the antimalarial action of chloroquine in rodent malaria by drugs known to reduce cellular glutathione levels. *Biochem Pharmacol* **2003**, *66*, 809-17, doi:10.1016/s0006-2952(03)00396-4.
179. Huang, X.; Sun, P.; Qin, Y.; Wang, X.J.; Wang, M.; et al. Disulfiram attenuates MCMV-Induced pneumonia by inhibition of NF- κ B/NLRP3 signaling pathway in immunocompromised mice. *Int Immunopharmacol* **2022**, *103*, 108453, doi:10.1016/j.intimp.2021.108453.
180. Lin, M.H.; Moses, D.C.; Hsieh, C.H.; Cheng, S.C.; Chen, Y.H.; et al. Disulfiram can inhibit MERS and SARS coronavirus papain-like proteases via different modes. *Antiviral Res* **2018**, *150*, 155-63, doi:10.1016/j.antiviral.2017.12.015.
181. Fillmore, N.; Bell, S.; Shen, C.; Nguyen, V.; La, J.; et al. Disulfiram use is associated with lower risk of COVID-19: A retrospective cohort study. *PLoS One* **2021**, *16*, e0259061, doi:10.1371/journal.pone.0259061.
182. Spivak, A.M.; Planelles, V. Novel latency reversal agents for HIV-1 cure. *Annu Rev Med* **2018**, *69*, 421-36, doi:10.1146/annurev-med-052716-031710.
183. Spivak, A.M.; Andrade, A.; Eisele, E.; Hoh, R.; Bacchetti, P.; et al. A pilot study assessing the safety and latency-reversing activity of disulfiram in HIV-1-infected adults on antiretroviral therapy. *Clin Infect Dis* **2013**, *58*, 883-90, doi:10.1093/cid/cit813.
184. Elliott, J.H.; McMahon, J.H.; Chang, C.C.; Lee, S.A.; Hartogensis, W.; et al. Short-term administration of disulfiram for reversal of latent HIV infection: A phase 2 dose-escalation study. *Lancet HIV* **2015**, *2*, e520-e9, doi:10.1016/S2352-3018(15)00226-X.
185. Knights, H.D.J. A critical review of the evidence concerning the HIV latency reversing effect of disulfiram, the possible explanations for its inability to reduce the size of the latent reservoir in vivo, and the caveats associated with its use in practice. *AIDS Res Treat* **2017**, *2017*, 8239428, doi:10.1155/2017/8239428.
186. McMahon, J.H.; Evans, V.A.; Lau, J.S.Y.; Symons, J.; Zerbato, J.M.; et al. Neurotoxicity with high-dose disulfiram and vorinostat used for HIV latency reversal. *AIDS* **2022**, *36*, 75-82, doi:10.1097/qad.0000000000003091.
187. López-Huertas, M.R.; Jiménez-Tormo, L.; Madrid-Elena, N.; Gutiérrez, C.; Vivancos, M.J.; et al. Maraviroc reactivates HIV with potency similar to that of other latency reversing drugs without inducing toxicity in CD8 T cells. *Biochem Pharmacol* **2020**, *182*, 114231, doi:10.1016/j.bcp.2020.114231.
188. Khan, S.; Singhal, S.; Mathur, T.; Upadhyay, D.J.; Rattan, A. Antifungal potential of disulfiram. *Med Mycol J* **2007**, *48*, 109-13, doi:10.3314/jjmm.48.109.
189. Krajaejun, T.; Lohnoo, T.; Yingyong, W.; Rujirawat, T.; Kumsang, Y.; et al. The repurposed drug disulfiram inhibits urease and aldehyde dehydrogenase and prevents in vitro growth of the oomycete *pythium insidiosum*. *Antimicrob Agents Chemother* **2019**, *63*, e00609-19, doi:10.1128/AAC.00609-19.
190. Harrison, J.J.; Turner, R.J.; Ceri, H. A subpopulation of *Candida albicans* and *Candida tropicalis* biofilm cells are highly tolerant to chelating agents. *FEMS Microbiol Lett* **2007**, *272*, 172-81, doi:10.1111/j.1574-6968.2007.00745.x.
191. Hao, W.; Qiao, D.; Han, Y.; Du, N.; Li, X.; et al. Identification of disulfiram as a potential antifungal drug by screening small molecular libraries. *J Infect Chemother* **2021**, *27*, 696-701, doi:10.1016/j.jiac.2020.12.012.
192. De Brucker, K.; Bink, A.; Meert, E.; Cammue, B.P.; Thevissen, K. Potentiation of antibiofilm activity of amphotericin B by superoxide dismutase inhibition. *Oxid Med Cell Longev* **2013**, *2013*, 704654, doi:10.1155/2013/704654.
193. Yan, H.; Yang, H.; Wang, L.; Sun, X.; Han, L.; et al. Disulfiram inhibits IL-1 β secretion and inflammatory cells recruitment in *Aspergillus fumigatus* keratitis. *Int Immunopharmacol* **2022**, *102*, 108401, doi:10.1016/j.intimp.2021.108401.

8 Bibliography

194. Taylor, E.H.; Walker, E.; Bartelt, M.; Day, S.; Pappas, A. In vitro antimicrobial activity of diethyldithiocarbamate and dimethyldithiocarbamate against methicillin-resistant Staphylococcus. *Ann Clin Lab Sci* **1987**, *17*, 171-7.
195. Phillips, M.; G., M.; Nedunchezian, D.; Lukrec, A.; Howard, R.G. Disulfiram inhibits the in vitro growth of methicillin-Resistant Staphylococcus aureus. *Antimicrob Agents Chemother* **1991**, *35*, 785-7, doi:10.1128/AAC.35.4.785.
196. Frazier, K.R.; Moore, J.A.; Long, T.E. Antibacterial activity of disulfiram and its metabolites. *J Appl Microbiol* **2019**, *126*, 79-86, doi:10.1111/jam.14094.
197. Sheppard, J.G.; Frazier, K.R.; Saralkar, P.; Hossain, M.F.; Geldenhuys, W.J.; et al. Disulfiram-based disulfides as narrow-spectrum antibacterial agents. *Bioorganic Med Chem Lett* **2018**, *28*, 1298-302, doi:10.1016/j.bmcl.2018.03.023.
198. Long, T.E. Repurposing thiram and disulfiram as antibacterial agents for multidrug-resistant Staphylococcus aureus infections. *Antimicrob Agents Chemother* **2017**, *61*, e00898-17, doi:10.1128/aac.00898-17.
199. Chavva, H.; Meka, Y.; Long, T.E. Antimicrobial pharmacodynamics of vancomycin and disulfiram (Antabuse®) in Staphylococcus aureus. *Front Microbiol* **2022**, *13*, 1092257, doi:10.3389/fmicb.2022.1092257.
200. Peng, Y.; Wang, X.; Wang, H.; Xu, W.; Wu, K.; et al. Interleukin-4 protects mice against lethal influenza and Streptococcus pneumoniae co-infected pneumonia. *Clin Exp Immunol* **2021**, *205*, 379-90, doi:10.1111/cei.13628.
201. Serafin, M.B.; Foletto, V.S.; da Rosa, T.F.; Bottega, A.; Viana, A.R.; et al. Repositioning of disulfiram in association with vancomycin against Enterococcus spp. MDR and XDR. *Curr Microbiol* **2022**, *79*, 137, doi:10.1007/s00284-022-02794-9.
202. Lewis, A.D.; Riedel, T.M.; Kesler, M.B.A.; Varney, M.E.; Long, T.E. Pharmacological evaluation of disulfiram analogs as antimicrobial agents and their application as inhibitors of fosB-mediated fosfomycin resistance. *J Antibiot (Tokyo)* **2022**, *75*, 146-54, doi:10.1038/s41429-022-00500-2.
203. Liu, F.; Yu, J.; Zhang, Y.X.; Li, F.; Liu, Q.; et al. High-throughput tandem-microwell assay for ammonia repositions FDA-Approved drugs to inhibit Helicobacter pylori urease. *FASEB J* **2021**, *35*, e21967, doi:10.1096/fj.202100465RR.
204. Huang, W.; Zhang, J.; Liu, S.; Hu, C.; Zhang, M.; et al. Disulfiram enhances the activity of polymyxin B against Klebsiella pneumoniae by inhibiting lipid a modification. *Infect Drug Resist* **2022**, *15*, 295-306, doi:10.2147/idr.S342641.
205. Dubey, V.; Devnath, K.; Gupta, V.K.; Kalyan, G.; Singh, M.; et al. Disulfiram enhances meropenem activity against NDM- and IMP-producing carbapenem-resistant Acinetobacter baumannii infections. *J Antimicrob Chemother* **2022**, *77*, 1313-23, doi:10.1093/jac/dkac057.
206. Zhang, K.; Yang, X.; Yang, J.; Qiao, X.; Li, F.; et al. Alcohol dehydrogenase modulates quorum sensing in biofilm formations of Acinetobacter baumannii. *Microb Pathog* **2020**, *148*, 104451, doi:10.1016/j.micpath.2020.104451.
207. Pothineni, V.R.; Wagh, D.; Babar, M.M.; Inayathullah, M.; Solow-Cordero, D.; et al. Identification of new drug candidates against Borrelia burgdorferi using high-throughput screening. *Drug Des Devel Ther* **2016**, *10*, 1307-22, doi:10.2147/dddt.S101486.
208. Alvarez-Manzo, H.S.; Zhang, Y.; Shi, W.; Zhang, Y. Evaluation of disulfiram drug combinations and identification of other more effective combinations against stationary phase Borrelia burgdorferi. *Antibiotics (Basel)* **2020**, *9*, 542, doi:10.3390/antibiotics9090542.
209. Liegner, K.B. Disulfiram (tetraethylthiuram disulfide) in the treatment of lyme disease and babesiosis: Report of experience in three cases. *Antibiotics (Basel)* **2019**, *8*, 72, doi:10.3390/antibiotics8020072.
210. Younger, D.; Murphy, B. Antabuse for lyme disease: The way forward. *World J Neurosci* **2020**, *10*, 1-7, doi:10.4236/wjns.2020.101001.

211. Hamblin, K.A.; Flick-Smith, H.; Barnes, K.B.; Pereira-Leal, J.B.; Surkont, J.; et al. Disulfiram, an alcohol dependence therapy, can inhibit the in vitro growth of *Francisella tularensis*. *Int J Antimicrob Agents* **2019**, *54*, 85-8, doi:10.1016/j.ijantimicag.2019.04.002.
212. Nishimori, I.; Vullo, D.; Minakuchi, T.; Scozzafava, A.; Osman, S.M.; et al. Anion inhibition studies of two new β -carbonic anhydrases from the bacterial pathogen *Legionella pneumophila*. *Bioorganic Med Chem Lett* **2014**, *24*, 1127-32, doi:10.1016/j.bmcl.2013.12.124.
213. Nocentini, A.; Hewitt, C.S.; Mastrolorenzo, M.D.; Flaherty, D.P.; Supuran, C.T. Anion inhibition studies of the α -carbonic anhydrases from *Neisseria gonorrhoeae*. *J Enzyme Inhib Med Chem* **2021**, *36*, 1061-6, doi:10.1080/14756366.2021.1929202.
214. Urbanski, L.J.; Vullo, D.; Parkkila, S.; Supuran, C.T. An anion and small molecule inhibition study of the β -carbonic anhydrase from *Staphylococcus aureus*. *J Enzyme Inhib Med Chem* **2021**, *36*, 1088-92, doi:10.1080/14756366.2021.1931863.
215. Del Prete, S.; De Luca, V.; Nocentini, A.; Scaloni, A.; Mastrolorenzo, M.D.; et al. Anion inhibition studies of the beta-carbonic anhydrase from *Escherichia coli*. *Molecules* **2020**, *25*, 2564, doi:10.3390/molecules25112564.
216. Byrne, S.T.; Gu, P.; Zhou, J.; Denkin, S.M.; Chong, C.; et al. Pyrrolidine dithiocarbamate and diethyldithiocarbamate are active against growing and nongrowing persister *Mycobacterium tuberculosis*. *Antimicrob Agents Chemother* **2007**, *51*, 4495-7, doi:10.1128/AAC.00753-07.
217. Das, S.; Garg, T.; Chopra, S.; Dasgupta, A. Repurposing disulfiram to target infections caused by non-tuberculous mycobacteria. *J Antimicrob Chemother* **2019**, *74*, 1317-22, doi:10.1093/jac/dkz018.
218. Winters, C.G.; Basnet, R.M.; Faasualalie, P.E.; Shallom, S.J.; Zelazny, A.M.; et al. Disulfiram is effective against drug-resistant *Mycobacterium abscessus* in a zebrafish embryo infection model. *Antimicrob Agents Chemother* **2022**, *66*, e0053922, doi:10.1128/aac.00539-22.
219. Capasso, C.; Supuran, C.T. Inhibition of bacterial carbonic anhydrases as a novel approach to escape drug resistance. *Curr Top Med Chem* **2017**, *17*, 1237-48, doi:10.2174/1568026617666170104101058.
220. Li, Y.; Fu, S.Y.; Wang, L.H.; Wang, F.Y.; Wang, N.N.; et al. Copper improves the anti-angiogenic activity of disulfiram through the EGFR/Src/VEGF pathway in gliomas. *Cancer Lett* **2015**, *369*, 86-96, doi:10.1016/j.canlet.2015.07.029.
221. Dalecki, A.G.; Haeili, M.; Shah, S.; Speer, A.; Niederweis, M.; et al. Disulfiram and copper ions kill *Mycobacterium tuberculosis* in a synergistic manner. *Antimicrob Agents Chemother* **2015**, *59*, 4835-44, doi:10.1128/AAC.00692-15.
222. Menghani, S.V.; Rivera, A.; Neubert, M.; Hagerty, J.R.; Lewis, L.; et al. Demonstration of N,N-dimethyldithiocarbamate as a copper-dependent antibiotic against multiple upper respiratory tract pathogens. *Microbiol Spectr* **2021**, e0077821, doi:10.1128/Spectrum.00778-21.
223. Wehbe, M.; Anantha, M.; Backstrom, I.; Leung, A.; Chen, K.; et al. Nanoscale reaction vessels designed for synthesis of copper-drug complexes suitable for preclinical development. *PLoS One* **2016**, *11*, e0153416-e, doi:10.1371/journal.pone.0153416.
224. Totten, A.H.; Crawford, C.L.; Dalecki, A.G.; Xiao, L.; Wolschendorf, F.; et al. Differential susceptibility of mycoplasma and ureaplasma species to compound-enhanced copper toxicity. *Front Microbiol* **2019**, *10*, 1720, doi:10.3389/fmicb.2019.01720.
225. Saputo, S.; Faustoferri, R.C.; Quivey, R.G., Jr. A drug repositioning approach reveals that *Streptococcus mutans* is susceptible to a diverse range of established antimicrobials and nonantibiotics. *Antimicrob Agents Chemother* **2018**, *62*, e01674-17, doi:10.1128/aac.01674-17.
226. Haeili, M.; Moore, C.; Davis, C.J.; Cochran, J.B.; Shah, S.; et al. Copper complexation screen reveals compounds with potent antibiotic properties against methicillin-resistant *Staphylococcus aureus*. *Antimicrob Agents Chemother* **2014**, *58*, 3727-36, doi:10.1128/aac.02316-13.
227. Etheridge, M.L.; Campbell, S.A.; Erdman, A.G.; Haynes, C.L.; Wolf, S.M.; et al. The big picture on nanomedicine: The state of investigational and approved nanomedicine products. *Nanomedicine* **2013**, *9*, 1-14, doi:10.1016/j.nano.2012.05.013.

228. Hartwig, F.; Köll-Weber, M.; Süß, R. Preclinical in vitro studies with 3D spheroids to evaluate Cu(DDC)₂ containing liposomes for the treatment of neuroblastoma. *Pharmaceutics* **2021**, *13*, 894, doi:10.3390/pharmaceutics13060894
229. Zhao, L.; Wang, X.; Jiang, M.; Wu, X.; Zhang, M.; et al. A nanosystem of copper(II)-disulfiram for cancer treatment with high efficacy and few side effects. *Front Mater Sci* **2021**, *15*, 553-66, doi:10.1007/s11706-021-0576-2.
230. Ren, L.; Feng, W.; Shao, J.; Ma, J.; Xu, M.; et al. Diethyldithiocarbamate-copper nanocomplex reinforces disulfiram chemotherapeutic efficacy through light-triggered nuclear targeting. *Theranostics* **2020**, *10*, 6384-98, doi:10.7150/thno.45558.
231. Wu, P.Y.; Shen, Z.C.; Jiang, J.L.; Zhang, B.C.; Zhang, W.Z.; et al. A multifunctional theranostics nanosystem featuring self-assembly of alcohol-abuse drug and photosensitizers for synergistic cancer therapy. *Biomater Sci* **2022**, *10*, 6267-81, doi:10.1039/d2bm00803c.
232. Pereira, A.M.; Kaya, A.; Alves, D.; Ansari-Fard, N.; Tolaymat, I.; et al. Preparation and characterization of disulfiram and beta cyclodextrin inclusion complexes for potential application in the treatment of SARS-CoV-2 via nebulization. *Molecules* **2022**, *27*, 5600, doi:10.3390/molecules27175600.
233. Rolle, F.; Bincoletto, V.; Gazzano, E.; Rolando, B.; Lollo, G.; et al. Coencapsulation of disulfiram and doxorubicin in liposomes strongly reverses multidrug resistance in breast cancer cells. *Int J Pharm* **2020**, *580*, 119191, doi:10.1016/j.ijpharm.2020.119191.
234. Miao, L.; Su, J.; Zhuo, X.; Luo, L.; Kong, Y.; et al. mPEG_{5k}- b-PLGA_{2k}/PCL_{3.4k}/MCT mixed micelles as carriers of disulfiram for improving plasma stability and antitumor effect in vivo. *Mol Pharm* **2018**, *15*, 1556-64, doi:10.1021/acs.molpharmaceut.7b01094.
235. Mohammad, I.S.; Teng, C.; Chaurasiya, B.; Yin, L.; Wu, C.; et al. Drug-delivering-drug approach-based codelivery of paclitaxel and disulfiram for treating multidrug-resistant cancer. *Int J Pharm* **2019**, *557*, 304-13, doi:10.1016/j.ijpharm.2018.12.067.
236. Liu, P.; Wang, Z.; Brown, S.; Kannappan, V.; Tawari, P.E.; et al. Liposome encapsulated disulfiram inhibits NFκB pathway and targets breast cancer stem cells in vitro and in vivo. *Oncotarget* **2014**, *5*, 7471-85, doi:10.18632/oncotarget.2166.
237. Najlah, M.; Said Suliman, A.; Tolaymat, I.; Kurusamy, S.; Kannappan, V.; et al. Development of injectable PEGylated liposome encapsulating disulfiram for colorectal cancer treatment. *Pharmaceutics* **2019**, *11*, 610, doi:10.3390/pharmaceutics11110610.
238. Solak, K.; Mavi, A.; Yilmaz, B. Disulfiram-loaded functionalized magnetic nanoparticles combined with copper and sodium nitroprusside in breast cancer cells. *Mater Sci Eng C* **2021**, *119*, 111452, doi:10.1016/j.msec.2020.111452.
239. Zhang, L.; Tian, B.; Li, Y.; Lei, T.; Meng, J.; et al. A copper-mediated disulfiram-loaded pH-triggered PEG-shedding TAT peptide-modified lipid nanocapsules for use in tumor therapy. *ACS Appl Mater Interfaces* **2015**, *7*, 25147-61, doi:10.1021/acsami.5b06488.
240. Wang, Z.; Tan, J.; McConville, C.; Kannappan, V.; Tawari, P.E.; et al. Poly lactic-co-glycolic acid controlled delivery of disulfiram to target liver cancer stem-like cells. *Nanomedicine* **2017**, *13*, 641-57, doi:10.1016/j.nano.2016.08.001.
241. Kang, X.; Cai, Y.; Wang, Q.; Wang, C.; Chen, W.; et al. Near-infrared light triggered activation of pro-drug combination cancer therapy and induction of immunogenic cell death. *Int J Pharm* **2021**, *607*, 120972, doi:10.1016/j.ijpharm.2021.120972.
242. Zhou, L.; Yang, L.; Yang, C.; Liu, Y.; Chen, Q.; et al. Membrane loaded copper oleate PEGylated liposome combined with disulfiram for improving synergistic antitumor effect in vivo. *Pharm Res* **2018**, *35*, 147, doi:10.1007/s11095-018-2414-5.
243. He, H.; Markoutsas, E.; Li, J.; Xu, P. Repurposing disulfiram for cancer therapy via targeted nanotechnology through enhanced tumor mass penetration and disassembly. *Acta Biomater* **2018**, *68*, 113-24, doi:10.1016/j.actbio.2017.12.023.
244. Tang, H.X.; Liu, C.G.; Zhang, J.T.; Zheng, X.; Yang, D.Y.; et al. Biodegradable quantum composites for synergistic photothermal therapy and copper-enhanced chemotherapy. *ACS Appl Mater Interfaces* **2020**, *12*, 47289-98, doi:10.1021/acsami.0c14636.

245. Jiapaer, Z.; Zhang, L.; Ma, W.; Liu, H.; Li, C.; et al. Disulfiram-loaded hollow copper sulfide nanoparticles show anti-tumor effects in preclinical models of colorectal cancer. *Biochem Biophys Res Commun* **2022**, *635*, 291-8, doi:10.1016/j.bbrc.2022.10.027.
246. Lan, Q.H.; Du, C.C.; Yu, R.J.; Zhai, J.; Shi, Y.; et al. Disulfiram-loaded copper sulfide nanoparticles for potential anti-glioma therapy. *Int J Pharm* **2021**, *607*, 120978, doi:10.1016/j.ijpharm.2021.120978.
247. Abu-Serie, M.M.; Eltarahony, M. Novel nanoformulated diethyldithiocarbamate complexes with biosynthesized or green chemosynthesized copper oxide nanoparticles: An in vitro comparative anticancer study. *Int J Pharm* **2021**, *609*, 121149, doi:10.1016/j.ijpharm.2021.121149.
248. Kang, X.; Wang, J.; Huang, C.H.; Wibowo, F.S.; Amin, R.; et al. Diethyldithiocarbamate copper nanoparticle overcomes resistance in cancer therapy without inhibiting P-glycoprotein. *Nanomedicine* **2023**, *47*, 102620, doi:10.1016/j.nano.2022.102620.
249. Chen, W.; Yang, W.; Chen, P.; Huang, Y.; Li, F. Disulfiram copper nanoparticles prepared with a stabilized metal ion ligand complex method for treating drug-resistant prostate cancers. *ACS Appl Mater Interfaces* **2018**, *10*, 41118-28, doi:10.1021/acsami.8b14940.
250. Meng, Z.; Wang, H.; Fang, X.; Liu, Z.; Yang, Z.; et al. Surface decoration via physical interaction of cupric diethyldithiocarbamate nanocrystals and its impact on biodistribution and tumor targeting. *ACS Appl Mater Interfaces* **2021**, *13*, 36894-908, doi:10.1021/acsami.1c09346.
251. Peng, Y.; Liu, P.; Meng, Y.; Hu, S.; Ding, J.; et al. Nanoscale copper(II)-diethyldithiocarbamate coordination polymer as a drug self-delivery system for highly robust and specific cancer therapy. *Mol Pharm* **2020**, *17*, 2864-73, doi:10.1021/acs.molpharmaceut.0c00284.
252. Peng, X.; Pan, Q.; Zhang, B.; Wan, S.; Li, S.; et al. Highly stable, coordinated polymeric nanoparticles loading copper(II) diethyldithiocarbamate for combinational chemo/chemodynamic therapy of cancer. *Biomacromolecules* **2019**, *20*, 2372-83, doi:10.1021/acs.biomac.9b00367.
253. Lu, Y.; Pan, Q.; Gao, W.; Pu, Y.; He, B. Reversal of cisplatin chemotherapy resistance by glutathione-resistant copper-based nanomedicine via cuproptosis. *J Mater Chem B* **2022**, *10*, 6296-306, doi:10.1039/d2tb01150f.
254. Li, X.; Du, K.; Sun, J.; Feng, F. Apoferritin as a carrier of Cu(II) diethyldithiocarbamate and biomedical application for glutathione-responsive combination chemotherapy. *ACS Appl Bio Mater* **2020**, *3*, 654-63, doi:10.1021/acsabm.9b01014.
255. Said Suliman, A.; Khoder, M.; Tolaymat, I.; Webster, M.; Alany, R.G.; et al. Cyclodextrin diethyldithiocarbamate copper II inclusion complexes: A promising chemotherapeutic delivery system against chemoresistant triple negative breast cancer cell lines. *Pharmaceutics* **2021**, *13*, 84, doi:10.3390/pharmaceutics13010084.
256. Wu, W.; Yu, L.; Pu, Y.; Yao, H.; Chen, Y.; et al. Copper-enriched Prussian blue nanomedicine for in situ disulfiram toxification and photothermal antitumor amplification. *Adv Mater* **2020**, *32*, 2000542, doi:10.1002/adma.202000542.
257. Shi, H.; Suo, Y.; Zhang, Z.; Liu, R.; Liu, H.; et al. Copper(II)-disulfiram loaded melanin-dots for cancer theranostics. *Nanomedicine* **2021**, *32*, 102340, doi:10.1016/j.nano.2020.102340.
258. Zhang, H.; Song, F.; Dong, C.; Yu, L.; Chang, C.; et al. Co-delivery of nanoparticle and molecular drug by hollow mesoporous organosilica for tumor-activated and photothermal-augmented chemotherapy of breast cancer. *J Nanobiotechnology* **2021**, *19*, 290, doi:10.1186/s12951-021-01025-w.
259. Xu, Y.; Kong, Y.; Xu, J.; Li, X.; Gou, J.; et al. Doxorubicin intercalated copper diethyldithiocarbamate functionalized layered double hydroxide hybrid nanoparticles for targeted therapy of hepatocellular carcinoma. *Biomater Sci* **2020**, *8*, 897-911, doi:10.1039/c9bm01394f.
260. Hou, L.; Liu, Y.; Liu, W.; Balash, M.; Zhang, H.; et al. In situ triggering antitumor efficacy of alcohol-abuse drug disulfiram through Cu-based metal-organic framework nanoparticles. *Acta Pharm Sin B* **2021**, *11*, 2016-30, doi:10.1016/j.apsb.2021.01.013.

8 Bibliography

261. Zhao, L.; Wang, X.; Lou, H.; Jiang, M.; Wu, X.; et al. Buffet-style Cu(II) for enhance disulfiram-based cancer therapy. *J Colloid Interface Sci* **2022**, *624*, 734-46, doi:10.1016/j.jcis.2022.06.009.
262. Bozzuto, G.; Molinari, A. Liposomes as nanomedical devices. *Int J Nanomedicine* **2015**, *10*, 975-99, doi:10.2147/ijn.S68861.
263. Marengo, A.; Forciniti, S.; Dando, I.; Dalla Pozza, E.; Stella, B.; et al. Pancreatic cancer stem cell proliferation is strongly inhibited by diethyldithiocarbamate-copper complex loaded into hyaluronic acid decorated liposomes. *Biochim Biophys Acta Gen Subj* **2019**, *1863*, 61-72, doi:10.1016/j.bbagen.2018.09.018.
264. Nsairat, H.; Khater, D.; Sayed, U.; Odeh, F.; Al Bawab, A.; et al. Liposomes: Structure, composition, types, and clinical applications. *Heliyon* **2022**, *8*, e09394, doi:10.1016/j.heliyon.2022.e09394.
265. Ernsting, M.J.; Murakami, M.; Roy, A.; Li, S.D. Factors controlling the pharmacokinetics, biodistribution and intratumoral penetration of nanoparticles. *J Control Release* **2013**, *172*, 782-94, doi:10.1016/j.jconrel.2013.09.013.
266. Danaei, M.; Dehghankhold, M.; Ataei, S.; Hasanzadeh Davarani, F.; Javanmard, R.; et al. Impact of particle size and polydispersity index on the clinical applications of lipidic nanocarrier systems. *Pharmaceutics* **2018**, *10*, 57, doi:10.3390/pharmaceutics10020057.
267. Nag, O.K.; Awasthi, V. Surface engineering of liposomes for stealth behavior. *Pharmaceutics* **2013**, *5*, 542-69, doi:10.3390/pharmaceutics5040542.
268. Bleher, S.; Buck, J.; Muhl, C.; Sieber, S.; Barnert, S.; et al. Poly(sarcosine) surface modification imparts stealth-like properties to liposomes. *Small* **2019**, *15*, 1904716, doi:10.1002/smll.201904716.
269. Henry, B.D.; Neill, D.R.; Becker, K.A.; Gore, S.; Bricio-Moreno, L.; et al. Engineered liposomes sequester bacterial exotoxins and protect from severe invasive infections in mice. *Nat Biotechnol* **2015**, *33*, 81-8, doi:10.1038/nbt.3037.
270. Ferreira, M.; Pinto, S.N.; Aires-da-Silva, F.; Bettencourt, A.; Aguiar, S.I.; et al. Liposomes as a nanoplatform to improve the delivery of antibiotics into *Staphylococcus aureus* biofilms. *Pharmaceutics* **2021**, *13*, 321, doi:10.3390/pharmaceutics13030321.
271. Wang, Y. Liposome as a delivery system for the treatment of biofilm-mediated infections. *J Appl Microbiol* **2021**, *131*, 2626-39, doi:10.1111/jam.15053.
272. Ferreira, M.; Ogren, M.; Dias, J.N.R.; Silva, M.; Gil, S.; et al. Liposomes as antibiotic delivery systems: A promising nanotechnological strategy against antimicrobial resistance. *Molecules* **2021**, *26*, 2047, doi:10.3390/molecules26072047.
273. Guo, R.; Liu, Y.; Li, K.; Tian, B.; Li, W.; et al. Direct interactions between cationic liposomes and bacterial cells ameliorate the systemic treatment of invasive multidrug-resistant *Staphylococcus aureus* infections. *Nanomedicine* **2021**, *34*, 102382, doi:10.1016/j.nano.2021.102382.
274. Thorn, C.R.; Thomas, N.; Boyd, B.J.; Prestidge, C.A. Nano-fats for bugs: The benefits of lipid nanoparticles for antimicrobial therapy. *Drug Deliv Transl Res* **2021**, *11*, 1598-624, doi:10.1007/s13346-021-00921-w.
275. Wang, D.-Y.; van der Mei, H.C.; Ren, Y.; Busscher, H.J.; Shi, L. Lipid-based antimicrobial delivery-systems for the treatment of bacterial infections. *Front Chem* **2020**, *7*, 872, doi:10.3389/fchem.2019.00872.
276. Alavi, S.E.; Koochi Moftakhari Esfahani, M.; Raza, A.; Adelnia, H.; Ebrahimi Shahmabadi, H. PEG-grafted liposomes for enhanced antibacterial and antibiotic activities: An in vivo study. *NanoImpact* **2022**, *25*, 100384, doi:10.1016/j.impact.2022.100384.
277. Ahmed, K.; Muiruri, P.W.; Jones, G.H.; Scott, M.J.; Jones, M.N. The effect of grafted poly(ethylene glycol) on the electrophoretic properties of phospholipid liposomes and their adsorption to bacterial biofilms. *Colloids Surf A Physicochem Eng Asp* **2001**, *194*, 287-96, doi:10.1016/S0927-7757(01)00817-2.

278. Nwabuike, J.C.; Pant, A.M.; Govender, T. Liposomal delivery systems and their applications against *Staphylococcus aureus* and Methicillin-resistant *Staphylococcus aureus*. *Adv Drug Deliv Rev* **2021**, *178*, 113861, doi:10.1016/j.addr.2021.113861.
279. Zhang, Y.; Zhao, Y.; Dong, D.; Li, X.; Li, Z.; et al. Effects of isosorbide mononitrate loaded nanoparticles conjugated with anti-*Staphylococcus aureus* α -toxin on *Staphylococcus aureus* biofilms. *Exp Ther Med* **2020**, *19*, 1267-74, doi:10.3892/etm.2019.8344.
280. Ommen, P.; Hansen, L.; Hansen, B.K.; Vu-Quang, H.; Kjems, J.; et al. Aptamer-targeted drug delivery for *Staphylococcus aureus* biofilm. *Front Cell Infect Microbiol* **2022**, *12*, 814340, doi:10.3389/fcimb.2022.814340.
281. Makhathini, S.S.; Kalhapure, R.S.; Jadhav, M.; Waddad, A.Y.; Gannimani, R.; et al. Novel two-chain fatty acid-based lipids for development of vancomycin pH-responsive liposomes against *Staphylococcus aureus* and methicillin-resistant *Staphylococcus aureus* (MRSA). *J Drug Target* **2019**, *27*, 1094-107, doi:10.1080/1061186x.2019.1599380.
282. Wehbe, M.; Anantha, M.; Shi, M.; Leung, A.W.; Dragowska, W.H.; et al. Development and optimization of an injectable formulation of copper diethyldithiocarbamate, an active anticancer agent. *Int J Nanomedicine* **2017**, *12*, 4129-46, doi:10.2147/IJN.S137347.
283. Al Badri, Y.N.; Chaw, C.S.; Elkordy, A.A. Insights into asymmetric liposomes as a potential intervention for drug delivery including pulmonary nanotherapeutics. *Pharmaceutics* **2023**, *15*, 294, doi:10.3390/pharmaceutics15010294.
284. Liu, H.; Kong, Y.; Liang, X.; Liu, Z.; Guo, X.; et al. The treatment of hepatocellular carcinoma with SP94 modified asymmetrical bilayer lipid-encapsulated Cu(DDC)(2) nanoparticles facilitating Cu accumulation in the tumor. *Expert Opin Drug Deliv* **2023**, *20*, 145-58, doi:10.1080/17425247.2023.2155631.
285. Li, Q.; Chao, Y.; Liu, B.; Xiao, Z.; Yang, Z.; et al. Disulfiram loaded calcium phosphate nanoparticles for enhanced cancer immunotherapy. *Biomaterials* **2022**, *291*, 121880, doi:10.1016/j.biomaterials.2022.121880.
286. Chen, M.; Huang, Z.; Xia, M.; Ding, Y.; Shan, T.; et al. Glutathione-responsive copper-disulfiram nanoparticles for enhanced tumor chemotherapy. *J Control Release* **2022**, *341*, 351-63, doi:10.1016/j.jconrel.2021.11.041.
287. Huang, Z.; Ding, Y.; Luo, Y.; Chen, M.; Zeng, Z.; et al. ROS-triggered cycle amplification effect: A prodrug activation nanoamplifier for tumor-specific therapy. *Acta Biomater* **2022**, *152*, 367-79, doi:10.1016/j.actbio.2022.08.072.
288. Paun, R.A.; Dumut, D.C.; Centorame, A.; Thuraisingam, T.; Hajduch, M.; et al. One-step synthesis of nanoliposomal copper diethyldithiocarbamate and its assessment for cancer therapy. *Pharmaceutics* **2022**, *14*, 640, doi:10.3390/pharmaceutics14030640.
289. Zheng, Z.; Zhang, J.; Jiang, J.; He, Y.; Zhang, W.; et al. Remodeling tumor immune microenvironment (TIME) for glioma therapy using multi-targeting liposomal codelivery. *J Immunother Cancer* **2020**, *8*, e000207, doi:10.1136/jitc-2019-000207.
290. Liu, H.; Kong, Y.; Liu, Z.; Guo, X.; Yang, B.; et al. Sphingomyelin-based PEGylation Cu (DDC)₂ liposomes prepared via the dual function of Cu²⁺ for cancer therapy: Facilitating DDC loading and exerting synergistic antitumor effects. *Int J Pharm* **2022**, *621*, 121788, doi:10.1016/j.ijpharm.2022.121788.
291. Najlah, M. Drug repurposing supported by nanotechnology: A promising strategy to fight cancer. *Ther Deliv* **2021**, *12*, 267-9, doi:10.4155/tde-2021-0009.
292. Patzelt, S.; Pigors, M.; Steenbock, H.; Diel, L.; Boch, K.; et al. Increased fibrosis in a mouse model of anti-laminin 332 mucous membrane pemphigoid remains unaltered by inhibition of aldehyde dehydrogenase. *Front Immunol* **2021**, *12*, 812627, doi:10.3389/fimmu.2021.812627.
293. Nagai, N.; Yoshioka, C.; Mano, Y.; Ito, Y.; Okamoto, N.; et al. Effect of eye drops containing disulfiram and low-substituted methylcellulose in reducing intraocular pressure in rabbit models. *Curr Eye Res* **2015**, *40*, 990-1000, doi:10.3109/02713683.2014.971187.
294. Wang, S.; Li, D.; Ito, Y.; Nabekura, T.; Wang, S.; et al. Bioavailability and anticataract effects of a topical ocular drug delivery system containing disulfiram and hydroxypropyl-beta-

- cyclodextrin on selenite-treated rats. *Curr Eye Res* **2004**, *29*, 51-8, doi:10.1080/02713680490513209.
295. Kanai, K.; Ito, Y.; Nagai, N.; Itoh, N.; Hori, Y.; et al. Effects of instillation of eyedrops containing disulfiram and hydroxypropyl- β -cyclodextrin inclusion complex on endotoxin-induced uveitis in rats. *Curr Eye Res* **2012**, *37*, 124-31, doi:10.3109/02713683.2011.622853.
296. Qu, Y.; Li, A.; Ma, L.; Iqbal, S.; Sun, X.; et al. Nose-to-brain delivery of disulfiram nanoemulsion in situ gel formulation for glioblastoma targeting therapy. *Int J Pharm* **2021**, *597*, 120250, doi:10.1016/j.ijpharm.2021.120250.
297. Landegren, J.; Borglund, E.; Storgårds, K. Treatment of scabies with disulfiram and benzyl benzoate emulsion: A controlled study. *Acta Derm Venereol* **1979**, *59*, 274-6.
298. Lajarin-Reinares, M.; Pena-Rodríguez, E.; Cañellas-Santos, M.; Rosell-Vives, E.; Cortés, P.; et al. Repurposing disulfiram as an antimicrobial agent in topical infections. *Antibiotics (Basel)* **2022**, *11*, 1752, doi:10.3390/antibiotics11121752.
299. Bonnekoh, H.; Vera, C.; Abad-Perez, A.; Radetzki, S.; Neuenschwander, M.; et al. Topical inflammasome inhibition with disulfiram prevents irritant contact dermatitis. *Clin Transl Allergy* **2021**, *11*, e12045, doi:10.1002/clt2.12045.
300. Celes, F.S.; Trovatti, E.; Khouri, R.; Van Weyenbergh, J.; Ribeiro, S.J.; et al. DETC-based bacterial cellulose bio-curatives for topical treatment of cutaneous leishmaniasis. *Sci Rep* **2016**, *6*, 38330, doi:10.1038/srep38330.
301. Xie, C.; Yan, J.; Cao, S.; Liu, R.; Sun, B.; et al. Bi-layered disulfiram-loaded fiber membranes with antibacterial properties for wound dressing. *Appl Biochem Biotechnol* **2022**, *194*, 1359-72, doi:10.1007/s12010-021-03663-0.
302. Zhang, X.; Xiang, J.; Hong, Y.; Shen, L. Recent advances in design strategies of tough hydrogels. *Macromol Rapid Commun* **2022**, *43*, 2200075, doi:10.1002/marc.202200075.
303. Li, Y.; Rodrigues, J.; Tomás, H. Injectable and biodegradable hydrogels: Gelation, biodegradation and biomedical applications. *Chem Soc Rev* **2012**, *41*, 2193-221, doi:10.1039/c1cs15203c.
304. Zawani, M.; Fauzi, M.B. Injectable hydrogels for chronic skin wound management: A concise review. *Biomedicines* **2021**, *9*, 527, doi:10.3390/biomedicines9050527.
305. Dimatteo, R.; Darling, N.J.; Segura, T. In situ forming injectable hydrogels for drug delivery and wound repair. *Adv Drug Deliv Rev* **2018**, *127*, 167-84, doi:10.1016/j.addr.2018.03.007.
306. Parhi, R. Cross-linked hydrogel for pharmaceutical applications: A review. *Adv Pharm Bull* **2017**, *7*, 515-30, doi:10.15171/apb.2017.064.
307. Huang, H.; Qi, X.; Chen, Y.; Wu, Z. Thermo-sensitive hydrogels for delivering biotherapeutic molecules: A review. *Saudi Pharm J* **2019**, *27*, 990-9, doi:10.1016/j.jpsps.2019.08.001.
308. Cobrado, L.; Azevedo, M.M.; Silva-Dias, A.; Ramos, J.P.; Pina-Vaz, C.; et al. Cerium, chitosan and hamamelitannin as novel biofilm inhibitors? *J Antimicrob Chemother* **2012**, *67*, 1159-62, doi:10.1093/jac/dks007.
309. Sami El-banna, F.; Mahfouz, M.E.; Leporatti, S.; El-Kemary, M.; A. N. Hanafy, N. Chitosan as a natural copolymer with unique properties for the development of hydrogels. *Appl Sci* **2019**, *9*, 2193, doi:10.3390/app9112193.
310. Rahmanian-Devin, P.; Baradaran Rahimi, V.; Askari, V.R. Thermosensitive chitosan- β -glycerophosphate hydrogels as targeted drug delivery systems: An overview on preparation and their applications. *Adv Pharmacol Pharm Sci* **2021**, *2021*, 6640893, doi:10.1155/2021/6640893.
311. Supper, S.; Anton, N.; Seidel, N.; Riemenschnitter, M.; Schoch, C.; et al. Rheological study of chitosan/polyol-phosphate systems: Influence of the polyol part on the thermo-induced gelation mechanism. *Langmuir* **2013**, *29*, 10229-37, doi:10.1021/la401993q.
312. Cho, J.; Heuzey, M.C.; Bégin, A.; Carreau, P.J. Physical gelation of chitosan in the presence of beta-glycerophosphate: The effect of temperature. *Biomacromolecules* **2005**, *6*, 3267-75, doi:10.1021/bm050313s.

313. Saravanan, S.; Vimalraj, S.; Thanikaivelan, P.; Banudevi, S.; Manivasagam, G. A review on injectable chitosan/beta glycerophosphate hydrogels for bone tissue regeneration. *Int J Biol Macromol* **2019**, *121*, 38-54, doi:10.1016/j.ijbiomac.2018.10.014.
314. Ruel-Gariépy, E.; Leclair, G.; Hildgen, P.; Gupta, A.; Leroux, J.C. Thermosensitive chitosan-based hydrogel containing liposomes for the delivery of hydrophilic molecules. *J Control Release* **2002**, *82*, 373-83, doi:10.1016/S0168-3659(02)00146-3.
315. Zhong, M.; Kou, H.; Zhao, P.; Zheng, W.; Xu, H.; et al. Nasal delivery of D-penicillamine hydrogel upregulates a disintegrin and metalloprotease 10 expression via melatonin receptor 1 in alzheimer's disease models. *Front Aging Neurosci* **2021**, *13*, 660249, doi:10.3389/fnagi.2021.660249.
316. Pakzad, Y.; Fathi, M.; Omid, Y.; Mozafari, M.; Zamanian, A. Synthesis and characterization of timolol maleate-loaded quaternized chitosan-based thermosensitive hydrogel: A transparent topical ocular delivery system for the treatment of glaucoma. *Int J Biol Macromol* **2020**, *159*, 117-28, doi:10.1016/j.ijbiomac.2020.04.274.
317. Ghasemi Tahrir, F.; Ganji, F.; Mani, A.R.; Khodaverdi, E. In vitro and in vivo evaluation of thermosensitive chitosan hydrogel for sustained release of insulin. *Drug Deliv* **2016**, *23*, 1038-46, doi:10.3109/10717544.2014.932861.
318. Qi, X.; Qin, X.; Yang, R.; Qin, J.; Li, W.; et al. Intra-articular administration of chitosan thermosensitive in situ hydrogels combined with diclofenac sodium-loaded alginate microspheres. *J Pharm Sci* **2016**, *105*, 122-30, doi:10.1016/j.xphs.2015.11.019.
319. Zhao, Y.; Liu, J.G.; Chen, W.M.; Yu, A.X. Efficacy of thermosensitive chitosan/ β -glycerophosphate hydrogel loaded with β -cyclodextrin-curcumin for the treatment of cutaneous wound infection in rats. *Exp Ther Med* **2018**, *15*, 1304-13, doi:10.3892/etm.2017.5552.
320. Wang, W.; Zhang, P.; Shan, W.; Gao, J.; Liang, W. A novel chitosan-based thermosensitive hydrogel containing doxorubicin liposomes for topical cancer therapy. *J Biomater Sci Polym Ed* **2013**, *24*, 1649-59, doi:10.1080/09205063.2013.789357.
321. Huang, P.; Su, W.; Han, R.; Lin, H.; Yang, J.; et al. Physicochemical, antibacterial properties, and compatibility of ZnO-NP/chitosan/ β -glycerophosphate composite hydrogels. *J Microbiol Biotechnol* **2022**, *32*, 522-30, doi:10.4014/jmb.2111.11024.
322. Zang, S.; Mu, R.; Chen, F.; Wei, X.; Zhu, L.; et al. Injectable chitosan/ β -glycerophosphate hydrogels with sustained release of BMP-7 and ornidazole in periodontal wound healing of class III furcation defects. *Mater Sci Eng C Mater Biol Appl* **2019**, *99*, 919-28, doi:10.1016/j.msec.2019.02.024.
323. Sheshala, R.; Quah, S.Y.; Tan, G.C.; Meka, V.S.; Jnanendrappa, N.; et al. Investigation on solution-to-gel characteristic of thermosensitive and mucoadhesive biopolymers for the development of moxifloxacin-loaded sustained release periodontal in situ gels. *Drug Deliv Transl Res* **2019**, *9*, 434-43, doi:10.1007/s13346-018-0488-6.
324. Tucker, L.J.; Grant, C.S.; Gautreaux, M.A.; Amarasekara, D.L.; Fitzkee, N.C.; et al. Physicochemical and antimicrobial properties of thermosensitive chitosan hydrogel loaded with fosfomicin. *Mar Drugs* **2021**, *19*, md19030144, doi:10.3390/md19030144.
325. Wu, Y.; Wei, W.; Zhou, M.; Wang, Y.; Wu, J.; et al. Thermal-sensitive hydrogel as adjuvant-free vaccine delivery system for H5N1 intranasal immunization. *Biomaterials* **2012**, *33*, 2351-60, doi:10.1016/j.biomaterials.2011.11.068.
326. Bhuiyan, M.H.; Houlton, J.; Clarkson, A.N. Hydrogels and nanoscaffolds for long-term intraparenchymal therapeutic delivery after stroke. *Methods Mol Biol* **2023**, *2616*, 379-90, doi:10.1007/978-1-0716-2926-0_26.
327. Ren, S.; Dai, Y.; Li, C.; Qiu, Z.; Wang, X.; et al. Pharmacokinetics and pharmacodynamics evaluation of a thermosensitive chitosan based hydrogel containing liposomal doxorubicin. *Eur J Pharm Sci* **2016**, *92*, 137-45, doi:10.1016/j.ejps.2016.07.002.
328. Rassouli, A.; Kiani, K.; Hosseinzadeh Ardakani, Y.; Akbari Javar, H.; Khanamani Falahatipour, S. A comparative pharmacokinetic study of a novel sustained release danofloxacin formulation and the conventional product in rabbits. *Vet Res Forum* **2021**, *12*, 253-7, doi:10.30466/vrf.2019.105313.2504.

8 Bibliography

329. Asfour, M.H.; Abd El-Alim, S.H.; Awad, G.E.A.; Kassem, A.A. Chitosan/ β -glycerophosphate in situ forming thermo-sensitive hydrogel for improved ocular delivery of moxifloxacin hydrochloride. *Eur J Pharm Sci* **2021**, *167*, 106041, doi:10.1016/j.ejps.2021.106041.
330. Sheshala, R.; Wai, N.Z.; Said, I.D.; Ashraf, K.; Lim, S.M.; et al. Poloxamer and chitosan-based in situ gels loaded with orthosiphon stamineus benth. Extracts containing rosmarinic acid for the treatment of ocular infections. *Turk J Pharm Sci* **2022**, *19*, 671-80, doi:10.4274/tjps.galenos.2021.40121.
331. Li, Y.; Li, G.; Sha, X.; Li, L.; Zhang, K.; et al. An intelligent vancomycin release system for preventing surgical site infections of bone tissues. *Biomater Sci* **2020**, *8*, 3202-11, doi:10.1039/d0bm00255k.
332. Mellinghoff, S.C.; Vehreschild, J.J.; Liss, B.J.; Cornely, O.A. Epidemiology of surgical site infections with *Staphylococcus aureus* in europe: Protocol for a retrospective, multicenter study. *JMIR Res Protoc* **2018**, *7*, e63, doi:10.2196/resprot.8177.
333. Romling, U.; Balsalobre, C. Biofilm infections, their resilience to therapy and innovative treatment strategies. *J Intern Med* **2012**, *272*, 541-61, doi:10.1111/joim.12004.
334. Kleinschmidt, S.; Huygens, F.; Faoagali, J.; Rathnayake, I.U.; Hafner, L.M. *Staphylococcus epidermidis* as a cause of bacteremia. *Future Microbiol* **2015**, *10*, 1859-79, doi:10.2217/fmb.15.98.
335. López-Cortés, L.E.; Gálvez-Acebal, J.; Rodríguez-Baño, J. Therapy of *Staphylococcus aureus* bacteremia: Evidences and challenges. *Enferm Infecc Microbiol Clin (Engl Ed)* **2020**, *38*, 489-97, doi:10.1016/j.eimc.2020.01.018.
336. Cahill, T.J.; Baddour, L.M.; Habib, G.; Hoen, B.; Salaun, E.; et al. Challenges in infective endocarditis. *J Am Coll Cardiol* **2017**, *69*, 325-44, doi:10.1016/j.jacc.2016.10.066.
337. Kaushik, A.; Kest, H. Pediatric methicillin-resistant *Staphylococcus aureus* osteoarticular infections. *Microorganisms* **2018**, *6*, 40, doi:10.3390/microorganisms6020040.
338. Otto, M. Staphylococcal biofilms. *Curr Top Microbiol Immunol* **2008**, *322*, 207-28, doi:10.1007/978-3-540-75418-3.
339. Zheng, Y.; He, L.; Asiamah, T.K.; Otto, M. Colonization of medical devices by staphylococci. *Environ Microbiol* **2018**, *20*, 3141-53, doi:10.1111/1462-2920.14129.
340. Tong, S.Y.C.; Davis, J.S.; Eichenberger, E.; Holland, T.L.; Fowler, V.G., Jr. *Staphylococcus aureus* infections: Epidemiology, pathophysiology, clinical manifestations, and management. *Clin Microbiol Rev* **2015**, *28*, 603-61, doi:10.1128/CMR.00134-14.
341. Stevens, D.L.; Bisno, A.L.; Chambers, H.F.; Everett, E.D.; Dellinger, P.; et al. Practice guidelines for the diagnosis and management of skin and soft-tissue infections. *Clin Infect Dis* **2005**, *41*, 1373-406, doi:10.1086/497143.
342. Liu, C.; Bayer, A.; Cosgrove, S.E.; Daum, R.S.; Fridkin, S.K.; et al. Clinical practice guidelines by the infectious diseases society of america for the treatment of methicillin-resistant *Staphylococcus aureus* infections in adults and children. *Clin Infect Dis* **2011**, *52*, e18-55, doi:10.1093/cid/ciq146.
343. Santajit, S.; Indrawattana, N. Mechanisms of antimicrobial resistance in ESKAPE pathogens. *Biomed Res Int* **2016**, *2016*, 2475067, doi:10.1155/2016/2475067.
344. Crabbé, A.; Jensen, P.Ø.; Bjarnsholt, T.; Coenye, T. Antimicrobial tolerance and metabolic adaptations in microbial biofilms. *Trends Microbiol* **2019**, *27*, 850-63, doi:10.1016/j.tim.2019.05.003.
345. Australian Commission on Safety and Quality in Health Care (ACSQHC). *AURA 2019: Third Australian report on antimicrobial use and resistance in human health*; ACSQHC: Sydney, **2019**.
346. Craft, K.M.; Nguyen, J.M.; Berg, L.J.; Townsend, S.D. Methicillin-resistant *Staphylococcus aureus* (MRSA): Antibiotic-resistance and the biofilm phenotype. *Medchemcomm* **2019**, *10*, 1231-41, doi:10.1039/c9md00044e.

347. European Centre for Disease Prevention and Control. *Antimicrobial resistance in the EU/EEA (EARS-Net) - Annual Epidemiological Report 2020*; ECDC: Stockholm, **2022**.
348. Lee, J.Y.H.; Monk, I.R.; Gonçalves da Silva, A.; Seemann, T.; Chua, K.Y.L.; et al. Global spread of three multidrug-resistant lineages of *Staphylococcus epidermidis*. *Nat Microbiol* **2018**, *3*, 1175-85, doi:10.1038/s41564-018-0230-7.
349. World Health Organization. *Antibacterial agents in clinical development: An analysis of the antibacterial clinical development pipeline, including tuberculosis*; WHO: Geneva, **2017**.
350. Dinarvand, M.; Spain, M.P.; Vafae, F. Pharmacodynamic functions of synthetic derivatives for treatment of methicillin-resistant *Staphylococcus aureus* (MRSA) and *Mycobacterium tuberculosis*. *Front Microbiol* **2020**, *11*, 551189, doi:10.3389/fmicb.2020.551189.
351. Sovari, S.N.; Vojnovic, S.; Bogojevic, S.S.; Crochet, A.; Pavic, A.; et al. Design, synthesis and in vivo evaluation of 3-arylcoumarin derivatives of rhenium(I) tricarbonyl complexes as potent antibacterial agents against methicillin-resistant *Staphylococcus aureus* (MRSA). *Eur J Med Chem* **2020**, *205*, 112533, doi:10.1016/j.ejmech.2020.112533.
352. Wang, X.; Bittner, T.; Milanov, M.; Kaul, L.; Munding, S.; et al. Pyridinium modified anthracenes and their endoperoxides provide a tunable scaffold with activity against Gram-positive and Gram-negative bacteria. *ACS Infect Dis* **2021**, *7*, 2073-80, doi:10.1021/acinfed.1c00263.
353. Feng, T.; Leptihn, S.; Dong, K.; Loh, B.; Zhang, Y.; et al. JD419, a *Staphylococcus aureus* phage with a unique morphology and broad host range. *Front Microbiol* **2021**, *12*, 602902, doi:10.3389/fmicb.2021.602902.
354. Walsh, L.; Johnson, C.N.; Hill, C.; Ross, R.P. Efficacy of phage- and bacteriocin-based therapies in combatting nosocomial MRSA infections. *Front Mol Biosci* **2021**, *8*, 654038, doi:10.3389/fmolb.2021.654038.
355. Richter, K.; Facal, P.; Thomas, N.; Vandecandelaere, I.; Ramezanpour, M.; et al. Taking the silver bullet colloidal silver particles for the topical treatment of biofilm-related infections. *ACS Appl Mater Interfaces* **2017**, *9*, 21631-8, doi:10.1021/acsami.7b03672.
356. Sánchez-López, E.; Gomes, D.; Esteruelas, G.; Bonilla, L.; Lopez-Machado, A.L.; et al. Metal-based nanoparticles as antimicrobial agents: An overview. *Nanomaterials (Basel)* **2020**, *10*, 292, doi:10.3390/nano10020292.
357. Thangamani, S.; Mohammad, H.; Younis, W.; Seleem, M.N. Drug repurposing for the treatment of staphylococcal infections. *Curr Pharm Des* **2015**, *21*, 2089-100, doi:10.2174/1381612821666150310104416.
358. Richter, K. Tackling superbugs in their slime castles: Innovative approaches against antimicrobial-resistant biofilm infections. *Microbiol Aust* **2019**, *40*, 165-8, doi:10.1071/MA19049.
359. Xu, L.; Tong, J.; Wu, Y.; Zhao, S.; Lin, B.L. A computational evaluation of targeted oxidation strategy (TOS) for potential inhibition of SARS-CoV-2 by disulfiram and analogues. *Biophys Chem* **2021**, *276*, 106610, doi:10.1016/j.bpc.2021.106610.
360. Gessner, P.K.; Gessner, T. Toxicology. In *Disulfiram and its Metabolite Diethyldithiocarbamate Pharmacology and status in the treatment of alcoholism, HIV infections, AIDS and heavy metal toxicity*, Hall, C.a., Ed.; Chapman and Hall: London, United Kingdom, **1992**; pp. 335-45.
361. Wiegand, I.; Hilpert, K.; Hancock, R.E. Agar and broth dilution methods to determine the minimal inhibitory concentration (MIC) of antimicrobial substances. *Nat Protoc* **2008**, *3*, 163-75, doi:10.1038/nprot.2007.521.
362. Peeters, E.; Nelis, H.J.; Coenye, T. Comparison of multiple methods for quantification of microbial biofilms grown in microtiter plates. *J Microbiol Methods* **2008**, *72*, 157-65, doi:10.1016/j.mimet.2007.11.010.
363. Richter, K.; Ramezanpour, M.; Thomas, N.; Prestidge, C.A.; Wormald, P.J.; et al. Mind "De GaPP": In vitro efficacy of deferiprone and gallium-protoporphyrin against *Staphylococcus aureus* biofilms. *Int Forum Allergy Rhinol* **2016**, *6*, 737-43, doi:10.1002/alr.21735.

8 Bibliography

364. Sopirala, M.M.; Mangino, J.E.; Gebreyes, W.A.; Biller, B.; Bannerman, T.; et al. Synergy testing by Etest, microdilution checkerboard, and time-kill methods for pan-drug-resistant *Acinetobacter baumannii*. *Antimicrob Agents Chemother* **2010**, *54*, 4678-83, doi:10.1128/aac.00497-10.
365. Hoogenkamp, M.A. Challenging dental unit water biofilms. [Doctoral Thesis, University of Amsterdam] Amsterdam, The Netherlands, **2021**.
366. Abrantes, P.; Africa, C.W.J. Measuring *Streptococcus mutans*, *Streptococcus sanguinis* and *Candida albicans* biofilm formation using a real-time impedance-based system. *J Microbiol Methods* **2020**, *169*, 105815, doi:10.1016/j.mimet.2019.105815.
367. Seixas, A.F.; Quendera, A.P.; Sousa, J.P.; Silva, A.F.Q.; Arraiano, C.M.; et al. Bacterial response to oxidative stress and rna oxidation. *Front Genet* **2021**, *12*, 821535, doi:10.3389/fgene.2021.821535.
368. Viola-Rhenals, M.; Patel, K.R.; Jaimes-Santamaria, L.; Wu, G.; Liu, J.; et al. Recent advances in antabuse (disulfiram): The importance of its metal-binding ability to its anticancer activity. *Curr Med Chem* **2018**, *25*, 506-24, doi:10.2174/0929867324666171023161121.
369. Baker, J.; Sitthisak, S.; Sengupta, M.; Johnson, M.; Jayaswal, R.K.; et al. Copper stress induces a global stress response in *Staphylococcus aureus* and represses *sae* and *agr* expression and biofilm formation. *Appl Environ Microbiol* **2010**, *76*, 150-60, doi:10.1128/aem.02268-09.
370. Dupont, C.L.; Grass, G.; Rensing, C. Copper toxicity and the origin of bacterial resistance - new insights and applications. *Metallomics* **2011**, *3*, 1109-18, doi:10.1039/C1MT00107H.
371. Solioz, M. Copper homeostasis in gram-positive bacteria. In *Copper and Bacteria*; SpringerBriefs in Biometals: London, **2018**; pp. 21-48.
372. Tsai, C.J.-Y.; Loh, J.M.S.; Proft, T. *Galleria mellonella* infection models for the study of bacterial diseases and for antimicrobial drug testing. *Virulence* **2016**, *7*, 214-29, doi:10.1080/21505594.2015.1135289.
373. Brackman, G.; Cos, P.; Maes, L.; Nelis, H.J.; Coenye, T. Quorum sensing inhibitors increase the susceptibility of bacterial biofilms to antibiotics in vitro and in vivo. *Antimicrob Agents Chemother* **2011**, *55*, 2655-61, doi:10.1128/aac.00045-11.
374. Desbois, A.P.; Coote, P.J. Wax moth larva (*Galleria mellonella*): An in vivo model for assessing the efficacy of antistaphylococcal agents. *J Antimicrob Chemother* **2011**, *66*, 1785-90, doi:10.1093/jac/dkr198.
375. Dalecki, A.G.; Crawford, C.L.; Wolschendorf, F. Targeting biofilm associated *Staphylococcus aureus* using resazurin based drug-susceptibility assay. *J Vis Exp* **2016**, e53925, doi:10.3791/53925.
376. Robertson, J.; McGoverin, C.; Vanholsbeeck, F.; Swift, S. Optimisation of the protocol for the LIVE/DEAD® BacLight™ bacterial viability kit for rapid determination of bacterial load. *Front Microbiol* **2019**, *10*, 801, doi:10.3389/fmicb.2019.00801.
377. Ferrer, M.D.; Rodriguez, J.C.; Álvarez, L.; Artacho, A.; Royo, G.; et al. Effect of antibiotics on biofilm inhibition and induction measured by real-time cell analysis. *J Appl Microbiol* **2017**, *122*, 640-50, doi:10.1111/jam.13368.
378. Gutiérrez, D.; Hidalgo-Cantabrana, C.; Rodríguez, A.; García, P.; Ruas-Madiedo, P. Monitoring in real time the formation and removal of biofilms from clinical related pathogens using an impedance-based technology. *PLoS One* **2016**, *11*, e0163966, doi:10.1371/journal.pone.0163966.
379. Fey, P.D.; Olson, M.E. Current concepts in biofilm formation of *Staphylococcus epidermidis*. *Future Microbiol* **2010**, *5*, 917-33, doi:10.2217/fmb.10.56.
380. Stiefel, P.; Rosenberg, U.; Schneider, J.; Mauerhofer, S.; Maniura-Weber, K.; et al. Is biofilm removal properly assessed? Comparison of different quantification methods in a 96-well plate system. *Appl Microbiol Biotechnol* **2016**, *100*, 4135-45, doi:10.1007/s00253-016-7396-9.
381. World Health Organization. *Global guidelines for the prevention of surgical site infection*; WHO: Switzerland, **2016**.

382. Iskandar, K.; Sartelli, M.; Tabbal, M.; Ansaloni, L.; Baiocchi, G.L.; et al. Highlighting the gaps in quantifying the economic burden of surgical site infections associated with antimicrobial-resistant bacteria. *World J Emerg Surg* **2019**, *14*, 50, doi:10.1186/s13017-019-0266-x.
383. Hoffmann, J.P.; Friedman, J.K.; Wang, Y.; McLachlan, J.B.; Sammarco, M.C.; et al. In situ treatment with novel microbiocide inhibits methicillin resistant *Staphylococcus aureus* in a murine wound infection model. *Front Microbiol* **2020**, *10*, 3106, doi:10.3389/fmicb.2019.03106.
384. Assolini, J.P.; Tomiotto-Pellissier, F.; da Silva Bortoleti, B.T.; Gonçalves, M.D.; Sahd, C.S.; et al. Diethyldithiocarbamate encapsulation reduces toxicity and promotes leishmanicidal effect through apoptosis-like mechanism in promastigote and ROS production by macrophage. *J Drug Target* **2020**, *28*, 1110-23, doi:10.1080/1061186x.2020.1783669.
385. Shanholtzer, C.N.; Rice, C.; Watson, K.; Carreon, H.; Long, T.E. Effect of copper on the antifungal activity of disulfiram (Antabuse®) in fluconazole-resistant *Candida* strains. *Med Mycol* **2022**, *60*, myac016, doi:10.1093/mmy/myac016.
386. Cvek, B.; Milacic, V.; Taraba, J.; Dou, Q.P. Ni(II), Cu(II), and Zn(II) diethyldithiocarbamate complexes show various activities against the proteasome in breast cancer cells. *J Med Chem* **2008**, *51*, 6256-8, doi:10.1021/jm8007807.
387. Kaul, L.; Abdo, A.I.; Coenye, T.; Krom, B.P.; Hoogenkamp, M.A.; et al. The combination of diethyldithiocarbamate and copper ions is active against *Staphylococcus aureus* and *Staphylococcus epidermidis* biofilms in vitro and in vivo. *Front Microbiol* **2022**, *13*, 999893, doi:10.3389/fmicb.2022.999893.
388. Thaarup, I.C.; Bjarnsholt, T. Current in vitro biofilm-infected chronic wound models for developing new treatment possibilities. *Adv Wound Care* **2020**, *10*, 91-102, doi:10.1089/wound.2020.1176.
389. Han, J.; Liu, L.; Yue, X.; Chang, J.; Shi, W.; et al. A binuclear complex constituted by diethyldithiocarbamate and copper(I) functions as a proteasome activity inhibitor in pancreatic cancer cultures and xenografts. *Toxicol Appl Pharmacol* **2013**, *273*, 477-83, doi:10.1016/j.taap.2013.09.009.
390. Brackman, G.; Garcia-Fernandez, M.J.; Lenoir, J.; De Meyer, L.; Remon, J.-P.; et al. Dressings loaded with cyclodextrin-hamamelitannin complexes increase *Staphylococcus aureus* susceptibility toward antibiotics both in single as well as in mixed biofilm communities. *Macromol Biosci* **2016**, *16*, 859-69, doi:10.1002/mabi.201500437.
391. Richter, K.; Thomas, N.; Claeys, J.; McGuane, J.; Prestidge, C.A.; et al. A topical hydrogel with deferiprone and gallium-protoporphyrin targets bacterial iron metabolism and has antibiofilm activity. *Antimicrob Agents Chemother* **2017**, *61*, e00481-17, doi:10.1128/aac.00481-17.
392. Van den Driessche, F.; Rigole, P.; Brackman, G.; Coenye, T. Optimization of resazurin-based viability staining for quantification of microbial biofilms. *J Microbiol Methods* **2014**, *98*, 31-4, doi:10.1016/j.jmimet.2013.12.011.
393. Grassi, L.; Batoni, G.; Ostyn, L.; Rigole, P.; Van den Bossche, S.; et al. The antimicrobial peptide lin-SB056-1 and its dendrimeric derivative prevent *Pseudomonas aeruginosa* biofilm formation in physiologically relevant models of chronic infections. *Front Microbiol* **2019**, *10*, 198, doi:10.3389/fmicb.2019.00198.
394. Wehbe, M.; Chernov, L.; Chen, K.; Bally, M.B. PRCosomes: Pretty reactive complexes formed in liposomes. *J Drug Target* **2016**, *24*, 787-96, doi:10.1080/1061186x.2016.1186169.
395. Sajithlal, G.B.; Chithra, P.; Chandrakasan, G. An in vitro study on the role of metal catalyzed oxidation in glycation and crosslinking of collagen. *Mol Cell Biochem* **1999**, *194*, 257-63, doi:10.1023/a:1006988719374.
396. Hassan, G.; Forsman, N.; Wan, X.; Keurulainen, L.; Bimbo, L.M.; et al. Non-leaching, highly biocompatible nanocellulose surfaces that efficiently resist fouling by bacteria in an artificial dermis model. *ACS Appl Bio Mater* **2020**, *3*, 4095-108, doi:10.1021/acsabm.0c00203.
397. Grassi, L.; Pompilio, A.; Kaya, E.; Rinaldi, A.C.; Sanjust, E.; et al. The anti-microbial peptide (lin-SB056-1)2-K reduces pro-inflammatory cytokine release through interaction with *Pseudomonas aeruginosa* lipopolysaccharide. *Antibiotics (Basel)* **2020**, *9*, 585, doi:10.3390/antibiotics9090585.

8 Bibliography

398. Caputo, F.; Clogston, J.; Calzolari, L.; Rösslein, M.; Prina-Mello, A. Measuring particle size distribution of nanoparticle enabled medicinal products, the joint view of EUNCL and NCI-NCL. A step by step approach combining orthogonal measurements with increasing complexity. *J Control Release* **2019**, *299*, 31-43, doi:10.1016/j.jconrel.2019.02.030.
399. Forier, K.; Raemdonck, K.; De Smedt, S.C.; Demeester, J.; Coenye, T.; et al. Lipid and polymer nanoparticles for drug delivery to bacterial biofilms. *J Control Release* **2014**, *190*, 607-23, doi:10.1016/j.jconrel.2014.03.055.
400. Rukavina, Z.; Vanić, Ž. Current trends in development of liposomes for targeting bacterial biofilms. *Pharmaceutics* **2016**, *8*, 18, doi:10.3390/pharmaceutics8020018.
401. Ibaraki, H.; Kanazawa, T.; Chien, W.-Y.; Nakaminami, H.; Aoki, M.; et al. The effects of surface properties of liposomes on their activity against *Pseudomonas aeruginosa* PAO-1 biofilm. *J Drug Deliv Sci Technol* **2020**, *57*, 101754, doi:10.1016/j.jddst.2020.101754.
402. Verhoef, J.J.; Anchordoquy, T.J. Questioning the use of PEGylation for drug delivery. *Drug Deliv Transl Res* **2013**, *3*, 499-503, doi:10.1007/s13346-013-0176-5.
403. Ahmed, K.; Gribbon, P.N.; Jones, M.N. The application of confocal microscopy to the study of liposome adsorption onto bacterial biofilms. *J Liposome Res* **2002**, *12*, 285-300, doi:10.1081/lpr-120016195.
404. Dong, D.; Thomas, N.; Thierry, B.; Vreugde, S.; Prestidge, C.A.; et al. Distribution and inhibition of liposomes on *Staphylococcus aureus* and *Pseudomonas aeruginosa* biofilm. *PLoS One* **2015**, *10*, e0131806-e, doi:10.1371/journal.pone.0131806.
405. Maurer, E.; Hörtnagl, C.; Lackner, M.; Grässle, D.; Naschberger, V.; et al. *Galleria mellonella* as a model system to study virulence potential of mucormycetes and evaluation of antifungal treatment. *Med Mycol* **2019**, *57*, 351-62, doi:10.1093/mmy/myy042.
406. Senior, N.J.; Titball, R.W. Isolation and primary culture of *Galleria mellonella* hemocytes for infection studies. *F1000Res* **2020**, *9*, 1392, doi:10.12688/f1000research.27504.2.
407. Bergin, D.; Reeves, E.P.; Renwick, J.; Wientjes, F.B.; Kavanagh, K. Superoxide production in *Galleria mellonella* hemocytes: Identification of proteins homologous to the NADPH oxidase complex of human neutrophils. *Infect Immun* **2005**, *73*, 4161-70, doi:10.1128/IAI.73.7.4161-4170.2005.
408. Sheehan, G.; Dixon, A.; Kavanagh, K. Utilization of *Galleria mellonella* larvae to characterize the development of *Staphylococcus aureus* infection. *Microbiology (Reading)* **2019**, *165*, 863-75, doi:10.1099/mic.0.000813.
409. Fuchs, B.B.; O'Brien, E.; Khoury, J.B.; Mylonakis, E. Methods for using *Galleria mellonella* as a model host to study fungal pathogenesis. *Virulence* **2010**, *1*, 475-82, doi:10.4161/viru.1.6.12985.
410. Ignasiak, K.; Maxwell, A. *Galleria mellonella* (greater wax moth) larvae as a model for antibiotic susceptibility testing and acute toxicity trials. *BMC Res Notes* **2017**, *10*, 428, doi:10.1186/s13104-017-2757-8.
411. Russell, W.M.S.; Burch, R.L. *The principles of humane experimental technique*; Methuen: London, **1959**; p. 252.
412. Kaul, L.; Grundmann, C.E.; Köll-Weber, M.; Löffler, H.; Weiz, A.; et al. A thermosensitive, chitosan-based hydrogel as delivery system for antibacterial liposomes to surgical site infections. *Pharmaceutics* **2022**, *14*, 2841, doi:10.3390/pharmaceutics14122841.
413. Allegra, E.; Titball, R.W.; Carter, J.; Champion, O.L. *Galleria mellonella* larvae allow the discrimination of toxic and non-toxic chemicals. *Chemosphere* **2018**, *198*, 469-72, doi:10.1016/j.chemosphere.2018.01.175.
414. Chenite, A.; Chaput, C.; Wang, D.; Combes, C.; Buschmann, M.D.; et al. Novel injectable neutral solutions of chitosan form biodegradable gels in situ. *Biomaterials* **2000**, *21*, 2155-61, doi:10.1016/S0142-9612(00)00116-2.
415. Zhou, H.Y.; Jiang, L.J.; Cao, P.P.; Li, J.B.; Chen, X.G. Glycerophosphate-based chitosan thermosensitive hydrogels and their biomedical applications. *Carbohydr Polym* **2015**, *117*, 524-36, doi:10.1016/j.carbpol.2014.09.094.

416. Khodaverdi, E.; Tafaghodi, M.; Ganji, F.; Abnoos, K.; Naghizadeh, H. In vitro insulin release from thermosensitive chitosan hydrogel. *AAPS PharmSciTech* **2012**, *13*, 460-6, doi:10.1208/s12249-012-9764-9.
417. Xing, J.; Qi, X.; Jiang, Y.; Zhu, X.; Zhang, Z.; et al. Topotecan hydrochloride liposomes incorporated into thermosensitive hydrogel for sustained and efficient in situ therapy of H22 tumor in Kunming mice. *Pharm Dev Technol* **2015**, *20*, 812-9, doi:10.3109/10837450.2014.926918.
418. Zheng, Y.; Wang, W.; Zhao, J.; Wu, C.; Ye, C.; et al. Preparation of injectable temperature-sensitive chitosan-based hydrogel for combined hyperthermia and chemotherapy of colon cancer. *Carbohydr Polym* **2019**, *222*, 115039, doi:10.1016/j.carbpol.2019.115039.
419. Kaya, G.; Oytun, F. Rheological properties of injectable hyaluronic acid hydrogels for soft tissue engineering applications. *Biointerface Res Appl Chem* **2020**, *11*, 8424-30, doi:10.33263/briac111.84248430.
420. Alinaghi, A.; Rouini, M.R.; Johari Daha, F.; Moghimi, H.R. Hydrogel-embedded vesicles, as a novel approach for prolonged release and delivery of liposome, in vitro and in vivo. *J Liposome Res* **2013**, *23*, 235-43, doi:10.3109/08982104.2013.799179.
421. Rybtke, M.; Chua, S.L.; Yam, J.K.H.; Givskov, M.; Yang, L.; et al. Gauging and visualizing c-di-GMP levels in *Pseudomonas aeruginosa* using fluorescence-based biosensors. In *c-di-GMP Signaling: Methods and Protocols, Methods in Molecular Biology*, Sauer, K., Ed.; Humana Press: New York, NY, **2017**; Volume 1657, pp. 87-98.
422. Chen, C.; Han, D.; Cai, C.; Tang, X. An overview of liposome lyophilization and its future potential. *J Control Release* **2010**, *142*, 299-311, doi:10.1016/j.jconrel.2009.10.024.
423. Franzé, S.; Selmin, F.; Samaritani, E.; Minghetti, P.; Cilurzo, F. Lyophilization of liposomal formulations: Still necessary, still challenging. *Pharmaceutics* **2018**, *10*, 139, doi:10.3390/pharmaceutics10030139.
424. Kannan, V.; Balabathula, P.; Thoma, L.A.; Wood, G.C. Effect of sucrose as a lyoprotectant on the integrity of paclitaxel-loaded liposomes during lyophilization. *J Liposome Res* **2015**, *25*, 270-8, doi:10.3109/08982104.2014.992023.
425. Wang, Y.; Grainger, D.W. Lyophilized liposome-based parenteral drug development: Reviewing complex product design strategies and current regulatory environments. *Adv Drug Deliv Rev* **2019**, *151-152*, 56-71, doi:10.1016/j.addr.2019.03.003.
426. Wessman, P.; Edwards, K.; Mahlin, D. Structural effects caused by spray- and freeze-drying of liposomes and bilayer disks. *J Pharm Sci* **2010**, *99*, 2032-48, doi:10.1002/jps.21972.
427. Bindu, B.; Bindra, A.; Rath, G. Temperature management under general anesthesia: Compulsion or option. *J Anaesthesiol Clin Pharmacol* **2017**, *33*, 306-16, doi:10.4103/joacp.JOACP_334_16.
428. Supper, S.; Anton, N.; Seidel, N.; Riemenschnitter, M.; Curdy, C.; et al. Thermosensitive chitosan/glycerophosphate-based hydrogel and its derivatives in pharmaceutical and biomedical applications. *Expert Opin Drug Deliv* **2014**, *11*, 249-67, doi:10.1517/17425247.2014.867326.
429. Szymańska, E.; Winnicka, K. Stability of chitosan-a challenge for pharmaceutical and biomedical applications. *Mar Drugs* **2015**, *13*, 1819-46, doi:10.3390/md13041819.
430. Zingel, C.; Sachse, A.; Rößling, G.L.; Müller, R.H. Lyophilization and rehydration of iopromide-carrying liposomes. *Int J Pharm* **1996**, *140*, 13-24, doi:10.1016/0378-5173(96)04566-8.
431. Sebaaly, C.; Trifan, A.; Sieniawska, E.; Greige-Gerges, H. Chitosan-coating effect on the characteristics of liposomes: A focus on bioactive compounds and essential oils: A review. *Processes (Basel)* **2021**, *9*, 445, doi:10.3390/pr9030445.
432. Nugraheni, P.S.; Soeriyadi, A.H.; Sediawan, W.B.; Ustadi; Budhijanto, W. Influence of salt addition and freezing-thawing on particle size and zeta potential of nano-chitosan. *IOP Conf Ser Earth Environ Sci* **2019**, *278*, 012052, doi:10.1088/1755-1315/278/1/012052.

433. Szekalska, M.; Sosnowska, K.; Wróblewska, M.; Basa, A.; Winnicka, K. Does the freeze-thaw technique affect the properties of the alginate/chitosan glutamate gels with posaconazole as a model antifungal drug? *Int J Mol Sci* **2022**, *23*, 6775, doi:10.3390/ijms23126775.
434. Huang, F.J.; Hung, C.C.; Chang, C.W.; Chao, J.H.; Hsieh, B.T. Evaluation of injectable chitosan-based co-cross-linking hydrogel for local delivery of (188)Re-LIPO-DOX to breast-tumor-bearing mouse model. *Anticancer Res* **2018**, *38*, 4651-9, doi:10.21873/anticancer.12770.
435. Kapałczyńska, M.; Kolenda, T.; Przybyła, W.; Zajączkowska, M.; Teresiak, A.; et al. 2D and 3D cell cultures - a comparison of different types of cancer cell cultures. *Arch Med Sci* **2018**, *14*, 910-9, doi:10.5114/aoms.2016.63743.
436. Irimia, T.; Dinu-Pîrvu, C.E.; Ghica, M.V.; Lupuleasa, D.; Muntean, D.L.; et al. Chitosan-based in situ gels for ocular delivery of therapeutics: A state-of-the-art review. *Mar Drugs* **2018**, *16*, md16100373, doi:10.3390/md16100373.
437. Dang, Q.F.; Zou, S.H.; Chen, X.G.; Liu, C.S.; Li, J.J.; et al. Characterizations of chitosan-based highly porous hydrogel—The effects of the solvent. *J Appl Polym Sci* **2012**, *125*, E88-E98, doi:10.1002/app.36681.
438. Ahmadi, R.; de Bruijn, J.D. Biocompatibility and gelation of chitosan-glycerol phosphate hydrogels. *J Biomed Mater Res A* **2008**, *86*, 824-32, doi:10.1002/jbm.a.31676.
439. Kim, S.; Nishimoto, S.K.; Bumgardner, J.D.; Haggard, W.O.; Gaber, M.W.; et al. A chitosan/beta-glycerophosphate thermo-sensitive gel for the delivery of ellagic acid for the treatment of brain cancer. *Biomaterials* **2010**, *31*, 4157-66, doi:10.1016/j.biomaterials.2010.01.139.
440. Jeong, S.; Jeong, S.; Chung, S.; Kim, A. Revisiting in vitro release test for topical gel formulations: The effect of osmotic pressure explored for better bio-relevance. *Eur J Pharm Sci* **2018**, *112*, 102-11, doi:10.1016/j.ejps.2017.11.009.
441. Duffy, C.; O'Riordan, D.; O'Sullivan, M.; Jacquier, J.C. In vitro evaluation of chitosan copper chelate gels as a multimicronutrient feed additive for cattle. *J Sci Food Agric* **2018**, *98*, 4177-83, doi:10.1002/jsfa.8939.
442. O'Dwyer, P.J.; Litou, C.; Box, K.J.; Dressman, J.B.; Kostewicz, E.S.; et al. In vitro methods to assess drug precipitation in the fasted small intestine - a PEARL review. *J Pharm Pharmacol* **2019**, *71*, 536-56, doi:10.1111/jphp.12951.
443. Panyamao, P.; Ruksiriwanich, W.; Sirisa-Ard, P.; Charumane, S. Injectable thermosensitive chitosan/pullulan-based hydrogels with improved mechanical properties and swelling capacity. *Polymers (Basel)* **2020**, *12*, 2514, doi:10.3390/polym12112514.
444. Uribe-Alvarez, C.; Chiquete-Félix, N.; Contreras-Zentella, M.; Guerrero-Castillo, S.; Peña, A.; et al. Staphylococcus epidermidis: Metabolic adaptation and biofilm formation in response to different oxygen concentrations. *Pathog Dis* **2016**, *74*, ftv111, doi:10.1093/femspd/ftv111.
445. Ji, Q.X.; Chen, X.G.; Zhao, Q.S.; Liu, C.S.; Cheng, X.J.; et al. Injectable thermosensitive hydrogel based on chitosan and quaternized chitosan and the biomedical properties. *J Mater Sci Mater Med* **2009**, *20*, 1603-10, doi:10.1007/s10856-009-3729-x.
446. Niranjana, R.; Koushik, C.; Saravanan, S.; Moorthi, A.; Vairamani, M.; et al. A novel injectable temperature-sensitive zinc doped chitosan/ β -glycerophosphate hydrogel for bone tissue engineering. *Int J Biol Macromol* **2013**, *54*, 24-9, doi:10.1016/j.ijbiomac.2012.11.026.
447. Lišková, J.; Douglas, T.E.; Beranová, J.; Skwarczyńska, A.; Božič, M.; et al. Chitosan hydrogels enriched with polyphenols: Antibacterial activity, cell adhesion and growth and mineralization. *Carbohydr Polym* **2015**, *129*, 135-42, doi:10.1016/j.carbpol.2015.04.043.
448. Pakzad, Y.; Ganji, F. Thermosensitive hydrogel for periodontal application: In vitro drug release, antibacterial activity and toxicity evaluation. *J Biomater Appl* **2016**, *30*, 919-29, doi:10.1177/0885328215614191.
449. Carlson, R.P.; Taffs, R.; Davison, W.M.; Stewart, P.S. Anti-biofilm properties of chitosan-coated surfaces. *J Biomater Sci Polym Ed* **2008**, *19*, 1035-46, doi:10.1163/156856208784909372.

450. Peterson, S.B.; Irie, Y.; Borlee, B.R.; Murakami, K.; Harrison, J.J.; et al. Different methods for culturing biofilms in vitro. In *Biofilm Infections*, Bjarnsholt, T., Jensen, P.Ø., Moser, C., et al., Eds.; Springer New York: New York, NY, **2011**; pp. 251-66.
451. Sheiko, S.S.; da Silva, M.; Shirvaniants, D.; LaRue, I.; Prokhorova, S.; et al. Measuring molecular weight by atomic force microscopy. *J Am Chem Soc* **2003**, *125*, 6725-8, doi:10.1021/ja0346779.
452. Rayfield, W.J.; Kandula, S.; Khan, H.; Tugcu, N. Impact of freeze/thaw process on drug substance storage of therapeutics. *J Pharm Sci* **2017**, *106*, 1944-51, doi:10.1016/j.xphs.2017.03.019.
453. Tarrant, E.; G, P.R.; McIlvin, M.R.; Stevenson, J.; Barwinska-Sendra, A.; et al. Copper stress in *Staphylococcus aureus* leads to adaptive changes in central carbon metabolism. *Metallomics* **2019**, *11*, 183-200, doi:10.1039/c8mt00239h.
454. Rowe, S.E.; Wagner, N.J.; Li, L.; Beam, J.E.; Wilkinson, A.D.; et al. Reactive oxygen species induce antibiotic tolerance during systemic *Staphylococcus aureus* infection. *Nat Microbiol* **2020**, *5*, 282-90, doi:10.1038/s41564-019-0627-y.
455. Pavelescu, L.A. On reactive oxygen species measurement in living systems. *J Med Life* **2015**, *8*, 38-42, PMID: 26361509.
456. Fiedler, S.; Heerklotz, H. Vesicle leakage reflects the target selectivity of antimicrobial lipopeptides from *Bacillus subtilis*. *Biophys J* **2015**, *109*, 2079-89, doi:10.1016/j.bpj.2015.09.021.
457. Fasnacht, M.; Polacek, N. Oxidative stress in bacteria and the central dogma of molecular biology. *Front Mol Biosci* **2021**, *8*, 671037, doi:10.3389/fmolb.2021.671037.
458. Li, L.; Zhong, S.; Shen, X.; Li, Q.; Xu, W.; et al. Recent development on liquid chromatography-mass spectrometry analysis of oxidized lipids. *Free Radic Biol Med* **2019**, *144*, 16-34, doi:10.1016/j.freeradbiomed.2019.06.006.
459. Zapotoczna, M.; Riboldi, G.P.; Moustafa, A.M.; Dickson, E.; Narechania, A.; et al. Mobile-genetic-element-encoded hypertolerance to copper protects *Staphylococcus aureus* from killing by host phagocytes. *mBio* **2018**, *9*, e00550-18, doi:10.1128/mBio.00550-18.
460. Rosario-Cruz, Z.; Eletsky, A.; Daigham, N.S.; Al-Tameemi, H.; Swapna, G.V.T.; et al. The copBL operon protects *Staphylococcus aureus* from copper toxicity: CopL is an extracellular membrane-associated copper-binding protein. *J Biol Chem* **2019**, *294*, 4027-44, doi:10.1074/jbc.RA118.004723.
461. Purves, J.; Thomas, J.; Riboldi, G.P.; Zapotoczna, M.; Tarrant, E.; et al. A horizontally gene transferred copper resistance locus confers hyper-resistance to antibacterial copper toxicity and enables survival of community acquired methicillin resistant *Staphylococcus aureus* USA300 in macrophages. *Environ Microbiol* **2018**, *20*, 1576-89, doi:10.1111/1462-2920.14088.
462. Iglar, C.; Rolff, J.; Regoes, R. Multi-step vs. single-step resistance evolution under different drugs, pharmacokinetics, and treatment regimens. *Elife* **2021**, *10*, e64116, doi:10.7554/eLife.64116.
463. Edwards, A.M.; Massey, R.C. Invasion of human cells by a bacterial pathogen. *J Vis Exp* **2011**, 2693, doi:10.3791/2693.
464. Langer, C.; Süß, R. HPLC-DAD-CAD-based approach for the simultaneous analysis of hydrophobic drugs and lipid compounds in liposomes and for cyclodextrin/drug inclusion complexes. *J Pharm Biomed Anal* **2021**, *201*, 114120, doi:10.1016/j.jpba.2021.114120.
465. Pumerantz, A.; Muppidi, K.; Agnihotri, S.; Guerra, C.; Venketaraman, V.; et al. Preparation of liposomal vancomycin and intracellular killing of methicillin-resistant *Staphylococcus aureus* (MRSA). *Int J Antimicrob Agents* **2011**, *37*, 140-4, doi:10.1016/j.ijantimicag.2010.10.011.
466. Kluzek, M.; Oppenheimer-Shaanan, Y.; Dadosh, T.; Morandi, M.I.; Avinoam, O.; et al. Designer liposomic nanocarriers are effective biofilm eradicators. *ACS Nano* **2022**, *16*, 15792-804, doi:10.1021/acsnano.2c04232.

8 Bibliography

467. Moghadas-Sharif, N.; Fazly Bazzaz, B.S.; Khameneh, B.; Malaekheh-Nikouei, B. The effect of nanoliposomal formulations on *Staphylococcus epidermidis* biofilm. *Drug Dev Ind Pharm* **2015**, *41*, 445-50, doi:10.3109/03639045.2013.877483.
468. Ferreira, M.; Aguiar, S.; Bettencourt, A.; Gaspar, M.M. Lipid-based nanosystems for targeting bone implant-associated infections: Current approaches and future endeavors. *Drug Deliv Transl Res* **2021**, *11*, 72-85, doi:10.1007/s13346-020-00791-8.
469. Bartomeu Garcia, C.; Shi, D.; Webster, T.J. Tat-functionalized liposomes for the treatment of meningitis: An in vitro study. *Int J Nanomedicine* **2017**, *12*, 3009-21, doi:10.2147/ijn.S130125.
470. Scriboni, A.B.; Couto, V.M.; Ribeiro, L.N.M.; Freires, I.A.; Groppo, F.C.; et al. Fusogenic liposomes increase the antimicrobial activity of vancomycin against *Staphylococcus aureus* biofilm. *Front Pharmacol* **2019**, *10*, 1401, doi:10.3389/fphar.2019.01401.
471. Bondarczuk, K.; Piotrowska-Seget, Z. Molecular basis of active copper resistance mechanisms in Gram-negative bacteria. *Cell Biol Toxicol* **2013**, *29*, 397-405, doi:10.1007/s10565-013-9262-1.
472. Massing, U.; Ingebrigtsen, S.G.; Škalko-Basnet, N.; Holsæter, A.M. Dual centrifugation - A novel "in-vial" liposome processing technique. *Liposomes* **2017**, doi:10.5772/intechopen.68523.
473. Nowak, D.; Jakubczyk, E. The freeze-drying of foods - The characteristic of the process course and the effect of its parameters on the physical properties of food materials. *Foods* **2020**, *9*, 1488, doi:10.3390/foods9101488.
474. Alonso, J.M.; Andrade Del Olmo, J.; Perez Gonzalez, R.; Saez-Martinez, V. Injectable hydrogels: From laboratory to industrialization. *Polymers (Basel)* **2021**, *13*, 650, doi:10.3390/polym13040650.
475. Moreira, C.D.F.; Carvalho, S.M.; Sousa, R.G.; Mansur, H.S.; Pereira, M.M. Nanostructured chitosan/gelatin/bioactive glass in situ forming hydrogel composites as a potential injectable matrix for bone tissue engineering. *Mater Chem Phys* **2018**, *218*, 304-16, doi:10.1016/j.matchemphys.2018.07.039.
476. Hartwig, F. Cu(DDC)₂-liposomen zur alternativen neuroblastomtherapie – Evaluierung der Toxizität anhand von 3D-sphäroiden. [Doctoral Thesis, Albert-Ludwigs-Universität Freiburg im Breisgau] Freiburg im Breisgau, **2020**.
477. Niaz, T.; Shabbir, S.; Noor, T.; Rahman, A.; Bokhari, H.; et al. Potential of polymer stabilized nano-liposomes to enhance antimicrobial activity of nisin Z against foodborne pathogens. *LWT-Food Sci Technol* **2018**, *96*, 98-110, doi:10.1016/j.lwt.2018.05.029.